Experimental study on wave-induced scour in front of sloping coastal structures and the influence of bed protection

W.M. Goedhart

Cover Photo:
Wave flume with bed protection and toe structure in front of sloping coastal structure

Experimental study on wave-induced scour in front of sloping coastal structures and the influence of bed protection

by

W.M. Goedhart

in partial fulfillment of the requirements for the degree of Master of Science in Hydraulic Engineering

at the Delft University of Technology,

to be defended publicly on Monday May 10, 2021 at 10:30 AM.

This study was part of the project Labwerk Coastal Structures (LabCoSts), which is supported by TKI Deltatechnologie.

Graduation committee:	Dr. ir. B. Hofland	TU Delft
	ing. C. Kuiper	TU Delft
	Dr. ir. M. A. de Schipper	TU Delft
	ir. W. J. Ockeloen	Van Oord

An electronic version of this thesis is available at http://repository.tudelft.nl/.

TU Delft
Delft University of Technology

TKI DELTATECHNOLOGIE

Preface

This report is the conclusion of my time studying Civil Engineering at the Delft University of Technology. It is written as part of obtaining the degree Master of Science in Hydraulic Engineering. Within this program I did a specialisation in the field of Coastal Engineering, with a focus on coastal structures. The report is the end product of the last 9 months in which I researched the phenomenon of scour in front of sloping coastal structures.

While the country was in lockdown and the university was closed for regular education due to the COVID-19 pandemic, I was allowed to continue my research in the laboratory of Hydraulic Engineering. Here I did physical model tests within the wave flume. While it felt a bit lonely at times at an almost abandoned laboratory and campus, I am very grateful that I was given this opportunity. My gratitude goes out to the staff that continued to work for some days a weeks in the laboratory. Their contribution to my research ranged from explaining how to operate the wave generator to helping me paint bed protection layer stones in a concrete mixer.

Besides working in the laboratory for about 3 months in the model testing phase, I worked from home and had contact with my graduation committee via video calls. I would like to thank them for their enthusiasm and available time in helping me reach this end product. I would like to thank my daily supervisor Coen Kuiper for always being available for fruitful discussions and review of my report. Thanks to the chair of my graduation committee and head of the laboratory Bas Hofland for providing me with the opportunity to do physical model testing, besides this his valuable new insights every time we met were of great help. Finally, I would also like to thank my external committee members Wouter Ockeloen and Matthieu de Schippper for their valuable input.
In addition, I have to thank TKI Deltatechnologie, part of the Dutch topsector water & maritime, for their funding of the work done in the laboratory. Without this funding I would not have been able to have such a long period of time available to conduct physical model testing within my research.

Besides these people who were directly involved with this project, I would also like to thank my friends, family and girlfriend for their support over the past years. Special thanks go out to Casper Jantzen for providing the foundation of this study. Being able to use the model set-up he constructed and having access to all measurement equipment allowed me to save a lot of time. Because of this, after only a couple of days of working in the laboratory valuable measurements could already be undertaken. Resulting in a very large and valuable data set. Besides this, he was also always available to answer all sorts of questions or discuss my results.

Thank you all for your support.

Wisse Goedhart
Rotterdam, April 2021

Summary

The erosion of the seabed in front of coastal structures induced by waves can lead to multiple types of failure in stability or function of the structure. On this topic most research has been done into erosion in front of vertical structures. For sloping structures a knowledge gap exists in the understanding of the processes that lead to erosion of seabed material directly in front of the structure. Available studies were done with regular waves or for a low number of waves. To fill this knowledge gap a series of studies was done at Delft University of Technology by MSc students. The present report is the second report in a series of studies into this topic. Here also results from the first study are included to create a large data set that will help determining what the main parameters are that lead to development of scour in front of sloping structures. Additionally, a method is presented that will help with predicting maximum scour depths when designing a sloping coastal structure.
To reach this goal a research question and a set of sub-questions have been formulated. The research question that is answered in the report is:

Can a set of design guidelines that include physical processes be created to predict the scour-deposition pattern at the toe of a sloping coastal structure.

In this study besides a constant transport over the whole bed two distinct types of scour are found in front of sloping structures. Being: (1) the standing wave pattern scour, and (2) the downrush flow scour directly adjacent to the structure. This second type of scour is not observed for vertical structures as here no significant run-up and run-down of waves on the surface of the structure is present. Besides these two types of scour, a constant transport of sediment was observed over the whole length of the flume. The direction of this transport was found to vary for variations in wave period when the wave height remained constant. For large wave periods transport offshore was observed while for short wave periods onshore transport was observed that resulted in accumulation of sediment at the base of the structure. Also, for some tests a small amount of sediment was trapped in the permeable structure, the bed protection and the wooden foreshore. The observed influence of this trapping of sediment was small and is neglected in analysis of scour development.

The first type of scour is found to primarily depend on the wave reflection coefficient K_r as the reflection of waves results in standing waves, influence of the wave reflection coefficient on the development of the maximum scour depth is found to follow a $K_r^{1.5}$ relation. For this relation better results for the development of the maximum scour depth are found for every structure than with the quadratic relation from Jantzen (2020). For larger wave reflection coefficients a more distinct standing wave pattern forms and the maximum standing wave scour depth increases. Material is deposited at the nodes and removed from the anti-nodes.
The downrush flow scour directly adjacent to the structure is found to directly depend on multiple parameters of which the relative water depth, the surf similarity parameter, the wave reflection coefficient, the roughness of the structure and the permeability of the structure are found to be most important in the present study and that of Jantzen (2020). For more rough structures there is less run-down of waves on the surface of the structure leading to lower flow velocities at the toe. As a result, for these cases less material will be removed and a lower maximum scour depth can be expected. Maximum scour depths directly in front of smooth impermeable structures are found to be about 2 to 3 times as large as for rough structures with the same slope angle. Opting for a rough structure when designing a sloping structure can therefore greatly reduce maximum scour directly adjacent to the structure. Besides the influences discussed here the maximum scour depth also depends on the type of sediment transport. In the present study for all tests the type of transport was found to be predominantly bed-load transport. The Xie (1981) criterion for suspended load or bed-load transport was found to give a good indication for the type of transport in these cases.

The following design formula, based on the work by Xie (1981) for vertical wall structures and where the relation with the wave reflection coefficient is included for sloping structures, is formulated as an answer to the research question for cases where bed-load transport of sediment is dominant:

$$\text{For } N \leq 24000 \text{ and } \frac{W_{p,t}}{L_p} < \frac{3}{8} L_p : \quad \frac{S_{max}(N)}{H_s} = \frac{0.3}{\left(\sinh \frac{2\pi h}{L_p}\right)^{1.35}} K_r^{1.5} \sqrt{\frac{N}{12000}} \tag{1}$$

By adding the influence of the reflection coefficient the formula is now made suitable for not only vertical wall cases ($K_r = 1$) but also for sloping wall cases where not all wave energy is reflected.

For temporal development of the spatially maximum scour depth the influence of the number of waves N is included. In combination with an estimation of the number of waves N_s ($= K_r \cdot 12000$) for which a substantial amount of scour occurs, development of the maximum depth is included in the formula. It is found that after the rapid increase in scour depth for the first waves this approach gives a good estimation of the maximum depth for cases where $\frac{N}{N_s} \geq 0.5$. No clear equilibrium maximum scour depth was observed after a certain amount of waves in the present study. Therefore, the maximum amount of waves tested on which the formula is based is added.
Also, a range for the length of the bed protection (measured from the waterline) is included to exclude cases with a long bed protection for which the formula is found to underpredict the maximum scour depth found in model tests.

Development of the maximum scour depth in this formula follows a square-root relation. This in contradiction with a recent formula from Den Bieman et al. (2019) where a linear relation is used. This linear relation is found to be suitable for only a low amount of waves for which the scour-deposition pattern has not fully developed. For a large amount of waves this linear relation is no longer suitable and a square-root relation like used in eq. (1) shows better results.
Performance of eq. (1) has been compared with measurements of the downrush flow scour hole and the standing wave scour. In model tests where waves with a low wave steepness were used the formula shows good results for all three tested structures. For a low number of waves ($\frac{N}{N_s} < 0.5$) the formula underpredicts the maximum scour depth. For a larger number of waves ($\frac{N}{N_s} \geq 0.5$), for which the maximum scour is important when designing, predicted values show good correspondence with results from model tests. The root-mean-square error of the formula with model results is in the order of 0.03 - 0.05 for these cases.
The formula is applicable for the maximum depth of both the scour hole directly adjacent to the structure ($x < \frac{3}{8}L_p$) and the standing wave scour hole at the first anti-node in front of the structure ($x > \frac{3}{8}L_p$) in cases without a long bed protection as indicated in the applicability given with the formula. The value of x used here is the distance of the end of the considered area measured from the waterline. $W_{p,t}$ is the distance from the waterline to the end of the structure, including bed protection. L_p is the peak wave length. It is important to note that the scour-deposition pattern is not significantly changed by the presence of bed protection but is truncated by the bed protection. In test that were outside of this range maximum scour depths were measured that are higher than the values calculated using eq. (1). Therefore, the formula is no longer suitable for these cases.

The large amount of tests included in the present study show clearly that for sloping coastal structures maximum scour depths are much lower than the incident wave height H_s in the case of irregular waves. Especially for rubble mound and rough structures maximum depths are found to be much lower. For 1:2.0 slopes the longest waves show maximum scour depths of about 0.5 H_s. Only for smooth structures maximum depths in the order of 1.0 H_s can be expected for very long waves. For cases where the relative water depth is in the range $0.075 \leq \frac{h}{\lambda_p} \leq 0.100$ the maximum scour depth rapidly decreases and is in the order of 0.25 H_s for rubble mound an rough structures. For smooth structures the maximum depth is in the order of 0.5 H_s. For the structures tested in the present study the wave reflection coefficient relation in the formula properly includes this influence of the difference in roughness. For more steep structures the formula seems to overpredict the depth of the scour hole directly adjacent to the structure for rough structures as these have large wave reflection coefficients while downrush flow is reduced by the rough surface. Performance for smooth steep structures is not known.

Influence of scour protection on the location of scour and the maximum scour depth is found to largely depend on the standing wave pattern and the downrush flow. The location of the end of the protection layer compared to the standing wave pattern determines whether scour or deposition can be expected at this position for the standing waves. Possibly some of the effect of the downrush flow scour is present at the end of the protection layer as scour is also observed when the protection ends at a location where deposition from the standing wave pattern is expected. Whether downrush flow is present further away from the slope at the end of a protection layer and how this is influenced by an increase in bed protection length is not know. For every test in this study scour is found directly at the end of the protection layer. Opposed to expectations the largest maximum scour depths were observed for layouts with a bed protection.
Bed protection with a length of 3/8 L_p (measured from the waterline) as proposed in some literature results in scour directly in front of the protection layer in the present study. However the hole that forms directly at the base of the structure when no protection is present is covered by the protection layer in these cases. Thus the hole closest to the structure forms in front of the protection layer at the first anti-node, 1/2 L_p from the waterline.
When designing scour protection for sloping structures it is therefore important to keep the locations of nodes and anti-nodes of the standing wave pattern and the magnitude of the downrush flow into account.

Contents

List of Figures

List of Tables

List of symbols

a	[m]	Wave amplitude
a_b	[m]	Wave amplitude at bottom
c_f	[-]	Friction coefficient
d	[m]	Diameter
d_n	[-]	Nominal diameter
d_{n50}	[-]	Median nominal diameter
d_{15}	[-]	Diameter exceeded by 85% of the material
d_{85}	[-]	Diameter exceeded by 15% of the material
D	[hr]	Test duration
D	[m]	Particle diameter
D_{50}	[m]	Median particle diameter
$d*$	[-]	Dimensionless particle diameter
C_f	[-]	Friction coefficient
Fr	[-]	Froude number
g	[m/s^2]	Gravitational acceleration
h	[m]	Water depth
h_o	[m]	Offshore water depth
h_t	[m]	Water depth above toe structure
H	[m]	Wave height
H_{m0}	[m]	Spectral wave height
H_s	[m]	Significant wave height
$H_{s,i}$	[m]	Significant incoming wave height
$H_{s,o}$	[m]	Significant outgoing wave height
Ir	[-]	Iribarren number (=ξ)
k	[1/m]	Wave number
K_r	[-]	Wave reflection coefficient
k_r	[m]	Roughness of bottom
KC	[-]	Keulegan-Carpenter number
L	[m]	Wavelength (=λ)
L_p	[m]	Peak wavelength (=λ_p)
N	[-]	Number of waves
N_0	[-]	Number of waves for which equilibrium conditions is reached
N_s	[-]	Number of waves during which a significant amount of scour occurs
n	[-]	Scale factor
P	[-]	Permeability
P	[-]	Rouse number
R^2	[-]	Coefficient of determination

Re	[-]	Reynolds number
$s_{o,p}$	[-]	Offshore peak wave steepness
$s_{n,p}$	[-]	Nearshore peak wave steepness
S	[m]	Scour depth
S_{max}	[m]	Maximum scour depth
$S_{max,3/8\lambda}$	[m]	Maximum scour depth over first 3/8 wavelength from waterline
T	[s]	Wave period
T_m	[s]	Mean wave period
T_p	[s]	Peak wave period
$T_{m-1,0}$	[s]	Spectral wave period
u	[m/s]	Velocity in x-direction
u_{mean}	[m/s]	Mean velocity in x-direction
$\hat{u_b}$	[m/s]	Orbital velocity at bed in x-direction
u_b	[m/s]	Maximum orbital velocity at bed in x-direction
u_{crit}	[m/s]	Critical velocity in x-direction
u_{max}	[m/s]	Maximum velocity in x-direction
u_{rms}	[m/s]	Root-mean-squared velocity in x-direction
$u_{2\%}$	[m/s]	Maximum velocity exceeded 2% of the time in x-direction
$\hat{u}_\delta$	[m/s]	Characteristic velocity at toe in x-direction
$u_\star$	[m/s]	Shear velocity in x-direction
We	[-]	Weber number
W	[m/s]	Sediment settling velocity
W_s	[m/s]	Sand particle settling velocity
W_t	[m]	Toe width
$W_{b,p}$	[m]	Width toe and bed protection
$W_{p,t}$	[m]	Width from waterline to end construction compared to peak wavelength
w	[m/s]	Velocity in z-direction
α	[-]	Slope angle
δ	[-]	Relative density
γ_f	[-]	Roughness coefficient
κ	[-]	Von Karman constant
λ	[m]	Wavelength
λ_p	[m]	Peak wavelength
μ	[kg/ms]	Dynamic viscosity
ν	[m^2/s]	Kinematic viscosity
ρ_s	[kg/m^3]	Density of solids
ρ_w	[kg/m^3]	Density of water
σ	[N/m]	Surface tension

τ_b	[N/m^2]	Bed shear stress in x-direction
τ_c	[N/m^2]	Critical bed shear stress in x-direction
$\tau_\star$	[-]	Dimensionless shear stress in x-direction
ψ_c	[-]	Shields stability parameter
ω	[1/s]	Angular frequency of waves
ξ	[-]	Iribarren number

1 Introduction

1.1 Background

In coastal areas all over the world coastal structures are present that protect people and infrastructure from the water. These type of structures have a large variety of functions and appearance. Structures can be divided into two main types, being: (1) Structures that protect or are part of coastal infrastructure such as ports and harbours; (2) Structures that prevent flooding of coastal areas or prevent erosion of a coastline. Examples of structures for both types of functions are breakwaters, dams, dikes and groynes. Structures range from consisting of a vertical wall to gentle rubble slopes. In this study the main focus will be on sloping structures.

Sloping coastal structures are constructed using a wide range of materials, of which rock, concrete, soil, wood and textiles are used most frequently. Structures commonly consist of a combination of materials that vary in size to come to the most functional and cost effective design. In this study the main materials that are used for construction are rock and wood.
A sloping coastal structure generally consists of several aspects, of which the armour layer, filter layer, core, toe and scour/bed protection are the most important aspects for this study. The armour layer (the outer layer) of the structure is exposed to wave attack and can consist of rubble, artificial concrete units or placed block revetments. These different types of layers vary in permeability, roughness and used material. The type of material used in the armour layer, the filter layer and the core have a large influence on absorption, transmission and reflection of the incoming wave energy. In this study these materials are varied to investigate the influence of these parameters on the erosion of the bed in front of the structure.

Such coastal structures are often build in areas where the bed consists of sediment material like sand, mud, clay and silt. Materials that can easily be displaced. Waves in front of a structure result in flow velocities near the bed that can lead to the sediment material being set in motion. Just in front of these structures velocities are influenced not only by the incoming wave energy but also by the energy that is reflected from the structure. This can result in large amounts of wave-induced erosion of the area in front of the structure.
Research has already been done into the influence of irregular waves on wave-induced erosion in front of vertical wall structures. For sloping structures some research with irregular waves has been done but this is limited to steep slopes (1:1.2), also the effect of bed protection has not been studied for these cases. This research in combination with an earlier study by Jantzen (2020) will try to fill this gap.

To reach this goal three types of sloping structures are tested in this study with irregular waves. Variations in toe and bed protection layout, sediment characteristics and hydraulic conditions will be tested for each structure. This will results in a large data set for which empirical relations can be derived for the development and behaviour of scour in front of all kinds of sloping structures.

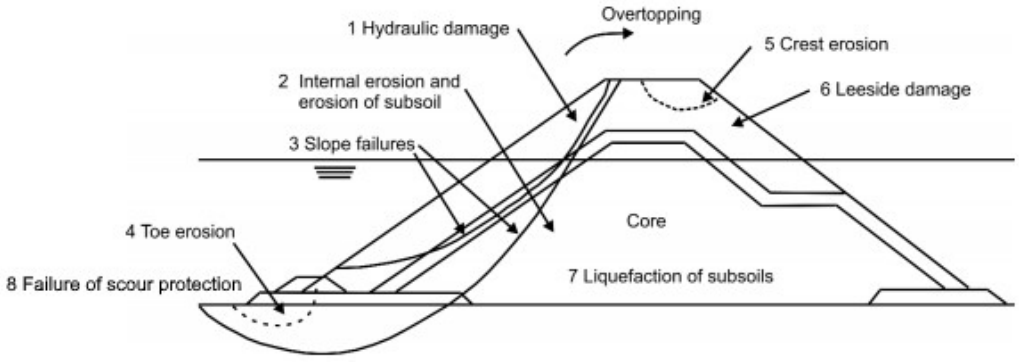

Figure 1.1: Standard rubble mound breakwater failure modes, from The Rock Manual (2007).

1.2 Problem description

Scour in front of a coastal structure and underneath the toe structure are important mechanisms that can cause breakwater failure. Figure 1.1 shows typical breakwater failure modes of which toe erosion/scour (4), erosion of the subsoil (2), slope failure (3) and failure of scour protection (8) are the types of failure on which this study is focused. All four types of failure can be the result of a scour hole forming in front of the structure. Therefore, when designing such a structure, taking into account this scour hole is an important aspect that influences design choices. The most common method used to prevent these types of failure is usage of a bed protection layer. A bed protection layer extends in front of the structure to make sure that no scour hole forms in the covered area. Using such a protection layer will result in scour being located further away from the main structure. Generally, holes that form here no longer significantly influence stability of the structure. Constructing such as scour protection over the whole length of the structure is an expensive operation. Especially when not sure whether such a protection is even necessary. For sloping structures no general set of guidelines is currently available that can be used to accurately determine whether scour can be expected close to the structure and what the dimensions of this scour hole will be. This makes it hard to judge whether bed protection is necessary.
When such a set of guidelines would be available a first estimation of the expected scour-deposition pattern could be made. These estimations can help with determining whether the costly bed protection in front of the structure will be necessary. A tool that currently can be used to check the necessity of bed protection is physical model testing. A scale model can be used to test the stability of the structure for individual cases, this is a costly and time-consuming method that has to be repeated for every individual case.

Knowledge gap
Several studies have been done into scour in front of breakwaters with and without a toe structure. Sumer and Fredsøe (2000) used physical model testing to study the scour-deposition pattern in front of rubble mound breakwaters. Here most tests were done with regular waves and only steep structures were used in combinations with irregular waves. Also, the influence of bed protection was studied only for cases with regular waves. In addition to this Gislason et al. (2009b) created a numerical model to calculate the scour-deposition pattern. This model works well for vertical-wall breakwaters but is lacking for sloping coastal structures.
Several other studies have been done to investigate the mechanisms that cause scour and deposition at and within a breakwater toe. For instance Dixen et al. (2008) studied suction removal of sediment from between armour blocks.

Recently studies have been done specifically for the case of rubble mound structures with a toe structure. Den Bieman et al. (2018) created a CFD (Computational Fluid Dynamics) model to simulate morphological change underneath a toe structure. Because of the lack in validation data for scour underneath toe structures no comparison can yet be made for the models predictive capabilities. The structure used in this model has a slope of 1:2.0 and an impermeable core. In addition to this Den Bieman et al. (2019) did physical model testing for a rock armoured structure with a toe. With the results of this experiments two expressions were developed. One for scour underneath the toe structure, the other for scour in front of the toe structure. The tested toe structure in these models consisted of the same material as the outer armour layer of the structure. Also, the structure that was used in this test was impermeable. These expressions are therefore not yet suitable for permeable rock armoured structures with a separate toe structure, such as breakwaters. Besides this, the tests were only done for a low number of waves which makes the expressions not suitable for determining the maximum equilibrium scour depth.

As stated there is no extensive set of design rules available to properly predict what the scour-deposition pattern in front of gentle sloping coastal structures will look like. Only information is available for very steep structures, a low number of waves or for regular waves. Also, the effect of scour protection is not completely included in the available studies. Because of this it is hard to predict the amount of scour that will occur and whether additional scour protection underneath and in front of the structure is required.
To fill the described knowledge gap a series studies is done at the Delft University of Technology. The present study is the second study on this topic and expands on the first study done by Jantzen (2020). In Jantzen (2020) investigation is done into the influence of bed protection on scour in front of sloped embankments. Here a rubble mound and a smooth sloping structure have been tested. This resulted in a design formula for determining the maximum scour depth over time and a formula to calculate the scour pattern in front of the structure over time.
In the present study the model tests done by Jantzen (2020) will be further expanded for an additional type of coastal structure and for several variations in bed material sizes and wave conditions. This will result in a large combined data set that will be analysed to investigate the influence of structural and hydraulic parameters on the scour-deposition pattern in front of sloping coastal structures.

Problem statement
It becomes clear that there is not enough knowledge available on the subject of scour at the foot of sloping coastal structures. Previous physical model studies have either been done for short testing times, rubble mound structures with steep slopes, impermeable structures or with toe structures that are made out of the main armour material. The problem statement therefore is:
When designing sloping coastal structures there are no elaborate guidelines or tools available to predict the scour-deposition pattern in front of the structure and include the influence of a toe structure and bed protection. This makes it difficult to predict whether additional scour protection will be needed.

Research objective
Objective of the research is filling the described knowledge gap. For this the physical model tests by Jantzen (2020) will be expanded for a new structure and other sediment particle sizes. With the combined test results from both studies better predictions can be made for the expected scour in front of sloping coastal structures. By further developing the formulas from Jantzen (2020) a tool will be available to estimate this expected scour pattern. Having expanded the tested conditions this tool will be applicable for a wider range of conditions.

1.3 Research question

To reach the desired goal of coming up with a set of design guidelines for estimating the amount of scour in front of a sloping structure a research question has been formulated. This research question is:

Can a set of design guidelines that include physical processes be created to predict the scour-deposition pattern at the toe of a sloping coastal structure.

1.4 Sub-questions

To help with answering this research question and to better understand the parameters influencing the results, the following sub-questions have been formulated:

- What is the relation between the relative water depth and the scour-deposition pattern?
- What effect does the wave steepness have on the scour-deposition pattern?
- What is the relation between the permeability of the structure, its corresponding reflection coefficient, and the scour-deposition pattern?
- What is the influence of the steady streaming flow on the scour-deposition pattern?
- What is the influence of the downrush flow on the scour-deposition pattern?
- How does the length of the scour protection influence the scour hole that forms directly in front of the protection?
- What influence do scale effects have on the scaling of sediment?
- How does scour develop over time?

The sub-questions formulated here are answered first to substantiate the response that is given to the main research question. The sub-questions are also used to determine the structures, sediment and wave conditions that are tested.
From earlier research it is clear that the parameters in the first five sub-questions all influence the scour in front of the structure. Further investigating their influence will help with better understanding their relation with the amount of scour and will allow for them to be used as parameters in the design formula(s) that will be created as a result of this research.

In several studies different definitions are used for the length of bed protection. In the present study the length is defined as the distance from the intersection of the waterline and the sloping structure to the end of the protection layer. It will therefore include not only the actual length of the protection layer but also the part of the structure that is in front of the waterline. Besides this, the values of S and S_{max} describing the bed profile and the maximum scour depth are taken to be positive when lower than the initial bed level. The scour depth is therefore given as a positive value in this study.

1.5 Structure of report

To be able to formulate an answer to all these questions this report first describes the studied literature, the model test setup and the tests results. Afterwards the results are analysed. This analysis is then used to answer the sub-questions and the research question. The report will have the following structure:

Available literature on relevant topics is discussed in section 2. Besides discussing the literature also considerations based on the literature are included here.

The methodology used in the physical model testing is discussed in section 3. Here the model setup and the tested conditions are described.

Results of the physical model tests are given in section 4. The results are presented of the laser measurements, photo measurements and flow measurements.

In section 5 the test results are analysed. Here the influence of individual parameters on the development of scour is described before the combined effect is presented in a design formula. This formula is then checked with available model tests results from literature. Also the model test results from this study will be compared with design formulas from literature.

The results of this study are discussed in section 6. Relevance of the new results and the addition they provide to the literature that is currently available is discussed. The shortcomings of the present study are also discussed here.

In the conclusion in section 7 the main research question and the sub-questions that have been formulated in the introduction are answered.

Recommendations for future research are given in section 8. These recommendations can further help filling the knowledge gap presented in this study.

Additionally at the end of the report several appendixes are included that contain a more elaborate overview of the testing conditions, used material, measurement results and calculations. These appendixes support the core of this report.

2 Literature

In this chapter the available literature on the topics discussed in this study is reviewed. The chapter has the following structure:

- Relevant and similar studies are discussed in section 2.1. Available literature is used to indicate the existing knowledge gap and support decision made in the methodology of this study.
- Important parameters that influence the amount of scour in front of a sloping structure are discussed in section 2.2, section 2.3 and in section 2.4. Where the influence of the water depth, the wave steepness and the influence of the permeability of the structure are considered.
- The sediment transport is discussed in section 2.5. Here the approach by Shields (1936) for the motion of sediment is considered. In section 2.6 the stability of sediment material under waves is discussed.
- Literature on scaling and scale effects is discussed in section 2.7 and section 2.8. Here approaches are discussed to make sure that model results can be used in prototype situations.

2.1 Relevant & similar studies

In this section an overview is given of the relevant studies that have been done into the topic of scour in front of coastal structures. First the work by Xie (1981) is discussed where an expression for the maximum scour depth was developed for vertical wall breakwaters. Based on the work by Xie (1981) Sumer and Fredsøe (2000) further studied the scour in front of steep rubble mound breakwaters. Here the expression by Xie (1981) was further extended and made usable for steep sloping rubble mound structures.

Removal of sediment from between armour blocks due to waves was studied in Dixen et al. (2008). Here it was determined for what critical values particles are removed from underneath the armour blocks.
Gislason et al. (2009b) developed a model to calculated 2-D flow in front of a breakwater which was coupled with a morphological model. This model was found to show good results for simulating scour in front of vertical wall breakwaters. For sloping wall cases the results were not satisfactory.

More recently two studies were done into the scour underneath and in front of toe structures of a rubble mound breakwater by Den Bieman et al. (2018) and Den Bieman et al. (2019). Here a CFD model was created to simulate morphological change around and under toe structures. Predictive capabilities of this model are not yet validated. Also model tests were done for scour at the toe of an impermeable rock armoured structure. Two expressions are developed for the scour underneath and in front of a toe structure.
Additionally, the research by Jantzen (2020) on which this study is an extension is also discussed.

2.1.1 Study by Xie (1981)

Xie (1981) researched scouring patterns in front of vertical-wall breakwaters. In the model tests done in this research it was noticed that two basic types of scouring patterns occurred. These patterns depended on the sand grain size and the wave characteristics. These patterns were called fine, dominant for small grain sizes, and coarse, dominant for large grain sizes. For small grain sizes the material is transported largely in suspension resulting in scour at the nodes and deposition at the anti-nodes of the standing waves. For large grain sizes the material was mainly transported as bed-load resulting in scour halfway between the nodes and anti-nodes and deposition at the nodes. Figure 2.1 shows these two basic scouring patterns.
To distinguish between these patterns based on the wave characteristics the velocity at the bed was used. The relation used by Xie (1981) is given in Equation 2.1. For several grain sizes the value of this parameter is given for which the change between the fine and coarse scouring pattern is expected.

$$\frac{u_{max} - u_{crit}}{W} \quad \text{or} \quad \frac{u*_m - u*_c}{W} \tag{2.1}$$

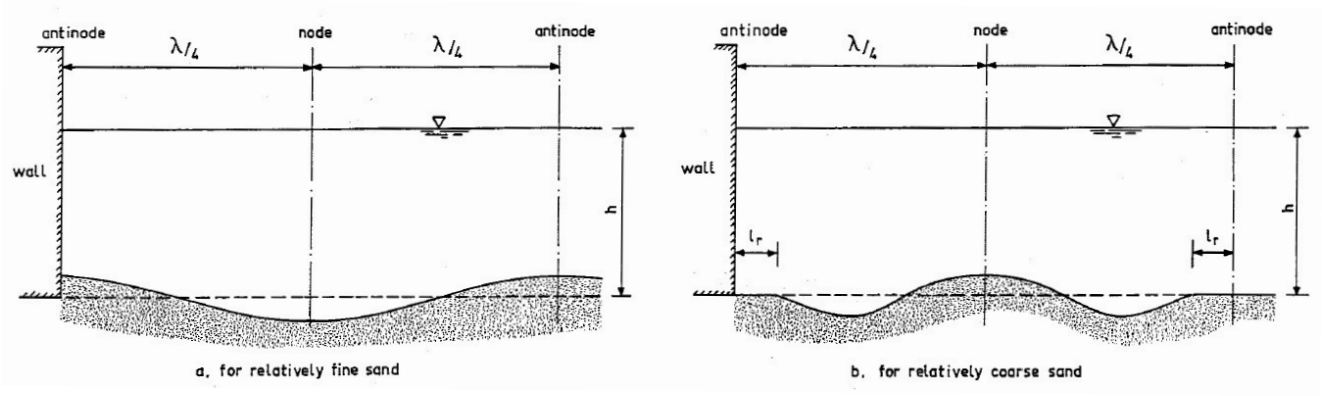

Figure 2.1: Basic scouring patterns in front of a vertical wall, from Xie (1981).

Xie (1981) found with his tests that the scour pattern due to flat waves ($s < 0.02$) needed more time to reach an equilibrium situation than the pattern due to steep waves ($s > 0.02$). For steep waves about 6500 - 7500 regular waves were needed to reach the final pattern, for flat waves 7500 to 10000 regular waves were need to reach this stage. It was also found that for steep waves the depth of the scour hole is smaller than for flatter waves.
The influence of a protective layer on the sea bed in front of the breakwater has also been investigated by Xie (1981). Tests have been done to investigate the length of this protection layer on the scouring profiles. The maximum depth of the scouring hole decreases with an increase in protection length and the width of this hole also decreases with an increasing length of the protection. Figure 2.2 shows the influence of a protective layer on the bottom profile. Figure 2.3 shows the relation between the length of the protection and the depth of the scour hole.

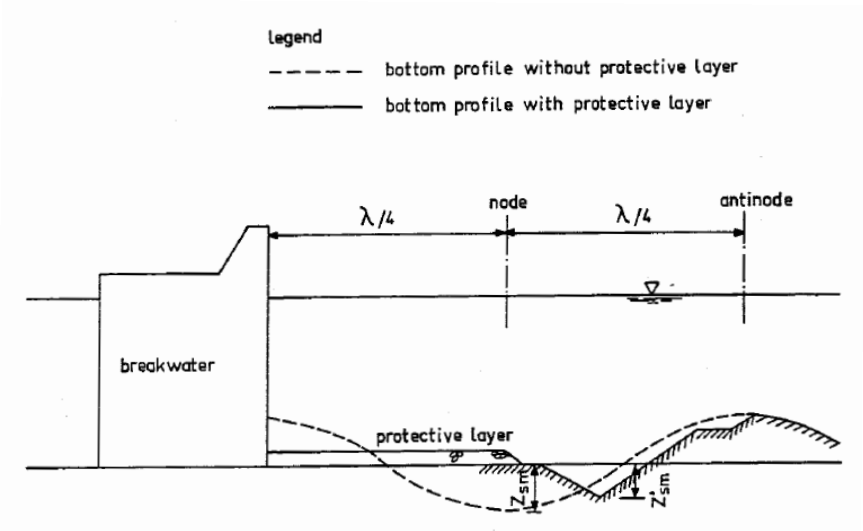

Figure 2.2: Influence of a protective layer, from Xie (1981).

An additional test was done where after reaching the equilibrium pattern for one type of regular wave a new regular wave condition was tested. A change in wave height and period will lead to a change in position of the nodes and anti-nodes which will give a more complicated situation. It was found that when a greater scouring depth is created by storm waves it is difficult to fill in the scouring hole according to the condition of the other waves. It is stated that this is probably a result of the orbital velocities at the bottom being influenced by the bottom geometry.

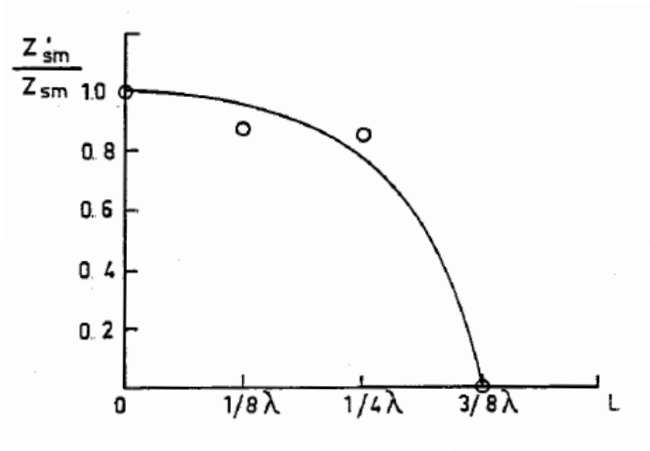

Figure 2.3: Influence of a protective layer on the depth of the scour hole, from Xie (1981).

In addition to testing with regular waves three test runs were done with irregular waves. The scouring pattern for irregular waves was found to be different than that of regular waves. The scour and deposition for irregular waves decreases fast with increasing distances from the breakwater. The parameters and results from two successful tests are given in table 2.1. Figure 2.4 shows the measured scouring depth compared to the wave height for these tests. For both tests the results are given for two cases. In the first case the measured scouring depth is compared to the significant wave height H_s. The second case compares the measured scouring depth to the mean wave height $\bar{H}$.

To determine the wave height and period of the irregular waves the zero-up-crossing method was used. For this the wave height was measured close to the surface of the vertical wall with a wave height meter that measures the standing wave. Half of this standing wave height is taken as the individual incident wave height. Xie (1981) also concluded that the energy ratio decreases fast when moving away from the vertical wall. It reaches half of that measured close to the wall at a distance of about 4λ from the vertical wall. After this it remains almost constant. Therefore it is concluded that the nodes and anti-nodes pattern vanishes completely when at least 4λ away from the vertical wall.

Table 2.1: Irregular wave tests done by Xie (1981)

Test	D50 [μm]	h [cm]	H [cm]	H_s [cm]	T [s]	T_P [s]	λ [cm]	h/λ [-]	H/λ [-]	Z_{sm} [cm]	$Z_{sm}/\bar{H}$ [-]	Z_{sm}/H_s[–]
1c	106	50	8.5	7.1	1.72	1.92	337	0.148	0.025	2.7	0.38	0.32
3c	106	50	7.1	4.8	1.69	1.90	270	0.111	0.026	3.0	0.63	0.42

From the results of these cases it seems that all the parameters for irregular wave cases are comparable with those of regular wave cases, except the time required to reach the equilibrium condition. For irregular waves it takes about twice as much time to reach the equilibrium condition, in this case 8 hours.

The scale of sand grains can be obtained via the similarity of the parameter in Equation 2.1 in model and in prototype. An approximation is:

$n_D = n_L^{0.25}$ for finer sand

$n_D = n_L^{0.5}$ for coarser sand

Where n_L is the length scale.
Xie found the scale of the scouring depth to be the same as the length scale.

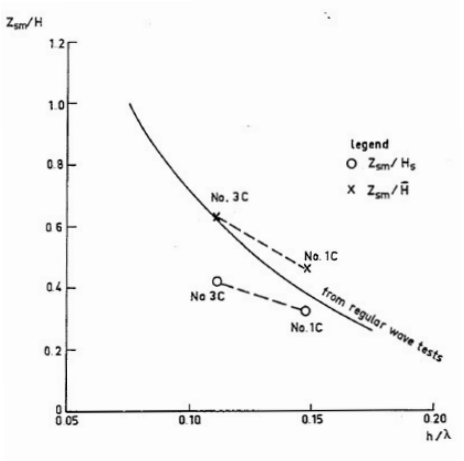

Figure 2.4: Measured scouring depth for relatively fine material under irregular waves, from Xie (1981).

Scour in front of vertical wall breakwaters has been extensively studied by Xie (1981). The grain size of the sediment particles is found to be an important parameter in the scour process as it determines whether bed-load or suspended load transport is dominant. For both types of transport a different scour-deposition pattern is found. Variations in sediment particle size will allow for comparison with both patterns found by Xie (1981)

Also, a relation between the length of a bed protection layer and the presence of a scour hole in the first $1/2\lambda$ from the vertical structure was found by Xie (1981) For a protection that extends $3/8\lambda$ from the structure no scour hole hole formed in this area. This raises the following two questions: (1) How to define the length of bed protection for sloping structures? (2) Does the influence of the length of the bed protection follow the same relation as found by Xie (1981) in fig. 2.3 for sloping structures?

2.1.2 Study by Sumer and Fredsøe (2000)

Sumer and Fredsøe (2000) studied the scour-deposition pattern in front of rubble mound breakwaters. It was found that the scour-deposition pattern in front of a breakwater takes the form of areas alternating from scour to deposition lying parallel to the breakwater, as can be seen in Figure 2.5. They also found that the scour depth decreases with a decreasing breakwater slope and in the case of irregular waves. It is stated that the difference between scour in front of vertical-wall and rubble-mound breakwater lies in the reflection coefficient associated with the structure.
The results of this study should only be used for the no-suspension mode of sediment transport (coarse sand).

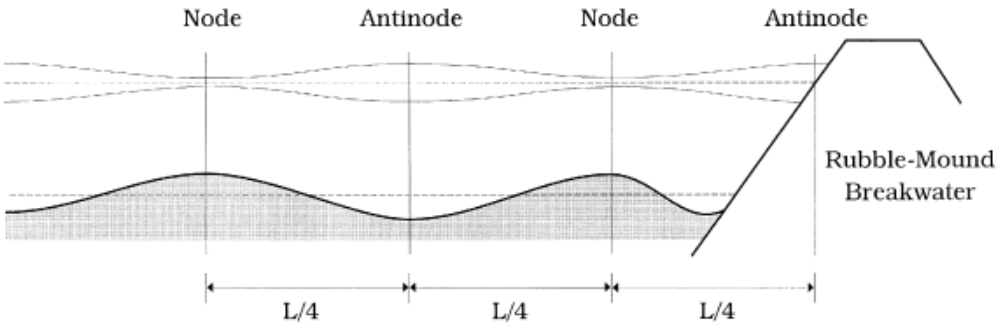

Figure 2.5: Schematic illustration of the scour/deposition pattern in the case of a rubble mound breakwater for coarse sand, from Sumer and Fredsøe (2000).

Sumer and Fredsøe (2000) tested with regular and irregular waves using the JONSWAP wave spectrum. Tests were done for rubble mound breakwater without scour protection and with scour protection (one layer and multiple

layers). For irregular waves it was found that scour and deposition decreases with an increasing distance from the breakwater, this behaviour is different from that for regular waves. This is due to the fact that for regular waves the nodes anti-nodes pattern extends over the whole length of the area in front of the structure. It is also found that the scour depth is lower in the case of irregular waves compared to regular waves.
They stated that the scour is caused by the steady streaming that is induced by standing waves. This steady streaming depends on the following quantities:

- The incident wave height H
- The incident wave period T
- The water depth h
- The breakwater slope α
- The bed roughness characterized by the sand-grain size d
- The water density ρ
- The water viscosity μ

The milder the slope of the breakwater the smaller the scour depth, this is due to a decrease of the strength of the steady streaming.

Sumer and Fredsøe (2000) came up with the following experimental expression for the maximum scour depth at a rubble mound breakwater:

$$\frac{S}{H} = \frac{f(\alpha)}{\left(\sinh = (\frac{2\pi h}{L})\right)^{1.35}} \tag{2.2}$$

Where $f(\alpha)$ is:

$$f(\alpha) = 0.3 - 1.77 \exp\left(-\frac{\alpha}{15}\right) \tag{2.3}$$

This expression is valid for breakwater slopes in the range of $30° \lesssim \alpha \leq 90°$

For the case of toe protection two experiments were done. For the first experiment an apron with one layer of stones was used. In the second experiment this apron consisted of several layers of stone.
For one layer of stones scour did not only appear at the edge of the toe protection but also underneath the apron. This resulted in a net downward displacement of the apron. This can be contributed to two effects. The waves stir up the sand underneath the apron and bring it into suspension near the bed. The existing steady streaming near the bed will carry this sediment away from the apron into the sand-bed section.
When a protection of multiple layers was used the apron slumped down into the scour hole an formed a protective slope. This can be seen as a desired effect of scour protection. This displacement develops slowly and is partly caused by wave action.

Sumer and Fredsøe (2000) researched scour for relatively steep rubble mound breakwaters. Model tests with irregular waves were only done for very steep (1:1.2) structures. The expression developed for the maximum scour depth based on regular waves is only valid for slopes that are steeper than 30°. For milder slopes this research cannot be used. The results here are also only suitable for the no-suspension mode of sediment transport. Influence of scour protection is tested in the form of a falling apron. Interesting to note is that Sumer and Fredsøe (2000) found a different scour pattern than Xie (1981) for bed load transport. While Xie found scour halfway between the nodes and anti-nodes and deposition at the nodes Sumer and Fredsøe (2000) found scour at the anti-nodes and deposition at the nodes.

More insight in the scour-deposition pattern in front of sloping structures and the differences with vertical structures is created by Sumer and Fredsøe (2000). It is stated that the scour-deposition pattern is caused by steady streaming for which the important parameters are listed. Parameters that can easily be varied between tests are: the incident wave height H, the incident wave period T and the bed roughness characterized by the sand grain size d.

2.1.3 Study by Dixen et al. (2008)

Dixen et al. (2008) researched the suction removal of sediment from between armour blocks due to waves. This study is an extension to a study done for the removal of sediment due to steady currents. In this new study the critical onset of suction is determined. The onset of suction is defined as the occurrence of entrainment of sediment grains/particles into the main body of het water. This onset of suction is determined by three different parameters:

- The sediment mobility number, based on sediment size
- The ratio of sediment size to stone size d/D
- The Keulegan-Carpenter (KC) number, based on the armour block/stone size

The Keulegan-Carpenter (KC) number is the ratio between the structure dimension and length scale of the orbital motion at th bed. It describes the importance of drag forces over inertia forces. It can be calculated using:

$$KC = \frac{\hat{u}_b T}{D} \tag{2.4}$$

Where $\hat{u}_b$ is the amplitude of the horizontal orbital velocity at the bed.

The tests show that the bed topography corresponding to the equilibrium stage in waves is completely different from that in the case of a steady current. Waves cause the bed to take the form of ripples. The stones will sit in the through areas of these ripples. The stones are initially undermined by the suction mechanism, resulting them to sink in the sand. As this continues the bed profile becomes wavy with dips near the stones. This bed profile develops into ripples. This formation of ripples is linked to the presence of recirculating cells generated by the oscillatory motion in the cavities caused by waves. This mechanism is similar to that at an ordinary ripple covered bed.

2.1.4 Study by Gislason et al. (2009a) & Gislason et al. (2009b)

Gislason et al. studied flow under standing waves. This work was divided in two parts:

In part 1 (Gislason et al. (2009a)) the shear stress distribution, energy flux and steady streaming for standing waves is discussed. Here the exchange of energy between the wave motion and the near bed oscillatory boundary layer is discussed. Additionaly, shear stress near the bed is determined. For this a numerical model is created. Simulations were done mainly for fully reflecting wall. The model was also used for some simulations of a plane sloping wall.

In part 2 Gislason et al. (2009b) used a 3-D general purpose Navier-Stokes solver to calculate 2-D flow in front of a breakwater. This model was coupled with a morphological model to calculate sediment transport and the scour-deposition pattern. Two elements were used in this model, the bed-load and the equation of continuity (mass balance) of sediment. The model was tested for two types of breakwater models. A vertical-wall breakwater and a sloping-wall breakwater.

The model shows good results for vertical-wall breakwaters. The equilibrium scour depth from the simulations agree fairly well with observations from experiments.
For the sloping-wall breakwater the scour-deposition pattern resembles that observed in previous experiments with breakwaters made of stones. It does not match the pattern observed in the model tests done in this study where the breakwater was made of an impermeable plywood plate. In the model for the sloping-wall breakwater the scour depth was predicted to be in the same order of magnitude as for the vertical-wall breakwater, this is in contrast to earlier experimental results were the scour depth was reduced by a factor of 2. Because of this it was concluded that the numerical results for the sloping-wall case appear to not be very satisfactory.

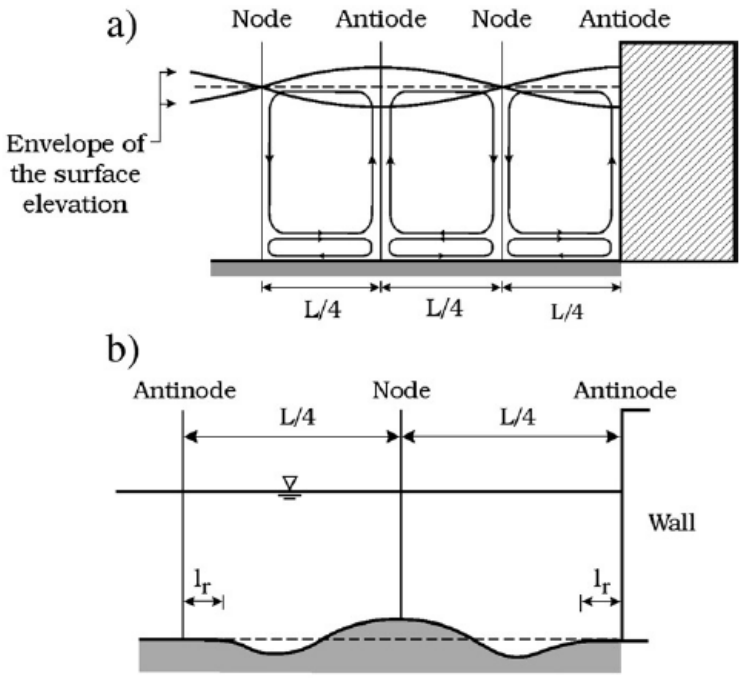

Figure 2.6: (a) Standing wave pattern in front of vertical-wall breakwater, (b) Scour-deposition pattern in front of vertical breakwater, from Gislason et al. (2009b).

An extension of the research by Sumer and Fredsøe (2000) was done in Gislason et al. (2009a), where the flow under standing waves at a smooth impermeable slope is further investigated. For this a numerical model was developed which was checked with the laboratory experiments. The main focus of this study are standing waves in front of a vertical wall but also some investigation is done into the the case of a sloping wall. Here a distribution of the bed shear stress in front of a sloping wall was determined. The resulting distribution is shown in fig. 2.7.
Near the toe of the sloping wall a strong offshore directed mean bed shear stress was found. Further away from the structure the sinusoidal variation was found to be identical to the variation in front of a vertical wall. Gislason et al. (2009a) also state that the presence of toe scour depends on the permeability of the structure. For porous structures toe scour is expected while for an impermeable structure no toe scour is present. The influence of the boundary layer over the slope is not included in the numerical model. The effect of this boundary layer is believed to not be significant according to Gislason et al. (2009a). No clear explanation is found for the differences between the laboratory experiments and the numerical model.

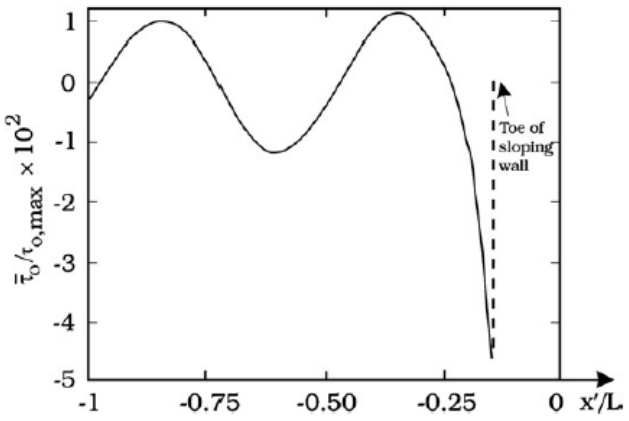

Figure 2.7: Mean bed shear stress in front of a sloping wall (slope 1:1.5), from Gislason et al. (2009a).

2.1.5 Study by Den Bieman et al. (2018)

Den Bieman et al. (2018) created a CFD (Computational Fluid Dynamics) model to simulate morphological change around and under toe structures. Within this model the dimensions of the toe structure and the hydraulic loading were varied to investigate their effect on scour. The results of this numerical model were compared with results from physical models. No comparison is done with data of bed level change inside the toe structure. Initial observations suggest that suspended sediment transport does play a role inside the toe structure. Because of this there are doubts about the assumption of bed load transport only in the sediment transport equations.
The model shows a remarkable scour-deposition pattern, it shows significant sedimentation inside the toe structure which is contrary to expectation. This seems to take place in almost all cases. The scour hole at the interface of the structure also look unrealistically narrow.

The work in Den Bieman et al. (2018) is mainly focused on sediment transport within the structure. When sediment transport within the toe is experienced comparison can be done with this model. The predictive capabilities of this model will still have to be shown by comparison with validation data.

2.1.6 Study by Den Bieman et al. (2019)

In a recent study by Den Bieman et al. (2019) two expressions for scour at the toe of impermeable rock armoured structures were created using physical model tests. One of these expressions is for scour in front of the structure. The other is for scour underneath the structure. The erosion volume seems to have a linear relation with the conditions, to describe this behaviour the following equations were created.

Scour underneath the structure:

$$\frac{\Delta V_{toe}}{H_{m0}^2} = C_{toe} \cdot N_{waves} \frac{H_{m0}}{d} \frac{d_{toe}}{d} \frac{D_{n50,toe}}{d} \frac{L_p}{d} \tag{2.5}$$

Scour in front of the structure:

$$\frac{\Delta z_{b,scour}}{H_{m0}} = C_{out} \cdot N_{waves} \frac{H_{m0}}{d} \frac{L_p}{d} \frac{d_{toe}}{d} \tag{2.6}$$

Where:

ΔV_{toe}	=	Volume change underneath the toe structure per meter structure width
$z_{b,scour}$	=	Scour depth outside the structure
H_{m0}	=	Spectral significant wave height
C_{toe}	=	Calibration constant for scour underneath the toe structure
C_{out}	=	Calibration constant for scour outside the structure
N_{waves}	=	Number of waves
d	=	Water depth
d_{toe}	=	Water depth above the toe structure
$D_{n50,toe}$	=	Nominal diameter of the toe structure material
L_p	=	Local wavelength associated with the peak wave period

For the current study eq. (2.6) is most relevant. Here the maximum scour depth is taken to follow a linear trend. It is concluded by Den Bieman et al. (2019) that the equation gives a somewhat conservative estimation of the maximum depth. Based on the model tests used in the study the following validity range is included with eq. (2.5) and eq. (2.6):

Table 2.2: Validity range of eq. (2.5) and eq. (2.6), from Den Bieman et al. (2019)

Variable	Range of validity
Number of waves [-]	$N_{waves} \leq 3000$
Relative wave height [-]	$0.29 \leq \frac{H_{m0}}{d} \leq 0.41$
Wave steepness [%]	$0.5 \leq s_{p,toe} \leq 3.4$
Structure slope [-]	1 : 2
Relative toe stone diameter [-]	$0.12 \leq \frac{D_{n50,toe}}{d} \leq 0.21$
Rock grading [-]	$1.5 \leq \frac{D_{n85,toe}}{D_{n15,toe}} \leq 1.74$
Ratio stone to sand diameter [-]	$\frac{D_{n85,toe}}{D_{n15,toe}} \geq 2.2 \cdot 10^2$
Relative water depth above toe [-]	$0.58 \leq \frac{d_{toe}}{d} \leq 0.79$

The model tests in this research were done with a structure with an impermeable core. In many coastal structures the core is permeable. This permeability will likely influence the amount of erosion and deposition and the wave reflection properties of the structure. It is expected that the use of an impermeable core will lead to the same or more scour compared to structures with a permeable core. Therefore, the results from this study are expected to be conservative.
The structure used in these tests did not have a separate toe structure. In this model the armour layer of the breakwater extended over the whole structure and was placed directly on the sand bed. The results from this study are therefore less suitable for coastal structures with toe structures consisting of other material and with filter and protection layers.

More knowledge on the influence of permeability and roughness of a sloping structure and the associated wave reflection can be created by testing additional structures. Also, the influence of various layouts in toe and bed protection on scour can be further researched. Development of the maximum scour depth over long periods of time is also not included in the work by Den Bieman et al. (2019).

2.1.7 Study by Jantzen (2020)

The present study is part of ongoing research into coastal structures at Delft University of Technology. As a part of this the topic of scour development in front of sloping structures has been studied in Jantzen (2020). The present study is an extension of the work by Jantzen and will combine new results with model test results from Jantzen (2020) to further extend knowledge on the topic.

In Jantzen (2020) the scour depth was found to be mainly influenced by the following processes:

- Downrush flow
- Damping sine wave pattern
- Undertow
- Asymmetric waves
- Sand dune development

Of these processes the downrush flow and the dampening sine wave pattern were determined to be the most significant processes leading to scour in front of a structure.

Model tests were done by Jantzen (2020) for two types of sloping structures, being an impermeable smooth slope and a rubble mound breakwater. Both structures had a 1:2.0 slope. Based on the results of these model tests a new design formula for determining the maximum scour depth in front of a sloping structure was developed based on the work by Xie (1981) and Sumer and Fredsøe (2000). In addition to their work the influence of the reflection coefficient K_r and the amount of waves was added by Jantzen (2020). Influence of the reflection coefficient was found to be quadratic while development of the scour depth for the number of waves follows a square root relation. This new design formula is given in eq. (2.7).

$$For\ N_0 = 12000\ and\ \frac{x}{L} < 1:$$

$$\frac{S_{max}(N)}{H_s} = \frac{0.3}{\left(\sinh\frac{2\pi h}{L}\right)^{1.35}} K_r^2 \sqrt{\frac{N}{N_0}} \tag{2.7}$$

Where:

S_{max}	=	The maximum scour depth
H_s	=	The significant incident wave height
h	=	The water depth in front of the structure
L	=	The peak wave length
K_r	=	The wave reflection coefficient
N	=	The number of waves
N_0	=	The number of waves for which an equilibrium is reached, $N_0 = 12000$

In addition to the equation for the maximum scour depth an expression for the bed profile in front of the structure was developed. This expression includes eq. (2.7) for the maximum scour depth and links this to a damped standing wave pattern that is present in front of the structure for irregular waves. This resulted in the following expression:

$$\frac{S(x,N)}{H_s} = S_{max} e^{(-0.85\frac{x}{L})} - \cos(4\pi\frac{x}{L}) K_r^2 \sqrt{\frac{N}{N_0}} \tag{2.8}$$

It was concluded by Jantzen (2020) that the location of maximum scour is mostly influenced by the length of the scour protection. The presence of scour or deposition of material in front of the structure is said to depend on a combination of the standing wave pattern and the downrush flow from the structure slope. When the end of the structure is near the anti-node of the standing wave pattern more scour can be expected than when close to a node of the standing wave pattern.

For determining the scour-deposition pattern Jantzen (2020) concluded that the peak wave period and the wavelength based on this peak wave period should be used. The node anti-node pattern of the standing waves was found to be determined by the peak wavelength.

The following relevant recommendations were given in Jantzen (2020) to further fill the knowledge gap on scour in front of embankments:

- Measured the bed profile more frequently to gain better insight in scour development over time.
- Test more variations in wavelength and wave steepness. This will extend knowledge on the influence of wave steepness, downrush flow and location of toe compared to node anti-node pattern.
- Test an additional structure with a different permeability and roughness to better understand the downrush flow.
- Vary ratio bed protection length - wavelength. This will give more insight in the combination of downrush flow scour and standing wave scour present at the end of the protection layer.
- Conduct model tests were fine sand is used. For this type of sand another scour-deposition pattern is expected which has not yet been studied for sloping structures.

Findings by Jantzen (2020) are used in determining the test conditions for the present study. Also the given recommendations are used for deciding what other parameters can be varied to further fill the current knowledge gap. The new results will be compared with the developed design formula and based on the larger data set the formula is optimised.

2.2 Influence of water depth

Multiple studies have already been done to investigate the relation between the water depth and the bottom orbital velocity. To calculate this velocity eq. (2.9), derived from linear wave theory, can be used. Here the water depth, wave period and wave height are used to calculate the velocity. Additionally eq. (2.10) and eq. (2.11) are given that describe the shear bottom stress for the calculated bottom orbital velocity and the friction at the bottom.

$$\hat{u_b} = \frac{\omega a}{\sinh 2\pi \frac{h}{L}} \tag{2.9}$$

$$\tau_b = \frac{1}{2}\rho C_f \hat{u_b}^2 \tag{2.10}$$

$$C_f = 0.237\left(\frac{a_b}{k_r}\right)^{-0.52} \quad \text{for} \quad a_b > 0.636k_r \tag{2.11}$$

Wiberg and Sherwood (2008) studied the near-bed wave orbital velocities and shear stresses depending on surface-wave parameters. This resulted in the relation given in fig. 2.8. Here the bottom orbital velocity as a function of the water depth is given for multiple wave periods. It is clear that the bottom velocity u_b reduces for increasing water depth and thus an increasing relative water depth h/λ. As a result the shear stress τ will reduce as well. As the shear stress on the bed particles reduces less material will be displaced and transported for an increase in relative water depth. Smaller scouring depths are therefore expected for an increase in relative water depth. This increase in relative water depth can be the result of an increase in water depth or an increase in wave period and thus wave length.

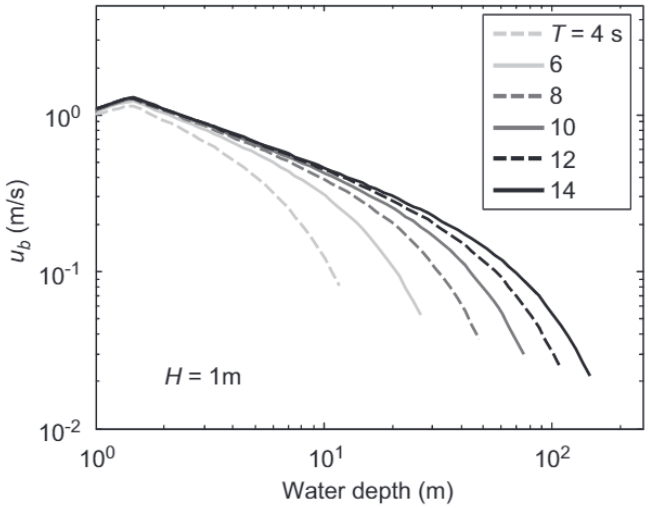

Figure 2.8: Bottom orbital velocity as a function of water depth, from Wiberg and Sherwood (2008).

2.3 Influence of wave steepness

Sato et al. (1969) studies scouring at the foot of coastal structures. Presented are the results of two-dimensional model experiments conducted to clarify the basic characteristics of scour and to find out some preventive measures against scouring around coastal structures. From the experiments and field investigation is it is concluded that the characteristics of waves just in front of structures, their reflection and wave-induced currents are the most important factors in scouring.

In the experiments for scour at the foot of a vertical sea wall it was found that the maximum scour depth was highest for waves with a low wave steepness. For a steepness of 0.02 to 0.04 the scour depth is approximately equal to the height of the deep-water waves. For higher wave steepness the maximum scour depth decreases with an increase of the wave steepness.

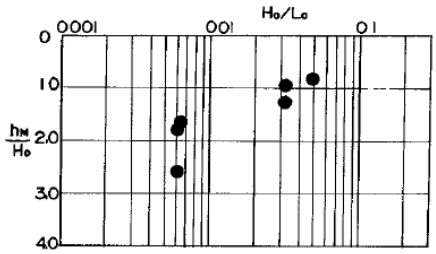

Figure 2.9: Relation between the largest maximum scouring depth and the wave steepness, from Sato et al. (1969).

For an inclined sea wall, the scouring depth decreases with the slope becoming less steep. For the case of a 30° seawall, which similar to a 1:2.0 slope, the position of the nodes and loops of the standing waves are shifted. When the distance of this shifting was close to a quarter of the wavelength, the foot of the wall was accreted from the beginning of the tests without any scour taking place.

Smith (1996) presents a method for estimating toe scour at a slope characterized by bottom velocity. For this wave, water level and structure parameters were considered. In this study results are presented to correlate the representative bottom velocity with relative depth, wave steepness and reflection.

It was concluded that scour in part depends on the reflection coefficient K_r. The horizontal bottom velocity increases for increasing reflection coefficients up to some maximum velocity, for higher reflection than this value the velocity reduces slightly. The reflection coefficient for which this velocity is highest depends on the slope steepness. It was found that for a 1:3.5 slope maximum velocity occurs at $K_r = 0.38$. For a 1:2.0 slope the maximum velocity is found for a K_r in the range of 0.44 – 0.48. For higher reflection coefficients the bottom velocity decreases, indicating that the scour potential decreases. This corresponds with earlier studies that state that scour ceases for high values of K_r.

On the influence of wave steepness on scour it was observed by Smith that maximum velocities occur at low wave steepness. Because the velocity is proportional to the wavelength it shows a decreasing trend with H_0/L_0.
The influence of depth is apparent if the velocity is normalized by the wave celerity. Maximum u/C occurs at lower deep-water wave steepness. The data shows increasing velocity with increasing wave height. The deep-water wave steepness is found to not be a good parameter to quantify the velocity because the velocity is directly proportional to both wave height and wavelength.

Reflecting on Sato et al. (1969) where maximum scour was observed for storm waves with steepness in the range of 0.02 – 0.04, and a decrease in scour was observed for increasing wave steepness. Laboratory results from Smith (1996) show that the offshore velocity decreases with increasing wave steepness, but the highest velocities occurred for minimum deep-water wave steepness. The results from the laboratory show that scour is not directly related to deep-water wave steepness.
Smith (1996) concluded that for 1:2.0 slopes maximum bottom velocities are found for a reflection coefficient K_r of 0.44 - 0.48. Whether this is also the case when the permeability and the roughness of the structure is varied has to be checked.

2.4 Effects of structure permeability and wave reflection

2.4.1 Permeability

The permeability of a structure has an influence on the stability of the armour layer and the wave reflection. The permeability depends on the size of filter layers and the core of the structure.
More water can penetrate the structure when it is more permeable, this will reduce the forces on the armour units. As a result, larger permeability will lead to a more stable structure.

Van der Meer (1988) came up with a notional permeability factor P, to describe the permeability of a structure with respect to the stability.
The lower boundary of P is given for an armour layer placed on an impermeable core (sand or clay) with a thin filter layer. For this situation, the value of P = 0.1, examples of this situation are seawalls and revetments. The upper boundary is given by a homogenous structure, that consist only of armour rocks. For this case P = 0.6. Two additional values of P are given. P = 0.4 for an armour layer with a filter placed on a permeable core. P = 0.5 for an armour layer placed on a permeable core without the use of a filter layer. For breakwaters, this value of P is generally in the range of 0.4 – 0.5 depending on the composition of the structure.

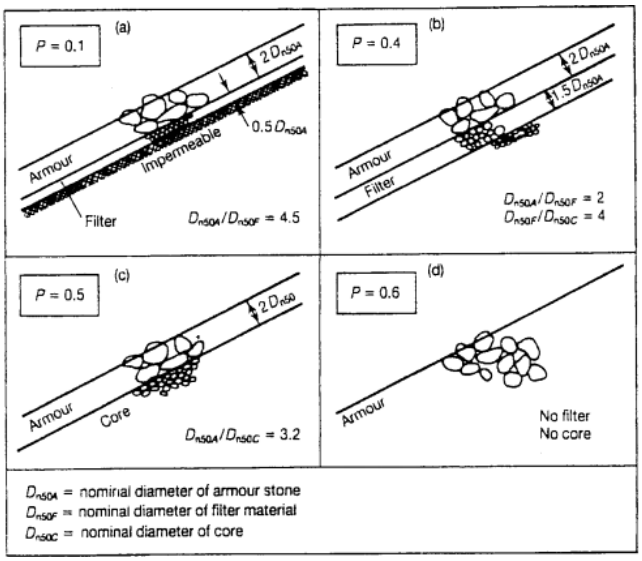

Figure 2.10: Notional permeability factor P for various structures, from Van der Meer (1988).

2.4.2 Wave reflection

Several equations have been produced to calculate the wave reflection for impermeable and permeable slopes.

Van der Meer (1995) presents formulae developed by Battjes (1974), Seelig and Ahrens (1981) and Postma (1989) and compares their fit with data from several tests. It was found that the best fit for the data was given by Postma (1989). In Postma (1989) the following relationship for calculating the wave reflection based on the notional permeability, the wave steepness, and the slope angle was derived:

$$K_r = 0.081 \cdot P^{-0.14} \cdot \cot\alpha^{-0.0.78} \cdot s_{op}^{-0.44} \tag{2.12}$$

Where:

P	=	Notional permeability
$\cot\alpha$	=	Slope angle of structure
s_{op}	=	Offshore wave steepness

From this formula it is clear that the wave reflection increases with an increase of the notional permeability. For more permeable structures the reflection coefficient decreases resulting in a lower reflection of wave energy. It also shows that for increasing wave steepness the reflection decreases, resulting in less energy being reflected. In the

study for scour at the foot of coastal structures by Sato et al. (1969) it was found that for large wave steepness the amount of scour at the toe was lowest and scour was maximum for low wave steepness. The expectation is therefore that a decrease in the reflection coefficient will result in a lower scour depth in front of the breakwater structure. When the wave reflection increases above a value for which the velocity is maximum, found to be in the range of K_r = 0.44 - 0.48 for a 1:2.0 slope by Smith (1996), the bottom velocity will also decrease slightly.

Zanuttigh and Van der Meer (2007) further studied the wave reflection of coastal structures. A new formula was developed that fits all kinds of slopes. By analysing existing formulas (including the one by Postma), comparing them with data and refitting them a new formula was developed. This formula uses two calibration coefficients that depend on the roughness of the structure.

The wave period has been adopted at the toe structure to come up with a parameter ξ_0 that is useful for representing bi-modal spectra. This parameter allows to incorporate different slopes into the formula.

$$\xi_0 = \frac{\tan(\alpha)}{\sqrt{(2\pi H_{m0})/(g T_{m-1,0}^2)}} \tag{2.13}$$

A new reflection formula was developed that satisfies all the following requirements (Zanuttigh and Van der Meer, 2007):

- Its shape can reproduce all different slope tyes
- Its represents physical bounds
- It gives a relationship with the roughness factor γ_f in the wave overtopping discharge formula

The new formula is:

$$K_r = \tanh(a \cdot \xi_0^b) \tag{2.14}$$

The coefficients to be used in this formula are given in table 2.3.

Table 2.3: Coefficients to be used in equation 2.14, (Zanuttigh and Van der Meer, 2007)

Data type	a	b	γ_f
Rock permeable	0.12	0.87	0.40
Armour units	0.12	0.87	various
Rock impermeable	0.14	0.90	0.55
Smooth	0.16	1.43	1.00

Using this formula the found reflection for a smooth slope is almost double that of a rock impermeable slope. Results from model tests with a smooth slope are therefore expected not to be representable for impermeable structures with a rubble armour layer.

2.5 Sediment transport

For this research it will be important to define what kind of sediment transport is present as it has a big influence on the scouring pattern as described by Xie (1981). This pattern depends on the sediment grain size and the wave characteristics. For small grain sizes the sediment is usually transported in suspension while for larger grain sizes the transport is usually in the form of bed-load. For both these types of transport formulas exist.

2.5.1 Shields

The approach by Shields (1936) considers the friction force caused by water on the bed. When a certain value is exceeded the grains will start to move. This is given as a relation between a dimensionless shear stress and the particle Reynolds number. The critical value of the velocity is described with the Shields parameter ψ_c, which is a stability parameter. In Equation 2.15 this relation is given. Figure 2.11a show the relation between the Shields parameter and the particle Reynolds number.

$$\psi_c = \frac{\tau_c}{(\rho_s - \rho_w)gd} = \frac{u*_c^2}{(\rho_s - \rho_w)gd} \tag{2.15}$$

van Rijn (1984) replaced the particle Reynolds number Re∗ with the dimensionless particle diameter d∗. This presentation of the Shields relation has the advantage that no iteration of $u*_c$ is required. This new relation can be seen in Figure 2.11b.

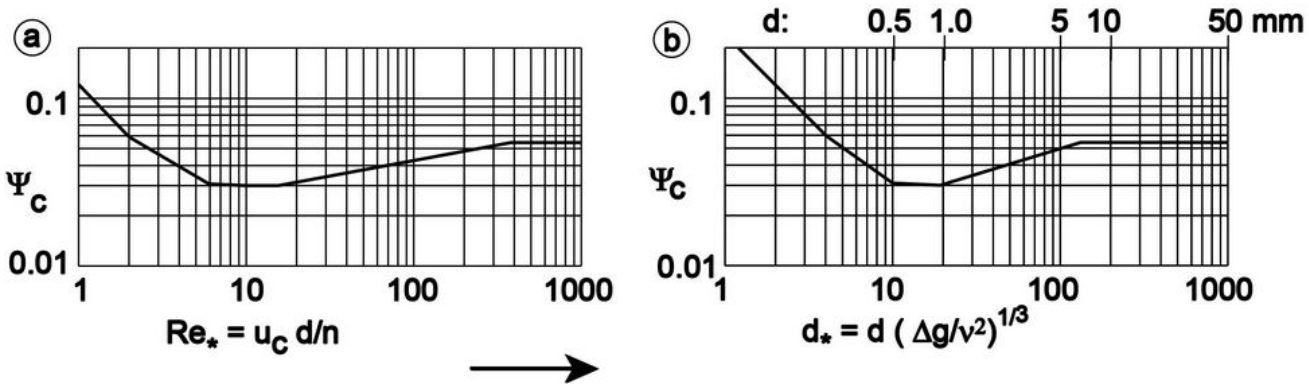

Figure 2.11: Critical shear stress according to Shields (a) - van Rijn (b), from Schiereck (2003).

It is difficult to determine what the exact threshold is for which the bed material will become in motion. This can be divided in multiple stages of transport depending on the Shields parameter.

2.5.2 Rouse

Rouse (1937) developed an approach for predicting the mode of sediment transport. In this approach the Rouse number P is calculated. This is a non-dimensional number that describes the mode of transport of sediment. The Rouse number can be calculated using the expression in equation 2.16.

The Rouse number is based on uniform flow and is therefore not directly suitable for wave-induced flow. It does give an indication of the possible type of transport for maximum flow velocities.

$$P = \frac{W}{\kappa u_*} \tag{2.16}$$

Where:

W	=	The sediment settling velocity
κ	=	The von Karman constant (=0.4)
u_*	=	The shear velocity

The type of sediment transport corresponding to the Rouse number is given in table 2.4. A division was made between bed load, suspended load (50%), suspended load (100%) and wash load.

Table 2.4: Rouse numbers for transport (Rouse, 1937)

Type of transport	Rouse number
Bed load	P > 2.5
Suspended load (50%)	1.2 > P >2.5
Suspended load (100%)	0.8 > P >1.2
Wash load	P < 0.8

2.6 Stability under waves

The stability of the loose material under waves is not that different from the stability in flow. In this section two methods are presented which are based on the work by Shields (1936).

2.6.1 Stability in non-breaking waves - Modified Shields

By combining the shear stress under a wave with the stability relation by Shields, that relates the shear stress to the grain diameter, the modified Shields relation for waves can be found. The results from this slightly differ from the original results by Shields, probably due to different boundary development in oscillatory flow (Schiereck, 2003). For large grain sizes this method shows similar results as the original approach by Shields for uniform flow. For smaller sizes this modified approach shows a lower mobility parameter. The threshold will therefore be rather high compared to the threshold in uniform flow. An explanation for this is that an unstable grain in oscillatory flow can not move a long distance before the flow decreases. This effect can be seen in fig. 2.12.

An equation that can be used to determine for which size the material will start to move is Equation 2.17. With the maximum orbital velocity $\hat{u}_b$, the wave period and the relative density this material size can be determined.

$$d_{n50} = 2.15 \frac{\hat{u}_b^{2.5}}{\sqrt{T}(\Delta g)^{1.5}} \tag{2.17}$$

The max orbital velocity can be calculated using the following equation based on linear wave theory. Where ω is the angular frequency, a is the wave amplitude, k is the wave number and h is the water depth.

$$\hat{u}_b = \omega a_b = \frac{\omega a}{\sinh kh} \tag{2.18}$$

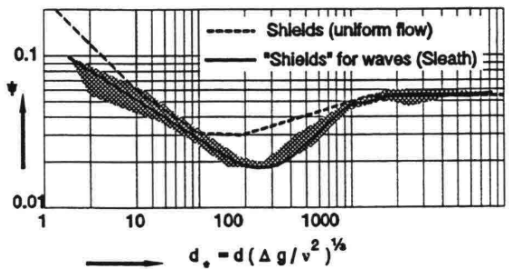

Figure 2.12: Modified Shields diagram, From Schiereck (2003).

2.6.2 Stability in breaking waves - Hudson

A next step for the modified Shields approach is taking the structure slope and the breaking of waves into account. Hudson (1953) proposed Equation 2.19 for the stability of stones on a slope. This formula is valid for slopes in the range of $1.5 < \cot\alpha < 4.0$. The K_D value in this formula is a dimensionless stability coefficient that depends on the kind of element and includes the accepted degree of damage.

$$\frac{H_{sc}}{\Delta d} = \sqrt[3]{K_D \cot\alpha} \tag{2.19}$$

This formula has several limitations. The wave period is not included, this means that the inertia force are not taken into account. It also does not include the permeability of a structure. The effect of energy dissipation is therefore not included. Also the number of waves is not included, this determines whether the equilibrium situation is reached. The Hudson relation is based on slopes in the range of 1:1.5 - 1:6. These equations were also derived for deep water conditions and are not suitable for shallow water.

2.7 Scaling

2.7.1 General scaling rules

The similarity between a real-world prototype and its model can be distinguished in three parts (Hughes, 1993):

- Geometric similarity
- Kinematic similarity
- Dynamic similarity

Geometric similarity
Geometric similarity requires similarity in shape between the prototype and the model. A model is geometrically undistorted if the vertical and horizontal scales are the same.

Kinematic similarity
Kinematic similarity implies geometric similarity and indicates a similarity of motion between the model and the prototype. This requires constant ratios of time, velocity, acceleration and discharge.

Dynamic similarity
Dynamic similarity requires that all force ratios in the two system are identical. This means that there must be constant prototype-model ratios of all forces acting on the system. This requirement arises from Newton's second law.

Heller (2011) concluded that exact model similarity would require a model operating in a miniature universe where all physical parameters are scaled. However, it is already challenging to model two force quantities correctly.If the fluid in the model is identical to that of the prototype, only one force ratio can be identical, thus dynamic similarity is impossible. Therefore, the most relevant ratio has to be selected for scaling, the scale effects due to the other ratios have to be negligible.

The most important numbers for scaling are (Schiereck, 2003):

- Froude: $Fr = \frac{u^2}{gh}$ ratio inertia - gravitation
- Reynolds: $Re = \frac{uL}{\nu}$ ratio inertia - viscosity
- Weber: $We = \frac{\rho u^2 L}{\sigma}$ ratio inertia - surface tension
- Cauchy: $Ca = \frac{\rho u^2}{E}$ ratio inertia - elasticity
- Strouhal: $St = \frac{L}{uT}$ ratio local inertia - convective inertia
- Iribarren: $Ir = \xi = \frac{tan(\alpha)}{\sqrt{H/L}}$ ratio slope steepness - wave steepness

Frostick et al. (2011) describes that for wave models the relevant forces are the forces of gravity, friction and surface tension. To have true dynamic similarity the Fr, Re and We number should therefore be the same in the model and in the prototype. This is not possible, so true similarity is not possible.
However, the importance of friction is often small. If the size of the model is not too small, Weber similitude can be neglected. When the Reynolds number in the model is in the same range as for the prototype, Reynolds similarity can also be neglected. If these two criteria are met Froude scaling alone can be used for scaling the forces.

Frostick et al. (2011) states that the following scaling criteria have to be fulfilled for similitude in rubble mound breakwaters:

- Overall structural dimensions are scaled geometrically (geometric similarity).

- Flow hydrodynamics (waves) need to conform to the Froude criterion.
- Turbulent flow conditions have to exist throughout the primary armour layer (Re>3000).
- It is best to operate at larger scales when possible.

2.7.2 Froude scaling

For wave models where the importance of friction is negligible or very small Froude scaling is usually used. Froude scaling enables to maintain constant ratios between various terms in the equations of motion to have dynamic similarity. With Froude scaling all times are scaled with $N_t = \sqrt{N_L}$. Where N_L is the ratio of the lengths in the prototype and model. This relationship is required because the gravitational acceleration g is the same in the model and in the prototype.

For rectangular cross sections with an uniform depth the Froude number is:

$$Fr = \frac{u^2}{gh} \tag{2.20}$$

Using Froude scaling the following typical scaling relationships in terms of the length scale can be derived:

Wave height (m)	$n_H = n_L$
Time (s)	$n_T = n_L^{0.5}$
Velocity (m/s)	$n_H = n_L^{0.5}$
Acceleration (m/s^2)	$n_a = 1$
Discharge (l/s/m)	$n_q = n_L^{1.5}$
Mass (kg)	$n_M = n_\rho \cdot n_L^3$
Pressure (kN/m^2)	$n_P = n_\rho \cdot n_L$
Force (kN)	$n_F = n_\rho \cdot n_L^3$

The Keulegan-Carpenter (KC) number can be correctly scaled using Froude scaling and is applicable for sediment and rock protection as well as structures. The KC number is identical in model and prototype if the bed material is geometrically scaled, because they depend only on the ratio of bed material size to wave orbital excursion.
In rough turbulent flow the current drag coefficients and wave friction factors are identical in model and prototype, provided that the bed material is geometrically scaled. The bed shear-stresses in rough turbulent flow scale velocity-squared provided that the bed material is geometrically scaled and the water densities are identical (Frostick et al., 2011).
The Shields parameter in rough turbulent flow is identical in model and prototype. The threshold Shields parameter of rock protection is identical in model and prototype when the rock in the model is large enough that viscous effects can be ignored. For quartz in fresh water this responds to D > 5 mm. For smaller rocks and sediment the threshold Shields parameter varies and will generally not correspond between model and prototype.

Some sediment dynamic quantities are correctly scaled by Froude scaling, when the bed material is geometrically scaled and has the same density as the prototype. For this really small sediment or a large model has to be used. Because the model scale is limited by the size of the wave flume in this study no large model can be used. To reach similarity of the bed material sand particles with very small diameters have to be used.

2.7.3 Permeability scaling

The scaling of permeability is usually achieved by equating the hydraulic gradient at the interface between rock layers in prototype and model. This can be done by equating the Forchheimer resistance of the materials (Frostick et al., 2011).

However, when the size grading of the underlayer and core materials are not well-established and cannot be assured in the construction, a distorted material size might give over-optimistic results for the stability analysis, so that it may be unsafe to apply such a permeability correction. Furthermore, sand incursion into the core can occur at prototype scale and result in drastically reduced permeability. In these cases geometrically scaled material can give unconservative results. It can be seen that the benefits and disadvantages in permeability scaling must be carefully weighed, depending on the goal of the study and the client's needs and specifications.

2.7.4 Scaling of sediment

In Henriquez et al. (2008) a study is done for the scaling of sediment in the nearshore to find suitable sediment properties to model intra wave sediment transport. Using Froude scaling leads to the correct reproduction of wave steepness, shoaling, refraction and diffraction. Wave flumes are usually filled with water which leads to only two other scalable variables, the sediment diameter and the density.

Using lightweight sediment gives the opportunity to preserve several similarity parameters. This is possible for a bed load model, which is a combination of the Reynolds number, the Shields number and the relative settling velocity. Another possibility is using the suspended model, this uses a combination of the Dean number and the Shields number. A consequence of this is that the sediment grain diameter is larger, and the sediment density is smaller in the physical model compared to the prototype.

The settling velocity and the Dean number are both ratios between turbulence and settling velocity but focus on different processes. Turbulence by bed friction depends on the sediment diameter and hydraulic conditions, turbulence by wave breaking depends only on the hydraulic conditions. This suggests that the Dean number should be used when the area of interest is dominated by wave breaking.
Both the bed-load and suspended model will have similar scale effects since their mismatch in the Sleath number and relative length parameter is about the same.

The density of sediment is important when considering particle accelerations. Horizontal pressure gradients and inertia forces can have a significant impact on the total force balance of a sediment particle. This can be expressed with the Sleath number.

During half a wave cycle sediment is picked up, brought into suspension and settles again. Usually the parameter is thought of as the ratio of settling time to wave period. An alternative of this parameter is the ratio of turbulence generated by wave breaking to the settling velocity. Turbulent energy from wave breaking scales with the ratio of wave height to wave period.

Another similarity parameter is the relative length parameter, which is the ratio of a typical length to the sediment diameter. Scale effects from this parameter are unclear. Experiments indicate that bedform patterns depend on the relative length parameter.

On the scaling of fine sand De Vries (1982) concluded that fine sand is present in many coastal areas, these prototypes are difficult to scale because the conditions for roughness, currents and waves are hard to fulfil at the same time. Using bed-material in the model that is lighter than sand has restrictions because liquefaction may occur. For scale models on coastal morphology substantial deviation from the Froude condition can be expected

Frostick et al. (2011) states that the scaling of sediment transport rate does not usually follow directly from Froude scaling. The scaling of sediment required knowledge on the form of sediment transport and a formula that is appropriate to model this. As stated earlier the Shields threshold value for sediment is not similar in model and prototype when using Froude scaling. For these cases some adjustments of the scaling must be made. Normally the dependencies found in expressions for the bedload transport will be used for this. This introduces uncertainty into the scaling as different formulae have different dependencies.

Using sediment in the model that varies in density from prototype situation results in new difficulties when scaling to prototype situations. Not enough is yet known to confidently use material with a lower density in the model tests. Using small material will result in most of the material properties remaining the same between model and prototype.

2.8 Scale effects

Scale effects occur when the used scaling law does not correctly reproduce the physical conditions from the prototype. The model and scale effects are difficult to estimate and depend on the parameters that are being investigated.

In short-wave hydrodynamic models the scale effects result primarily from the assumption that gravity is the dominant force balancing inertial forces, this is called Froude scaling. When using this assumption for scaling the other physical forces, such as viscosity, elasticity and surface tension, will be scaled incorrectly. These scale effects have to be quantified.
For Froude scaled models the nonsimilitude of viscous forces and the surface tension can lead to scale effects involving wave energy frictional dissipation, wave breaking dissipation and air inclusion. It is important to recognize these scale effects and analyse them (Wolters et al., 2007).

Heller (2011) listed several practices to deal with scale effects:

- Avoidance, to avoid significant scale effects in a Froude model it is required to satisfy limiting values for the force ratios. Often rules of thumb are applied.
- Compensation, By giving up exact geometric similarity of some parameters an improved model-prototype similarity can sometimes be reached.
- Length distortion, uses different scaling factors for the height, width and length to decrease some scale effects. Disadvantages are that 2D and 3D flow is modelled incorrect.
- Correction, adjust results for the scale effect when enough information about the scale effect is available.

Scale effects are unavoidably when using small scale hydraulic models with sand particles. Froude scaling is found to be the best approach to scaling these types of models. It is expected that waves will not result in significant scale effects when using Froude scaling. Scale effects from the sediment transport are however harder to judge.

3 Methodology

In this chapter the methodology used for the model testing and to gather data is explained. It contains an overview of the wave flume facility, given in section 3.1. The model set-up used is shown in section 3.2. Section 3.3 contains the hydraulic and structural conditions that will be tested. An overview of the test program that is used is given in section 3.4.

The methodology applied in this research mainly follows the methodology as applied by Jantzen (2020). To be able to extend the analysis by Jantzen (2020) variations are made in the testing program. Additionally, further research also helps with scaling the results to other structural and hydraulic conditions. Deviations are done on the following topics:

- The tested structures, see section 3.2.1
- Grain size of the sand that is used, see section 3.2.2
- Measurement set-up, see section 3.2.3
- Hydraulic testing conditions, see section 3.3.1

An overview of the values of the most significant parameters from the present study compared to the values used by Jantzen (2020) is given in the following table:

Table 3.1: Overview variations in testing with Jantzen (2020)

Parameter	**Jantzen (2020)**	**Current study**
Wave height, H_s [m]	0.14 & 0.18	0.14 & 0.18
Peak wave period, T_p [s]	1.6 & 2.5	1.6, 1.9, 2.1 & 2.5
Offshore wave steepness, $s_{o,p}$ [%]	1.4, 1.7 & 3.5	1.4, 1.7, 2.0, 2.5 & 3.5
Test duration, D [Hr]	8 - 128	8 - 16
Length of bed protection, $W_{b,p}$ [m]	1.00	0.62 & 1.00
Slope angle structures, α [-]	1:2.0	1:2.0
Grain size sand, D_{50} [μm]	260	170 & 220
Permeability structure [-]	Impermeable & Permeable	Impermeable & Permeable
Roughness structure [-]	Smooth & rubble	Rubble
Type of structure [-]	Smooth impermeable & Rubble mound	Rubble mound & Impermeable rubble revetment

3.1 Wave flume set-up

For these test the wave flume at the TU Delft laboratory of Hydraulic Engineering is used. The dimensions of this flume are given in Table 3.2. The flume is equipped with a electrical piston-type wave generator, with a stroke of 2.00 m. It can create all types of waves with a H_s of up to 0.2 m and is equipped with active reflection compensation. Testing with a combination of waves and flow is also possible in this flume.

Set-up of the flume is the same as in Jantzen (2020). All structures and measurement devices are placed at the same locations in the wave flume. A side view of the wave flume is given in fig. 3.1.

Table 3.2: Dimensions wave flume Hydraulic Engineering Laboratory TU Delft

Dimension	size [m]
Effective length	39.00
Width	0.79
Height	1.00
Typical working depth	0.5 - 0.7

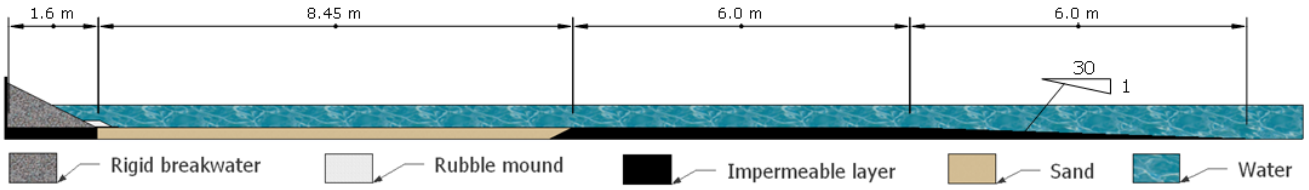

Figure 3.1: Side view of wave flume (Jantzen, 2020).

3.2 Model set-up

In this section the individual components of the model set-up are discussed. First the different types of structures that are tested are described in section 3.2.1. After that the set-up of the foreshore is described in section 3.2.2. The measurement equipment and that way these are used is described in section 3.2.3.

3.2.1 Structure set-up

My thesis deals with three different structures. Two of them were also tested by Jantzen (2020). The results of his tests will also be used in the analysis. All structures have a seaward slop of 1:2.0 and have a similar foreshore and crest level. Variations between the structures are in structure porosity and roughness. As a result, the wave reflection, wave run-up, wave run-down and flow velocities near the structure will vary. The tested structures are:

- Impermeable structure with smooth surface, tested in Jantzen (2020)
- Permeable rubble mound structure, tested in this thesis and in Jantzen (2020)
- Rubble mound revetment on impermeable layer, tested in this thesis

A side by side comparison of these structures can be seen in fig. 3.2. More detailed cross sections of the structures can be found in appendix A.1.

Table 3.3: Properties of materials used for construction

Material	Type	ρ_s [kg/m$_3$]	d_{n50} [mm]	d_{n15} [mm]	d_{n85} [mm]
Stones for permeable breakwater	Grauwacke	2550	38	30	44
Stones for revetment	Grauwacke	2550	30	24	38
Stones for toe structure	Grauwacke	2550	38	30	44
Stones for filter and bed protection	Basalt	3000	7.8	6.2	8.8

Permeable breakwater

The permeable rubble mound breakwater used in this study is present at the hydraulic engineering laboratory as it was already made for earlier research. This structure consist of stones that are glued together using epoxy. Epoxy was used to make sure that the shape of the breakwater does not change due to wave attack as this is outside the scope of this study. No displacement of stones also means that no rebuilding between tests is required. A cross section of the permeable breakwater is given in appendix A and the properties of the stones used for this structure are given in table 3.3. For a more detailed description and the decisions made when designing the structure is refered to Jantzen (2020).

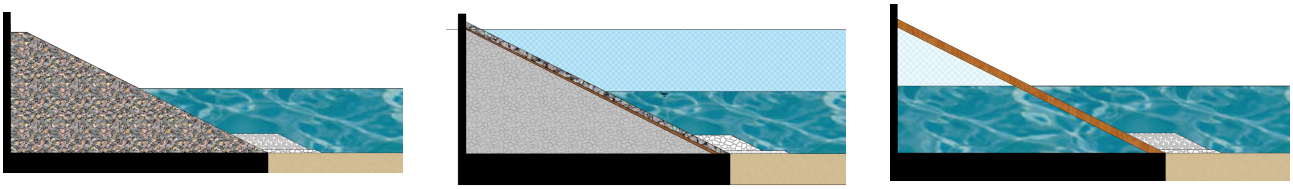

(a) Rubble mound structure.

(b) Impermeable revetment.

(c) Impermeable smooth slope.

Figure 3.2: Side view of the three tested structures.

Revetment

The rubble mound revetment structure used in this research was specifically made for this study and was placed on top of the permeable breakwater that remained inside the flume. The structures consists of a wooden plank that functions as an impermeable underlayer. On top of the plank a layer of stones was placed with a thickness of 2 times d_{n50}. These stones were glued together and on the underlayer using epoxy. This is done to prevent movement of individual stones. The design of this revetment structure can be seen in appendix A, the properties of the used material are given in table 3.3.
Because this new structure was placed on top of the permeable breakwater it extended further offshore and over the sand bed. An additional box was placed on the flume floor to make sure that the sand pit begins at the end of the revetment structure. A result of this extension is that the sand pit in front of the structure is slightly shorter than it is in front of the two other structures. Figure 3.3 shows the revetment structure inside the wave flume and also shows the extension of the box underneath the structure.

Figure 3.3: Revetment structure in wave flume, without toe and protection layer.

Toe structure

The toe structure used in this research is the same for every test that includes a toe. It is constructed with the exact same stones as used by Jantzen (2020), the same material is also used for the permeable breakwater. This toe is not glued together like the breakwater as it is not used for every test and has to be removed when preparing a new test set-up. The toe has a width of 5 times d_{n50} and a height of 2 times d_{n50} as generally used in practice. This results in approximately a height of 8 cm and a width of 20 cm.

Filter and protection layer

For some tests a toe structure is constructed which is placed on top of a filter layer. Additional tests are done were this filter layer will be extended offshore to also function as a bed protection. These layers will be constructed using the same material. The properties of this material are given in table 3.3 and in appendix A. For construction the same type of stones, with a similar d_{n50}, are used as by Jantzen (2020). Only difference is that in the present study the material has a more narrow grading. The filter and protection layer will have a thickness of 2 millimeters over its whole length. The length of the layer will depend on the test set-up, the used length is mentioned for each test in section 3.4.

3.2.2 Foreshore set-up

In front of the sloping structure over a length of 8.45 m a sand pit is constructed as can be seen in fig. 3.4. This layer of sand has a thickness of 0.20 m. In addition to the sand used in earlier research two additional types of sand, varying in grain size, were tested with this set-up. An overview of these three types of sand is given in table 3.4. The sieving curve of each of these types of sand is given in appendix A.
After each test the flume is drained and the sand bed is returned to its original flat state using a wooden board. This board is placed on top of the flume walls and can be moved over the whole length of the sand pit to ensure that the thickness of the sand layer is approximately the same for every test. When needed extra sand is added.

Further away from the structure at the end of the sand pit a wooden box is placed that will enable a transition from a flat solid bed to the sand bed. This box has a height of 0.20 m, a length of 6.0 m and has the same width as the flume. In front of this box a ramp is placed with a slope of about 1/30 to ensure a realistic transition from this box to the bottom of the wave flume. This slope and the decrease in water depth will influence the waves that are travelling towards the sand bed and the coastal structure.

The set-up used here is constructed using the same material as used by Jantzen (2020). Here the design was based on the set-up used in Den Bieman et al. (2019). This similarity in foreshore allows for comparison of the results from these three studies.

Table 3.4: Sand properties

Type of sand	D_{15} [mm]	D_{50} [mm]	D_{85} [mm]
Sand used by Jantzen (2020)	0.21	0.26	0.32
M32	0.16	0.22	0.25
M34	0.15	0.17	0.23

Figure 3.4: Sand pit facing structure (left) and sand pit and foreshore facing wave maker (right).

3.2.3 Measurement set-up

The following types of equipment were used for gathering data:

- Wave gauges for measuring the wave signal
- Laser sensors for measuring the bed profile
- EMS for measuring flow velocities
- Cameras for measuring scour development over time

Wave gauges

A total of 6 wave gauges are used for measuring the waves. Three of these wave gauges are located in deep water near the wave maker. The other three are placed on the flat foreshore just in front of the sand pit. These are located approximately 1 wavelength from the transitional slope to ensure that the influence of this slope on the measured waves is small. Placement closer to the structure is not possible as the measurement cart would be blocked from measuring the whole profile of the sand bed. The location of the wave gauges can be seen in fig. 3.5.
The wave gauges return a voltage signal over time depending on the amount of water that is above the sensors. This signal of each wave gauge is processed to produce a wave signal.By placing three wave gauges close together it is possible to separate this signal into an incoming and outgoing reflected wave. With this method the incoming wave height and the wave reflection of the structure can be calculated. Both are important parameters for analysing the scouring pattern. The analysis is based on the incident wave conditions measured at the foreshore, unless mention differently.

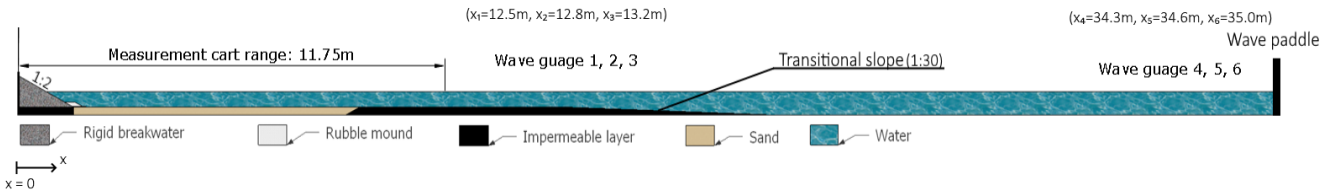

Figure 3.5: Location measurement equipment along wave flume, adapted from Jantzen (2020).

Measurement cart

The measurement cart is equipped with two laser sensors and one EMS measurement device. The cart is placed on top of rails that are placed on the walls of the flume. This will enable the cart to be driven over the whole length of the sand pit. The cart can be seen in fig. 3.6. On the far right side of this photo a wheel can be seen that is used to determine the exact position of the measurement cart over the flume length.

The two laser sensors will be used to measure the sand bed level in detail. These laser sensors measure the transit time of laser pulses between the sensor and the bed. Using this time and the speed of light in water the distance can be determined accurately. When measuring the bed using these lasers a reference frame is present within the flume, this will enable comparison between measurements. The laser sensors measure 10000 points per meter. Each of these measurements is linked to a position over the flume length as measured with the wheel attached to the cart.
When measuring the bed with the lasers sensors they are lowered to a fixed height just below the water surface. As can be seen in fig. 3.6 the lasers are mounted within small grey boxes. These boxes have a glass bottom enabling the lasers to be placed below the water level without getting wet.The lowering of the sensors is done by hand and can cause some small differences between measurements in the order of 1 mm.

Besides the laser sensors the cart is also equipped with an electromagnetic spectrum meter (EMS). EMS is used for measuring the flow velocities within the wave flume. The flow is measured for several tests close to the bed and higher in the water column for multiple locations over the flume length. The oscillatory flow that is measured is investigated over a longer period of time to determine whether there is net flow into one direction.
For three tests the velocity is measured 0.10 m above the initial sand bed level. This is done every 1.5 m over the length of the sand bed, starting in front of the coastal structure. When a toe structure is present the velocity is measured 0.20 m above the initial bed level at the location of the toe. For one test more extensive velocity measurements have been done. Here at every position measurements have been done at 0.10, 0.20 and 0.30 m above the initial bed level. For the first meter in front of the structure measurements were done every 0.25 m. Further offshore measurements were done every 0.50 m until a distance of 6.00 m from the structure.

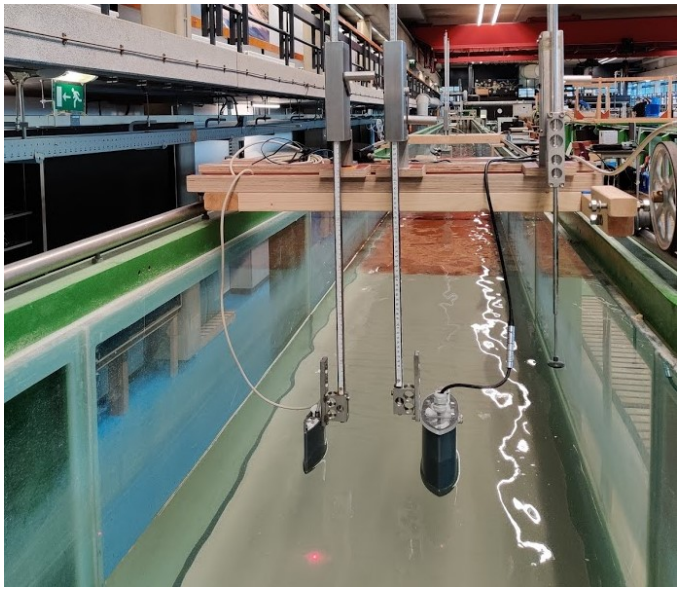

Figure 3.6: Measurement cart equipped with laser sensors and EMS (far right).

Cameras

Along the flume two cameras are placed that take photos of the side of the flume. This is done for an area of about three meters in front of the structure. Photos are taken at a fixed time interval of half an hour during the whole duration of a test. In addition to the laser scans that are used as the primary measurement to determine the sand profiles the photos can be used to determine the profile as well. Photos are taken to be able to verify laser measurements and have an indication about scour development over time. Scour development over time can be investigated as photos are taken at a more frequent time interval than laser measurements.
It is important to note that the side view of the flume may not give an exact representation of the scour in front of the toe as the presence of the flume wall may influence the flow here.

3.3 Test conditions

The test conditions that were varied in model testing are the type of structure, the hydraulic conditions and the set-up of the toe and bed protection. Both these conditions are varied to gain better insight of their influence on the scour-deposition pattern. These variations are described here.

3.3.1 Hydraulic conditions

The wave conditions that were used in this study are divided in two types of waves. These are long waves and short waves. The long waves have peak wave period of 2.5 seconds while the short waves have a peak wave period of 1.6 seconds. Both waves are tested with the same wave height of 0.14 meters. These values are entered into the wave making software that can be used for the wave generator in the laboratory. This program creates a standard JONSWAP spectrum, with peak enhancement factor 3.3, that the piston-type wave generator will recreate. Active reflection compensation (ARC) is used for these tests. The wave spectrum of both conditions are given in appendix B.

The wave gauges that measure the hydraulic conditions are placed at two positions, as described in section 3.2.3. The conditions measured near the wave generator are seen as the offshore wave conditions that are not affected by a changing water depth. The waves that are measured with the wave gauges located at the foreshore are seen as the nearshore wave conditions. These waves are influenced by the change in water depth due to the ramp in front of the foreshore. As the water depth remains constant from these gauges towards the structure, neglecting the small changes in sand bed profile, it is assumed that the wave conditions at the structure are the same as the conditions measured at the wave gauges.

3.3.2 Toe and bed protection set-up

Besides testing with the three structures described in section 3.2 variations in structural layout at the base of the structure have been tested. Three different toe layouts are tested in this study. These are:

- No toe and protection layer
- Toe with filter layer, no protection layer
- Toe with filter layer that is extend to function as a protection layer

These three layouts are tested for both wave conditions. This is done for all structures and types of sand. Resulting in a total of 18 tests. These tests and the extra tests that have been performed are given in section 3.4.

The set-up with a toe and filter layer is constructed as described in section 3.2.1. The filter layer used has a length of approximately 0.25 m and spans the whole width of the flume.
Additional tests are done with not only a toe structure with a filter layer but also a bed protection. This bed protection is constructed from the same material as the filter layer underneath the toe. But instead of having a length of 0.25 m this layer is extend with 0.75 m, resulting in a layer with a total length of 1.00 m. This layer is again placed over the whole width of the flume. Every 0.25 meter the colours of the stones used for the protection layer are changed. As a results, after a test has been finished, it is clear to see if stones are displaced and where displaced stones originate from. In addition to the test with a layer of 1.00 m one extra test is done for a length of 0.62 m. This additional test is used to judge the influence of the length of the bed protection on the development of scour.

3.4 Test program

To be able to answer the research question and its sub-questions a test program is created. Based on this variations in conditions are determined. Tests are done to check the influence of wave steepness, wave reflection, a toe structure, bottom protection, sediment grain size and wave height. In this section the naming of each individual test is explained and an overview is given of each individual test and its corresponding parameters.

Explanation test naming

In the name of each of the tests the parameters that are varied are listed. In table 3.5 these parameters are given and the naming for each variation is given. Below some examples are given of how this table should be interpreted.

For example a test with the permeable breakwater with no toe, the coarse sand and the long wave, with height 0.14 m, is named:
Per_D26_H14_T25_NoToe

A test with the revetment with a toe and protection layer, the fine sand and the short wave, with height 0.14 m, is named:
Rev_D17_H14_T16_ToeProt

Table 3.5: Individual test naming explained

Parameter	Variation	Naming
Type of construction	Impermeable plank/ Permeable breakwater/ Revetment	Im / Per / Rev
Type of sand	D_{50} = 170 μm / D_{50} = 220 μm / D_{50} = 260 μm	D17 / D22 / D26
Wave height entered in wave maker	0.14 m / 0.18 m	H14 / H18
Wave period	1.6 s / 2.5 s	T16 / T25
Presence of toe and bottom protection	No toe / Toe / Toe & protection / Toe & shorter protection	NoToe / Toe / ToeProt / ToeProt*

Test program

In table 3.6 an overview is given of all tests that have been done in the present study. It contains information on the used sediment, the wave conditions, structural layout and total testing time. Table 3.7 contains all tests that have been done in the earlier study by Jantzen (2020). In the present study a reanalysis has been done of these wave conditions as an error was found in the wave analysis for the permeable structure. Because of this the measured wave height and reflection in table 3.7 is lower than presented in the report by Jantzen (2020). Included in the second column of these tables is also the test naming as used in Jantzen (2020).
Explanation of parameters in table:

- $H_{s,i}$ The significant incoming wave height measured in front of the structure, between brackets is value entered in wave maker
- T_p The peak wave period
- $W_{b,p}$ Offshore extension toe and bed protection, measured from the point where the structure meets the bed.
- $W_{p,t}$ Offshore extension structure, toe and bed protection compared to wavelength, measured from the point where the waterline meets the structure. Expressed in peak wavelength λ_p
- D Test duration.
- $s_{o,p}$ The offshore wave steepness.
- K_r Reflection coefficient of incoming waves.

Table 3.6: Test series, for a structure with a 1:2 slope

Test		Structure	Sand type	$D_{50,Sand}[\mu m]$	$H_{s,i}$[cm]	T_p[s]	$W_{b,p}$[m]	$W_{p,t}$[-]	D[hour]	$s_{o,p}$[%]	Kr [%]
Per_D22_H14_T25_NoToe	(B.1.1b)	Permeable	m32	220	12.7 (14)	2.5	0	$0.17\lambda_p$	8	1.4	36
Per_D22_H14_T25_Toe	(B.1.2.b)	Permeable	m32	220	12.5 (14)	2.5	0.25	$0.22\lambda_p$	8	1.4	33
Per_D22_H14_T16_NoToe	(B.1.6)	Permeable	m32	220	11.6 (14)	1.6	0	$0.28\lambda_p$	8	3.5	23
Per_D22_H14_T16_Toe	(B.1.7)	Permeable	m32	220	11.6 (14)	1.6	0.25	$0.37\lambda_p$	8	3.5	24
Per_D22_H14_T16_ToeProt	(B.1.8)	Permeable	m32	220	11.6 (14)	1.6	1.00	$0.63\lambda_p$	8	3.5	24
Per_D17_H14_T25_NoToe	(B.2.1)	Permeable	m34	170	12.7 (14)	2.5	0	$0.17\lambda_p$	8	1.4	37
Per_D17_H14_T25_Toe	(B.2.2)	Permeable	m34	170	12.7 (14)	2.5	0.25	$0.22\lambda_p$	8	1.4	34
Per_D17_H14_T25_Toe_b	(B.2.2b)	Permeable	m34	170	13.0 (14)	2.5	0.25	$0.22\lambda_p$	16	1.4	34
Per_D17_H14_T25_ToeProt	(B.2.3)	Permeable	m34	170	12.7 (14)	2.5	1.00	$0.38\lambda_p$	16	1.4	37
Per_D17_H14_T16_NoToe	(B.2.4)	Permeable	m34	170	11.7 (14)	1.6	0	$0.28\lambda_p$	8	3.5	26
Per_D17_H14_T16_Toe	(B.2.5)	Permeable	m34	170	11.0 (14)	1.6	0.25	$0.37\lambda_p$	8	3.5	25
Per_D17_H14_T16_ToeProt	(B.2.6)	Permeable	m34	170	11.7 (14)	1.6	1.00	$0.63\lambda_p$	8	3.5	27
Per_D17_H14_T21_NoToe	(B.2.7a)	Permeable	m34	170	12.6 (14)	2.1	0	$0.20\lambda_p$	8	2.0	31
Per_D17_H14_T19_NoToe	(B.2.7b)	Permeable	m34	170	12.4 (14)	1.9	0	$0.23\lambda_p$	16	2.5	28
Per_D17_H14_T21_Toe	(B.2.8)	Permeable	m34	170	13.3 (14)	2.1	0.25	$0.27\lambda_p$	8	2.0	41
Per_D17_H18_T25_Toe	(B.2.9)	Permeable	m34	170	16.3 (18)	2.5	0.25	$0.22\lambda_p$	8	1.7	41
Per_D17_H14_T25_ToeProt*	(B.2.10)	Permeable	m34	170	13.2 (14)	2.5	0.62	$0.30\lambda_p$	16	1.4	36
Rev_D17_H14_T25_NoToe	(C.2.1)	Revetment	m34	170	12.7 (14)	2.5	0	$0.17\lambda_p$	8	1.4	51
Rev_D17_H14_T25_Toe	(C.2.2)	Revetment	m34	170	12.7 (14)	2.5	0.25	$0.22\lambda_p$	8	1.4	51
Rev_D17_H14_T25_ToeProt	(C.2.3)	Revetment	m34	170	12.6 (14)	2.5	1.00	$0.38\lambda_p$	8	1.4	51
Rev_D17_H14_T16_NoToe	(C.2.4)	Revetment	m34	170	11.9 (14)	1.6	0	$0.28\lambda_p$	8	3.5	33
Rev_D17_H14_T16_Toe	(C.2.5)	Revetment	m34	170	11.9 (14)	1.6	0.25	$0.37\lambda_p$	8	3.5	34
Rev_D17_H14_T16_ToeProt	(C.2.6)	Revetment	m34	170	11.9 (14)	1.6	1.00	$0.63\lambda_p$	8	3.5	33

Table 3.7: Test series Jantzen (2020), for a structure with a 1:2 slope

Test		Structure	Sand type	$D_{50,Sand}[\mu m]$	$H_{s,i}$[cm]	T_p[s]	$W_{b,p}$[m]	$W_{b,s}$[-]	D[hour]	$s_{o,p}$[%]	Kr [%]
Im_D26_H14_T16_NoToe	(A.0.1)	Impermeable	m32	260	12.4 (14)	1.6	0	$0.28\lambda_p$	10	3.5	63
Im_D26_H14_T25_NoToe	(A.0.2)	Impermeable	m32	260	13.5 (14)	2.5	0	$0.17\lambda_p$	66	1.4	81
Im_D26_H14_T25_Toe	(A.0.3)	Impermeable	m32	260	13.4 (14)	2.5	0.25	$0.22\lambda_p$	16	1.4	78
Im_D26_H14_T25_ToeProt	(A.0.4)	Impermeable	m32	260	13.5 (14)	2.5	1.00	$0.38\lambda_p$	32	1.4	77
Im_D26_H14_T16_Toe	(A.0.5)	Impermeable	m32	260	12.2 (14)	1.6	0.25	$0.37\lambda_p$	128	3.5	61
Per_D26_H14_T25_NoToe	(B.0.1)	Permeable	m32	260	13.4 (14)	2.5	0	$0.17\lambda_p$	32	1.4	35
Per_D26_H14_T25_Toe	(B.0.2)	Permeable	m32	260	13.5 (14)	2.5	0.25	$0.22\lambda_p$	16	1.4	36
Per_D26_H18_T25_Toe	(B.0.3)	Permeable	m32	260	17.5 (18)	2.5	0.25	$0.22\lambda_p$	22	1.7	36
Per_D26_H14_T25_ToeProt	(B.0.4)	Permeable	m32	260	13.7 (14)	2.5	1.00	$0.38\lambda_p$	8	1.4	37
Per_D26_H14_T25_Toe	(B.0.5)	Permeable	m32	260	13.7 (14)	2.5	0.25	$0.22\lambda_p$	8	1.4	37

4 Test results

This chapter contains the measurement results of the laboratory tests. First, in section 4.1 the results of the bed measurements with the laser sensors are presented. These measurements are the main focus of this research. Secondly, in section 4.2 the results of the photo cameras are given. These cameras were used to record the scour development in front of the coastal structure over time. In addition, the combined development of the bed profiles measured with the laser sensors and the cameras is given in section 4.3. Finally, section 4.4 contains the results of the flow measurements that were done during several tests.

4.1 Laser measurements

In this section the results of the laser sensor measurements are given. In section 4.1.1 the method used for determining the bed level out of the raw laser measurement data is explained. The maximum measured scour depth for each test is given in section 4.1.2. In section 4.1.3 and section 4.1.4 an overview of the resulting bed profiles for both tested structures are given. The bed profile of each individual test is given in appendix C.

4.1.1 Method

The processing of the laser measurement data in this research is based on the method used in the research by (Jantzen, 2020), which has been slightly altered. To come to a representative profile for every measurement the following procedure has been applied:

Step 1: The measurement data of the laser sensors is processed. This raw data contains a voltage signal indicating the time it takes the laser signal to be reflected of the bed and be received by the laser sensor. With the properties of the laser and the speed of light in water this signal is converted into the distance between the laser sensor and the bed. This data has a high resolution and contains a distance measurement every 0.1 mm over the whole length of the sand bed. It will therefore contain small local differences that are not of importance for this research.

Step 2: Filtering of the data is done to remove small ripples, that are present over the whole sand bed, from the measured bed profile. This is done because these small ripples, length $\approx$ 10 cm height $\approx$ 2 cm, are not important for the structural stability of the coastal structure, which is the main focus of this study. It is also not possible to correctly scale these ripples to a larger scale as found by O'Donoghue et al. (2006). Where ripples from large-scale experiments were compared with small-scale experiments.

These steps result in individual bed profiles of which examples can be seen in fig. 4.1. The resulting individual profiles will be used for further analysis. The method described here has also been applied to the measurement data from Jantzen (2020).
To be able to compare between tests and with literature the bed level is divided by the measured incident wave height $H_{s,i}$ in front of the structure. This results in the dimensionless value $\frac{S}{H_s}$ that is generally used to describe the scour depth in front of a coastal structure. Additionally, for each test the starting point from which the bed is analysed is the intersection between the still water level and the coastal structure. At this location, which is called the reference point in this study, there is always an anti-node in the wave pattern. All distances offshore from this reference point will be divided by the peak wave length, again enabling comparison between tests with different wave conditions.

For every test the profile is measured using the laser sensors after 1, 2, 4 and 8 hours of testing. Some tests have been extended with 8 hours, for these tests an additional measurement has been done after 16 hours. Additionally, for some tests extra measurements are done in between these set measurement moments. The measurements that are done for the initial profile (before wave generation) and after 8 hours have been done at 5 fixed positions over the flume width. As a results, for these measurements 5 cross sections over the whole length of the flume can be created. By taking the mean of these 5 cross sections local differences and individual measurement errors are filtered out of the resulting profile. An example of this method can be seen in fig. 4.1.

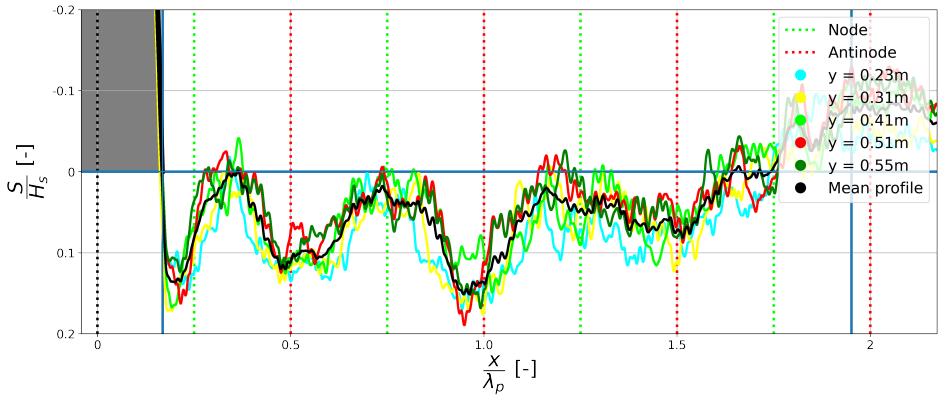

Figure 4.1: Example of individual filtered cross sections of single scans after 8 hours of testing and mean of filtered sections, for test Per_D17_H14_T25_NoToe

The measurement that are done at other time steps are only available for one cross section, therefore they might include larger deviations and possibly measurement errors. Additionally it can be seen in fig. 4.1 that the maximum depth of the produced mean is lower than that of some of the individual cross sections. Therefore the maximum measured depths at other time steps tend to be large compared to the measurements done after 8 hours. This variation between individual measurements and the method used to produce the mean depth after 8 hours is visualised in fig. 4.2.

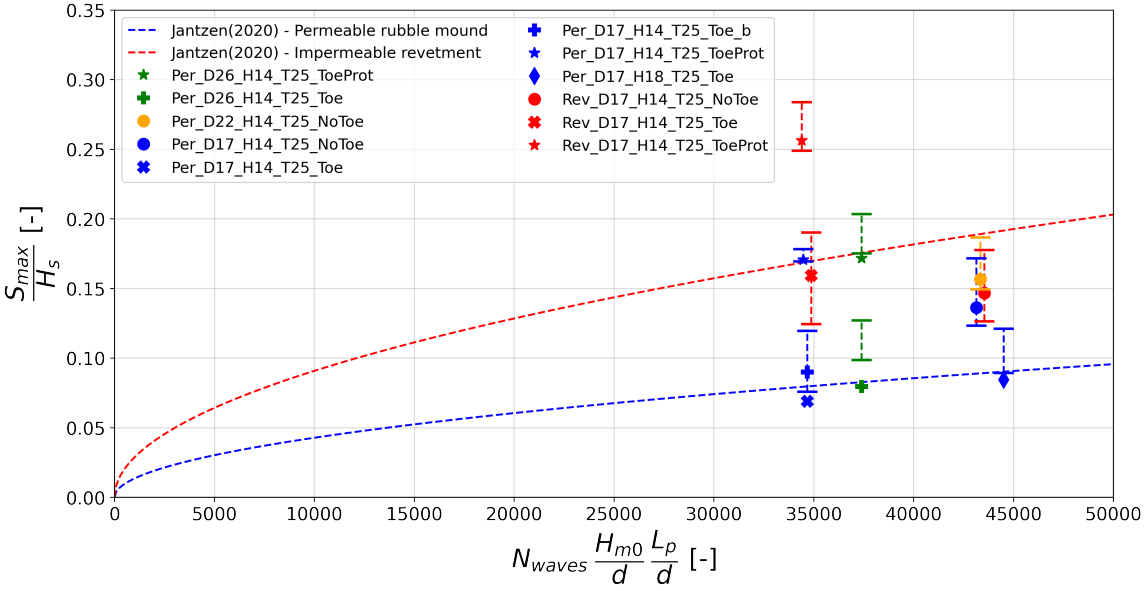

Figure 4.2: Maximum depth scour hole of mean profiles with individual profile range after 8 hours of testing.

In fig. 4.2 it can be seen that for some tests the determined 8 hour mean is within the range of the individual cross sections. For some other tests, mainly the situations with a toe and no scour protection, the determined 8 hour mean is lower than the maximum depth of each individual cross section. This is a results of a variation in size and location of the scour hole over the width of the flume.
In general, after 8 hours of testing, the individual cross section measurements vary with 0.05 - 0.10 $\frac{S_{max}}{H_s}$. It is assumed that this is also the case for the measurements done at other time steps. Since for these time steps only one cross section is measured instead of 5 cross sections, as is done after 8 hours, and no mean can be determined the maximum depth at these steps can vary a lot between each step. As a result for some measurements the depth seems to decrease after an increase in testing time. Since for every test measurements are done after at least 1, 2, 4 and 8 hours of testing the trend of the scour development over time will still be distinguishable. This development over time is further analysed in section 5.5.

4.1.2 Scour in front of the coastal structure

The measured bed profiles are further processed to find the location of the largest scour compared to the structure. For this the scour in front of the structure is analysed in two ways. The results of these analysis are given in table 4.1. The two methods used are:

1. For scour close to the main sloping structure only the the sand bed up to a distance of 3/8 times the peak wavelength λ_p from the waterline is considered. In this case the waterline is the location were the still water level intersects with the sloping structure. The largest depth of the scour hole, if present, in this area for each test is listed in table 4.1. Here also the location of the deepest point and the distance to the end of the main sloping structure is given for every test. When there is no scour in the considered area, in the case of deposition or presence of bed protection, the total scour is given as zero.

2. Additionally scour over a distance of 2 times the peak wavelength λ_p from the waterline is considered. This area includes the main part of the used sand pit for all wave conditions. Table 4.1 contains the maximum depth of the profile in this area, the location of this point and the corresponding distance to the end of the main structure.

Table 4.1: Maximum scour depth and locations for all tests, after 8 hours of waves

	Over first $3/8\lambda_p$ from waterline			Over first $2\lambda_p$ from waterline			
Test name	**$S_{max}/H_{s,i}$ [-]**	**Location [-]**	**Distance [-]**	**$S_{max}/H_{s,i}$ [-]**	**Location [-]**	**Distance [-]**	**Observation**
Per_D22_H14_T25_NoToe	0.16	$0.19\lambda_p$	$0.02\lambda_p$	0.16	$0.19\lambda_p$	$0.02\lambda_p$	Same location
Per_D22_H14_T25_Toe	0.13	$0.23\lambda_p$	$0.06\lambda_p$	0.13	$0.23\lambda_p$	$0.06\lambda_p$	Same location
Per_D22_H14_T16_NoToe	0	-	-	0.04	$1.11\lambda_p$	$0.83\lambda_p$	Deposition at structure
Per_D22_H14_T16_Toe	0	-	-	0.05	$0.88\lambda_p$	$0.60\lambda_p$	Deposition at structure
Per_D22_H14_T16_ToeProt	0	-	-	0.05	$1.31\lambda_p$	$1.03\lambda_p$	Deposition at structure
Per_D17_H14_T25_NoToe	0.14	$0.20\lambda_p$	$0.03\lambda_p$	0.15	$0.96\lambda_p$	$0.79\lambda_p$	
Per_D17_H14_T25_Toe	0.07	$0.29\lambda_p$	$0.12\lambda_p$	0.12	$0.90\lambda_p$	$0.73\lambda_p$	
Per_D17_H14_T25_Toe_b	0.09	$0.26\lambda_p$	$0.09\lambda_p$	0.11	$0.94\lambda_p$	$0.77\lambda_p$	
Per_D17_H14_T25_ToeProt	0	-	-	0.17	$0.41\lambda_p$	$0.24\lambda_p$	Bed protection ends at $3/8\lambda_p$
Per_D17_H14_T16_NoToe	0	-	-	0.06	$1.31\lambda_p$	$1.03\lambda_p$	Deposition at structure
Per_D17_H14_T16_Toe	0	-	-	0.08	$1.42\lambda_p$	$1.14\lambda_p$	Deposition at structure
Per_D17_H14_T16_ToeProt	0	-	-	0.06	$1.95\lambda_p$	$1.67\lambda_p$	Deposition at structure
Per_D17_H14_T21_NoToe	0.01	$0.23\lambda_p$	$0.03\lambda_p$	0.09	$0.94\lambda_p$	$0.74\lambda_p$	
Per_D17_H14_T19_NoToe	0	-	-	0.11	$0.95\lambda_p$	$0.72\lambda_p$	Deposition at structure
Per_D17_H14_T21_Toe	0.03	$0.375\lambda_p$	$0.17\lambda_p$	0.15	$0.48\lambda_p$	$0.27\lambda_p$	
Per_D17_H18_T25_Toe	0.08	$0.28\lambda_p$	$0.11\lambda_p$	0.13	$0.93\lambda_p$	$0.76\lambda_p$	
Per_D17_H14_T25_ToeProt*	0.15	$0.35\lambda_p$	$0.18\lambda_p$	0.21	$0.92\lambda_p$	$0.75\lambda_p$	Bed protection ends at $3/10\lambda_p$
Rev_D17_H14_T25_NoToe	0.15	$0.20\lambda_p$	$0.03\lambda_p$	0.18	$0.52\lambda_p$	$0.35\lambda_p$	
Rev_D17_H14_T25_Toe	0.16	$0.26\lambda_p$	$0.09\lambda_p$	0.17	$0.49\lambda_p$	$0.32\lambda_p$	
Rev_D17_H14_T25_ToeProt	0	-	-	0.26	$0.45\lambda_p$	$0.28\lambda_p$	Bed protection ends at $3/8\lambda_p$
Rev_D17_H14_T16_NoToe	0	-	-	0.08	$0.46\lambda_p$	$0.18\lambda_p$	Deposition at structure
Rev_D17_H14_T16_Toe	0	-	-	0.06	$0.93\lambda_p$	$0.65\lambda_p$	Deposition at structure
Rev_D17_H14_T16_ToeProt	0	-	-	0.07	$1.47\lambda_p$	$1.19\lambda_p$	Deposition at structure
Im_D26_H14_T16_NoToe	0	-	-	0.11	$0.45\lambda_p$	$0.28\lambda_p$	Deposition at structure
Im_D26_H14_T25_NoToe	0.50	$0.20\lambda_p$	$0.03\lambda_p$	0.50	$0.20\lambda_p$	$0.03\lambda_p$	Same location
Im_D26_H14_T25_Toe	0.39	$0.27\lambda_p$	$0.10\lambda_p$	0.46	$0.50\lambda_p$	$0.33\lambda_p$	
Im_D26_H14_T25_ToeProt	0	-	-	0.47	$0.46\lambda_p$	$0.29\lambda_p$	Bed protection ends at $3/8\lambda_p$
Im_D26_H14_T16_Toe	0	-	-	0.09	$0.42\lambda_p$	$0.25\lambda_p$	Deposition at structure
Per_D26_H14_T25_NoToe	0.21	$0.19\lambda_p$	$0.02\lambda_p$	0.21	$0.19\lambda_p$	$0.02\lambda_p$	Same location
Per_D26_H14_T25_Toe	0.07	$0.24\lambda_p$	$0.07\lambda_p$	0.16	$1.47\lambda_p$	$1.30\lambda_p$	
Per_D26_H18_T25_Toe	0.13	$0.26\lambda_p$	$0.09\lambda_p$	0.13	$0.26\lambda_p$	$0.09\lambda_p$	Same location
Per_D26_H14_T25_ToeProt	0	-	-	0.17	$0.47\lambda_p$	$0.30\lambda_p$	Bed protection ends at $3/8\lambda_p$
Per_D26_H14_T25_Toe	0.08	$0.25\lambda_p$	$0.08\lambda_p$	0.12	$1.00\lambda_p$	$0.83\lambda_p$	

In addition, table 4.1 contains for every test that is analysed with this method some observations. For some tests both methods return the same maximum scour hole. Also, for some tests there was no scour in the area considered close to the structure. For these tests it listed that there was deposition instead of erosion in front of the main structure. In other tests the area was covered by the bed protection and no scour hole formed.

For further analysing the results of this study a division is made between the first scour hole, in the $3/8\lambda$ area, which is mainly influenced by the structure and the deepest scour hole over the length of the sand pit, in the 2λ area, which is mainly influenced by the standing wave pattern. These processes are further described and analysed in section 5.1.

4.1.3 Permeable rubble mound breakwater

Most of the tests are done with the permeable rubble mound breakwater as described in section 3.2.1. For this structure long waves and short waves are tested, exact wave conditions for each test are given in appendix B. For the long waves (T_p = 2.5 s) the wave reflection of the structure is about 35 %, for the short waves (T_p = 1.6 s) this reflection is about 25 %. Additionally extra wave conditions were tested to check the influence of the wavelength, wave steepness, wave height and bottom protection on scour development. Test were done using two types of bed material. These were "coarse" sand with a size of D_{50} = 220 μm and "fine" sand with a size of D_{50} = 170 μm.

The resulting depth of the scour hole in the area in front of the permeable breakwater is given in table 4.1. The bed profile for each test after 8 hours of waves is given in appendix C.1. Figure 4.3 shows the bed profile of one of these tests.

From table 4.1 it is clear that the non-dimensional scouring depth $\frac{S_{max}}{H_s}$ is largest for waves with a high peak wave period and wave reflection. For the tests with low periods and wave reflections there is no scour directly in front of the structure. Further analysis including the influence of these parameters and how they interact is done in section 5.

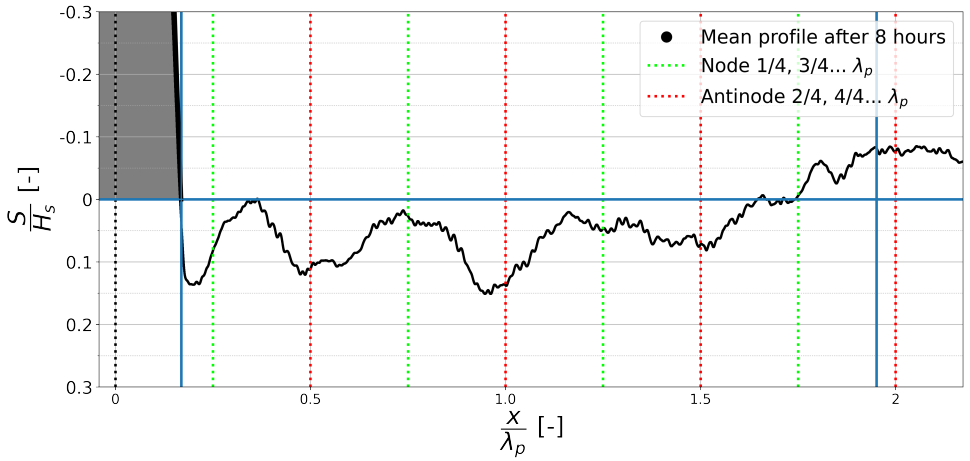

Figure 4.3: Bed profile of test Per_D17_H14_T25_NoToe.

4.1.4 Impermeable rubble mound revetment

In addition to the tests with the permeable rubble mound breakwater tests were done with an impermeable rubble mound revetment. For this structure the same variations were tested as for the Permeable breakwater. The main purpose of testing with this structure is determining the influence of the wave reflection on the scour development. For the revetment structure the wave reflection for long waves (T_p = 2.5 s) is about 51 %, for the short waves (T_p = 1.6 s) the reflection is about 33 %. All test for this structure have been done using the "fine" sand with a size of D_{50} = 170 μm. The resulting depth of the scour hole for all tests done with the revetment is given in table 4.1. The individual bed profiles can be found in appendix C.2.

For the revetment, as for the permeable breakwater, the non-dimensional scour depth is largest for high wave periods and wave reflections. Compared to the permeable breakwater the tests with a low wave period show similar behaviour in front of the structure. This behaviour and the influence of the reflection will be further discussed in section 5.

4.2 Photo measurements

Besides the bed profile measurements with the laser sensors cameras were used for interval capturing of the bed profile development. Two cameras are placed alongside the flume that photograph the side of the flume every 30 minutes. Together the cameras capture the first 3.0 m in front of the structure. For each picture the deepest point in front of the structure is selected manually and is compared to a reference point. As a result the development of the maximum scour depth in front of the structure can be tracked.
The deepest point that is selected from this side view includes the ripple pattern that is described in section 4.1. These ripples have heights that are in the same order as the scour depth in the model, as a result this influences the maximum scour depth that is measured using this method. The ripples cannot be correctly scaled to prototype situation. Therefore, the photo measurements will only be used for investigating the bed profile development over time.

As found for the laser measurements the tests that are done with the short wave period show accretion of sediment in front of the structure instead of scour. The results of the tests with the short waves are therefore separated from the tests where scour is observed.

4.2.1 Photo measurements scour

The photo measurements of the tests are separated into three cases, being the permeable breakwater tests, the revetment tests and the impermeable smooth slope tests. In fig. 4.4 the analysis of the permeable structure and the revetment are given. Here it can be seen that after a development in the first hours the maximum scour depth becomes somewhat constant for both cases. For the permeable structure most of the development seems to halt after about 2 to 4 hours of testing. For the revetment significant development seems to stop after about 4 hours of testing. For both cases tests where a larger scouring depth is observed take longer to reach this constant state than tests with a smaller scouring depth.

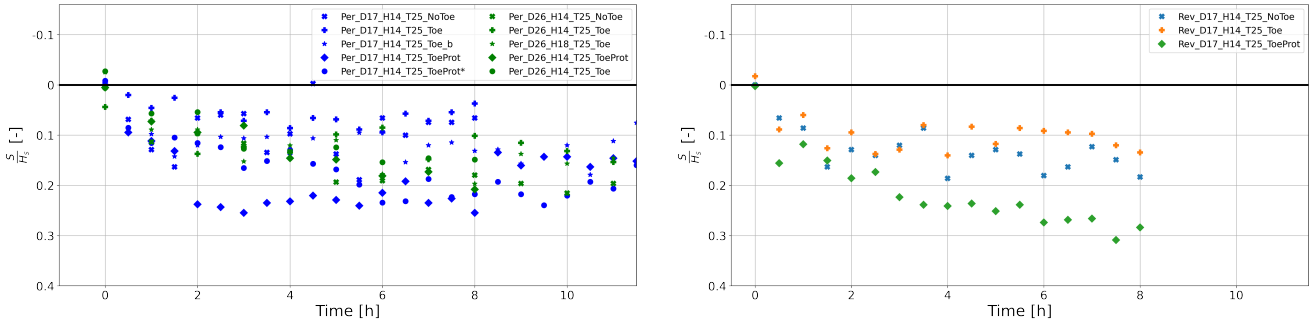

(a) Permeable breakwater.

(b) Revetment.

Figure 4.4: Development maximum depth.

For the impermeable smooth structure larger scouring depths are observed. As for the two other structures cases with a larger maximum scour depth take longer to develop towards this maximum scouring depth. The development is given in fig. 4.5 for the impermeable smooth structure. The development of the maximum depth of the scour hole for this structure does not seem to reach a somewhat constant state, as the other structures, but keeps becoming larger. This effect is witnessed for more tests and is further described in section 5.5, here it is linked to a constant loss of sediment that is observed for all tests with long waves. It is concluded that the scour-deposition pattern reaches a situation close to an equilibrium situation while this steady sinking of the complete bed profile continues. Therefore the development of the maximum scour depth linked to the scour-deposition pattern does no longer significantly increase after about 8 hours of testing for the impermeable smooth slope. The constant increase in maximum depth that is observed after this is expected to be completely caused by the constant loss of sediment.

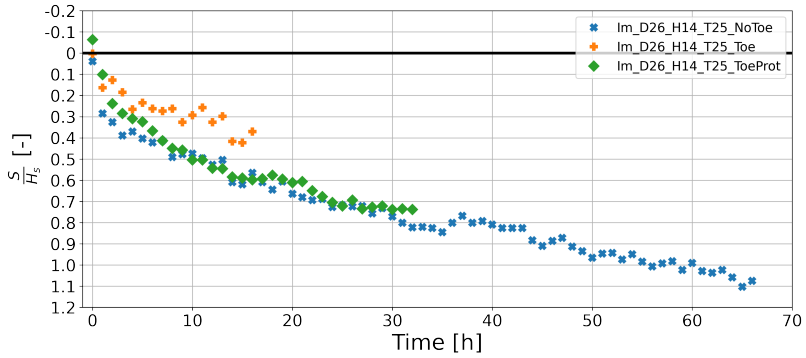

Figure 4.5: Development maximum depth, for impermeable smooth structure (tests from Jantzen (2020)).

For all three structures different timescales are found for reaching a constant maximum scour depth. For each structure the associated timescale is given in table 4.2. It is found that for an increase in reflection coefficient and maximum scour depth the time required to reach this maximum depth increases. This is in line with findings from Sumer and Fredsøe (2000), where an increase in timescale was found for cases with larger scouring depths.

The timescales found here will be included in section 4.3 where the development of the bed profile over time is further studied by including the results from the laser measurements.

Table 4.2: Resulting timescales scour development for tested structures

Structure	**Average K_r [-]**	**Timescale [HR]**	**Number of waves [-]**
Permeable breakwater	0.36	2 - 4	3000 - 6000
Revetment	0.51	2 - 4	3000 - 6000
Impermeable smooth slope	0.79	4 - 8	6000 - 12000

4.2.2 Photo measurements accretion

For all tests with the short waves with a peak wave period of 1.6 seconds accretion is found at the the toe of the structure. No significant differences are observed between the three tested structures. In fig. 4.6 the development of the accretion can be seen for every test with these short waves. Development seems to follow a linear trend, which is added, in the first 8 hours. This trend is not influenced by the type of structure and the associated wave reflection coefficient. Also the sediment particle size seems to have no influence on the development. It is therefore concluded that main mechanism resulting in accretion in front of the structure are the wave conditions. For these shorter waves it seems that an onshore directed mean transport of sediment is present. This transport seems to be offshore directed for the tests with the long waves.

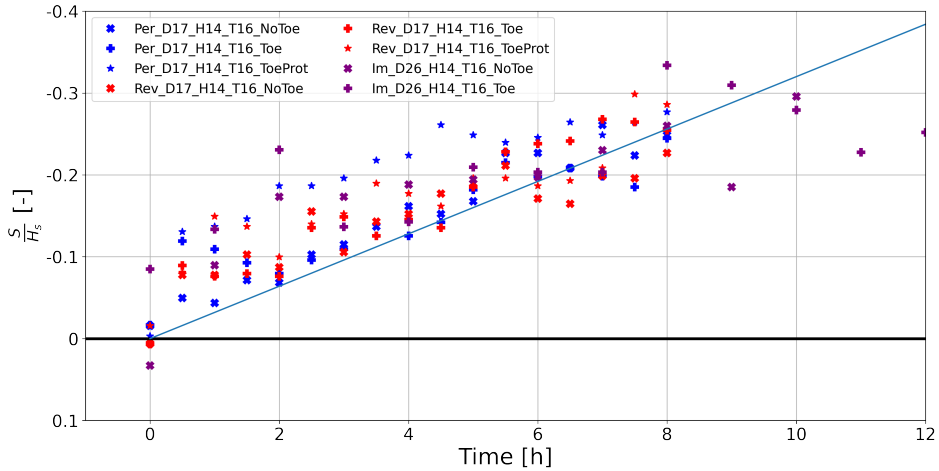

Figure 4.6: Development accretion in front of structures for short wave tests.

4.3 Development over time from laser and photo measurements

The number of waves that is needed to reach a state where the maximum scour depth no longer shows a substantial increase varies between the tested structures, this value will be called N_s. In the present study and that of Sumer and Fredsøe (2000) it is found that for cases with a larger maximum scour depth a longer time period and more waves are needed to reach this state. The time it takes to reach this somewhat constant state is listed for each of the tested structures in table 4.3. The values here are based on the tests with long waves (T_p = 2.5s) for which the largest maximum scour is present. This increase in number of waves seems related to an increase in the wave reflection coefficient K_r for these structures. The approximate number of waves needed to reach this constant state for each structure is found to be:

Permeable rubble mound structure, N = ±4500
Impermeable revetment, N = ±6000
Impermeable smooth slope, N = ±9000

Table 4.3: Resulting timescales after which maximum scour depth no longer shows substantial increase, based on photo and laser measurements

		Photo measurements		Laser measurements	
Structure	**Average K_r [-]**	**Timescale [hour]**	**Number of waves [-]**	**Timescale [hour]**	**Number of waves [-]**
Permeable rubble mound	0.36	2 - 4	3000 - 6000	2 - 4	3000 - 6000
Impermeable revetment	0.51	2 - 4	3000 - 6000	4	6000
Impermeable smooth slope	0.79	4 - 8	6000 - 12000	4 - 8	6000 - 12000

Development of the maximum scour depth from the laser and photo measurements is given in fig. 4.7. Here it can be seen that results from both types of measurements show the same trend. Also, measured maximum scour depth values are similar. An increase in wave reflection shows an increase in time for which a substantial amount of scour occurs for both types of measurements.

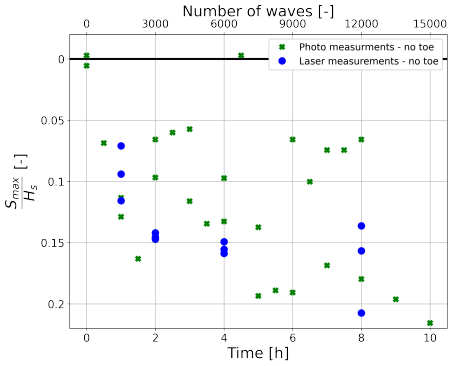

(a) Permeable breakwater with no toe.

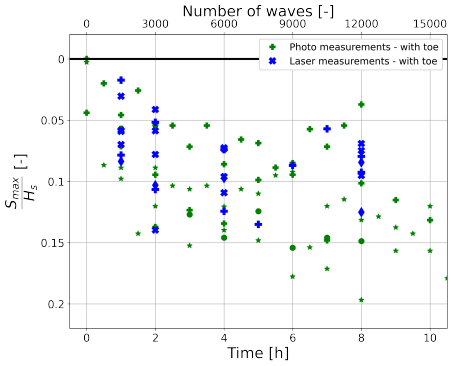

(b) Permeable breakwater with toe.

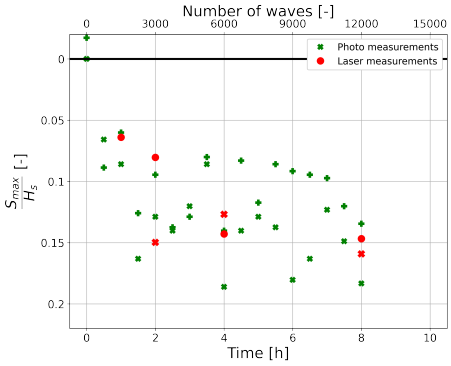

(c) Impermeable rubble revetment.

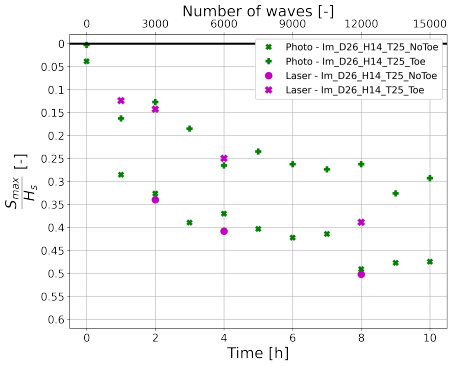

(d) Impermeable smooth slope.

Figure 4.7: Development maximum scour depth in first hours of testing for long waves, from photo and laser measurements.

4.4 Flow measurements

For several test flow velocities are measured using EMS. Measurements are done for both a peak wave period of 1.6 and 2.5 seconds as it is expected that these will show different flow patterns. Additionally, for both the permeable breakwater and the impermeable revetment velocities for these wave conditions are measured to investigate the influence of the structure and the amount of wave reflection. Measurements are done for the following tests, in addition measurements done for three tests series by Jantzen (2020) are also analysed.

- Per_D17_H14_T16_ToeProt
- Rev_D17_H14_T25_Toe
- Rev_D17_H14_T16_NoToe
- Per_D17_H14_T25_Toe_b
- Per_D26_H14_T25_NoToe
- Im_D26_H14_T16_Toe
- Im_D26_H14_T25_ToeProt

For the first three tests the velocity measurements are done at 0.10 meter above the initial bed level. Beginning at the structure measurements are done every 1.5 meters in offshore direction over the whole length of the sand pit. For the fourth test more elaborate measurements are done. For this test the velocities are measured at every position at 0.10, 0.20, and 0.30 meter above the initial bed level. Additionally measurements are done every 0.50 meter in offshore direction, again covering the whole length of the sand pit. For all tests in the present study an additional measurement has been done above the toe structure, at 0.20 meter above initial bed level. Measurements at each location were done for about 5 minutes.
Figure 4.8 shows the velocity over time and the mean flow velocity for one of these test. In this figure positive values mean that flow is away from the structure. It can be clearly observed in this figure that there is oscillatory flow of which the magnitude varies for irregular waves.

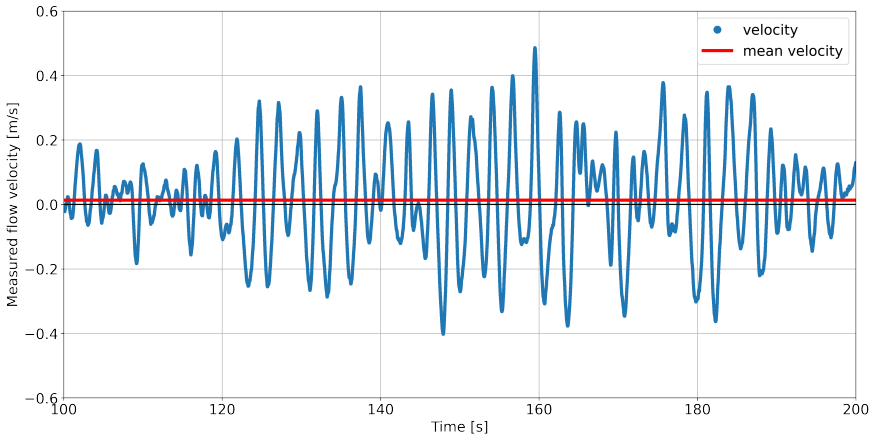

Figure 4.8: Flow velocity 0.10m above bed, 3.5m in front of structure, for test Rev_D17_H14_T25_Toe.

For all measurements the velocities at multiple significant locations are reported in table 4.4. Here the 2%-exceedance value of the absolute velocity is used to indicate maximum flow velocities that are regularly present. This value is given for the fist anti-node in front of the structure at $1/2\lambda$ from the waterline, the second node in front of the structure at $3/4\lambda$ from the waterline and above the toe structure. Measurements are done at 0.10 meter above the initial sand bed level. For the toe structure measurements are done 0.20 meter above the initial sand bed level. For some tests measurements are not available at every location.
As expected for a standing wave pattern, flow velocities are lowest at the node while they are largest at the anti-node. The velocity at the toe is significantly larger than the velocities in front of the structure. Velocities are also found to be larger for an increase in wave reflection.

Table 4.4: Measured flow velocities at 0.10 m above bed

Test	T_p [s]	u_{mean} [m/s]	Direction	$u_{2\%}$ at 1/2λ [m/s]	$u_{2\%}$ at 3/4λ [m/s]	$u_{2\%,toe}$ [m/s]
Per_D17_H14_T16_ToeProt	1.6	-0.01	Onshore	-	0.26	0.34
Per_D26_H14_T25_NoToe	2.5	-0.01	Onshore	0.26	0.31	0.36
Per_D17_H14_T25_Toe_b	2.5	0.03	Offshore	0.25	0.33	0.45
Rev_D17_H14_T16_NoToe	1.6	0.01	Offshore	-	0.24	0.31
Rev_D17_H14_T25_Toe	2.5	0.01	Offshore	0.26	0.36	0.58
Im_D26_H14_T16_Toe	1.6	0.01	Offshore	0.28	0.33	-
Im_D26_H14_T25_ToeProt	2.5	0.02	Offshore	0.30	0.40	

More results of the flow measurements at all three locations can be found in appendix D. Here for each location the maximum onshore and offshore velocity that was measured over a period of 5 minutes is given. Additionally the 2%-exceedance value for both the onshore and offshore directed velocity is given in addition to the 2%-exceedance value of the absolute velocity.
For the permeable structure it is observed that at every location (including the toe) for tests with the long waves (T_p = 2.5 s) maximum offshore directed velocities are larger than the onshore directed velocities. This is not the case for the short waves (T_p = 1.6 s) where maximum onshore directed velocities are found to be slightly larger than offshore directed velocities. This pattern is less clear for structures with an increase in wave reflection coefficient.

The measured flow velocities for each location are further analysed in section 5. Here the measurements are included in analysing the influence of the wave conditions and are linked to the sediment transport and the sediment transport direction.

5 Analysis

This chapter presents the analysis of the test results from section 4. The main focus of the analysis is to come to a good understanding and estimation of the wave-induced scour in front of the sloping coastal structure. The analysis starts with with the individual effects of the separate parameters. At the end of the chapter the combined effect is described by a dedicated design formula. The analysis comprises the following steps:

Step 1: What is the effect of the differnent wave characteristics on the scour-deposition pattern? (Section 5.1)

Step 2: What is the effect of the length of the bed protection on the scour-deposition pattern? (Section 5.2)

Step 3: What is the effect of the sediment suspension mode and the transport direction on the scour-deposition pattern? (Section 5.3)

Step 4: What is the effect of the sand grain diameter on the scour-deposition pattern? (Section 5.4)

Step 5: What is the combined effect of all parameters on the development of the scour-deposition pattern over time? (Section 5.5)

Step 6: Present the dedicated design formula and describes its performance for the test results of the present study. (section 5.6)

Step 7: Provides a comparison between the results from this study and other design methods. (Section 5.7)

5.1 Influence waves on scour-deposition pattern

In this section the influence of the hydraulic parameters on the scour-deposition pattern is analysed. First the influence of the water depth is discussed in section 5.1.1. Secondly the wave steepness is discussed in section 5.1.2. Then the wave reflection and the steady streaming induced by standing waves is discussed in section 5.1.3 and section 5.1.4. In the last section, section 5.1.5, the influence of the downrush flow on the presence of scour at the foot of the structure is discussed.
The hydraulic parameters that are analysed here influence the orbital velocities near the bed that lead to initiation of motion and transport of sediment particles. The main parameters that influence the orbital velocity near the bottom are:

- The water depth
- The wave height
- The wave period
- The shape of waves

The relation between these parameters and the bottom orbital velocity, eq. (5.1), and the resulting bottom shear stress, eq. (5.2), for linear, regular waves are given below. Also, a relation for the bottom friction is given in eq. (5.3). These equations are based on linear wave theory where it is assumed that the waves have a sinusoidal shape.

$$\hat{u_b} = \frac{\omega a}{\sinh 2\pi \frac{h}{L}} \tag{5.1}$$

$$\tau_b = \frac{1}{2}\rho C_f \hat{u_b^2} \tag{5.2}$$

$$C_f = 0.237\left(\frac{a_b}{k_r}\right)^{-0.52} \quad \text{for } a_b > 0.636k_r \tag{5.3}$$

5.1.1 Relative water depth

The relative water depth h/λ is an important parameter that expresses the interaction between the waves and the bed. Where h is the water depth and λ the local (peak) wavelength. The relative water depth determines the magnitude of the orbital velocity close to the bed compared to the velocity at water level.

From literature it is clear that the bottom velocity u_b reduces for increasing water depth h/λ, and as a result the shear stress τ on the bed will reduce as well. Taking into account that the shear stress on the bed, eq. (5.2), uses the velocity squared a change in bottom velocity has a large influence on the amount of shear stress acting on the

sediment particles of the bed.
Therefore less scour and deposition is expected for an increase in water depth. For the relative water depth this means that for an increase in water depth or a decrease in wave length (through a decrease in wave period) the magnitude of the scour-deposition caused by wave-induced velocities decreases.

Xie (1981) indeed found that the relative water depth has a large influence on the depth of the scour hole. With his vertical wall tests Xie found that for shallow water (h/λ = 0.05 - 0.10) the depth of the scour hole is approximately equal to the wave height. For larger relative water depths the maximum depth of the scour hole decrease rapidly. For values of about 0.15 h/λ Xie found the depth to be in the order of 0.4 times the wave height.

The relative water depths for the wave conditions that are tested in this study and in Jantzen (2020) are given in table 5.1. Here the peak wave period is used to calculate the local peak wavelength, λ_p. It also contains the bottom orbital velocity calculated using eq. (5.1). In both studies tests are done with irregular waves. The conclusions from Xie (1981) on the influence of the relative water depth are based on regular waves.
The maximum relative scour depth for the tests with the permeable breakwater have been added in this table. The value presented here is the average value of the relative scour dept of the tests done for the given conditions. This table also contains the scour depth for the vertical wall tests by Xie. These values are calculated using eq. (5.4), which is a relation between the maximum scour depth and the relative water depth for fine sediment, developed in Xie (1981). The results from this study follow the same increasing trend as found with the approach by Xie, albeit lower. It is therefore expected that the functional form of eq. (5.4) is a proper indication of the influence of the relative water depth.

$$\frac{S}{H_s} = \frac{0.3}{\left(\sinh 2\pi \frac{h}{\lambda_p}\right)^{1.35}} \tag{5.4}$$

The relation between the maximum scour depth over the first 2λ in front of the structure and the relative water depth is given for each test in fig. 5.1. Here it can be seen that relative water depth has indeed a large influence on the maximum scour depth. For an increase in relative water depth the maximum depth of the scour hole decreases. This is in line with the findings by Xie (1981) described above.
In the figure it can also be seen that the type of slope influences the maximum scour. On the influence of the structure and the associated parameters is commented in section 5.1.3 to section 5.1.5. The variation in grain size of the sediment for the tests with the permeable breakwater shows no significant changes in this figure. This influence of the size of the sediment is further discussed in section 5.4.

Table 5.1: Influence relative water depth for tested wave conditions

T_p [s]	h [m]	λ_p [m]	h/λ_p [-]	u_b [m/s]	S_{max}/H_s [-], from Xie (1981)	Average $S_{max}/H_{s,i}$ permeable breakwater[-]
1.6	0.4	2.84	0.141	0.24	0.30	0.07
1.9	0.4	3.48	0.115	0.27	0.41	-
2.1	0.4	3.91	0.102	0.29	0.50	0.12
2.5	0.4	4.74	0.084	0.31	0.66	0.15

It can be concluded that the relative water depth is an important parameter that heavily influences the magnitude of the scour deposition pattern. Especially for cases where the relative water depth is large a large reduction in maximum scour can be expected compared to cases with a smaller relative water depth. Therefore this parameter should be included in formula that predicts the maximum scour, as is done in the formulas by Xie (1981), Sumer and Fredsøe (2000) and Jantzen (2020). The performance of these formulas at including this influence is discussed in section 5.7.

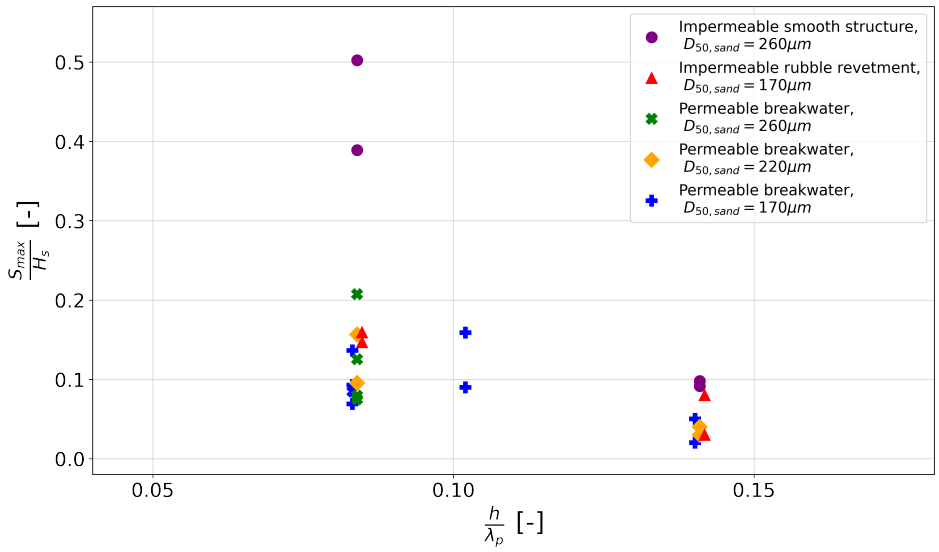

Figure 5.1: Influence relative water depth on maximum scour depth after 8 hours of testing.

5.1.2 Wave steepness

One of the main parameters that has been varied in the model tests is the peak wave period T_p. Most tests have been done with a wave period of 1.6 or 2.5 seconds. Additionally one test has been done with a period of 1.9 seconds and two tests have been done with a wave period of 2.1 seconds. As the wave height is kept constant for every test, changes in wave period will result in a change in wave steepness. A result is that, waves with a low peak wave period are steeper than waves with a high peak wave period. We consider the wave steepness for waves in the "shallow" part close to the structure.

It is noticed that for test with larger wave periods and thus a smaller wave steepness the magnitude of the scour and deposition is largest. This magnitude decreases with a decrease in wave period and an increase in wave steepness. Beside this, the relative water depth also changes with variations in wave period. This makes it difficult to individually consider the influence of the relative water depth and the wave steepness. The effect of the water depth on the bottom orbital velocity is described in the previous section. The water depth only influences the magnitude of the bottom orbital velocity. For an increase in relative water depth the orbital velocities at the bottom decrease. This does however not influence the standing wave pattern. As a result, the location of the nodes and anti-nodes do not change and scour and deposition is still expected at the same locations, albeit lower in magnitude. Therefore, changes in the location of scour and deposition for variations in wave period are expected to be a result of the change in wave steepness and not the change in relative water depth.

At some point when the wave period decreases and the wave steepness increases the scour-deposition pattern changes from scour in front of the structure to deposition in front of the structure. In table 4.1 it is noted for which tests deposition was found in front of the structure after 8 hours of testing. An overview of the results of the variations in wave steepness can be seen in table 5.2. Here both the offshore "deep" water wave steepness $s_{o,p}$ and the nearshore "shallow" water wave steepness $s_{n,p}$ are given. For both cases the wave steepness is calculated with the peak local wavelength. The offshore wave steepness has not been influenced by the bottom and is dependent on the conditions that are created by the wave maker. The nearshore wave steepness has been influenced by the bottom as the waves propagate over a slope before reaching the flat bed area in front of the structure. In this analysis mainly the offshore wave steepness will be used as these effects of the bottom are not included here. This will allow for comparison of the results with cases where only the offshore wave characteristics are known.
In this table also the ratio of horizontal distance from waterline to toe, $W_{p,t}$, to wavelength, λ_p, is given. For the tests where deposition was found at the toe of the structure this toe is close to the first node of the standing wave pattern. When only considering the influence of the standing wave pattern there is deposition at a node. The influence of the structural end in combination with the flow from the surface of the structure is further investigated in section 5.2.

Table 5.2: Expected influence wave steepness, tests with no toe and bed protection

$s_{o,p}$ [%]	$s_{n,p}$ [%]	Tp [s]	$H_{s,i}$ [cm]	Kr [%]	λ_p [m]	$W_{p,t}$ / λ_p [-]	$S_{max}/H_{s,i}$ [-]	Pattern in front of structure
1.4	2.7	2.5	12.7	37	4.74	0.17	0.14	Erosion
1.8	3.2	2.1	12.6	32	3.91	0.20	0.07	Combination
2.2	3.6	1.9	12.4	28	3.48	0.23	0	Deposition
3.4	4.1	1.6	11.7	26	2.84	0.28	0	Deposition

In fig. 5.2 the bed profiles of the tests described in table 5.2 are given. Here it can be seen that for an increase in wave steepness there is more deposition in front of the structure. Also, the tests with an offshore wave steepness of 1.4% and 1.8% show the same scour-deposition pattern, which can be linked to the standing wave pattern caused by reflection of waves. The profile for the offshore wave steepness of 2.2% shows a similar pattern from a distance of about 0.4λ away from the waterline. The profile for the offshore wave steepness of 3.4% does not seem to follow this standing wave pattern, as wave reflection here is low. For the test with a wave steepness of 2.2% only a measurement after 16 hours is available, which has been included here, due to a mistake in test set-up.
The profiles showing this standing wave pattern do show differences if compared to the initial bed level. For the waves with an offshore wave steepness of 1.4% the mean level of the profile is lowered compared to the initial profile. For the steeper waves this mean level only shows small changes compared to the initial bed level. A possible explanation of this is that the wave steepness influences the direction and magnitude of a large scale morphological change that is observed over the whole length of the sand pit.

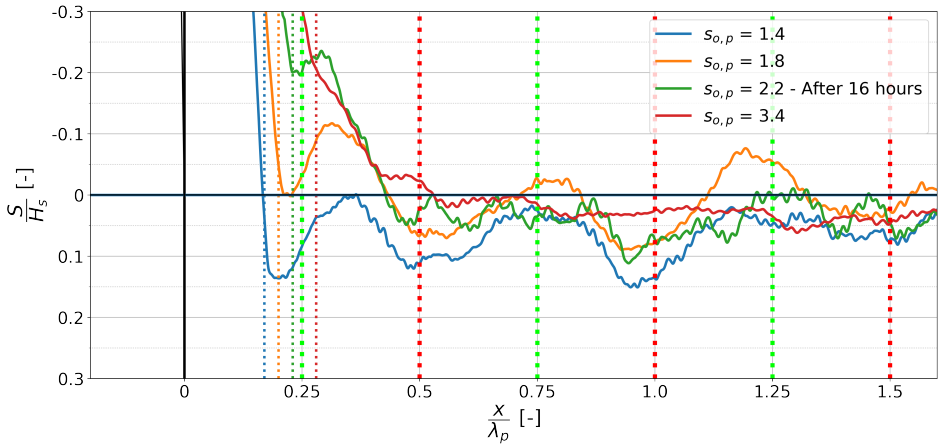

Figure 5.2: Scour pattern in front of permeable breakwater for a variation in wave steepness.

All cases of sediment deposition in front of the structure are for a wave period of 1.6 or 1.9 seconds and an offshore wave steepness of 3.4% or 2.2%. As the 1.9 seconds period has only been tested once and contains only a measurement after 16 hours, in the next part only the condition with a period of 1.6 seconds ($s_{o,p}$ = 3.4%) is considered. This period is tested for all three types of structure and shows deposition at the toe for every layout. There are however noticeable differences in the total bed profile between the results for the permeable breakwater and the revetment. For both structures deposition is observed directly at the foot of the structure. In the case of the revetment scour is observed at the first anti-node in front of the structure. This pattern was also observed in the tests by Jantzen (2020) where the same wave conditions were used for an impermeable smooth structure. For the permeable breakwater this is not the case, there is deposition at the first anti-node. It is therefore expected that not only the relative water depth and wave steepness but also the wave reflection and flow from the surface of the structure influence the presence of scour or deposition in front of the structure.
Besides this it was found that the amount of material deposited in front of the structure keeps increasing over time while the pattern more offshore, linked to the standing waves, does not significantly change after some time for both the permeable breakwater and the revetment. This pattern is also observed for the impermeable smooth structure where very long testing times were used.

Based on these observations it is expected that the scour-deposition pattern influenced by the standing waves does no longer change significantly after some time while the influence of the wave steepness and the associated bed changes stay present. Two main processes are present that both have their own characteristics and timescales.

These processes are:

- The standing wave pattern, dependent on the wave reflection
- The large-scale morphological changes, dependent on the wave characteristics such as the wave steepness

The influence of the standing wave pattern and the associated wave reflection is further analysed in section 5.1.3 and section 5.1.4. The timescale associated with both processes is further analysed in section 5.5.

The influence of the wave steepness on the scour deposition pattern and the maximum scour is significant. Especially close to the structure large differences are observed for variations in wave steepness. For some value of the offshore wave steepness scour is no longer observed directly at the foot of the structure. In the cases that have been studied here the pattern shows a clear change from scour to deposition in front of the structure for an offshore wave steepness that is larger than 2.0%. It is expected that this value changes for structures with different slope angles. The driving mechanism behind this influence of the wave steepness is not known.

5.1.3 Wave reflection

Another important parameter that influences the scour in front of coastal structures is the wave reflection. For vertical structures, as used in the study by Xie (1981), all of the wave energy is reflected resulting in an outgoing wave height that is the same as the incoming wave height. As a result of this wave reflection a standing wave pattern forms. At some locations the incoming and outgoing wave counteract each other resulting in a region with lower wave heights and lower near-bed velocities. In other regions the incoming and outgoing wave amplify each other resulting in regions with large wave heights and larger near-bed velocities.

For sloping structures this behaviour is different as part of the wave energy is not reflected by the structure but is absorbed. As a resulted the reflected wave height is lower than the incoming wave height. A standing wave pattern is still present for these cases but becomes less prominent. There are a lot of parameters that determine how much of the wave energy is absorbed by a sloping structure. The main ones are (Zanuttigh and Van der Meer, 2007):

- The breakwater slope α
- The wave steepness s (or the incident wave height and wavelength)
- The roughness of the structure
- The permeability of the structure

All of these parameters, excluding the structure slope, are varied in this study to determine the influence of the wave reflection on scour-deposition pattern. The wave reflection is in the range of 23% - 51% in this study. When including the measurement done by Jantzen (2020), which included an impermeable smooth slope, the range becomes 23% - 81%. Additionally, the results by Xie (1981), for tests with similar wave conditions, can be added. As a vertical wall was used here, the reflection for each test is considered to be 100%. It is important to note that the results from Xie (1981) for the long waves are for regular waves. For each structure tested in the present study and in Xie (1981) and Jantzen (2020) the measured reflection and maximum scour depth is calculated. The results, together with relevant wave and sand parameters, are given in table 5.3.

Table 5.3: Influence wave reflection for structures without toe and bed protection

Type of structure	**Slope [-]**	**$D_{50,Sand}$ [μm]**	**Type of waves**	**T_p [s]**	**$s_{n,p}$ [%]**	**h/λ_p or h/λ [-]**	**Kr [%]**	**$S_{max}/H_{s,i}$ [-]**
Permeable breakwater	1:2.0	170	Irregular	2.5	2.7	0.084	37	0.15
Revetment	1:2.0	170	Irregular	2.5	2.7	0.084	51	0.18
Impermeable slope, from Jantzen (2020)	1:2.0	260	Irregular	2.5	2.7	0.084	81	0.50
Vertical wall, from Xie (1981)	-	106 & 200	**Regular**	2.4	1.8	0.075 - 0.100	100	0.82
Permeable breakwater	1:2.0	170	Irregular	1.6	4.1	0.141	26	0.06
Revetment	1:2.0	170	Irregular	1.6	4.1	0.141	33	0.08
Impermeable slope, from Jantzen (2020)	1:2.0	260	Irregular	1.6	4.1	0.141	63	0.11
Vertical wall, from Xie (1981)	-	106	Irregular	1.7	2.6	0.111 - 0.148	100	0.37

From these results it is clear that, as described by Smith (1996), for an increase in wave reflection the maximum scour increases. This can be observed for both the short and long waves that have been tested in all three studies. For the tested long waves, T_p = 2.5 s, no decrease in maximum scour was observed at the foot of the sloping structures

by Jantzen (2020) and in this study for high wave reflection coefficients, this is in contradiction with findings from Smith (1996) were for high wave reflection values and a slope of 1:2.0 maximum scour slightly decreased. An explanation for this is that for sloping structures the downrush of the structure causes scour directly at the foot of the structure (Sumer and Fredsøe, 2000). The influence of downrush is further discussed in section 5.1.5.

As expected in the case of the vertical wall, with about 100% wave reflection, the largest scour hole forms. On average the depths of the scour hole in these case are however not 1.00 $S/H_{s,i}$, which is often used as a first estimate for scour in front of a vertical wall (Schiereck, 2003). Xie (1981) states that the maximum scour in front of a vertical wall decreases quickly with an increase in relative water depth, as is also found in section 5.1.1. The effect of an increase in relative water depth can also be seen in table 5.3 where for the tests with shorter waves, where this parameter is higher, the maximum scour depth is lower.

The comparison between the studies is further visualised in fig. 5.3, where the measured reflection and maximum scour depth are plotted for each individual test without a bed protection. All the points in this figure are for long waves (T_p = 2.5 seconds) that are tested. In addition some tests done by Xie with regular waves with a wave period of 2.4 seconds are added. In this figure again the trend of an increasing scour depth for an increase in reflection can be seen. In the formula developed in Jantzen (2020) for determining the maximum depth of the scour hole the influence of the reflection is taken to be quadratic. In Schiereck (2003) the erosion is said to be roughly linearly proportional to the reflection coefficient. Both relations are combined with the formula developed by Xie (1981), eq. (5.4) , to include the influence of the relative water depth and have been added in the figure.
The linear relation of Schiereck (2003) seems to overpredict the maximum scour in front of the structure for all cases that do not have a wave reflection of 100%. The quadratic relation proposed by Jantzen (2020) fits better with the observations of this study. For all three structures the measured scour is in line with the quadratic relation. For the structures with a low wave reflection, in this case the permeable breakwater, the accuracy is lower than for higher wave reflection coefficients.

For the shorter waves that are tested (T_p = 1.6 seconds) the maximum scour is significantly lower than for the long waves. This can be contributed to the following factors:

- Larger relative water depth h/λ, as discussed in section 5.1.1
- Larger wave steepness, as discussed in section 5.1.2
- Lower wave reflection

A combination of all of these three factors, which individually all cause less scour, results in a large reduction of the maximum scour depth. The scour closest to the structure is also not directly in front of the structure, as can be seen in table 4.1. Additionally, as described in section 5.1.2 deposition at the foot of the structure is found for most of these cases.

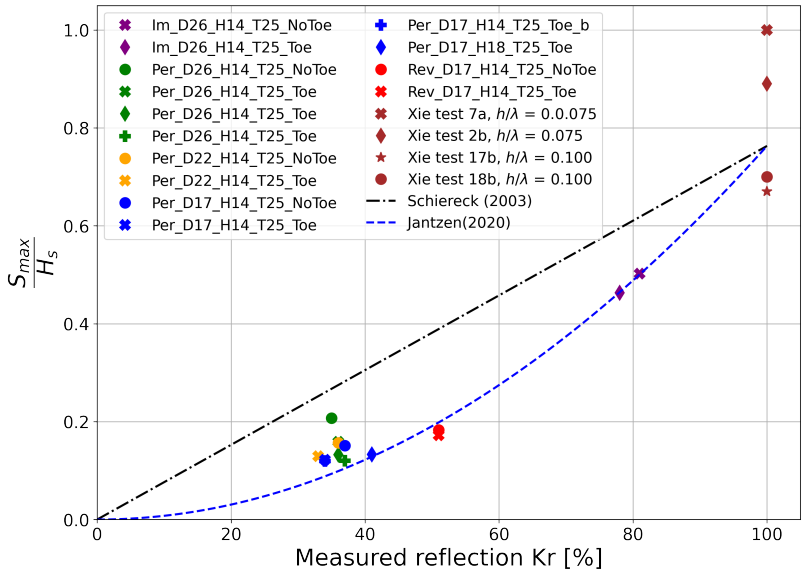

Figure 5.3: Relation between wave reflection and measured maximum scour, for relative water depth h/λ = 0.084.

The amount of wave reflection from a coastal structure plays an important part in the scour-deposition process as the reflection of waves results in the presence of standing waves. It is found here that the influence of the wave reflection coefficient K_r on the maximum scour follows a quadratic relation. By adding this relation in the maximum scour equation developed by Xie (1981) a good fit is found with the results from the tests done in this study. As a result of this relation, for structures with low reflection coefficients significantly less scour can be expected than for structures with high reflection coefficients. Taking into account the parameters that influence the amount of wave reflection while designing coastal structures can greatly reduce the amount of maximum scour.

5.1.4 Steady streaming flow

Sumer and Fredsøe (2000) stated that scour in front of vertical walls and sloping breakwaters is caused by the steady streaming flow that is induced by standing waves. Their research was primarily done with regular waves and bed load transport of sediment and stated that steady streaming flow depends on the following parameters:

- The incident wave height H
- The incident wave period T (or the incident wavelength L)
- The bed roughness characterized by the sand-grain size d
- The water depth h
- The breakwater slope α
- The water density ρ
- The water viscosity μ

The first three of these parameters have also been varied in this study. The other parameters are kept constant for every test. Sumer and Fredsøe (2000) stated that for the same incident wave conditions the scour deposition pattern for a rubble mound breakwater is essentially the same as for a vertical wall. A difference that was observed is that for the anti-node point at the structure no scour occurs at the vertical breakwater while a substantial amount of scour occurs at this location for the rubble mound breakwater. They found no clear explanation for this behaviour. This behaviour is also observed in the present study.

These findings are in line with the results from Gislason et al. (2009a) where besides the standard node - anti-node scour pattern additional scour or deposition was found at the toe of the structure. They linked this toe scour to the porosity of the structure and expect that no scour is present here for impermeable structures while there is scour for permeable structures. This influence of porosity is not in agreement with the results of this study and the study by Jantzen (2020), where not only for the permeable breakwater but also for an impermeable revetment and impermeable smooth slope toe scour was present for the tested long waves. It is therefore expected that the downrush flow from the structure cannot be neglected and plays an important part in the presence of scour directly at the foot of the structure. In the following section this is further discussed.

In appendix E velocities in front of the structure are calculated using the approach developed by Hughes and Fowler (1995). Here horizontal and vertical RMS velocities are calculated for variations in wave reflection. Maximum horizontal and vertical velocities are found to be larger for more reflective structures. Minimum horizontal and vertical velocities are also found to be lowest for more reflective structures.

The steady streaming flow that is induced by standing waves results in a pattern of nodes and anti-nodes where flow velocities vary. For an increase in wave reflection of the structure the flow at the anti-nodes of this pattern increases while at the nodes the flow decreases. For increasing wave reflection coefficients, larger flow is expected at the anti-nodes resulting in a larger maximum scour depth. At the nodes it is expected that an increase in wave reflection leads to more material being deposited here as the flow decreases. The link between flow and the maximum scour depth here is supported by the findings in the previous section were a quadratic relation was found between the wave reflection and the maximum scour depth.

5.1.5 Downrush flow

From the analysis done in the previous sections it is clear that there is an additional process that influences the amount of scour directly adjacent to a sloping structure. It is expected that this scour is caused by the breaking of waves on the sloping structure and the associated flow velocities. This process will be called the downrush flow, in some literature this is referred to as backflow. On the topic of downrush flow from a sloping structure and its effect on scour at the toe of the structure no extensive research has been done. Most studies focus on the effect of the run-up and run-down of waves and its effect on wave overtopping or on the stability of the armour layer.

Recently studies have been done into the stability of rock toes and velocity at the toe of a sloping structure. van Gent and van der Werf (2014) studied the rock toe stability of rubble mound breakwaters with a 1:2.0 slope. Here an expression for the characteristic velocity $\hat{u}_\delta$ at the toe was developed. This expression is given in eq. (5.5). Where the incident wave height H_s, the spectral wave period $T_{m-1,0}$, the wave number k and the water depth above the toe h_t are used to calculate this characteristic velocity. With the wave conditions that are measured for the 4 wave periods that are tested in this study the characteristic velocity $\hat{u}_\delta$ at the toe can be calculated. The resulting velocities are given in table 5.4. It can be seen that, as expected, velocities increase for an increasing wave period. Also a comparison is made with the orbital velocity $\hat{u}_b$, calculated using eq. (5.1) based on linear wave theory.
van Gent and van der Werf (2014) compared the resulting velocities using eq. (5.5) with velocity measurements at a toe for irregular waves. For irregular waves each individual wave leads to a different velocity at the toe. It is concluded that velocities calculated with eq. (5.5) compared well with the 2%-exceedance value of the maximum velocity per wave. As a result the calculated velocities are suitable for estimation of toe stability (van Gent and van der Werf, 2014). Also the influence of the wave steepness on the amount of damage was studied. The results showed that the influence of wave steepness, or wave period, is clearly present. Conditions with a low wave steepness result in more damage than conditions with a high wave steepness.

$$\hat{u}_\delta = \frac{\pi H_s}{T_{m-1,0}} \frac{1}{\sinh kh_t} \tag{5.5}$$

Table 5.4: Calculated an measured velocities at toe of rubble mound structure

					Calculated velocities		Measured velocities		
T_p [s]	$H_{s,i}$ [m]	$T_{m-1,0}$ [s]	h_t [m]	k [-]	$\hat{u}_\delta$ [m/s]	$\hat{u}_b$ [m/s]	$u_{2\%,toe}$ [m/s]	$u_{2\%}$ at 1/2λ [m/s]	$u_{2\%}$ at 3/4λ [m/s]
1.6	0.116	1.5	0.4	1.8	0.30	0.24	0.34	-	0.26
1.9	0.124	1.7	0.4	1.4	0.40	0.27	-	-	-
2.1	0.129	1.9	0.4	1.1	0.45	0.29	-	-	-
2.5	0.127	2.2	0.4	0.9	0.54	0.31	0.45	0.25	0.33

Besides calculating these velocities, velocity measurements have been done for several tests. This includes tests with a wave period of 1.6 and 2.5 seconds. Here measurements have been done over the length of the sand pit and above the toe structure. These measurements at the toe structure are of particular interest here. In fig. 5.4 the velocity above the toe for a test with the permeable breakwater and long waves is given. Measurements are done for 5 minutes at a height of 0.20 and 0.30 meter above the initial bed (water depth at the toe is 0.40 meter) and are presented in fig. 5.4 for one of these tests. Measurements lower in the water column were not possible due to the presence of the toe. It can be seen here that the maximum offshore directed velocities (positive values) are larger than the maximum onshore directed velocities at 0.20 m above the bed. Also the mean velocity is found to be larger and directed offshore lower in the water column. It is expected that both these findings are caused by the breaking of waves on the structure and the resulting downrush flow.
The maximum values measured at the toe are also in line with the calculated values of $\hat{u}_\delta$ in table 5.4 using the approach by van Gent and van der Werf (2014). Especially for short waves the 2%-exceedance value of the velocity compares well with the calculated value. For the longer waves the approach slightly overestimates the velocity.
Measured velocities of $u_{2\%}$ at the second anti-node in front of the structure are similar to the calculated values of the maximum orbital velocity $\hat{u}_b$ for the significant wave height. Using linear wave theory to calculate $\hat{u}_b$ therefore gives a good first estimation of the maximum flow velocity that can occur above the bed for standing waves.

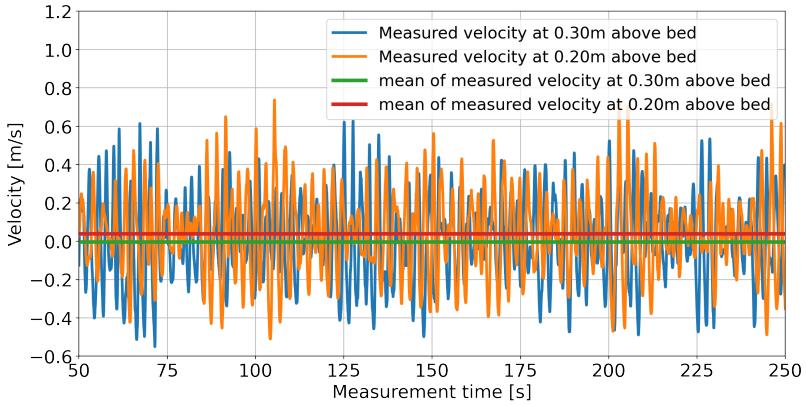

Figure 5.4: Measured velocity above toe for test Per_D17_H14_T25_Toe_b.

When comparing the values of $\hat{u}_\delta$ with the bottom orbital velocities $\hat{u}_b$ in table 5.4 and the measured $u_{2\%,toe}$ it is clear that the velocities at the toe are significantly larger than the orbital velocities at the bottom caused by the standing waves. It is therefore expected that the toe scour caused by the downrush flow has a larger scour potential than the standing wave pattern. This is in line with the bed profile measurements for the long waves. These profiles show significant scour at the toe of the structure while the node of the standing wave pattern causes deposition at this location as the associated velocities here are low, see fig. E.1a and fig. E.1b. This shows that the downrush flow counteracts this effect and results in a scour hole at the foot of the structure. The depth of this hole is similar or even larger, depending on the amount of wave reflection, than that of the hole at the first anti-node. The bed profiles for all tested structures are given in fig. 5.5b. This in combination with the measured and calculated velocities at the toe, which are larger than velocities at the anti-node, lead to the conclusion that the scour potential of the downrush flow is larger than that of the standing wave pattern for the tested long waves.

Additionally, measurements of the flow velocity have also been done for the revetment and the impermeable smooth slope for which wave reflection coefficients are larger than for the permeable rubble mound structure. Here the measured flow velocities at the toe are larger than for the rubble mound structure and are significantly larger than the measured velocity at the second anti-node. For an increase in wave reflection an increase in downrush flow scour potential can therefore be expected.

For the shorter waves that are tested the wave length is shorter which results in a smaller orbital motion. This in combination with the accretion of sediment that is found at the toe for short waves, which is visible in fig. 5.5a, indicate that flow velocities at the toe are smaller for the shorter waves. As a result, the downrush flow is less important for shorter waves. At some point the downrush flow is no longer the most relevant mechanism determining whether deposition or scour occurs at the toe of the structure.

In addition, the influence of the three tested structures on the amount of downrush flow scour is further investigated. In table 5.5 the mean diameter D_{50} of the used sand, the hydraulic conditions and the maximum depth of the downrush scour hole is given. Here also the roughness coefficient γ_f of the structures is given. This coefficient has a large influence on the amount of run-up and run-down, the values are from Van der Meer (2002) and CIRIA et al. (2007). In fig. 5.5 the bed profile of every test described in table 5.5 is given. All comparisons here are done for structures without a toe and bed protection. Important to note here is that the wave reflection, which also plays an important part in the scour processes, is also influenced by the roughness of the structure.

Table 5.5: Influence structure on downrush flow, all with 1:2.0 structure slope

Type of structure	Roughness coefficient γ_f [-]	$D_{50,Sand}$ [μm]	Type of waves	T_p [s]	$s_{n,p}$ [%]	h/λ [-]	Kr [%]	$u_{2\%,toe}$ [m/s]	$S_{max}/H_{s,i}$ first 3/8 λ [-]
Permeable rubble mound	0.4	170	Irregular	2.5	2.7	0.084	37	0.45	0.14
Permeable rubble mound	0.4	220	Irregular	2.5	2.7	0.084	37	-	0.16
Permeable rubble mound, from Jantzen (2020)	0.4	260	Irregular	2.5	2.7	0.084	37	-	0.21
Impermeable revetment	0.55	170	Irregular	2.5	2.7	0.084	51	0.58	0.15
Smooth impermeable, from Jantzen (2020)	1.0	260	Irregular	2.5	2.7	0.084	79	-	0.50
Permeable rubble mound	0.4	170	Irregular	1.6	4.1	0.141	26	0.34	0
Permeable rubble mound	0.4	220	Irregular	1.6	4.1	0.141	26	-	0
Impermeable revetment	0.55	170	Irregular	1.6	4.1	0.141	33	0.31	0
Smooth impermeable, from Jantzen (2020)	1.0	260	Irregular	1.6	4.1	0.141	62	-	0

For the long waves a lower roughness coefficient results in less scour directly in front of the structure, as can be seen in fig. 5.5b. An increase in roughness results in a decrease in wave run-up and run-down. As a result, the flow velocities also decrease. Therefore, the velocity of the downrush flow decreases with an increase in roughness, this results in a decrease in the downrush flow scour potential. For the smooth impermeable structure it can be seen that the downrush flow scour is larger than the standing wave scour at the first anti-node. For the other two structures, which are more rough, this is not the case. Between the permeable breakwater and the impermeable revetment no clear differences are observed. This is unexpected as the structures show a significant difference in roughness coefficient, permeability and amount of wave reflection. Between the variations in sand diameter some differences are visible for the tested long waves. For smaller values of D_{50} less erosion is experienced. Influence of the sand diameter on the amount of erosion is further discussed in section 5.4.

As described in the previous sections it can be seen that for the short waves no scour but accretion occurs directly at the toe of the structure. From the start of testing accretion is observed directly at the structure. Therefore no clear influence of the roughness of each structure on the downrush flow can be distinguished. This is also observed in the flow measurements done at the toe where no increase in $u_{2\%,toe}$ is found for the less rough structure.
What is observed is that accretion at the toe seems to increase more rapidly for an increase in roughness. It is expected that due to the decrease in wave reflection orbital velocities from the standing waves decrease which results in more deposition of material.
At the first anti-node of the standing wave pattern in front of the structure in the first hours of testing some scour is observed. Over time the depth of the scour hole here decreases and accretion is observed at the anti-node as well. It is therefore expected that besides the downrush flow scour and the standing wave scour another large-scale process is present over the length of the flume that causes sediment transport. This process is further discussed in section 5.3.2 and section 5.5.1.

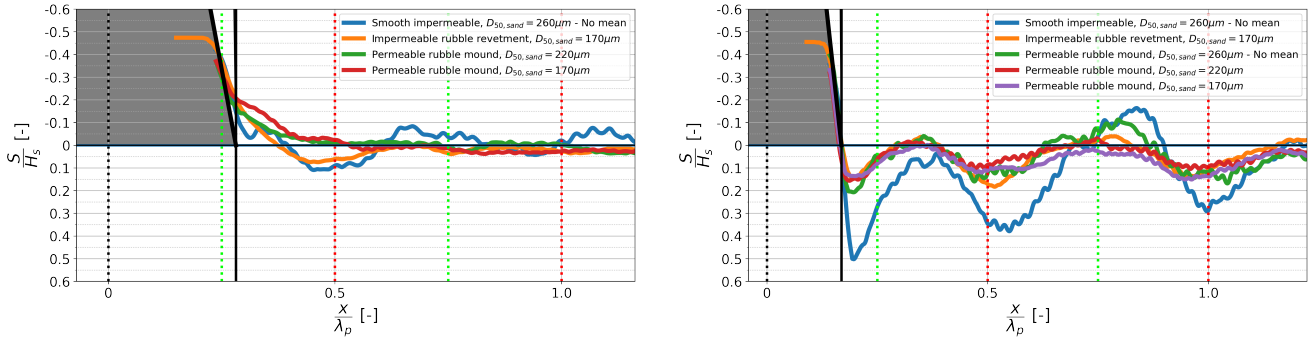

(a) Bed profile short waves, Tp = 1.6 s.

(b) Bed profile long waves, Tp = 2.5 s.

Figure 5.5: Downrush scour comparison for tested structures, after 8 hours of testing.

It can be concluded that, depending on wave characteristics, the downrush flow can play an important part in the scour that is experienced close to sloping coastal structures. In some cases the downrush flow creates a scour hole directly in front of the structure. As scour close to the structure can cause instability or even failure of the structure it is important to include the influence of downrush flow when considering scour at sloping coastal structures. The amount of downrush flow and its influence at the foot of the structure depends on many parameters such as the relative water depth, the wave steepness, the wave reflection, the roughness of the slope and the permeability of the structure. The influence of the first three parameters have been discussed in the previous sections. In general the influence of the downrush flow is larger for smooth slopes and smaller for rough slopes. For the permeability no significant difference between downrush flow scour has been experienced for the tests done in this study. Both parameters also influence the amount of wave reflection and thus the amount of standing wave scour.

For making a first estimation of the downrush flow scour potential eq. (5.5) developed by van Gent and van der Werf (2014), for calculating the toe stability at rubble mound structures with a 1:2.0 slope and a water depth that is between 1.2 and 4.5 times the wave height, can be used. This equation gives a characteristic velocity $\hat{u}_\delta$ at the toe of the sloping structure that is similar to maximum velocities measured at the toe in this study. This calculated value can be compared with the bottom orbital velocity $\hat{u}_b$ that is calculated using the design wave conditions. When the characteristic velocity $\hat{u}_\delta$ is significantly larger than the bottom orbital velocity $\hat{u}_b$ scour directly at the toe can be expected.

This approach is suitable for rubble mound structures. In this study it is found that for less rough and more impermeable structures the flow velocities at the toe increase. For these cases the approach underestimates the maximum velocity at the toe. For these types of structures large flow velocities and downrush flow scour potential can be expected for structures that have high wave reflection coefficients.
To prevent large downrush flow scour holes from forming a rough structure can be used. It is found in this study that with the same wave conditions, for smooth structures the depth of the downrush scour hole is in order of two times the depth of the downrush scour hole for structures with a rough slope. Also taking into account the location of the standing wave scour in relation to the location of the downrush scour hole can help reduce the maximum scour depth, as further discussed in the next section.

5.2 Influence bed protection length on scour-deposition pattern

Variations in bed protection length were tested to investigate the influence of the length of the bed protection on the scour-deposition pattern. The set-up of the bed protection is presented in section 3.2. The bed protection material was a closed filter. Only when a scour hole is present at the offshore end the layer was undermined and material started to displace and settle into this hole. No displacement of stones was witnessed due to wave-induced velocities near the bed. For all tests with the bed protection deposition of sand on top of the layer was observed. The amount of deposited material varied between tests. Most accretion is observed for the tests for shorter waves where, also without the bed protection, accretion was observed in front of the structure.
The resulting bed profiles for long waves and variations in bed protection layout are given in fig. 5.6. Here besides the two tests varying in bed protection length also the tests with and without a toe are added for comparison. Also, the location of the end of the filter/protection layer is given for every layout.

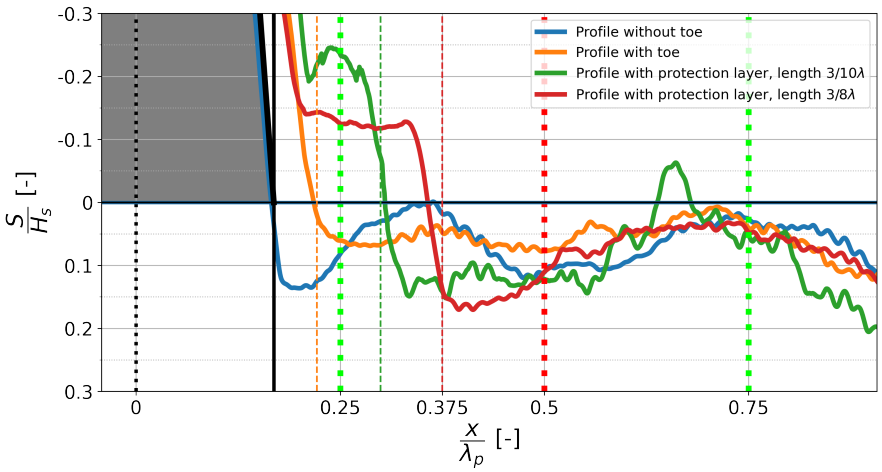

Figure 5.6: Bed profiles for long waves and permeable rubble mound structure with varying bed protection layout.

For the tested wave conditions the measured scour depth for each condition is found to be highest for the layouts with bed protection. This was in accordance with Jantzen (2020) and differed from expectations, as usually it is assumed that the scour hole directly at the toe is the deepest. Once this fist hole is protected it is generally assumed that the second hole is less deep as concluded in figures presented in Sumer and Fredsøe (2000) for irregular waves. An overview of the measured maximum depth of the scour hole depending on the tested layout is given in table 5.6. The maximum scour over the whole area in front of the structure and for the first $3/8\lambda$ are given here. An area with a length of $3/8\lambda$ from the waterline is considered here as it will include the first hole at the structure but not the hole caused by the anti-node of the standing wave pattern, which is present at a distance of $1/2\lambda$ from the waterline. For the long waves this area also corresponds to a combination of the width of the first scour hole and the width of the structure from the waterline to the toe.
Also, the width of the filter and/or bed protection layer $W_{b,p}$, the total width of the structure measured from the waterline $W_{p,t}$ and the total width compared to the wavelength $W_{p,t}$ / λ_p are given. A sketch explaining these parameters is given in fig. 5.7.

Table 5.6: Influence position structural end, for long waves and permeable breakwater

Layout	$W_{b,p}$ [m]	$W_{p,t}$ [m]	λ_p [m]	$W_{p,t}$ / λ_p [-]	$S_{max}/H_{s,i}$ [-]	$S_{max,3/8\lambda}/H_{s,i}$ [-]
No toe	0.00	0.80	4.74	0.17	0.15	0.14
Toe	0.25	1.05	4.74	0.22	0.12	0.08
Toe & short bed protection	0.60	1.40	4.74	0.30	0.21	0.15
Toe & long bed protection	1.00	1.80	4.74	0.38	0.17	-

For the test with the long waves the resulting bed profiles, given in section 4.1, show deposition of material or the least amount of scour at the nodes of the standing wave pattern. The first node of this pattern is located just in front of the coastal structure. For the layouts with the bed protection the protection layer even extends beyond this node. Therefore, the node and its associated deposition are an important aspect determining the maximum depth of the first scour hole. For the layout with only a toe, which ends just before the node, the measured maximum scour depth is lowest. It is expected that this is due to the standing wave pattern that counteracts the scour caused by the downrush flow from the structure, as discussed in section 5.1.5. This is supported by the observation that for layouts where the structural end is close to this node the second or third scour hole is deeper than the first hole. When the length of the layer extends beyond this node, as for both types of bed protection tested, the structure end becomes closer to the second anti-node, at $1/2\lambda$ from the waterline, where scour is expected. When the structure end approaches this anti-node the maximum depth of the scour hole becomes larger as the downrush flow from the structure might be working together with this standing wave scour. Whether the velocity of the downrush flow has decreased further away from the toe is not know. The resulting increase in maximum scour depth can be seen in table 5.6 where the maximum scour depth increases when the structural end is past the first node and approaches the anti-node.

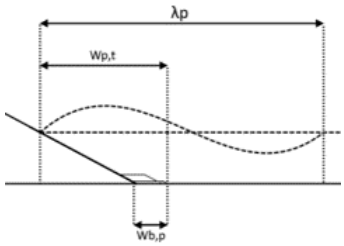

Figure 5.7: Definition of bed protection length values used in present study.

The depth of the first scour hole that forms directly in front of the structure is compared for every layout in fig. 5.8a. Here only the maximum depth within the first $3/8\lambda$ from the waterline, $S_{max,3/8\lambda}$, is considered for every layout. The value of $S^*_{max,3/8\lambda}$ that is used on the y-axis here is the maximum depth of this first hole for the layout without a toe or bed protection. It can be seen that only when the bed protection covers the whole first $3/8\lambda$ no hole forms in this area. This is also visible in fig. 5.6. No large influence on the maximum scour depth for the whole area in front of the structure is observed in fig. 5.8b for variations in bed protection layout.

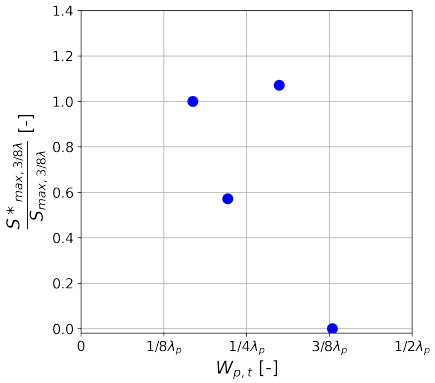

(a) Downrush flow scour hole, first $3/8\lambda$.

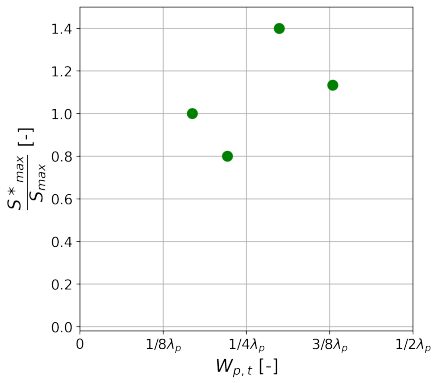

(b) Over whole length, first 2λ.

Figure 5.8: Influence bed protection length on maximum scour depth.

These findings are similar to that of Xie (1981) for vertical structures. In fig. 2.3 a similar relation can be observed as for the results of this study in fig. 5.8a. For the vertical wall tests by Xie no scour was observed at the end of a protection layer with a length of $3/8\lambda$. This pattern is not observed for tests with a sloping wall. Here always a hole formed directly at the end of the layer for every protection length tested.

5.3 Effect sediment suspension mode and transport direction on scour-deposition pattern

In this section the sediment transport mode is analysed. This is done using several approaches. In section 5.3.1 the mode of sediment transport is analysed using literature and visual observations. Approaches by Shields (1936), Rouse (1937) and Xie (1981) are used to quantify the mode of sediment transport. The results from these three approaches will be checked with visual observations from the model testing.
In the second section, section 5.3.2, the flow measurements are further analysed to determine the mean flow direction depending on wave conditions. Here a comparison between the flow direction and the observed sediment transport direction is made.

5.3.1 Mode and amount of sediment transport

Several methods have been developed to determine the amount and mode of sediment transport. The approaches that are used here have been developed by Shields (1936), Rouse (1937) and Xie (1981). Each approach will be used to indicate the amount of sediment movement and type of sediment transport. Visual observations will be compared with the results from literature.

Values calculated using the three approaches are given in table 5.7. For more elaborate calculations for each individual test is referred to appendix F.

Table 5.7: Sediment transport values

Type of sand	$D_{50,Sand}[\mu m]$	Settling velocity W [m/s]	T_p [s]	u_b [m/s]	$\hat{u}_b$ [m/s]	Rouse number [-]	Range Xie criterion [-]
Sand used by Jantzen (2020)	260	0.037	1.6	0.24	0.155	-	-
Sand used by Jantzen (2020)	260	0.037	2.5	0.31	0.170	-	-
M32	220	0.030	1.6	0.24	0.145	1.6	4.6
M32	220	0.030	2.5	0.31	0.159	1.5	6.5 - 6.7
M34	170	0.020	1.6	0.24	0.131	1.1	7.4 - 8.0
M34	170	0.020	1.9	0.27	0.136	1.0	8.9
M34	170	0.020	2.1	0.29	0.138	1.0	9.9 - 10.1
M34	170	0.020	2.5	0.31	0.143	1.0	10.5 - 11.4

Shields and modified Shields

For stability in non-breaking waves the modified Shields approach can be used. This approach is developed by Sleath (1978) and combines the shear stress under a wave with the stability relation developed in Shields (1936). For all tests the calculated orbital velocity for which material starts to move, $\hat{u}_b$, is found to be significantly smaller than the bottom orbital velocity, u_b, calculated from linear wave theory. Based on this the sediment is expected to be in motion.

Rouse

Rouse (1937) developed an approach for predicting the mode of sediment transport. In this approach the Rouse number P is calculated. This is a non-dimensional number that describes the mode of transport of sediment. With the Rouse number transport is divided into three regimes, these are the bed load, the suspended load and the wash load regime. Table 5.8 shows which type of transport is present depending on the Rouse number. The Rouse number is based on a flowing fluid and not on wave-induced flow. Therefore the results of the analysis with the Rouse approach are only used to give an indication of the possible sediment transport for the maximum flow velocities.
According to the approach by Rouse (1937) for the sand with a D_{50} of 260 μm and 220 μm all test conditions result in suspended load (50%) transport for the maximum orbital velocity. For all test conditions using the sand with a D_{50} of 170 μm the mode of transport is suspended load (100%) for the maximum orbital velocity. V ariations in hydraulic conditions tested in this research only have a small influence on the Rouse number for maximum velocities.

Table 5.8: Rouse numbers for transport (Rouse, 1937)

Type of transport	Rouse number
Bed load	P > 2.5
Suspended load (50%)	1.2 > P >2.5
Suspended load (100%)	0.8 > P >1.2
Wash load	P < 0.8

Xie

The sediment transport was also studied extensively in the study by Xie (1981) into scour in front of vertical wall breakwaters. Two scouring patterns were observed depending on the dominant type of sediment transport. These patterns were for fine sediment and for coarse sediment. The following criterion for the fine scouring pattern has been formulated by Xie:

$$\frac{u_{max} - u_{crit}}{W} \geq 16.5 \tag{5.6}$$

Where:

u_{max} = The maximum velocity at the bottom
u_{crit} = The critical velocity of sand particles
W = The sediment settling velocity

Multiple methods have been developed to determine the critical velocity for sand particles under oscillatory waves. Xie (1981) found the formula by Bagnold (1946) to be most close to his results. Using this formula to calculate the critical velocity for all types of sand and wave conditions the earlier determined settling velocity and maximum velocity at the bed are used to determine in which of the patterns defined by Xie the tests in this study fall. It is found that according to the criterion by Xie (1981) all tests done in this research qualify as the "coarse" pattern. Values range from 4.6 to 8.0 for the shorter waves and from 6.5 to 11.4 for the longer waves. This means that bedload transport is dominant over suspended load transport and that according to Xie (1981) scour is present halfway between nodes and anti-nodes and there is deposition at the nodes. Individual results for each tests can be found in appendix F.
The critical velocity found for each material (9.0 - 11.6 cm/s) following the approach used by Xie is lower than the maximum orbital velocity for the initiation of motion found using the Sleath (1978) approach. The velocities found using this approach are about 40 % larger than those found using the approach by Xie.

Visual observations

During the model testing the movement of sediment was visually observed and documented in short videos of about 1 minute. In addition to the videos, the interval capturing for the photo measurements allows a first estimation of differences in sediment suspension between tests. An example of one of these photos that shows some sediment suspension is given in fig. 5.9. During testing it is observed that most sediment movement is present in the lower quarter of the water column. During some periods sediment remained suspended but most material was observed to be transported on or just above the bed.
The visual observations of the type of sediment transport correspond with the calculations done in the previous sections. These clearly showed that the critical velocities for which particles start to move are significantly lower than the maximum orbital velocities for the tested wave conditions. Additionally, clear bedload dominance was observed, this matches witch the calculations using literature. Some visual observations were done by Jantzen, who used more coarse material during testing. For him it was clearly visible that more suspended sediment was present for the material tested in the present study compared to that used in Jantzen (2020).

During testing there were periods of time when almost no sediment transport was observed. This was during periods with small waves in front of the structure. During other periods when there were large waves, that were close to breaking, a lot of movement and suspension was observed. This shows that for irregular waves the amount of sediment transport changes constantly and behaviour is different than for regular waves. A result of this is it that timescales for reaching equilibrium bed conditions are different for irregular waves compared to regular waves.

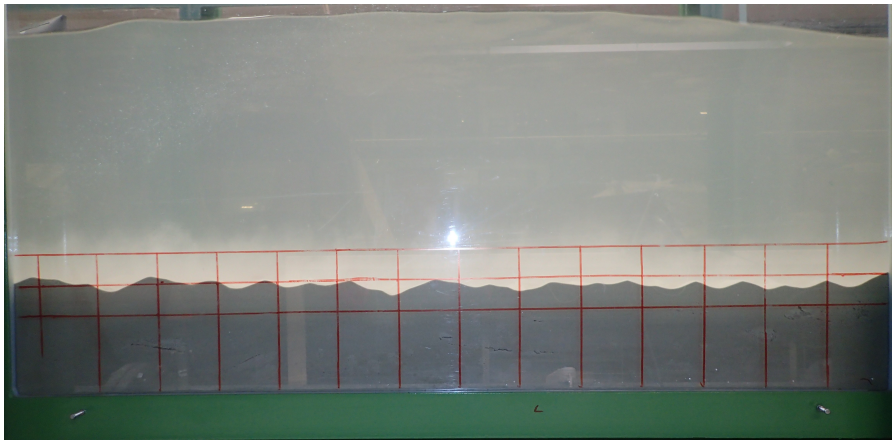

Figure 5.9: Wave-induced sediment suspension.

5.3.2 Transport direction

As described in section 4.4 the flow velocities for 4 tests, varying in wave period and tested structure, have been measured. For every test the mean flow at each individual measurement location has been determined. This is done to find if there is mean flow in one direction and how this is influenced by wave and structure parameters. Figure 5.10 shows these mean flow velocities for test Per_D17_H14_T25_Toe_b. This figure shows that the mean flow over most of the sand pit area is relatively constant and is directed offshore. The magnitude of this velocity is however very low, about 0.03 m/s. Close to the structure this mean flow pattern changes and is no longer constant.

Measurement for the three other tests confirm that from a distance of about 0.5 - 0.75 times the wavelength away from the structure the mean flow becomes almost constant. The results of all tests are given in table 5.9. From these results it seems that the mean flow velocity is offshore directed for most test and that the mean velocity is largest for larger wave periods.

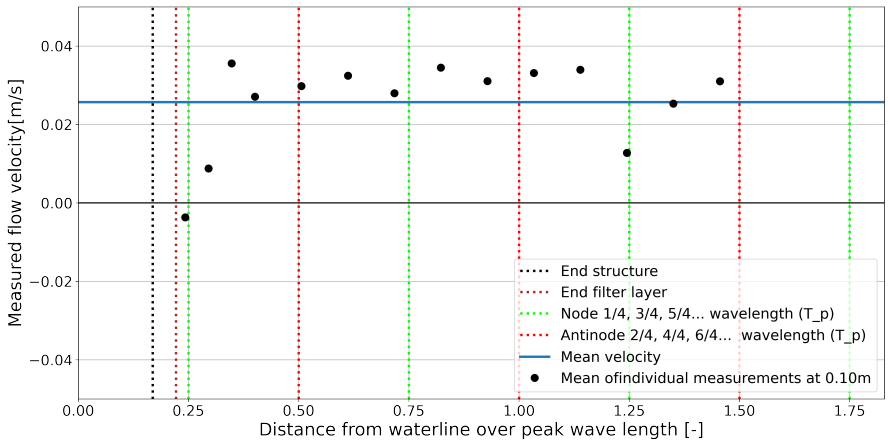

Figure 5.10: Mean flow velocity at 0.10 m above initial bed for test Per_D17_H14_T25_Toe_b.

The measurements show that flow velocities are highest for larger wave periods, this corresponds with the calculations done in section 5.3.1 where larger bottom orbital velocities were found for longer wave periods. The maximum velocities that are measured are slightly higher than the maximum velocities calculated using eq. (5.1). This equation uses the significant wave height H_s to calculate the maximum velocity. In reality for irregular waves there are larger and smaller wave heights than this H_s, resulting in larger and smaller flow velocities for individual waves as can be seen in fig. 4.8. Overall this calculated maximum velocity matches well with the average maximum flow velocity when looking at multiple individual waves. It is therefore expected that the accuracy of the results in section 5.3.1 is good.

Table 5.9: Measured flow velocities

Test	Structure	T_p [s]	Mean flow velocity [m/s]	Direction
Per_D17_H14_T25_Toe_b	Permeable breakwater	2.5	0.03	Offshore
Per_D17_H14_T16_ToeProt	Permeable breakwater	1.6	-0.01	Onshore
Rev_D17_H14_T25_Toe	Impermeable revetment	2.5	0.01	Offshore
Rev_D17_H14_T16_NoToe	Impermeable revetment	1.6	0.01	Offshore

Jantzen (2020) expected that the offshore directed mean flow was probably caused by the presence of an undertow caused by the breaking of waves on the foreshore. As a result, sediment was transported offshore. This offshore transport of sediment was also observed in this study, as over time sand started to accumulate on the wooden foreshore in front of the sand pit. This was especially the case for the tests with higher peak wave periods. For these wave periods the found mean flow velocities in table 5.9 are also largest. For the shorter waves the measured mean flow velocity is smaller and the direction varies between onshore and offshore.

To further observe the offshore sediment loss for the long waves the evolution of the sand pit volume over time is investigated for every test. This is done by determining the mean bed level from the structural end to a distance of 7.5 m offshore form the foot of the structure. This bed level is compared to the initial bed level to determine whether the amount of sediment in this area has changed, based on the method in Jantzen (2020). For every test with long waves it is found that the bed level decreases over time. This decrease seems to follow a linear trend in time, see fig. 4.5. This is in agreement with the findings in Jantzen (2020) were the total loss of sediment was constant over time for waves with a T_p = 2.5 s and $s_{o,p}$ = 1.4 %. That the volume change over time follows a linear trend can be clearly seen in fig. 5.11 where the volume change compared to the initial bed profile is given for every test. For an increase in wave period an increase in this constant loss is observed. Longer test duration up to 30 and 60 hours were also studied in Jantzen (2020), where it was found that for these longer duration this linear trend still continued.
The wave reflection does not seem to influence the sediment loss as for the three tested structures, with reflection coefficients of about 37%, 51% & 79%, the volume change is similar. Also, changes in roughness or permeability do not seem to influence the sediment loss. It is therefore concluded that the direction of the sediment transport is caused by the wave properties and not the structural properties.

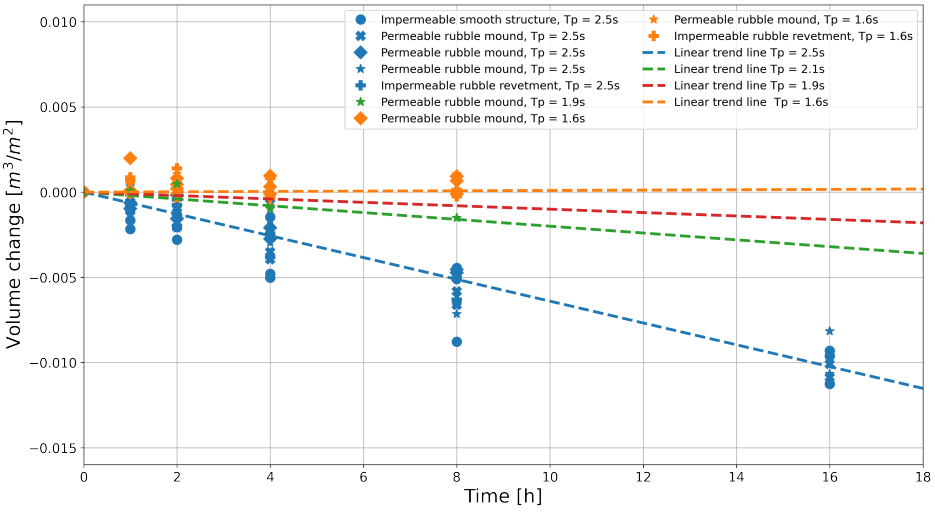

Figure 5.11: Volume change over time for tested wave periods.

The sediment loss for shorter waves, T_p = 1.6 s, is also investigated. It is found that for these wave condition no significant sediment loss is experienced during testing. This is in line with the visual observations where it was observed that the accumulation of sediment at the offshore end of the sand pit was much smaller for the short waves compared to the long waves. Also, for the short waves deposition instead of scour is found at the foot of the structure.

5.4 Influence sand grain diameter on scour-deposition pattern

In this section the influence of the sediment size on the scour-deposition pattern is analysed. This is done to get a better insight in possible effects and problems that can occur when scaling the model tests to prototype situations. The influence of variations in sediment particle size on the scour-deposition pattern are investigated.

To determine the influence of the sediment size on the scouring pattern a comparison is made between several tests. The only variation between these tests is the size of the used sediment, all other hydraulic and structural conditions are kept the same. All types of sand used in this research and in Jantzen (2020), of which the properties are described in section 3.2.2, have been tested with the permeable rubble mound breakwater. Tests have been done with "long" waves, Tp = 2.5 s, and with "short" waves, Tp = 1.6 s.

A comparison of the bed profiles for each type of sand after testing with the long waves is given in fig. 5.12a, this figure shoes the profiles for tests without a toe and protection layer. From the resulting profiles it can be seen that the scouring pattern is similar for every type of sediment. The locations of the peaks and troughs is roughly the same for every test and corresponds to the standing wave pattern.
In table 5.10 an overview is given of these test containing the maximum measured scour depth in front of the structure after 8 hours of testing. For two of the profiles used in this table no mean profile can be made using the method as described in section 4.1.1. This is not possible for these two tests as only one cross section has been measured after 8 hours of testing. For determining the maximum scour for these two tests the profiles of the individual cross sections are used. As described in section 4.1.1 the individual cross sections show local differences over the width of the flume. The maximum scour for both individual profiles may therefore over or underpredict the actual mean scour depth present over the flume width.

Table 5.10: Max long wave scour for varying sediment size

Test name	$D_{50,Sand}[\mu m]$	$H_{s,i}$ [cm]	T_p [s]	$S_{max,3/8\lambda}/H_{s,i}$ [-]	$S_{max}/H_{s,i}$ [-]	Xie criterion [-]	Note
Per_D17_H14_T25_NoToe	170	12.7	2.5	0.14	0.15	10.5	-
Per_D22_H14_T25_NoToe	220	12.7	2.5	0.16	0.16	6.7	-
Per_D26_H14_T25_NoToe	260	13.4	2.5	0.21	0.21	5.0	No mean profile
Per_D17_H14_T25_Toe	170	12.7	2.5	0.08	0.12	10.5	-
Per_D22_H14_T25_Toe	220	12.5	2.5	0.13	0.13	6.5	No mean profile
Per_D26_H14_T25_Toe	260	13.7	2.5	0.12	0.17	5.0	-

From the results presented in table 5.10 it seems that for an increase in particle size the depth of the first scour hole also increases. Due to only having two comparisons and the lack of a mean profile for two of the used tests, not enough data is present to properly judge this behaviour. Especially since the tests with shorter waves, for which the results are given in table 5.11, seem to show a different behaviour.

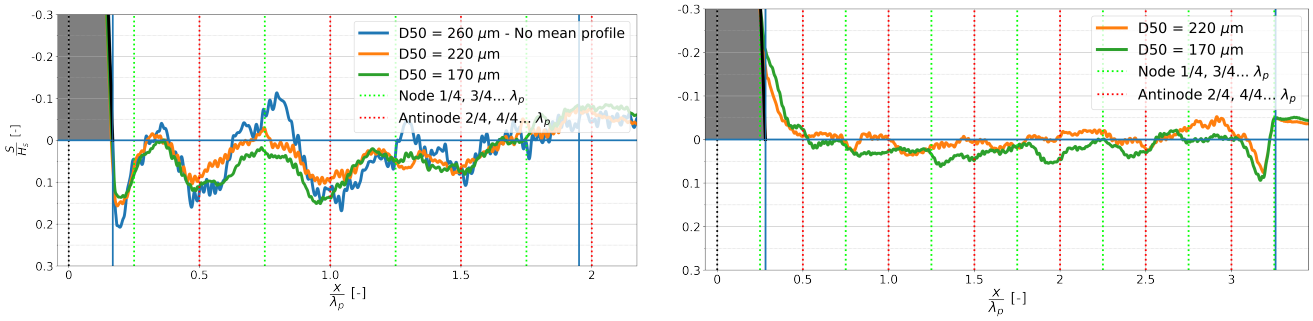

(a) After 8 hours of long waves.

(b) After 8 hours of short waves.

Figure 5.12: Comparison of bed profiles of tests with no toe for varying sediment sizes, after 8 hours of waves.

No additional short wave conditions have been tested for the permeable breakwater in Jantzen (2020), due to this a comparison between bed profiles for the shorter waves can only be made for the two types of finer sediment used in the present study. For the shorter waves, Tp = 1.6 s, the observed scouring patterns in fig. 5.12b show a different behaviour for variations in grain size than for the long waves. The resulting maximum scour and transport values

for the three tested toe layouts are given in table 5.11.
For the short waves the bed profiles show most scour for the finer sediment, which is in contradiction with the findings for the longer waves. The bed profiles for the two used types of sediment show different patterns. The peaks and troughs, from a distance of about 1λ away from the breakwater, are not in the same location as was the case for the longer waves. Close to the structure similar patterns are observed. For all tests done with the permeable breakwater both types of sediment show deposition at the foot of the breakwater.

Table 5.11: Max short wave scour for varying sediment size

Test name	$\mathbf{D_{50,Sand}}[\mu m]$	$\mathbf{H_{s,i}}$ **[cm]**	$\mathbf{T_p}$ **[s]**	$\mathbf{S_{max,3/8\lambda}/H_{s,i}}$ **[-]**	$\mathbf{S_{max}/H_{s,i}}$ **[-]**	**Xie criterion [-]**
Per_D17_H14_T16_NoToe	170	11.7	1.6	-	0.06	7.4
Per_D22_H14_T16_NoToe	220	11.6	1.6	-	0.04	4.6
Per_D17_H14_T16_Toe	170	11.0	1.6	-	0.08	7.4
Per_D22_H14_T16_Toe	220	11.6	1.6	-	0.05	4.6
Per_D17_H14_T16_ToeProt	170	11.7	1.6	-	0.06	7.4
Per_D22_H14_T16_ToeProt	220	11.6	1.6	-	0.05	4.6

No clear pattern has been observed for the influence of the sediment particle size on the scour-deposition pattern. For the long waves a larger scour depth is found for more coarse particles while for the short waves this is the case for more fine particles. For both types of waves the differences in maximum scour for the variation in sediment size are small. Also for the long waves, where the pattern is determined by the standing waves, no differences are observed between locations of peaks and troughs between the particle sizes.
Therefore it is concluded that the sediment particle size only has a small influence on the scour-deposition pattern. For larger variations in particle size it is possible that the transport regime switches between bed-load and suspended load and the influence becomes large. In these cases a significant difference in scour-deposition pattern is expected as Xie (1981) found different scour behaviours for these regimes.

In table 5.10 and table 5.11 besides the maximum measured scour the value of the Xie criterion is listed. This values is based on the approach from Xie (1981) and is an indication of the mode of sediment transport. This values is influenced by the size of the sediment particles.
As described by Xie (1981) scouring patterns show large differences depending whether bed-load or suspended load transport is present. Xie states that for bed-load transport scour is halfway between the nodes and anti-nodes and deposition is found at the nodes. For suspended transport, material is transported towards the anti-nodes. Xie (1981) divided these two patterns into the "coarse" regime, for which bed-load transport is dominant, and into the "fine" regime, for which suspended load transport is dominant. All test done have been checked with the criterion developed by Xie to determine what regime is expected. For each type of sediment tested the criterion for the "fine" pattern is not met, thus the "coarse" pattern is present for every test condition according to Xie (1981). As a results all test should show deposition at the the nodes and scour halfway between the nodes and anti-nodes. For the long waves that are tested there is indeed deposition at the nodes. The scour however, is not observed halfway between the nodes and anti-nodes but at the anti-nodes.

Based on this comparisons with literature and the visual observations it is concluded that for the tests done in this research the bed-load transport regime is dominant. During testing there is also suspended transport present for extreme waves but the corresponding pattern is not dominant.

5.5 Combined effect of all parameters on the development of the scour-deposition pattern over time

In this section the development of the bed profile and the development of the maximum scouring depth is analysed over time. For this the changes in measured bed profile over time are investigated. This is done with the bed profiles that are determined using the laser measurements and the side view of the flume captured with the interval photo measurements. As described in section 5.1 a division is made between the scour pattern of the standing waves and the scour caused by the downrush flow. Development of the complete bed profile and the maximum scour depth over the whole area in front of the structure is studied in section 5.5.1. Here a division is made between the scour-deposition profile caused by the standing waves and large-scale morphological changes that are observed. The development of the downrush flow scour that is observed directly adjacent to the structure is further studied in section 5.5.2.
Development of both the bed profile and the downrush flow scour is in section 5.5.3 linked to the combined effect of the parameters that have been described in the previous sections. Based on the influence of these parameters a best approach is selected to include the effect of all important parameters in a design formula which is given in section 5.6. The findings and resulting patterns are compared with literature in section 5.7.

5.5.1 Development bed profile

Besides the maximum depth of the scour hole in front of the structure, the development of the complete bed profile is also studied. For this the bed profile measurements of every test is compared to investigate how the bed profile develops over time. It is important to note that, as described in section 4.1.1, the bed profile has only been measured for one fixed position over the flume width for most measurements. As a result the measurements that are done in between the initial and last measurement include larger deviations and possible measurement errors.

An example of the development of the bed profile of one of the tests is given in fig. 5.13a. The used layout is the revetment structure without a toe or protection layer, this set-up is tested for the long waves. It can be seen that the depth of the scour hole directly in front of the structure, which is caused by downrush flow, does not significantly increase after about 4 hours of testing. The complete bed profile does however show significant changes after 4 hours of testing. These are primarily observed at the locations of the nodes and anti-nodes of the standing waves. Here a decrease over the whole length of the sand pit is observed. The peaks at the nodes become lower and the troughs at the anti-nodes also become deeper compared to the initial profile. As a result, the total difference in height between the peaks and troughs does not seem to change a lot after 4 hours. This pattern is observed for every test done with the long waves. It is expected that this lowering of the bed profile is caused by the constant sediment loss that was observed for the tested long waves in section 5.3.2.

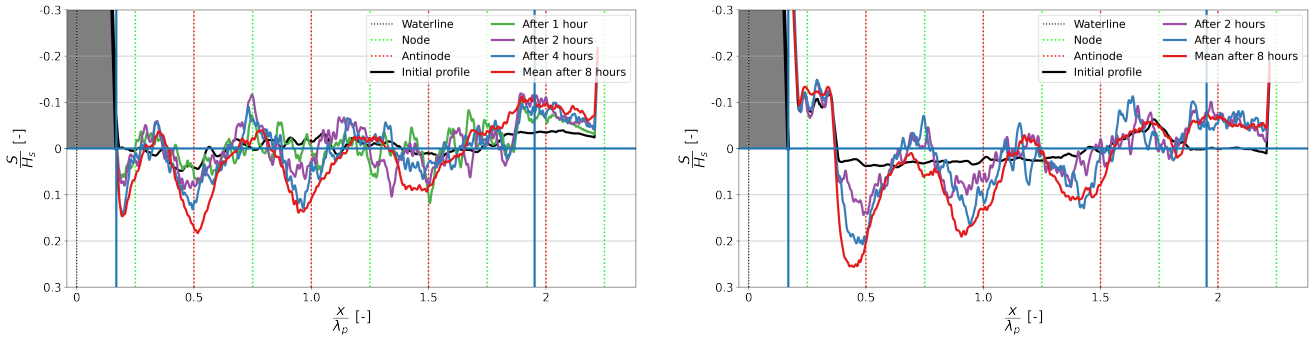

(a) development bed profile test Rev_D17_H14_T25_NoToe. (b) Development bed profile test Rev_D17_H14_T25_ToeProt.

Figure 5.13: Development of width-averaged bed profile over testing time, for long waves T_p = 2.5 s.

In the cases with a bed protection, the first anti-node of the standing wave pattern for the long waves is just in front of the bed protection. As a possible result, the first scour hole for this structure is a combination of the standing wave scour and some influence of the downrush flow. This is a possible explanation why the largest maximum scouring depths were found for tests with bed protection. In fig. 5.13b the development of one of these profiles can be seen. For this test the actual location of the nodes and anti-nodes also seems to be shifted slightly onshore.

Based on these observations in combination with the observed influence of the wave steepness in section 5.1.2, a division will be made between the complete bed profile development caused by the standing wave pattern and the large-scale morphological changes. The influence of the downrush flow is only local and is further discussed in section 5.5.2. The divided processes are:

- The standing wave scour, linked to the node - anti-node pattern
- The large-scale morphological changes
- The downrush flow scour

In fig. 5.14 a sketch is given of these three processes to indicate their influence on the development of the bed profile.

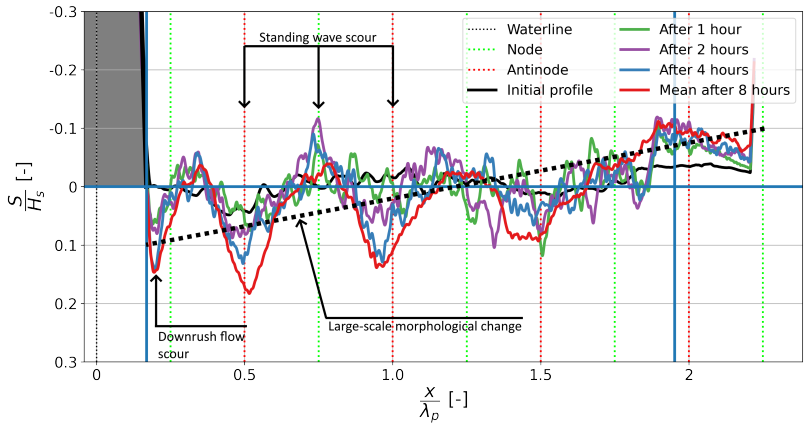

Figure 5.14: Processes in development bed profile.

Standing wave scour

As described above, the standing wave scour seems to reach an equilibrium after which it stops developing. The relative height of the peaks and troughs compared to mean level does no longer increase. Compared to the initial level these peaks and troughs become lower but this process is linked to the large-scale morphological changes that are discussed next.
The time it takes the standing wave scour to reach the equilibrium varies between tests. As for most tests the bed level has only been measured with the lasers after 1, 2, 4 and 8 hours of testing the exact moment when the equilibrium is reached cannot be determined with the bed profiles. For this the results of the photo measurements give a better insight as these are taken every 30 minutes of testing.

For the laser measured bed profiles most cases with the long waves seem to reach an equilibrium after 4 hours of testing. Especially after 8 hours of testing and onwards the scour deposition pattern from a distance of $3/4\lambda$ from the waterline does no longer show significant changes. Closer to the structure the pattern is more influenced by the downrush flow, see section 5.5.2.

With the photo measurements only the first 2.5 - 3.0 meter in front of the structure is considered. For the long waves this means that only the development of the first scour hole can be investigated. Here a combination of the the downrush flow scour and the standing wave scour is expected to influence the development of the profile. The timescale for development of the standing wave scour was found to increase with an increase in the wave reflection coefficient of the structure in section 4.2. The time for which a somewhat constant maximum scour depth was reached ranged from 2 to 8 hours depending on the tested structure and bed protection.

Large-scale morphological changes

For some tested wave conditions the bed profile shows a constant change over the testing time, as described in section 5.3.2. Although small, here a constant loss of sediment was observed for the tests with long waves. This loss remained constant even for very long testing times. With a decrease in wave period and thus a decrease in wavelength and an increase in wave steepness less sediment is lost, this loss is found to remain constant over time.

For the short waves no significant loss of sediment is measured. The change in volume for the four tested wave periods are given in table 5.12. As can be seen in table 5.12, the bed change is about 0.1 - 0.6 mm/h depending on the tested wave condition. Here also the relevant wave conditions for each tested wave period are listed.
A possible explanation for this behaviour is the mean transport direction of the sediment. For the long waves an offshore directed transport is experienced and sand starts to accumulate past the offshore end of the sand pit. For the short waves this accumulation of sand is seen at the onshore end. Therefore it is concluded that the main transport direction is offshore for the long waves but that this is not the case for the short waves. No significant onshore directed flow and transport has been measured for the short waves besides the accumulation at the structure.

Table 5.12: Morphological change for tested wave conditions

Wave condition	$\mathbf{T_p}$ [s]	$\mathbf{s_{o,p}}$ [%]	$\mathbf{s_{n,p}}$ [%]	**Kr** [%]	**Volume change** [$\frac{m^3}{m^2}/hour$]
Short wave	1.6	3.4	4.1	26	0
Intermediate wave 1	1.9	2.2	3.6	28	-0.0001
Intermediate wave 2	2.1	1.8	3.2	32	-0.0002
Long wave	2.5	1.4	2.7	37	-0.0006

For the development of the maximum depth of the complete profile a division is made between long waves, T_p = 2.5 s, and short waves, T_p = 1.6 s. Since both wave conditions show different patterns comparison of the development is done individually for each wave condition.

Development long waves

As concluded earlier, the tests with the long waves show larger scouring depths than the tests with the short waves. This is caused by a variation in hydraulic parameters of which the influence is discussed in section 5.1. This division results in fig. 5.15 where the development of the maximum scour depth over two wavelengths in front of the structure is given for the tests with long waves. Figure 5.16 shows this development for the tests with short waves. Additionally, in both figures the expressions for the maximum scour depth by Den Bieman et al. (2019) and Jantzen (2020) have been added.

When looking at the development of the maximum depth for the long waves in fig. 5.15 a pattern is clearly visible. After a rapid increase the development of maximum depth slows down and becomes almost constant. This slowing down of the development seems to happen faster for the structures with the lower wave reflection compared to the structure with a high wave reflection, in line with the findings for the photo measurements in section 4.2. This constant state is reached after about 4 hours of testing, or 6000 long waves, for the permeable breakwater and the revetment. After this still a small increase of the maximum depth is observed which can primarily be linked to the constant loss of sediment described above.
For the smooth impermeable structure not enough measurements are present to properly judge when the maximum depth no longer shows a significant increase. It does seem that after 4 hours of testing this constant state has not been reached yet. For this structure this seems to be more in the order of 8 hours.

In table 4.1 in section 4.1.2 a difference in location of the maximum scour hole is observed between the tested structures. The tests with the permeable breakwater without bed protection show a maximum scour depth at a distance of one wavelength from the waterline while for the revetment maximum scour is at a distance of half a wavelength. For both structures scour occurs at an anti-node of the standing wave pattern. For irregular waves maximum scour is expected at the first anti-node away from the structure as for irregular waves the standing wave pattern dampens and so the scour decreases with increasing distance from the structure (Sumer and Fredsøe, 2000). The exact reason why for some cases with the permeable breakwater the maximum scour is not at the first anti-node of the standing wave pattern is unknown.

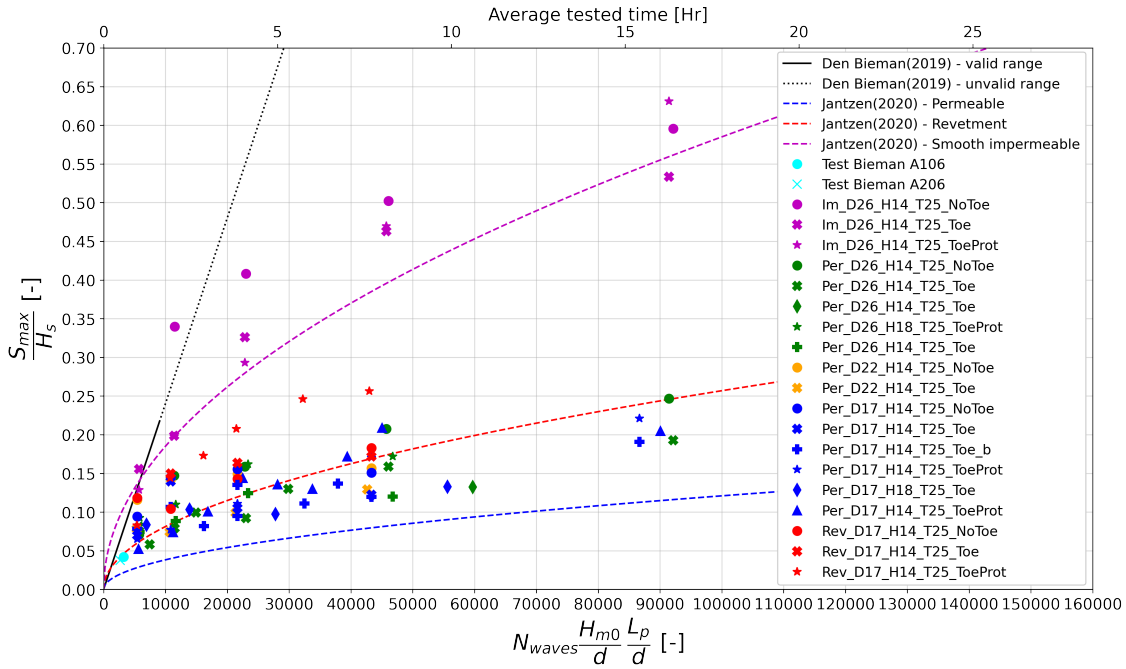

Figure 5.15: Development maximum measured depth, over first 2λ from the structure, over time for long waves.

Development short waves

The maximum depth for the tests with short waves in fig. 5.16 shows a similar development pattern as the long waves. After a rapid increase the development slows down and becomes almost constant. The timescale of this development is similar to that of the long waves. After about 2 to 4 hours of testing, or 4500 - 9000 waves, the constant state seems to be reached. Here after this time no significant increase in depth is observed as no sediment loss or clear transport direction is observed for the short waves.
For the tests with short waves no clear difference between the structures is visible like it is for the long waves. The type of structure and the associated wave reflection does not seem to have a large influence on the maximum scouring depth. Because of this it is expected that for these short waves the other hydraulic conditions, which remain the same for each test, are the main mechanism determining the scour-deposition profile.

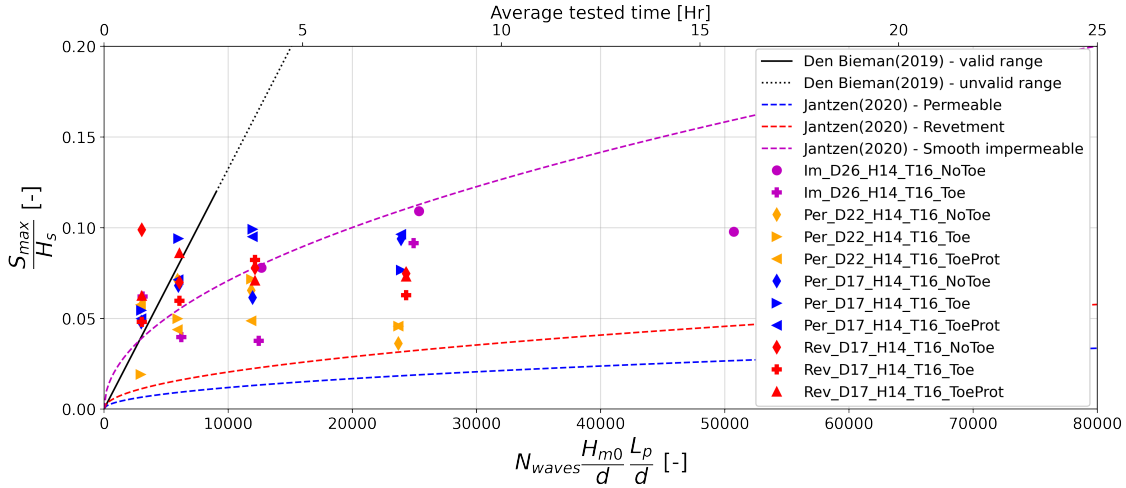

Figure 5.16: Development maximum measured depth, over first 2λ from the structure, over time for short waves.

5.5.2 Development downrush scour hole

For the development of the downrush scour hole directly at the toe of the structure the tests with the long waves will be investigated. For these cases the fist anti-node is located away from the base of the slope. Also, larger downrush flow is expected for cases where the Iribarren number ξ is larger. As concluded in section 5.5.1 for the short waves no scour hole forms directly in front of the structure. Because of this the influence of downrush flow for the short waves is not further discussed here.

In fig. 5.17 for all measurements done with long waves the maximum depth of the first scour hole at the toe is given. This does not include the tests done with bed protection as here this first hole at the toe of the structure is covered by the bed protection and so this separate hole does not form. The first hole that is present at the end of the bed protection is expected to be caused by a combination of the downrush flow and the anti-node scour of the standing wave pattern. Whether downrush flow really is present here, and if the magnitude has reduced, is not known. Therefore it is not included here. For every test measurements have been done after 1, 2, 4 and 8 hours of testing. For some tests additional measurements are done every hour or an additional 8 hours have been tested where a measurement is done after 16 hours. In this figure also formulas developed by Den Bieman et al. (2019) and Jantzen (2020) are added to be checked with the measurements. Further analysis of their predictive capabilities is done in section 5.7.

To be able to compare the development over time between tests the horizontal axis is made proportional to the number of waves. Included here are also the significant incident wave height and the peak wave length. These are all normalized using the water depth in front of the structure. This allows for easier comparison between tests where these are varied.

$$\frac{S(N)_{max}}{H_s} = \frac{0.3}{\left(\sinh \frac{2\pi h}{L}\right)^{1.35}} K_r^2 \sqrt{\frac{N}{12000}} \tag{5.7}$$

In fig. 5.17 the formula developed by Jantzen (2020), shown in eq. (5.7), for the estimating the development of the maximum scour depth has been added for the permeable breakwater, the revetment and the impermeable smooth slope. In this formula a factor 0.3 or 0.4 is used depending on the type of sediment transport. Xie (1981) proposed that a value of 0.3 should be used for bed load dominant cases and that for suspended load dominance 0.4 should be used. In section 5.3 it is concluded that bed load transport is dominant in all the tests that are done, so the value of 0.3 will be used here. The resulting scour depth for the number of waves using this approach is given in fig. 5.17.

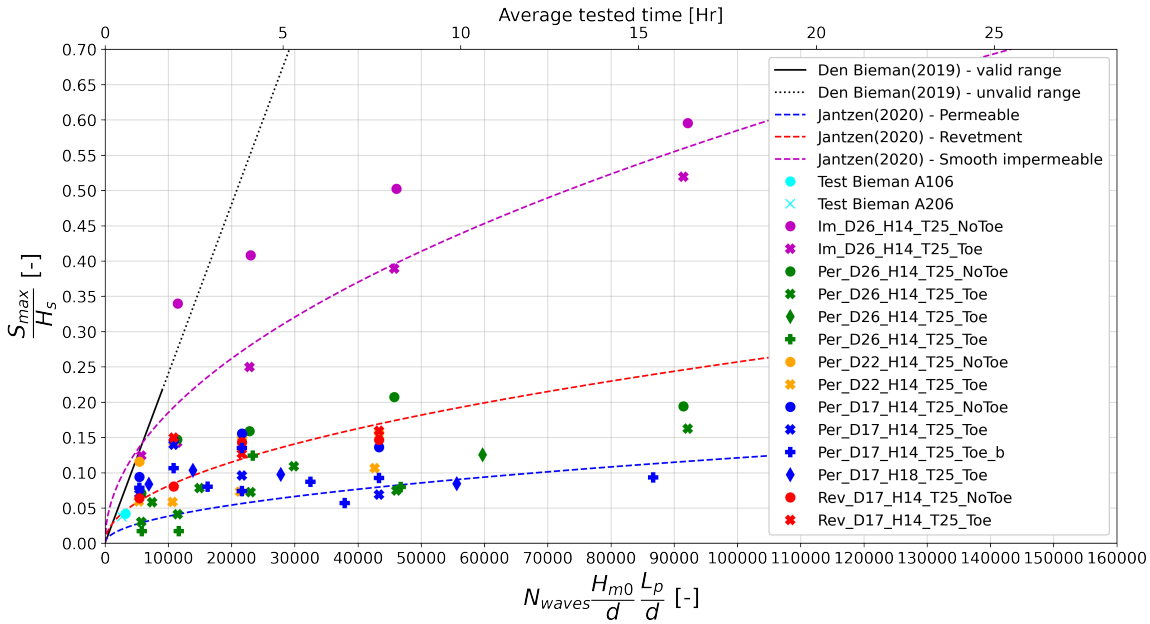

Figure 5.17: Development maximum measured depth downrush scour hole over time for tests with large T and no bed protection.

In fig. 5.17 it can be seen that at the start of testing the depth of the first scour hole increases rapidly. After some time this increase slows down and the depth becomes almost constant. The timescale of this slowing down varies between the tested structures. For the permeable breakwater and the revetment at a horizontal axis value of about 20000 this depth of the scour hole seems to become almost constant, which for these tests is after about 4 hours of testing. For the impermeable smooth slope a significant increase is still observed after 4 hours of testing. Especially the layout with a toe shows a large increase in depth after this time.
For the tests that have been done for 16 hours only a small increase in maximum scour depth is observed after an extra 8 hours of testing. This may partly be a result of the large-scale loss of sediment observed.

5.5.3 Combined influence of parameters

In this section the influence on the maximum scour depth of all the parameters that have been described in this chapter is combined to form one design formula. The most important parameters are selected and included in the design formula. The predictive capability of this formula is then compared with the results of the model tests of this study and other relevant studies. In section 5.7 the resulting design formula is further compared to literature.

Influence water depth

The relative water depth h/λ is one of the main parameters that determines the magnitude of the flow velocities at the bottom. Thus it has a large influence on the amount of scour and has to be included in a design formula. The following relation that was proposed by Xie (1981) for the influence of the relative water depth properly includes the effect.

$$\frac{S_{max}}{H_s} \propto \frac{1}{\left(\sinh \frac{2\pi h}{\lambda_p}\right)^{1.35}}$$

This can be seen in fig. 5.18 were for the permeable breakwater tests this relation has been compared with the individual measurements. Most test results follow this trend. Some outliers are present (red and purple points) because these are the test results for the impermeable revetment and impermeable smooth structure and the given trend line is for the permeable breakwater for which a smaller maximum scour depth is expected.

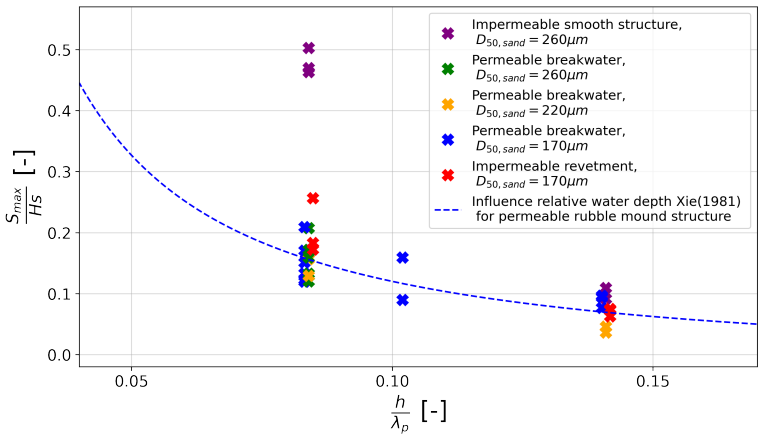

Figure 5.18: Influence relative water depth on maximum scour depth after 8 hours of testing.

Influence wave reflection

In fig. 5.19 the relation of the reflection and the maximum scour depth is considered. In both cases that are given here the relative water depth h/λ_p and the number of waves N is the same for every included test. The only variation is the wave reflection coefficient of the structure. For the long waves (T_p = 2.5s) in fig. 5.19a the relative water depth h/λ_p is 0.084. For the short waves (T_p = 1.6s) in fig. 5.19b the relative water depth h/λ_p is 0.141. For both cases the maximum scour depth of the mean profile after 8 hours of testing is used.
As discussed in section 5.1.3 the quadratic relation fits well with the results for long waves, as can be seen in fig. 5.19a. Especially for higher wave reflection coefficients. For the short waves that are tested accretion is found at the toe, only further offshore a scour-deposition pattern formed. In this pattern an increase in maximum scour

depth for increasing wave reflection is observed. For the short wave tests in fig. 5.19b this is not as clear. Changes in maximum depth are very small for these waves and no clear relation like the quadratic relation for the long waves can be observed. As the longer waves are determined to be the design conditions the quadratic relation is suitable for design wave conditions.

The results of the tests by Xie (1981) that are added in fig. 5.19a are for regular waves. For a vertical wall it is expected that the maximum scour depth is lower for irregular waves than for regular waves. Results are expected to more in the range of the added quadratic relation for 100% wave reflection. The results from Xie (1981) in fig. 5.19b are for irregular waves and show a better fit with the added relation when considering differences in relative water depth.

$$\frac{S_{max}}{H_s} \propto K_r^2$$

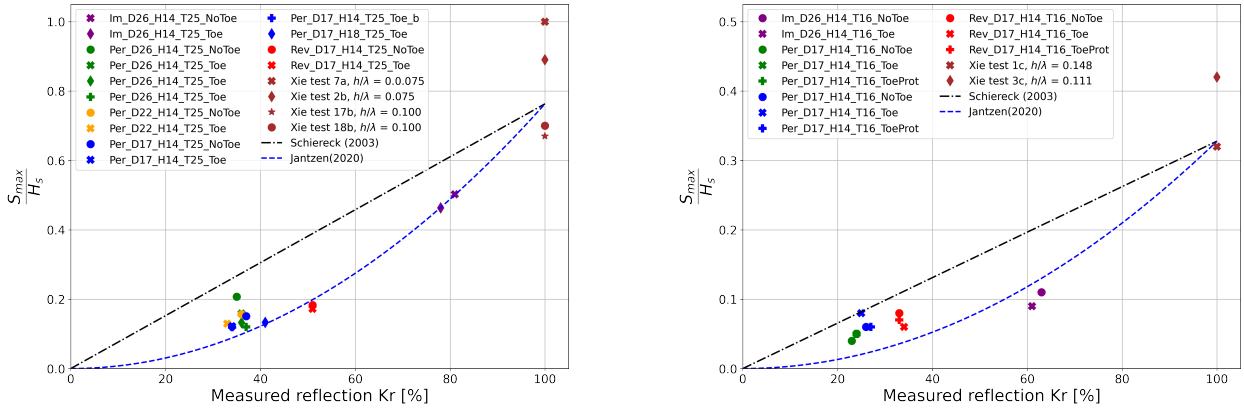

(a) For long waves (T_p = 2.5s).

(b) For short waves (T_p = 1.6s).

Figure 5.19: Influence reflection relation formula Jantzen (2020).

Influence downrush flow

The amount of downrush flow depends on many parameters, as discussed in section 5.1.5, and only has a large influence for cases without a bed protection and a large wave period. These parameters are the relative water depth, the wave steepness, the wave reflection, the roughness of the slope and the permeability of the structure. All these parameters are already included by including the effect of the relative water depth and the wave reflection in the design formula. Overall the design formula does a good job of predicting both the downrush flow scour and the standing wave scour, as these show similar depths. This is further discussed in section 5.6. Because of this no separate parameter is included for the effect of the downrush flow.

Relation number of waves

The influence of the number of waves on the development of scour is discussed in section 4.3. In section 5.5.1 it was found that the design formula from Jantzen (2020) does not describe the rapid increase in maximum scour depth in the first few hours of waves. For longer periods the squared relation used in the formula is a better description. As the main focus are the maximum scour depths that arise over time this relation is suitable. When looking at development over short periods of time (in the order of 0 - 3000 waves) the equation developed by Den Bieman et al. (2019), where a linear relation is used, is more suitable.

Table 5.13: Resulting timescales after which maximum scour depth no longer shows substantial increase, based on photo and laser measurements

Structure	Average K_r [-]	Timescale [hour]	Number of waves [-]
Permeable rubble mound	0.36	2 - 4	4500
Impermeable revetment	0.51	4	6000
Impermeable smooth slope	0.79	4 - 8	9000

The development of the maximum depth of the scour hole for longer periods of time is given in the following relation:

$$\frac{S_{max}}{H_s} \propto \sqrt{\frac{N}{N_s}}$$

$$Where\ N_s = K_r \cdot 12000$$

This relation will be included in the formula in the following way:

$$\frac{S_{max}}{H_s} \propto \frac{1}{K_r^{0.5}} \sqrt{\frac{N}{12000}}$$

The value of N_s included here is based on the findings for the three structures tested in the present study, which are summarised in table 5.13. The value of N/K_r for which most substantial scour has occurred is determined for each structure. Resulting values are given in table 5.14. Here it can be seen that for all structures this value is about 12000. This resulted in the given relation for N_s.

Most designers are interested in the maximum scour depth for a large amount of waves, thus situations where $\frac{N}{N_s} \geq 1$. While this section gives some guidance on the scour periods on smaller timescales. Larger reflection coefficients lead to longer required timescales to come to an equilibrium state and for these cases maximum scour depth for values lower than $\frac{N}{N_s} = 1$ may be relevant.

Table 5.14: Influence number of waves, for tests with long waves

Structure	**K_r [-]**	**N [-]**	**N/K_r [-]**	**calculated N_s [-]**
Permeable rubble mound	0.36	4500	12500	4300
Impermeable revetment	0.51	6000	11765	6100
Impermeable smooth slope	0.79	9000	11392	9500

Effect sediment suspension mode and transport direction

The suspension mode value that is used in the formula is based on the research by Xie (1981). Here two types of scouring patterns were found, being a coarse and a fine sand pattern. A value of 0.3 is used for coarse sand (or bed-load transport) and a value of 0.4 for fine sand (or suspended load transport) is used. In table 5.15 the resulting RMSE and coefficient of determination are given for both values and additionally some in-between values are included. Here it can be seen that the fit of the formula is better for values between the 0.3 and 0.4 than for the used value of 0.3 for bed-load transport. The suspension mode value for which the fit of the formula is best varies between the type of scour that are considered. In general the fit seems to be best for values around 0.35.
As differences are only small and not enough is known on the scaling of sediment it is chosen to keep using the values proposed by Xie (1981). For bed-load transport a value of 0.3 will be used. As no tests are done where suspended load transport is dominant it cannot be judged whether the associated value is also usable for sloping wall structures.

For bed-load dominant transport:

$$\frac{S_{max}}{H_s} \propto 0.3$$

Expected relation for suspended load dominant transport:

$$\frac{S_{max}}{H_s} \propto 0.4$$

Table 5.15: Influence suspension mode value

		No bed protection tests Over first 3/8λ		Including bed protection tests Over first 2λ		No bed protection tests Over first 2λ	
		RMSE [-]	**R^2 [-]**	**RMSE [-]**	**R^2 [-]**	**RMSE [-]**	**R^2 [-]**
Bed-load transport	0.30	0.048	0.80	0.060	0.71	0.052	0.75
	0.33	0.045	0.83	0.052	0.78	0.045	0.81
	0.35	0.047	0.82	0.048	0.81	0.043	0.83
Suspended load transport	0.40	0.055	0.71	0.048	0.81	0.046	0.79

5.6 Resulting design formula

Taking into account all the parameters as discussed in the previous sections results in the formulation of a design formula. This formula will be an extension of the formula developed by Xie (1981) and Jantzen (2020) described in section 2. In section 5.6.1 all test results will be compared with this design formula by Jantzen (2020). Here the capabilities of this formula are judged. Following this in section 5.6.2 an improvement to this design formula is proposed and checked with the model test results.

5.6.1 Design formula by Jantzen (2020)

The design formula proposed by Jantzen (2020), given in eq. (5.8), is similar to the formula that is developed in the previous section. Difference between both formulas is that in eq. (5.8) the amount of waves N_0 for which an equilibrium situation is reached is a constant value while for the newly proposed formula this is changed to N_s which is the amount of waves during which a substantial amount of scour occurs. The value of N_s varies and depends on the type of structure and its associated reflection coefficient.

$$For\ N_0 = 12000\ and\ \frac{x}{L} < 1:$$

$$\frac{S_{max}(N)}{H_s} = \frac{0.3}{\left(\sinh\frac{2\pi h}{L}\right)^{1.35}} K_r^2 \sqrt{\frac{N}{N_0}} \tag{5.8}$$

In fig. 5.20 the expression developed by Jantzen is compared with model tests done in this study and the study by Jantzen. In fig. 5.20a the expression is compared with the scour hole directly adjacent to the structure, over the first 3/8λ from the waterline. In fig. 5.20b it is compared with the maximum depth over the first 2λ. Fort both situations the coefficient of determination has been added. It can be seen that the expression by Jantzen does a decent job at estimating the maximum amount of scour for both cases. Performance is slightly better for the depth of the first hole than for the largest hole over the whole length. Here the formula underpredicts the maximum depth for almost all tests. Additionaly, in table 5.16 the root mean squared (RMS) error for the fit of the empirical relation for multiple test durations is listed.

This underprediction of the maximum scour depth over the whole profile can also be seen in fig. 5.15, which contains the test results for long waves, where the formula by Jantzen has been added for the permeable breakwater, the revetment and the impermeable structure. For all cases the underprediction is visible in this figure. Especially for the first hours it underpredicts the maximum scour depth.
Compared with short waves in fig. 5.16 it can be seen that the formula does no good job at predicting scour for short waves. Here between the different structures no clear difference is visible between the maximum amount of scour, while in the expression by Jantzen the structure and its associated reflection are an important factor in determining the maximum scour depth.

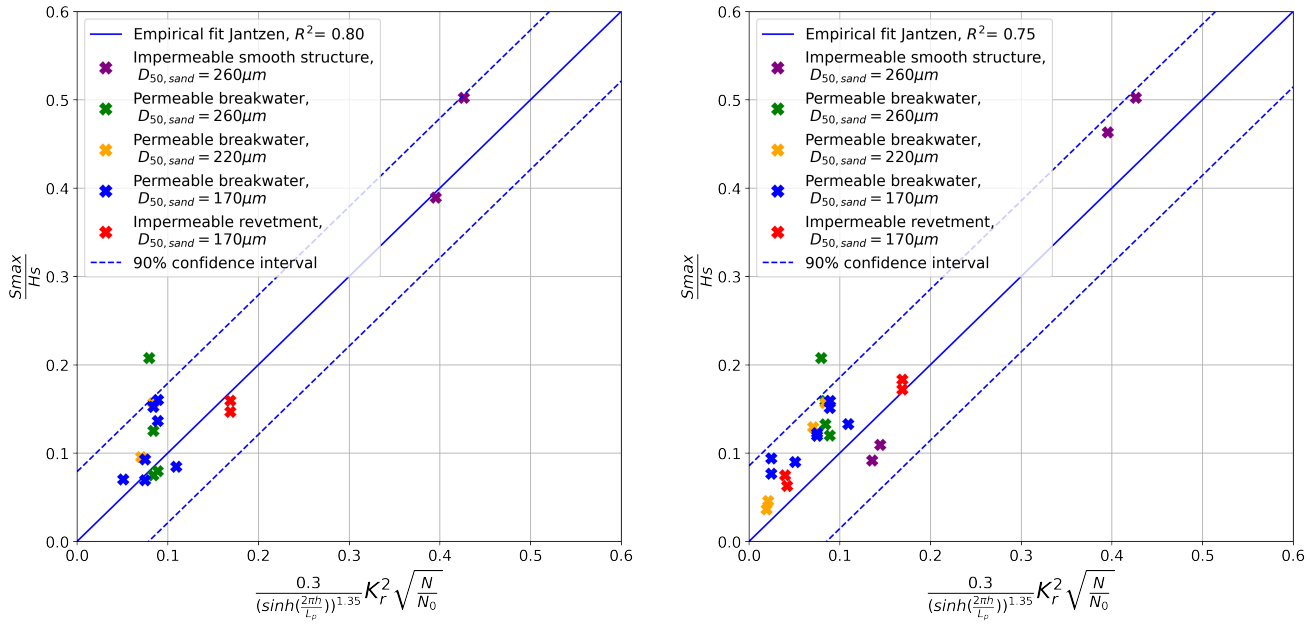

(a) Largest hole first $3/8\lambda_p$ after 8 hours of testing.

(b) Largest hole first $2\lambda_p$ after 8 hours of testing.

Figure 5.20: Comparison empirical relation Jantzen (2020) with measurement data.

Concluding, the expression by Jantzen (2020) is suitable for predicting the maximum depth of the first scour hole, over the first $3/8\lambda$ from the waterline, when considering a large amount of waves with long wave periods and low wave steepness. When looking at a smaller number of waves it underpredicts the maximum scour. For these cases a more conservative and linear approach, like the expression by Den Bieman et al. (2019) is more suitable.
When considering the maximum scour depth over a larger area in front of the coastal structure the expression by Jantzen (2020) gives a decent first estimation when keeping in mind the slight underprediction as seen in fig. 5.20b.

Table 5.16: Root mean square error of test results compared with empirical formula Jantzen (2020)

Area considered	Test duration	Number of tests	R^2 [-]	RMSE - all tests [-]	RMSE - small wave steepness [-]	n	RMSE - large wave steepness [-]	n
First $3/8\lambda$	4 hours	17	0.35	0.063	0.063	17	**Sedimentation**	-
First $3/8\lambda$	8 hours	17	0.80	0.048	0.048	17	**Sedimentation**	-
First $3/8\lambda$	16 hours	17	0.95	0.040	0.040	5	**Sedimentation**	-
First 2λ	4 hours	24	0.41	0.064	0.066	19	0.054	11
First 2λ	8 hours	24	0.75	0.052	0.061	14	0.041	8
First 2λ	16 hours	9	0.88	0.085	0.083	8	0.107	1

5.6.2 Improvement design formula

Below the new design formula is given. This formula is similar to the formula developed by Jantzen (2020), only difference is that N_0 is changed to the relation for N_s which is not a constant but depends on the wave reflection K_r of the structure. In this way the variation in amount of material displaced, which depends on the wave reflection coefficient, is included. For cases with a larger maximum scour depth more material is going to be displaced and for this more waves are needed. Based on model tests with 3 structures varying in wave reflection coefficient it was found that including this relation for N_s makes a good first estimation of including this effect. Rewriting results in the following design formula:

$$\frac{S_{max}(N)}{H_s} = \frac{0.3}{\left(\sinh \frac{2\pi h}{L}\right)^{1.35}} K_r^{1.5} \sqrt{\frac{N}{12000}} \tag{5.9}$$

Performance of the improved design formula with the data of the model tests done in this study is checked in the following section. Here a division is made between the downrush scour hole and the maximum scour depth of all combined processes. A comparison with literature and model data from others is made in section 5.7.

5.6.3 Performance new design formula

Performance of the new design formula is checked with the results of the laser measurements. Comparison is done with both the data on the maximum downrush flow scour depth (the maximum scour depth within $3/8\lambda$ from the waterline) and with the maximum measured scour depth for the whole area in front of the structure (being the first 2λ from the waterline). For both cases this comparison is given in fig. 5.21 after 8 hours of waves. Here the x-axis is the calculated value from eq. (5.9), the y-axis is the measured value. When values are to the left of the line the formula underpredicts the maximum scour depth, when they are to the right of the line the formula overpredicts the maximum scour depth.

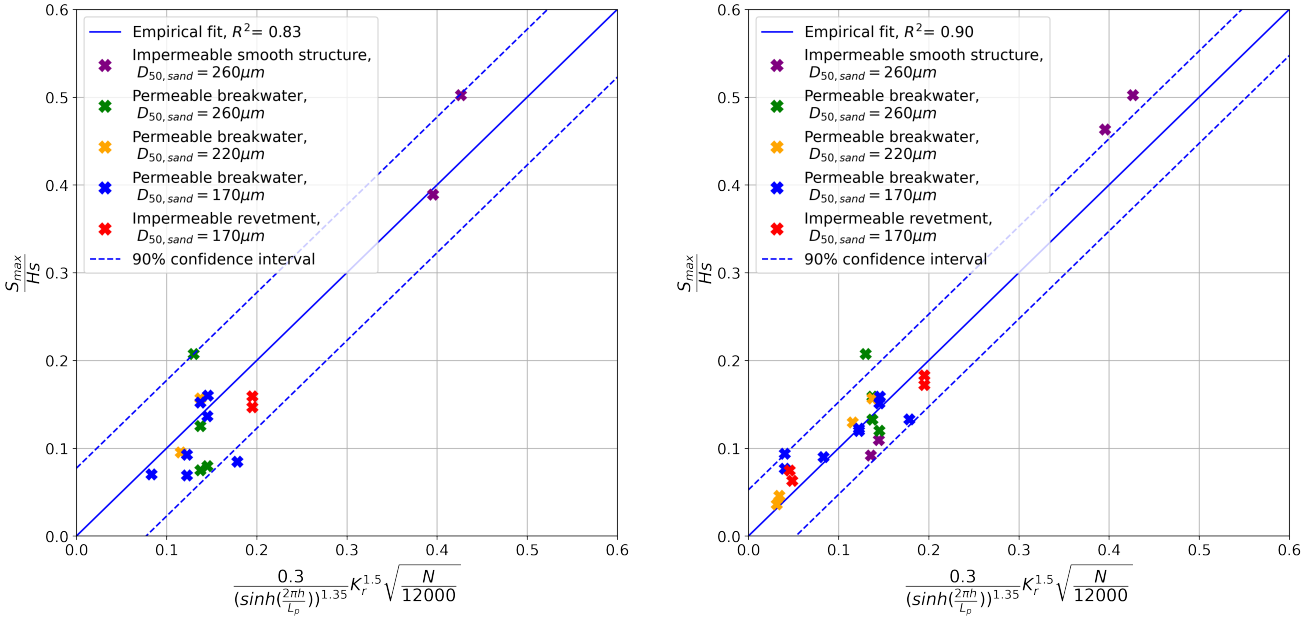

(a) Maximum depth downrush flow scour hole.

(b) Maximum depth scour hole over first 2λ.

Figure 5.21: Comparison new design formula with measurement data, after 8 hours of testing.

Performance for both types of scour is further discussed in the following sections. In table 5.17 the coefficient of determination R^2 and the root mean square error RMSE for the design formulas is given for both types of scour.

Performance for downrush flow scour

The new design formula shows a small increase in performance for the maximum depth of the downrush flow scour hole compared to the original formula. Where for the formula by Jantzen (2020) the coefficient of determination R^2 was 0.80, the value has increased to 0.83 for the adjusted design formula. Also the value of the RMSE has decreased slightly. When comparing fig. 5.21a to the results of the old formula in fig. 5.20a it can be seen that the new formula has mainly influenced the results for the permeable breakwater. With the formula by Jantzen (2020) maximum scour was mainly underpredicted for this structure while for the new formula maximum scour is slightly overpredicted.
A possible explanation for this is that the development of the downrush scour hole does not follow the same relation for N_s. Results from the flow measurements in section 4.4 show that the maximum flow velocity directly at the toe is larger than it is at the first anti-node. Larger flow velocities result in more material being displaced. Therefore it is expected that the development of the depth of the downrush scour hole has another timescale than the development of the standing wave scour holes and that a substantial amount of scour occurs for a different number of waves.

Performance for maximum scour depth

The new design formula shows an improved fit with the data of the maximum scour depth in front of the structure as can be seen in fig. 5.21b. For this maximum scour depth the area 2λ in front of the structure is considered. When compared to the the original design formula developed by Jantzen (2020) the coefficient of determination R^2

has significantly increased for all measurement moments, also the value of the RMSE has decreased. Making the number of waves N_s dependable on the wave reflection coefficient K_r therefore seems a good addition to improve the formula for maximum scour in the area in front of the structure.

Table 5.17: Comparison between new design formula and design formula by Jantzen (2020)

Area considered	Formula	Test duration	Number of tests	R^2 [-]	RMSE - all tests [-]	RMSE - small wave steepness [-]	n	RMSE - large wave steepness [-]	n
First 3/8λ	Jantzen (2020)	4 hours	17	0.35	0.063	0.063	17	**Sedimentation**	-
First 3/8λ	New formula	4 hours	17	0.70	0.041	0.041	17	**Sedimentation**	-
First 3/8λ	Jantzen (2020)	8 hours	17	0.80	0.048	0.048	17	**Sedimentation**	-
First 3/8λ	New formula	8 hours	17	0.83	0.046	0.046	17	**Sedimentation**	-
First 3/8λ	Jantzen (2020)	16 hours	5	0.95	0.040	0.040	5	**Sedimentation**	-
First 3/8λ	New formula	16 hours	5	0.96	0.037	0.037	5	**Sedimentation**	-
First 2λ	Jantzen (2020)	4 hours	24	0.41	0.064	0.066	14	0.054	8
First 2λ	New formula	4 hours	24	0.68	0.046	0.044	14	0.048	8
First 2λ	Jantzen (2020)	8 hours	24	0.75	0.052	0.061	14	0.041	8
First 2λ	New formula	8 hours	24	0.90	0.032	0.039	14	0.033	8
First 2λ	Jantzen (2020)	16 hours	6	0.80	0.082	0.072	5	0.107	1
First 2λ	New formula	16 hours	6	0.92	0.050	0.032	5	0.107	1

Overall the new addition to the design formula improves the results for the model tests done in this study for all measurements done after 4, 8 and 16 hours of testing as can be seen in table 5.17. Especially predictive capabilities for the maximum scour depth in the first 2λ in front of the structure the formula has significantly increased. For the downrush flow scour accuracy is a bit lower but still good. Also, a large improvement is made for the predictive capabilities after 4 hours of testing.

Applicable range design formula

Based on the performance for both cases of scour the applicability of the formula for both cases is formulated. Here a division is again made for using the formula to predict the maximum depth of the downrush scour hole and to predict the maximum depth of the standing wave scour over the whole area in front of the structure. The formula is applicable when:

For the maximum downrush scour hole depth:

$$x < \frac{3}{8}\lambda_p \ \ and \ \ \frac{W_{p,t}}{\lambda_p} < \frac{3}{8}\lambda_p$$

For the maximum scour depth of the standing wave scour in front of the structure:

$$x > \frac{3}{8}\lambda_p \ \text{ and } \ \frac{W_{p,t}}{\lambda_p} < \frac{3}{8}\lambda_p$$

The value of x here is the distance of the end of the considered area from the waterline, where the waterline is zero. An indication of the definition of the parameters used is given in fig. 5.22.

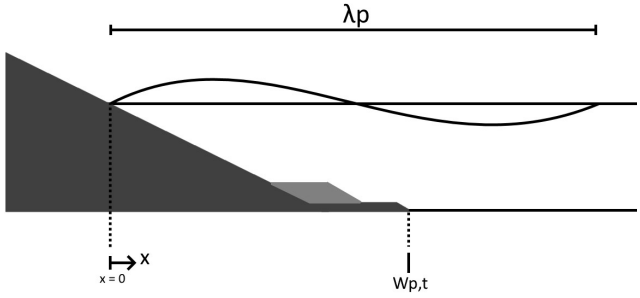

Figure 5.22: Sketch parameters validity formula

Performance for cases where $N > N_s$

When designing a coastal structure the maximum scour depths for long periods of time are of most interest. In these cases often the number of waves N will be larger than the number of waves N_s during which a significant amount of scour occurs. When comparing the measured development of the maximum scour depth with the design formula there are two options for cases where $N > N_s$. (1) When the number of waves N is equal or larger than the value of N_s the equilibrium depth is reached and $\frac{N}{N_s} = 1$ should be used. (2) For a large number of waves the square root relation in the formula results in only a small increase in maximum scour depth when $N > N_s$. This matches with the measurements in the present study and therefore the relation may still be suitable for most cases and values of N larger than N_s can be used.

Comparison between the measurements results and the formula by Jantzen (2020) is done using option 2 in fig. 5.15, fig. 5.16 and fig. 5.17 in section 5.5. In the tests in the present study a constant loss of sediment was observed for waves with a low wave steepness which resulted in a constant lowering of the bed profile. This method properly includes this effect as the maximum scour depth still increases when $N > N_s$.

Both methods are added in fig. 5.23 and in fig. 5.24 where they are compared with the maximum scour depth over the first $3/8\lambda$ and 2λ from the waterline. Here from the moment when N is equal to N_s there is a separation in predicted values. For each structure the bottom line represents option 1, here the maximum scour depth becomes constant. Only a small constant increase is added to include the constant loss that was found in section 5.5.1. The top line represents option 2, here the maximum scour depth still follows the square root relation.

When comparing the figures a difference in performance for both methods is visible. For the downrush flow scour hole measured values fit well with both prediction methods. For the maximum depth over the larger area in front of the structure method 2 seems to give better results. This is a result of the variation in timescale between development of the downrush flow scour and the standing wave scour.
The value of N_s has been based mainly on development of the downrush flow scour hole. The downrush flow scour hole is found to reach a somewhat constant state faster than the standing wave scour pattern. Therefore using the current method of calculating N_s in combination with using $\frac{N}{N_s} = 1$ for a number of waves larger than N_s gives good results for the downrush flow scour hole.
The maximum depth over a larger area in front of the structure is found to take longer to reach this state than the downrush flow scour hole. Therefore method 2, for which the depth still increases after reaching N_s, shows better results for the larger area in front of the structure.

As method 2 shows good results for both types of scour with the test results from the present study it is chosen to use this method in the design formula. Using this method may be slightly conservative when considering a very large number of waves as it seems to overestimate the maximum depth of the downrush scour in these cases. As the downrush flow scour hole is closest to the structure and therefore potentially has the largest influence on failure of the structure some conservatism is deemed acceptable. Whether the found relation for the number of waves is also valid for cases outside of the testing range or when scaling to prototype situation is unknown. Using this method results in the following design formula for maximum scour:

$$For\ N \leq 24000:$$

$$\frac{S_{max}(N)}{H_s} = \frac{0.3}{\left(\sinh \frac{2\pi h}{L}\right)^{1.35}} K_r^{1.5} \sqrt{\frac{N}{12000}} \tag{5.10}$$

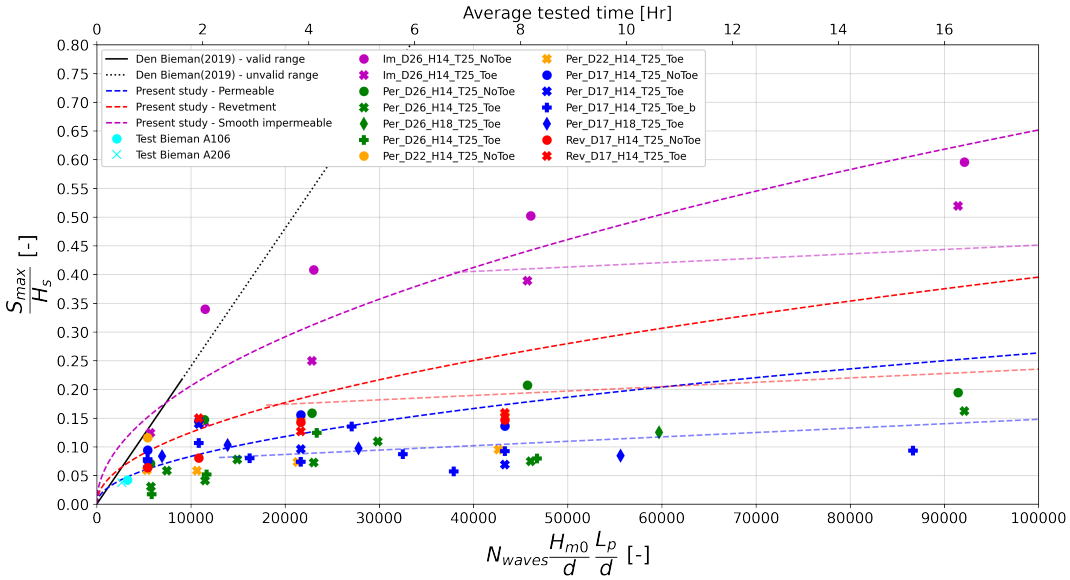

Figure 5.23: Comparison methods for cases where N > N_s, max scour depth first $3/8\lambda$.

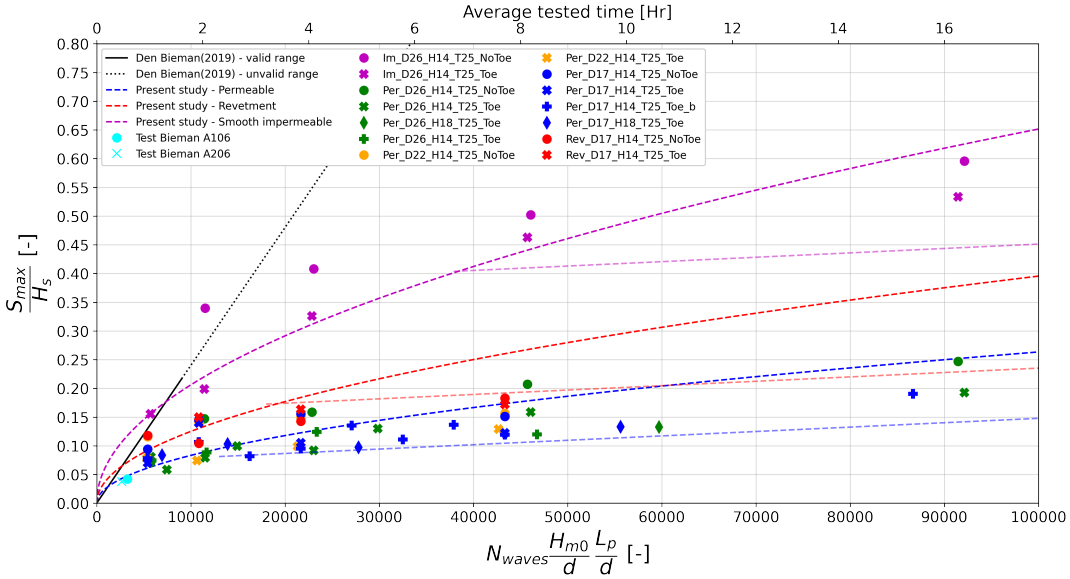

Figure 5.24: Comparison methods for cases where N > N_s, max scour depth first 2λ.

Influence length of bed protection

The presence of a bed protection is not included within the design formula. A bed protection is generally designed when it is found, with for example this design formula, that a large amount of scour occurs near the structure which can results in instabilities or failure of the structure.
When comparing model test results with a bed protection to model test results where no bed protection was used it was found that the largest scour depth occurred for the cases with a bed protection. It is expected that this happened due to a combination of the downrush flow scour and the presence of a standing wave anti-node close to the end of the protection layer. The design formula slightly underpredicts the maximum scour depth in these cases as it does not include this combined effect. This combined effect is also something to keep in mind when the toe of the breakwater is close to the location of the standing wave anti-node. Generally this is only the case for short waves (which were determined not to be the design conditions for scour in front of sloping structures) or for very mild sloping structures (which result in a low wave reflection coefficient).

Effect sand grain diameter

No significant influence of the sand grain diameter on maximum scour for variations of grain diameter was observed in this study, as described in section 5.4. Xie (1981) also found no obvious influence of the grain diameter on the development of the scour depth. Sumer and Fredsøe (2000) state that the grain diameter only slightly influences the scour pattern. Here for a decrease in particle size a small decrease in scour depth was observed. This pattern was not clearly observed in this study.

Based on both the results of this study and the findings in literature no parameter describing the sand grain diameter is included in the design formula.

5.7 Comparison with other literature

In this section the results and observations of the tests done in this study will be compared with literature. Here the focus will be on the predictive capabilities of the expressions for scour development. For this comparison will be done with test results from this study. Additionally the new design formula will be compared with test results from literature. Most of the literature that is used here also comments on the influence of sediment size and the type of sediment transport. This is discussed in section 5.3, section 5.4 and in section 6.
In section 5.7.1 a comparison will be made with the work of Xie (1981) where scour in front of a vertical wall breakwater was studied and expressions were developed for the development of scour over time. In the following section, section 5.7.2, additional investigations by Sumer and Fredsøe (2000) are added. Here the expressions from Xie (1981) were further developed for the case of sloping wall breakwaters. After this, in section 5.7.3, the more recent work by Den Bieman et al. (2019) is studied. Here also an expressions is developed which can be used to estimate scour in front of a sloping structure. Finally, the approach developed in this study which is based on work by Xie (1981) and Jantzen (2020), is compared with the available test results from this studied literature in section 5.7.4.

5.7.1 Comparison with Xie (1981)

Xie (1981) came up with two expressions to describe the increase in scour over time. The expressions are made for coarse material and fine material. This division is based on the coarse and fine scouring patterns that were found by Xie which depend on whether bed-load or suspended load transport is dominant. In **??** it was concluded that the bed-load transport regime, and thus the coarse pattern, is dominant for all tests done in this study. Comparison will therefore be done with eq. (5.11) and eq. (5.12). In **??** it was observed that the bed profile in front of a sloping wall does not follow the coarse pattern that is described by Xie. For this coarse transport regime Xie found scour halfway between the nodes and anti-nodes while for the sloping wall scour is found at the anti-nodes. The position of deposition is found to be at the nodes, which is in line with the coarse pattern by Xie.
As for a vertical wall no downrush is present this was not included in the study by Xie. Here no scour was present directly adjacent to the structure. The first scour hole formed at a distance of about 1/8 wavelength from the structure. An equilibrium scour depth was reached after about 4 hours. For irregular waves it is found that reaching an equilibrium takes twice as long. For the long waves tested in the present study the somewhat equilibrium condition was reached after about 4 to 8 hours of testing for structures with high wave reflection coefficients. It was also found by Xie that for a vertical wall the node anti-node scour patterns lasts for a distance of 4 wavelengths away from the breakwater for irregular waves. For the long waves tested in this study the sand bed only has a length of about 2 wavelengths. In this area the node anti-node scour pattern is still clearly visible.

Xie stated that the usage of a bed protection layer resulted in a decrease in depth of the first scour hole, as can be seen in fig. 2.3. It was found that no scour hole was present for a bed protection with a length of 3/8 wavelength. In this study this patterns is not observed. For the cases with a bed protection with this length the scour hole that forms directly in front of the protection is larger than it is without a bed protection. For a sloping wall there is downrush scour present which causes high flow velocities resulting in scour directly at the end of the structure. As for a vertical wall no downrush flow is present no downrush flow scour is present at the end of the protection layer. As a result, for these cases no significant scour can be expected when ending the protection just past the first scour hole of the standing wave pattern.

For estimating the maximum depth of the scour hole Xie developed eq. (5.12), where based on the relative water depth the maximum dimensionless scour depth can be calculated. This equation is only suitable for a vertical wall

and bed load sediment transport. By replacing the value of 0.3 with 0.4 the equation is made suitable for a case where suspended load transport is dominant. As the applicability of this equation is limited it was decided in both Sumer and Fredsøe (2000) and the present series of studies to expand on this expression and make it suitable for cases with sloping structures where not all wave energy is reflected.

$$\frac{Z_s}{Z_{sm}} = \left(\frac{t}{t_{max}}\right)^{0.4} \tag{5.11}$$

$$\frac{S_{max}}{H_s} = \frac{0.3}{\left(\sinh\frac{2\pi h}{L}\right)^{1.35}} \tag{5.12}$$

5.7.2 Comparison with Sumer and Fredsøe (2000)

An extension was done on the work of Xie (1981) by Sumer and Fredsøe (2000) to make the expression for the maximum scour depth applicable for sloping structures. Here the term in the upper part of the equation (which depends on the type of sediment transport) is replaced by a function depending on the slope of the structure, given in eq. (5.14). This is based on a rubble mound sloping structure and is applicable for slopes in the range of $30° < \alpha < 90°$. Adding this expression into eq. (5.12) results in eq. (5.13). Both the expression by Xie and Sumer and Fredsøe are compared wit the results of this study. In fig. 5.25 the maximum scour depth for the individual tests with the permeable breakwater after 2, 4 and 8 hours of testing are compared with both methods. As expected the approach by Xie heavily overestimates the amount of scour as this is based on vertical walls. The method by Sumer gives a good first estimation of the amount of scour. Important to note here is that the trendline here is for regular waves, a small amount of waves and a structure with a 1:1.75 slope as a 1:2.0 slope is outside the range of application for eq. (5.14). These notes give a good indication of the shortcomings of this approach.

$$\frac{S_{max}}{H_s} = \frac{f(\alpha)}{\left(\sinh\frac{2\pi h}{L}\right)^{1.35}} \tag{5.13}$$

Where $f(\alpha)$ is:

$$f(\alpha) = 0.3 - 1.77\exp\left(-\frac{\alpha}{15}\right) \tag{5.14}$$

Where α is the breakwater slope in degrees in the range of $30° \leq \alpha \leq 90°$.

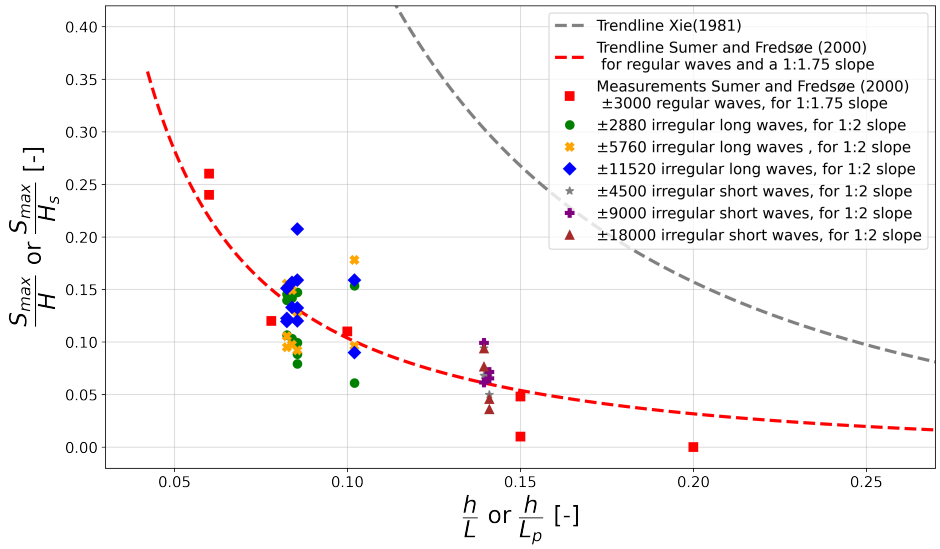

Figure 5.25: Comparison results rubble mound breakwater with Sumer and Fredsøe (2000).

Sumer and Fredsøe (2000) further investigated the time scale of the scour process for rubble mound breakwaters and came up with a nondimensional time scale for scour. This expression is given in eq. (5.15), where T_s is the time scale for which a substantial amount of scour occurs. It was found that for decreasing values of the relative water

depth h/λ the nondimensional time scale increases. Sumer and Fredsøe (2000) state that for a decreasing relative water depth the scour depth increases and more sediment has to be removed, resulting in an increase in time scale. Although the found values for the nondimensional time scale are at best suggestive they may help with assessing the time scale for corresponding real-life situations (Sumer and Fredsøe, 2000).

$$T^* = \frac{\left[g(s-1)d_{50}^3\right]^{1/2}}{H^2} T_s \tag{5.15}$$

5.7.3 Comparison with Den Bieman et al. (2019)

Den Bieman et al. (2019) found a linear relation between the maximum scour depth and the number of waves, this relation is plotted in fig. 5.15, fig. 5.16 and fig. 5.17. Additionally, two of the eleven tests done in their research, on which the relation is based, are added in these figures. Both tests are for similar wave conditions as the long waves in this study and can therefore be compared with results of the present study. The developed equation is given in eq. (5.16). Here the normalized wave height, peak wave length and water level above the toe are used, these are also used on the horizontal axis in fig. 5.15, fig. 5.16 and fig. 5.17. In this equation a calibration constant C_{out} is is used. This constant is derived from measurements and has a value of $C_{out} = 2.4 \cdot 10^{-5}$.
The equation is only valid for less than 3000 waves as only short test durations, in the order of 1 hour, were used. For this range, that can be seen in the three figures, the equation seems to be a conservative approach for predicting the scour depth. The linear trend is fitting as the scour increases rapidly in the first hours of testing. When the duration of test increases further the increase in depth becomes smaller. For these duration the equation by Den Bieman et al. (2019) is, as the given validity range states, no longer valid as it heavily overpredicts the depth of the scour hole. The equation is also not valid for longer durations as the increase does no longer follow a linear trend.

$$\frac{\Delta z_{b,scour}}{H_{m0}} = C_{out} \cdot N_{waves} \frac{H_{m0}}{d} \frac{L_p}{d} \frac{d_{toe}}{d} \tag{5.16}$$

Concluded, the equation by Den Bieman et al. (2019) is a good first estimate for scour in front of a sloping structure, when only interested in scour for a low number of waves. It seems to slightly overpredict the maximum scour depth found for tests in this study but can work as a conservative estimation. When interested in the scour for a large number of waves the equation is no longer suitable. It should therefore only be used for the validity range that is given in Den Bieman et al. (2019).

5.7.4 New design formula compared with model test results from literature

Because of the shortcomings of the three methods that are described above the current series of studies was done to further research processes that cause scour in front of sloping embankments. In the present study this resulted in the following design formula that was derived in section 5.6:

$$For\ N \leq 24000:$$
$$\frac{S_{max}(N)}{H_s} = \frac{0.3}{\left(\sinh \frac{2\pi h}{L}\right)^{1.35}} K_r^{1.5} \sqrt{\frac{N}{12000}} \tag{5.17}$$

From the literature that is described in the previous sections, results of model tests will be compared with the design formula. From these studies only tests that were done with irregular waves will be considered as these show significant differences with tests that are done for regular waves. All tests of which the maximum scour depth, the relative water depth, the incident wave height and the wave reflection coefficient is known are added in the comparison. When the wave reflection is not given in literature an approximation it is calculated with the approach of Zanuttigh and Van der Meer (2007) using the given wave conditions and structural geometry.

Tests results by Xie (1981) and Sumer and Fredsøe (2000) are added in fig. 5.26 where also the results for the maximum scour depth in the first $3/8\lambda$ for tests done in this study are given. Measurements by Xie (1981) are done of the first scour hole in front of the vertical structure. Sumer and Fredsøe (2000) measured the maximum scour depth at or near the breakwater, similar to the measurement in the first $3/8\lambda$ in the present study.
It can be seen here that the tests by Xie (1981), where only two successful tests with irregular waves were done, fit well with the predicted values of the design formula for reflection of all wave energy. This is as expected as for this case the formula is the same as the original formula of Xie.

The results by Sumer and Fredsøe (2000) show larger deviations from the predicted values of the design formula. Here the measured values are all lower than the predicted values. The exact explanation for this is not known. As the wave reflection coefficients are not given in Sumer and Fredsøe (2000) the values used here are an approximation. The influence of this is expected to be relatively small and not the cause of these significant differences.
A possible explanation for the large deviation is that Sumer and Fredsøe (2000) tested with a smaller number of waves. They found for one of the tests with irregular waves and a wave reflection coefficient of 0.95 that an equilibrium was already reached after about 1500 waves. This is much lower than the value of N_s = 9500 that is found for the most reflective structure in this study.
All tests by Sumer and Fredsøe (2000) were done with a rubble mound structure. It is found in this study that the roughness of the structure plays an important part in the depth of the downrush flow scour hole directly at the toe of the structure. Three structures with a constant slope but varying in roughness were tested with the same wave conditions in the present study. For a decrease in roughness the downrush flow scour shows a significant increase. This is a result of an increase in flow velocities at the toe of the structure caused by the wave run-down on the surface of the structure. For more rough structures more energy is absorbed, resulting in lower flow velocities at the toe. This effect is similar to the height of wave run-up decreasing with an increasing roughness. The test results for the maximum depth of the downrush flow scour hole from Sumer and Fredsøe (2000) are similar to that of rubble slopes in the present study. It is therefore expected that besides the wave reflection coefficient the roughness of the structure and possibly the slope angle also have to be included in a design formula to better predict the maximum depth of the hole directly adjacent to a sloping structure.

For the cases with a larger relative water depth no scour at the toe of the structure is observed for the results of Sumer and Fredsøe (2000). Here only the the maximum depth of the first hole in front of the structure was considered, similar to the downrush flow scour in the first $3/8\lambda$ in the present study. As can be seen in fig. 12c of Sumer and Fredsøe (2000) for a $h/\lambda = 0.13$ no scour hole formed directly in front of the structure, while a scour hole formed at the anti-node at a distance of $1/2\lambda$. This was also observed for the tests in the present study with a similar relative waterdepth, as can be seen in fig. 5.26.

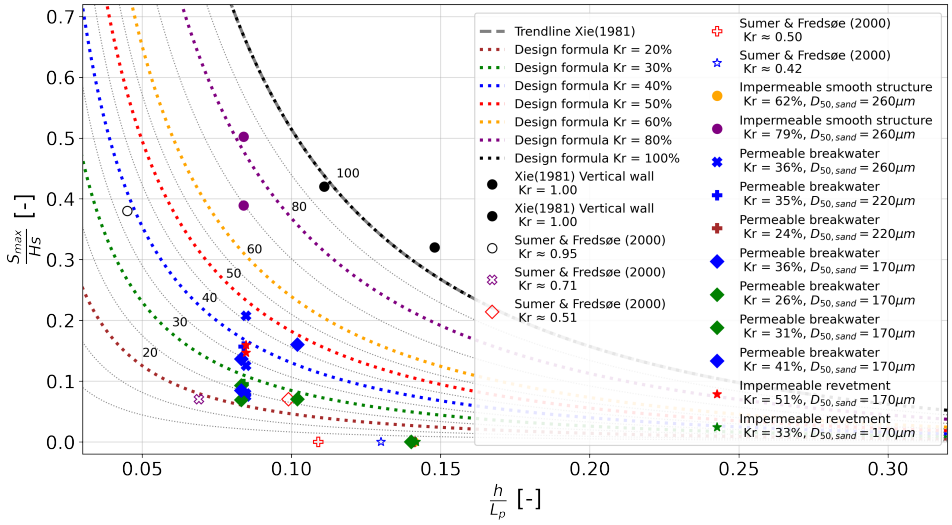

Figure 5.26: Design formula for 12000 waves with test results (first $3/8\lambda$) and model results Xie (1981) and Sumer and Fredsøe (2000).

Comparison of the results from Sumer and Fredsøe (2000) with the formula for the maximum scour depth in the first 2λ in front of the structure is not possible as only the depth of the scour hole directly at or near the structure is reported. For comparison the results have nevertheless been added. In fig. 5.27 the results from the present study and results from Xie (1981) are compared with the new design formula and the influence of the amount of wave reflection. Here again it can be observed that performance of the design formula in determining the maximum scour depth over the first 2λ is good. When comparing these figures it can be seen that not for all tests the downrush flow scour hole was the largest hole that formed after 8 hours of testing. Also when considering a larger area it can be seen that for cases where no downrush flow scour hole forms further offshore there is scour of which the depth can be estimated using the design formula.

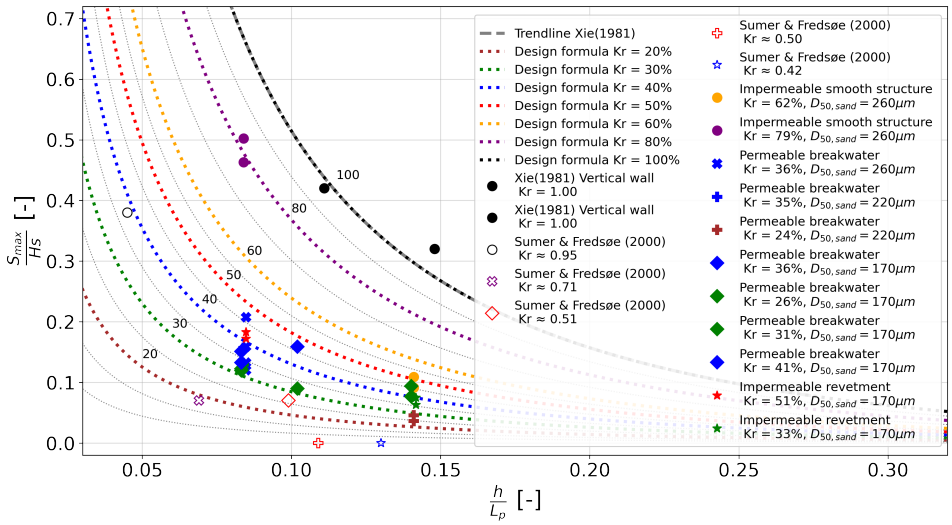

Figure 5.27: Design formula for 12000 waves with test results (first 2λ) and model results Xie (1981) and Sumer and Fredsøe (2000) for downrush flow scour hole.

Based on the situations tested in the present study and the comparison done with available literature the following test range is added that describe for which conditions the formula is determined. Here a division is made between using the formula for predicting the maximum depth of the downrush scour hole and for the maximum scour depth over the whole area in front of the structure.

Table 5.18: Tested range for which eq. (5.17) is found to be suitable for predicting maximum scour depth of the whole area in front of the structure.

Variable	**Range of testing**
Relative water depth [-]	$0.05 \leq \frac{h}{\lambda} \leq 0.15$
Wave reflection coefficient [-]	$K_r > 0.2$
Offshore wave steepness [-]	$1.4 \leq s_{o,p} \leq 3.5$
Nearshore wave steepness [-]	$2.6 \leq s_{n,p} \leq 4.1$
Ratio number of waves [-]	$\frac{N}{N_s} \geq 0.5$
Ratio wavelength to sand diameter [-]	$16000 \leq \frac{\lambda_p}{D_{50,sand}} \leq 28000$
Permeability structure [-]	Permeable & Impermeable
Roughness structure [-]	Rough rubble layer & Smooth layer

Table 5.19: Tested range for which eq. (5.17) is found to be suitable for predicting maximum downrush flow scour depth.

Variable	**Range of testing**
Relative water depth [-]	$0.05 \leq \frac{h}{\lambda} \leq 0.10$
Wave reflection coefficient [-]	$K_r > 0.2$
Offshore wave steepness [-]	$1.4 \leq s_{o,p} \leq 1.9$
Nearshore wave steepness [-]	$2.6 \leq s_{n,p} \leq 3.4$
Ratio number of waves [-]	$\frac{N}{N_s} \geq 0.5$
Ratio wavelength to sand diameter [-]	$18000 \leq \frac{\lambda_p}{D_{50,sand}} \leq 28000$
Permeability structure [-]	Permeable & Impermeable
Roughness structure [-]	Rough rubble layer & Smooth layer

6 Discussion

The aim of this research is to fill the current lack in available prediction methods for wave-induced scour in front of sloping coastal structures. For this a total of 34 model tests, including those by Jantzen (2020), have been done in which several parameters have been varied. Variations are in wave conditions, structural properties, test duration, toe and bed protection layouts and sediment grain size. The result is a large data set which is used to create a design formula useful for a first estimate of the maximum scour depth development in front of a sloping structure.
In this section the results of this study will be discussed. The relevance of the results and the addition these results provide to present literature is discussed. Additionally, some expectations are given for maximum scour depths for sloping structures that are useful when designing these structures. Afterwards, not included aspects that may be of influence in prototype situations and shortcomings of the present study are discussed. In addition some observations with respect to literature are given, also possible scale effects are discussed. This section supports the conclusions and recommendations that are given in the next sections.

Addition results to literature

The currently available approaches are only suitable for steep rubble mound structures and regular waves (Sumer and Fredsøe (2000)) or for a low number of waves for which no equilibrium maximum scour depth was yet reached (Den Bieman et al. (2019)). Model tests in the present study were, in addition to a rubble mound structure, done for a revetment structure and a smooth sloping structure. Also, long testing times were used which resulted in the maximum scour depth showing only small changes after a larger number of waves. Contrary to Sumer and Fredsøe (2000) no clear equilibrium scour depth was found. This may be a results of downrush flow influence or the presence of a large-scale transport of sediment that was observed. However, for design purposes the maximum depth of the holes that form directly adjacent to the structure and at the first anti-node in front of the structure are usually important. In that respect the developed formula provides reliable (RMSE = 0.03 - 0.05) results to calculate the scour depth at both locations for a large number of waves.

Relation results to design situations

It is clear from the present study that for sloping wall coastal structures maximum scour depths can be much lower than the incident wave height H_s in the case of irregular waves. Especially for rubble mound and rough structures maximum depths are much lower. For 1:2.0 slopes the longest waves show maximum depths of about 0.5 H_s. Only for smooth structures maximum depths in the order of 1.0 H_s can be expected for very long waves. For cases where the relative water depth $0.075 \leq \frac{h}{\lambda_p} \leq 0.100$ the maximum depth rapidly decreases and is in the order of 0.25 H_s for rubble mound an rough structures. For smooth structures the maximum depth is in the order of 0.5 H_s.

The largest maximum scour depths have been observed for waves with a low wave steepness. As a result, more operational swell conditions may results in larger maximum scour depths than possible design conditions where waves may be steep. Especially as no clear equilibrium has been observed in the present study, operational wave conditions can lead to large depths as they are present more often resulting in a large amount of waves. The formula developed in this study shows good results with tests for a large amount of waves. How this number of waves translates from the model to specific prototypes situations depends on the scale factor.

Maximum scour that forms due to standing waves can be properly predicted with the relation for the wave reflection K_r. This thesis shows that the effect of K_r is less than K_r^2 for some structures. It seems that for some most scour is expected earlier than for other structures. Therefore, the formula has been updated to $K_r^{1.5}$. Theoretical background for this has not yet been found, but the results give good agreement with this formula. Holes that form directly adjacent to the structure when no protection layer is present are harder to predict as here also the slope and the slope surface directly influence the scour depth.

Aspects and shortcomings to consider

When using the results of the present study one should take the following aspects into account:

- Only tests have been done where bed-load conditions are dominant. When considering cases where suspend load is dominant performance of the associated design formula has not been judged.

- Test conditions with a large wave steepness (s > 3%) in front of the structure showed accretion of sediment at the toe of the coastal structure. The exact reason for this behaviour is not known. But results are consistent with other publications, Sumer and Fredsøe (2000) and Jantzen (2020).
- The bed in front of the structure used in the model is horizontal. Many coastal structures have a sloped foreshore in front, therefore results may differ in these cases. For these cases the water depth decreases when waves propagate and the wave properties are influenced. Therefore, results may look different for these cases. It was chosen to use a horizontal bed in this study as first the physics of the more simple horizontal bed need to be understood. For further research sloping beds are recommended.
- In the present study the parameter N_s is introduced to describe the number of waves during which a substantial amount of scour occurs. Some discussion on this parameter for cases where the number of waves N is larger than N_s is already done in section 5.6.3. For results in the present study it is found that continuing with the square root relation for these cases is suitable. A case can also be made for using a maximum value of $\frac{N}{N_s} = 1$ as at some point an equilibrium depth will be reached. In the end it is chosen to use the square root relation in the developed formula as it best describes the model results.

For the developed design formula a table with the testing range is given for both the downrush flow scour hole adjacent to the structure and the complete area in front of the structure. This testing range gives an indication for which conditions the formula is expected to be valid. For cases outside of this range the formula may still be valid, but this is not checked in the present study. Some comparison is done with results from other studies in section 5.7.4. But, as described, only a low number of tests is available from literature for irregular waves. Tests that are available were done for a low number of waves or for steep structures for which downrush flow velocities are expected to be lower. Also, only the maximum depth of the first scour hole was reported in the available literature.

Influence downrush flow

On the influence of the downrush flow on the maximum scour depth a lot still remains uncertain. It is expected that only the hole that forms directly in front of the structure is influenced by the downrush flow. For an increase in roughness and permeability of the structure a decrease in maximum depth of this hole is found in the present study. It is expected that a change in slope angle also influence the downrush flow and the maximum scour depth.

When a bed protection is used it is not known whether the downrush flow extends over the layer and if the flow velocities are influenced by this. Whether the downrush flow therefore also leads to scour in front of a protection layer is therefore unknown.
Development of the scour hole directly adjacent to the structure is found to follow a similar pattern as development of the maximum standing wave scour depth. After a rapid increase development slows down and reaches a somewhat equilibrium condition. For the downrush flow scour this condition seems to be reached earlier than for the standing wave scour. The amount of waves required for reaching this condition varies depending on the type of tested structure. It is expected that this is due to larger flow velocities being observed at the toe than at the anti-nodes of the standing wave pattern.

Smith (1996) states that the bottom velocity increases with increasing wave reflection up to a maximum velocity. In the case of a 1:2.0 slope maximum bottom velocity was observed for reflection coefficients in the range of 0.44 - 0.48. For higher reflection coefficients the offshore directed bottom velocity decreased slightly with increasing reflection, resulting in a decrease in scour potential directly at the structure. These model test done by Smith (1996) were for shallow water, h/λ in the range of 0.05 - 0.10, similar to the present study.
This pattern was not observed in the present study. Here flow measurements for cases with higher reflection coefficients still showed an increase in maximum flow velocities. A possible explanation for this is that in the present study the increase in wave reflection was the result of variations in roughness of the structure while in Smith (1996) the slope angle of the structure was varied. Smith (1996) did observe maximum flow velocities for minimum deep-water wave steepness like in the present study. For the results of the present study the influence of the wave reflection coefficient K_r included in the formula properly predicts the maximum depth of the first hole adjacent to the structure. Whether this included relation of K_r also shows good result when using the formula for cases with a different slope angle is not known.

Bed protection

Based on the observations in section 5.2, when designing the toe and possible bed protection at the foot of a slopping coastal structure, it is advised to determine the standing wave pattern for the design wave conditions. The structural end can than be compared to the location of the nodes and anti-nodes of the standing wave pattern. This will help with determining whether a bed protection is beneficial and what length it should be. Also, the influence of the downrush flow, as discussed in section 5.1.5, should be taken into account as this often is the main process for the scour hole directly in front of the structure.
Considering the findings in this study, scour protection should be designed for waves with small wave steepness (s < 3%) near the structure as these result in the largest amount of erosion. A possibility is that the more frequent swell wave conditions are the design conditions instead of more extreme storm condition where wave periods are shorter and waves are steeper. When considering a bed protection design for the wave condition for which the largest amount of scour is expected it is advised to check this design also for other extreme conditions. Other conditions may result in a combined effect of downrush flow scour and standing wave scour that leads to a larger maximum scour depth than for the wave conditions for which the design is made.

The location of the scour hole compared to the main structure is important. Once a deep scour hole is located sufficiently far away from the structure, the geotechnical stability of the main structure can still be sufficient. This geotechnical stability is outside the scope of this research.

Observed scour-deposition pattern

A difference in scour-deposition pattern is observed between the results of Xie (1981) and that of Sumer and Fredsøe (2000) and the present study for cases where bed load transport is dominant. Xie (1981) found that scour is present halfway between the nodes and anti-nodes and that material is deposited at the nodes of the standing wave pattern. In Sumer and Fredsøe (2000) and the present study (both with sloping structures) scour was found at the anti-nodes and deposition at the nodes of the standing wave pattern. It is important to note that the test by Xie (1981) have been done with regular waves to investigate scour in front of a vertical wall and the tests by Sumer and Fredsøe (2000) have been done with regular and irregular waves using the JONSWAP wave spectrum to investigate scour in front of a rubble mound breakwater. For both regular and irregular waves the same pattern was observed by Sumer and Fredsøe (2000). In the present study also the JONSWAP wave spectrum has been used.
A clear explanation between the differences in scour-deposition pattern between these studies is not found. Whether the found patterns by Xie (1981) for bed-load and suspended load are valid for a sloping structure is therefore questionable. Also, whether such a distinct difference as described by Xie (1981) from one pattern to the other for variations in sediment particle size is realistic or that it changes more gradually and a lot of in between patterns are possible remains uncertain. Therefore, whether changing the value of 0.3 in formula to 0.4 like done by Xie (1981) to calculate the maximum scour depth is also valid for sloping structures in cases where suspended load transport is dominant remains unknown.

Scale effects and sediment transport mode

Scale effects arise when scaling the model tests results to prototype situations. In general Froude scaling is used for wave models. This allows for maintaining a constant ratio between various terms in the equations of motion.

According to De Vries (1982) and Frostick et al. (2011) the scaling of sediment transport usually does not follow this Froude condition. One of the reasons for this is that the Shields threshold value for the sediment is not similar in model and prototype when Froude scaling is used. Frostick et al. (2011) state that for these cases adjustments of the scaling must be made. For this normally dependencies found in expressions for bed-load transport are used. This method introduces new uncertainties into the scaling as different bed-load transport formula have different dependencies.

In table 6.1 the variations in parameters influencing the scour pattern that are linked to the sediment size are given for the tests done in this study. In Xie (1981) and Sumer and Fredsøe (2000) the influence of the relation between the wave height and the sediment size $H_{s,i}/D_{50,Sand}$ and the relation between the wavelength and the sediment size $\lambda_p/D_{50,Sand}$ are discussed. For the ratio between the wave height and the sediment size $H_{s,i}/D_{50,Sand}$, no obvious influence on the development of the scour depth was found for the sediment particle size by Xie (1981). In the results from this study an increase in this ratio results in no significant change in maximum scour depth for the

tests with low wave steepness. Sumer and Fredsøe (2000) state that the influence of the parameter $\lambda_p/D_{50,Sand}$ only slightly influences the scour pattern. For an increase in $\lambda_p/D_{50,Sand}$ the scour depth slightly decreases. This is in line with the findings in **??** where for waves with a low wave steepness less scour was observed for a decrease in sediment size.
Influence of both parameters on the maximum scour depth is small. Therefore, for first estimations of the maximum scour depth the influence of both parameters can be neglected. This confirms the findings of Xie (1981) and Sumer and Fredsøe (2000), that for a first approximation of the scour depth these values may be ignored.

Table 6.1: Ratio wavelength - sediment size & wave height - sediment size, for permeable breakwater tests with toe

$D_{50,Sand}[\mu m]$	$H_{s,i}$ [m]	T_p [s]	Wavelength λ_p [m]	$H_{s,i}$ / $D_{50,Sand}$ [-]	λ_p / $D_{50,Sand}$ [-]	$S_{max}/H_{s,i}$ [-]
170	0.117	1.6	2.84	688	16710	0.08
220	0.116	1.6	2.84	527	12910	0.05
170	0.127	2.5	4.74	747	27880	0.12
170	0.163	2.5	4.74	959	27880	0.13
220	0.127	2.5	4.74	577	21550	0.13
260	0.135	2.5	4.74	519	18230	0.14

Correctly scaling sediment dynamic quantities is possible with Froude scaling when the geometry of the material is scaled correctly and when the density of the material is the same. This is only possible when prototype material is very large. In this case scaling the finest sediment material used in this study to prototype situations would lead to very large sediment diameters, in the order of 2 - 5 millimeter for n_L = 10 - 30. Only for prototype situations with large grain sizes or for situations where n_L is small correct scaling of the sediment dynamics is possible. When considering the relation for the scaling of coarse sediment by Xie (1981), sediment diameters in the order of 1 - 2.5 millimeter are found for realistic prototype situation.

The scaling relationships using Froude scaling and the assumptions that are made when using this approach are discussed in section 2.7. Here also findings from literature describing issues that occur when scaling sediment can be found.
When using Froude scaling for the scaling of sediment transport the following relation is used:

$$n_q = n_L^{1.5} \text{ or } n_Q = n_L^{2.5}$$

Some indications of the possible sediment transport mode for the tested conditions are given in section 5.3 using literature. One of the indication values used here is the Rouse number proposed in Rouse (1937).
A high Rouse number indicates that there is more bed load transport and less suspended transport for the given flow conditions. For the fine sand tested in the present study, $D_{50,Sand}$ = 170 μm, the type of transport is suspended load (100%) according to definitions of the Rouse number. The more coarse sand that is used, $D_{50,Sand}$ = 220 μm, is in the suspended load (50%) transport regime. It is important to note that the Rouse number is determined for normal flow. In the present study however there is no uniform flow but orbital flow. The flow velocity used for determining the shear velocity used in calculating the Rouse number is based on the maximum orbital velocity for the present wave conditions. This maximum orbital velocity is based on the significant/peak wave conditions that are present during testing. As these conditions are only present for a portion of the testing time and wave periods are in the order of several seconds, maximum flow is only present for very short periods of time. This can be seen in fig. 4.8. It is therefore expected that during most periods of testing the Rouse number is higher and transport varies between suspended and bed load. This matches well with visual observations, as described in section 5.3.1, where low wave height periods with no suspended sediment and high wave height periods with a lot of movement and suspension were observed.

Based on these findings it is concluded that not enough is known to properly judge the scale effects acting on the transport of sediment when scaling to prototype situations. Using Froude relations for the scaling of the sediment transport results in dissimilarity between model and prototype for the threshold of motion. Another possible issue is the mode of transport changing due to the scaling of the material. Especially as prototype material is usually not large enough to reach similarity with the model material used in this study. This may result in a situation where for the model bed-load transport is dominant and for a prototype situation suspended load transport is dominant, resulting in a different scour-deposition pattern.
When taking into account the shortcomings described above, for a first estimation of the scour-deposition pattern

and the maximum scour when considering prototype situations where bed-load transport is dominant, the results of this study can be used.

7 Conclusion

In this chapter the research is concluded and an answer is given to the research questions. Three main processes are observed in the present study that result in a change in bed profile. Each of these processes and their influence will be discussed individually here. These processes are:

- The standing wave pattern
- The downrush flow from the structure slope
- A large-scale morphological change

Standing wave pattern
In confirmation with earlier studies the standing wave pattern is found to be the main driving mechanism for the scour-deposition pattern in front of a coastal structure. Standing waves form when waves are reflected of the structure. At the nodes of this pattern material is found to be deposited while at the anti-nodes material is removed. For irregular waves this standing wave pattern patterns dampens with increasing distance from the structure, resulting in less material being displaced. In Jantzen (2020) a quadratic relation was found between the wave reflection K_r and the maximum scour depth. In this study an additional structure was tested and this relation was changed to $K_r^{1.5}$ as this showed better results for development of the maximum scour depth for all structures.

Downrush flow
For tests with a sloping coastal structure a scour hole forms directly adjacent to the structure when no bed protection is present. This is expected to be the result of downrush flow from the surface of the sloping structure. The depth of this hole is found to depend on a lot of factors. In the present study and that of Jantzen (2020) the following parameters are found to be the most influential: the relative water depth h/λ_p, the surf similarity parameter (or Iribarren number) ξ, the amount of wave reflection, the roughness of the structure, the permeability of the structure and the presence of bed protection. For structures with the same slope angle the maximum depth of this hole is found to be 2 to 3 times larger for smooth structures than for rough rubble structures.

Large-scale morphological change
A constant transport of sediment is observed over the whole sand bed in the model tests. The wave reflection coefficient K_r and presence of bed protection are found to not influence this transport. Tests with a low wave steepness showed an offshore loss of sediment, which decreased for an increase in wave steepness. For wave steepness s > 3% at the structure onshore transport is found, resulting in accumulation of sediment at the structure. This large-scale change was found to remain constant over time up to at least 90,000 waves. The exact reason for this type of transport is not known.

Bed protection
The influence of the bed protection on the development of the bed in front of it largely depends on the standing wave pattern and the presence of downrush flow. When no downrush flow is present, which is the case for vertical structures, the location of the end of the bed protection compared to the standing wave pattern determines whether a scour hole forms at the end of the protection layer. For sloping structures this was not observed and largest scour depths are found for cases with bed protection. Whether this was a result of a combination of the downrush flow scour and the presence of a standing wave anti-node close to the end of the protection layer or that this is only a result of the anti-node is not yet known.

General scale effects

- When scaling the model to prototype situations scale effects arise for the transport of sediment. Only a small influence of the particle size on the scour-deposition pattern is found. For first approximations the influence of sediment size can be neglected as long as the type of transport remains similar. Not enough is know to properly judge all effects when scaling to specific prototype situations. It is expected that results of the present study are suitable for first estimations of prototype situations where bed-load transport is dominant.
- The influence of the sand ripples that form and migrate over time on the maximum scour depth and the effect it has when scaling the results is not known. As the sand ripples do not scale with the rest of the model these may result in scale effects. It is expected that influence of the sand ripples in prototype situations is small while possibly significant in the model situation. For this reason in processing the bed profile measurements in this study a mean profile was created to exclude most of the individual ripples from the results.

With the knowledge gap described in the introduction of this report the following research question was formulated to be answered in this study:

Can a set of design guidelines that include physical processes be created to predict the scour-deposition pattern at the toe of a sloping coastal structure?

In the present study a relation is found between the reflection coefficient K_r and the number of waves during which a substantial amount of scour occurs N_s for sloping structures. By including this relation in the formula developed for vertical walls by Xie (1981) the maximum depth of the scour hole can be calculated for a certain amount of waves. Also, development of the maximum depth is included by including the number of waves N in the formula. This results in the following design formula for cases where bed-load transport is dominant:

$$\text{For } N \leq 24000 \text{ and } \frac{W_{p,t}}{L_p} < \frac{3}{8} L_p : \\ \frac{S_{max}(N)}{H_s} = \frac{0.3}{\left(\sinh \frac{2\pi h}{L_p}\right)^{1.35}} K_r^{1.5} \sqrt{\frac{N}{12000}} \tag{7.1}$$

Included here are the maximum number of waves for which test results are compared with the formula. Also, a range for the length of the bed protection (measured from the waterline) is included to exclude cases with a long bed protection for which the formula is found to underpredict the maximum scour depth.
Performance of eq. (7.1) is found to be best for predicting the maximum scour depth at the first anti-node in front of the structure (RMSE = 0.032). Performance for the maximum scour depth directly adjacent to the structure is slightly less but still good (RMSE = 0.046). In this case the formula seems to slightly overpredict the maximum depth for most cases. The tested range for which the formula is found to be suitable is given in table 5.18 and table 5.19.
Upwards of about 3000 waves eq. (7.1) shows a good fit with the test results for most cases. Development for a lower number of waves seems to follow a more linear trend. It is expected that the formula is not suitable for cases where $\frac{N}{N_s} < 0.5$. In these cases the slightly conservative approach by Den Bieman et al. (2019), where a linear trend is used, is more suitable.

8 Recommendations

Based on the discussion and the conclusion recommendations for further research are formulated. These include conditions that have not been tested in the present study, additional measurements that can be done, improvements that can be made to the design formula and comments on scaling. Observations in the present study have led to the following set of recommendations which can further fill the knowledge gap identified in this study:

- No model test are done where suspended load sediment transport is dominant. Therefore performance of the developed formulas for these cases is not checked. In future research on the scour in front of sloping structures it can prove useful to have model tests were suspended load transport is dominant. This can then be used to see whether the expressions developed by Xie (1981), on which the design formula for suspended load transport is based, is also valid for wave-induced scour in front of sloping structures.
  For this a larger wave flume or lightweight material may be useful as in this study a combination of the finest sand available and the largest possible waves in the flume did not lead to suspended load dominance.

- More elaborate velocity measurements at and around the toe of the structure may give more insight in the parameters that influence the scour or deposition directly adjacent to the structure. Especially on the case of downrush flow little is yet known. Studies where this flow is considered focused mainly on the stability of the toe structure and not on the resulting sediment transport at the toe. As the downrush flow scour hole is the hole that forms closest to the structure better understanding of the velocities at the toe is of importance for structural stability. Varying the roughness and the permeability of the structure will give better insights on their effect on the downrush flow. In addition measurements can be done for cases with a bed protection to see whether influence of the downrush flow is still present at the end of the bed protection layer.

- Model tests with a larger scale may prove beneficial in determining the scale effects that occur when scaling the sediment transport from model to prototype. When the scale of the model is larger, similarity in sediment between model and prototype can more easily be reached with available sand grain sizes. In this way the threshold of motion and cohesive properties of the material can be similar for model and prototype situations.

- For exact similarity between model and realistic prototype situations the foreshore in the model should be sloping instead of being flat like it is in this study. Having a sloping foreshore influences the wave conditions near the structure as the water depth decreases which leads to the breaking of waves on the foreshore. This may influence flow and sediment transport patterns in front of the structure and should therefore be included to fully model the scour in front of a structure.

- Model tests with a 3-D model can further develop understanding of all the mechanisms that lead to scour in prototype situations. By including long-shore currents sediment in motion may be carried away from the structure resulting in larger scouring depths. Also, model tests with oblique waves are interesting to study as the assumption that maximum scour is largest for directly incident waves can be validated.

- A large-scale transport of sediment is witnessed in the present study that varied in amount of transported material and in transport direction for variations in wave period. For waves with a large wave steepness a small onshore transport was observed while for low wave steepness a clear offshore transport of material was present for which the amount of transported material increased with decreasing wave steepness. This transport was found to not be significantly influenced by the amount of wave reflection.
  Whether this behaviour is directly the result of the wave steepness, stokes drift (where possible influence of the wave period is not included) or another mechanism remains unknown. Future research into this pattern may explain the witnessed behaviour and can give insight on whether this can also be expected in prototypes situations.

References

Bagnold, R. A. (1946). Motion of waves in shallow water. interaction between waves and sand bottoms. *Proceedings of the Royal Society of London. Series A. Mathematical and Physical Sciences*, 187(1008):1–18.

CIRIA, CUR, and CETMEF (2007). The rock manual. *The use of rock in hydraulic engineering (2nd edition)*, C683, CIRIA, London. ISBN: 978-0-86017-683-1.

De Vries, M. (1982). Scale models in hydraulic engineering. *IHE lecture note*.

Den Bieman, J. P., Jacobsen, N. G., and van Gent, M. R. A. (2018). Scour at the toe of rock armoured structures. *Coastal Engineering Proceedings*, (36):papers.74.

Den Bieman, J. P., van Gent, M. R. A., and Hoonhout, B. M. (2019). Physical model of scour at the toe of rock armoured structures. *Coastal Engineering*, 154:103572.

Dixen, F. H., Sumer, B. M., and Fredsøe, J. (2008). Suction removal of sediment from between armor blocks. ii: waves. *Journal of Hydraulic Engineering*, 134(10):1405–1420.

Frostick, L. E., McLelland, S. J., and Mercer, T. G. (2011). *Users guide to physical modelling and experimentation: Experience of the HYDRALAB network*. CRC Press.

Gislason, K., Fredsøe, J., Deigaard, R., and Sumer, B. M. (2009a). Flow under standing waves: Part 1. shear stress distribution, energy flux and steady streaming. *Coastal engineering*, 56(3):341–362.

Gislason, K., Fredsøe, J., and Sumer, B. M. (2009b). Flow under standing waves: Part 2. scour and deposition in front of breakwaters. *Coastal engineering*, 56(3):363–370.

Heller, V. (2011). Scale effects in physical hydraulic engineering models. *Journal of Hydraulic Research*, 49(3):293–306.

Henriquez, M., Stive, M., Reniers, A., Ruessink, B., Stanton, T., and Foster, D. (2008). On the scaling of sediment transport in the nearshore. In *Coastlab 2008 Conference, IAHR*, pages 193–204.

Hudson, R. Y. (1953). Wave forces on breakwaters. *Transactions of the American Society of Civil Engineers*, 118(1):653–674.

Hughes, S. A. (1993). *Physical models and laboratory techniques in coastal engineering*, volume 7. World Scientific.

Hughes, S. A. and Fowler, J. E. (1995). Estimating wave-induced kinematics at sloping structures. *Journal of waterway, port, coastal, and ocean engineering*, 121(4):209–215.

Jantzen, C. (2020). Experimental study on the influence of bed protections on scour depth and scour development in front of sloped embankments. Master's thesis, Delft University of Technology, The Netherlands.

Kamphuis, J. (1975). Practical scaling of coastal models. In *Coastal Engineering 1974*, pages 2086–2101.

O'Donoghue, T., Doucette, J., van der Werf, J. J., and Ribberink, J. S. (2006). The dimensions of sand ripples in full-scale oscillatory flows. *Coastal Engineering*, 53(12):997–1012.

Postma, G. (1989). Wave reflection from rock slopes under random wave attack. *MSc thesis, Delft University of Technology, Department of Civil Engingineering*.

Rance, P. and Warren, N. (1969). The threshold of movement of coarse material in oscillatory flow. In *Coastal Engineering 1968*, pages 487–491.

Rouse, H. (1937). Modern conceptions of the mechanics of fluid turbulence. *Transactions of the American Society of Civil Engineers*, 102(1):463–505.

Sato, S., Tanaka, N., and Irie, I. (1969). Study on scouring at the foot of coastal structures. *Coastal Engineering in Japan*, 12(1):83–98.

Schiereck, G. J. (2003). *Introduction to bed, bank and shore protection*. DAP Press. ISBN: 97890-6562-4031.

Shields, A. (1936). Anwendung der aehnlichkeitsmechanik und der turbulenzforschung auf die geschiebebewegung. *PhD Thesis Technical University Berlin*.

Sleath, J. F. (1978). Measurements of bed load in oscillatory flow. *Journal of the waterway, port, coastal and ocean division*, 104(3):291–307.

Smith, E. R. (1996). *Potential toe scour and wave reflection at revetments*. Vicksburg MS: Coastal Engineering Research Center. US Army Corps of Engineers, Miscellaneous paper CERC-96-2.

Sumer, B. M. et al. (2002). *The mechanics of scour in the marine environment*. World Scientific Publishing Company. ISBN: 981-02-4930-6.

Sumer, B. M. and Fredsøe, J. (2000). Experimental study of 2d scour and its protection at a rubble-mound breakwater. *Coastal Engineering*, 40(1):59–87.

Van der Meer, J. (2002). Technisch rapport golfoploop en golfoverslag bij dijken. *Hydraulic Engineering Reports, TR33*.

Van der Meer, J. W. (1988). Rock slopes and gravel beaches under wave attack. *Delft Hydraulics Laboratory*.

Van der Meer, J. W. (1995). Conceptual design of rubble mound breakwaters. In *Advances In Coastal And Ocean Engineering: (Volume 1)*, pages 221–315. World Scientific.

van Gent, M. R. and van der Werf, I. M. (2014). Rock toe stability of rubble mound breakwaters. *Coastal Engineering*, 83:166–176.

van Rijn, L. (1989). *Handbook Sediment Transport by Currents and Waves*. Delft Hydraulics Report. Delft Hydraulics.

van Rijn, L. C. (1984). Sediment transport, part i: Bed load transport. *Journal of Hydraulic Engineering*, 110(10):1431–1456.

van Rijn, L. C. (1993). Sediment transport by currents and waves. In *Coastal Engineering 1992*, pages 2613–2628.

Wiberg, P. L. and Sherwood, C. R. (2008). Calculating wave-generated bottom orbital velocities from surface-wave parameters. *Computers & Geosciences*, 34(10):1243 – 1262.

Wolters, G., van Gent, M., Allsop, W., Hamm, L., and Mühlestein, D. (2007). Hydralab iii: Guidelines for physical model testing of rubble mound breakwaters. *Coasts, Marine Structures and Breakwaters: Adapting to Change - Proceedings of the 9th International Conference*.

Xie, S.-L. (1981). Scouring patterns in front of vertical breakwaters and their influences on the stability of the foundation of the breakwaters. TU Delft, Faculty of Civil Engineering and Geosciences, Hydraulic Engineering.

Zanuttigh, B. and Van der Meer, J. W. (2007). Wave reflection from coastal structures. In *Coastal Engineering 2006: (In 5 Volumes)*, pages 4337–4349. World Scientific.

A Appendix - Method

A.1 Cross sections structures

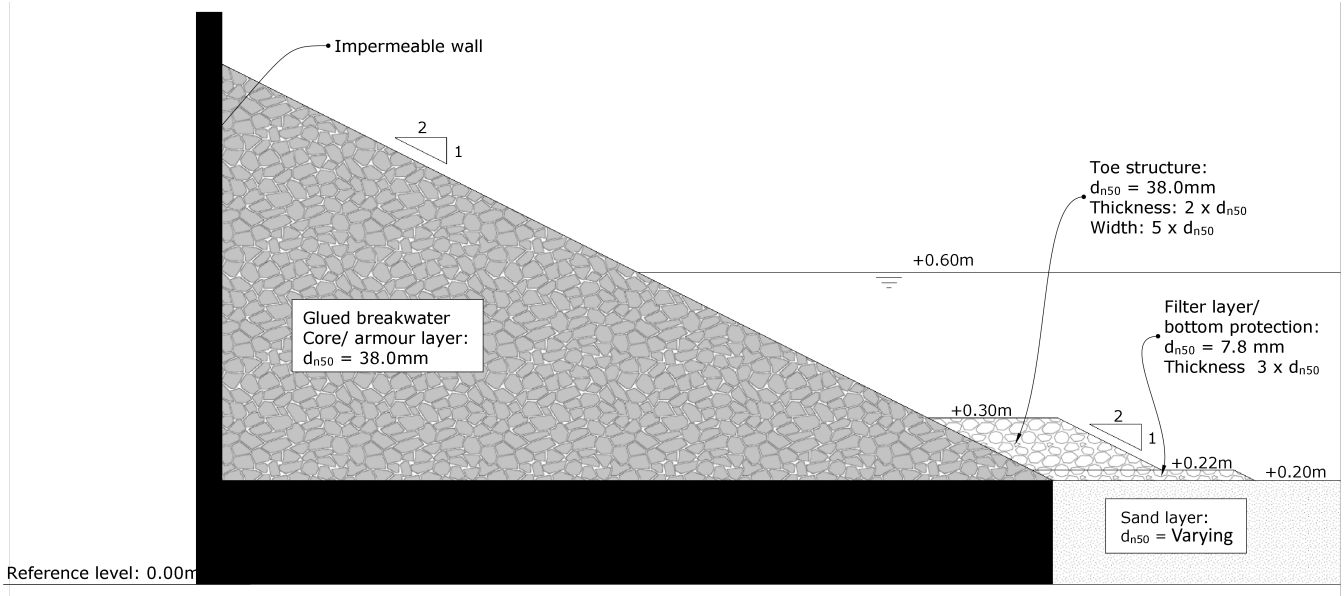

Figure A.1: Permeable breakwater cross section, from Jantzen (2020)

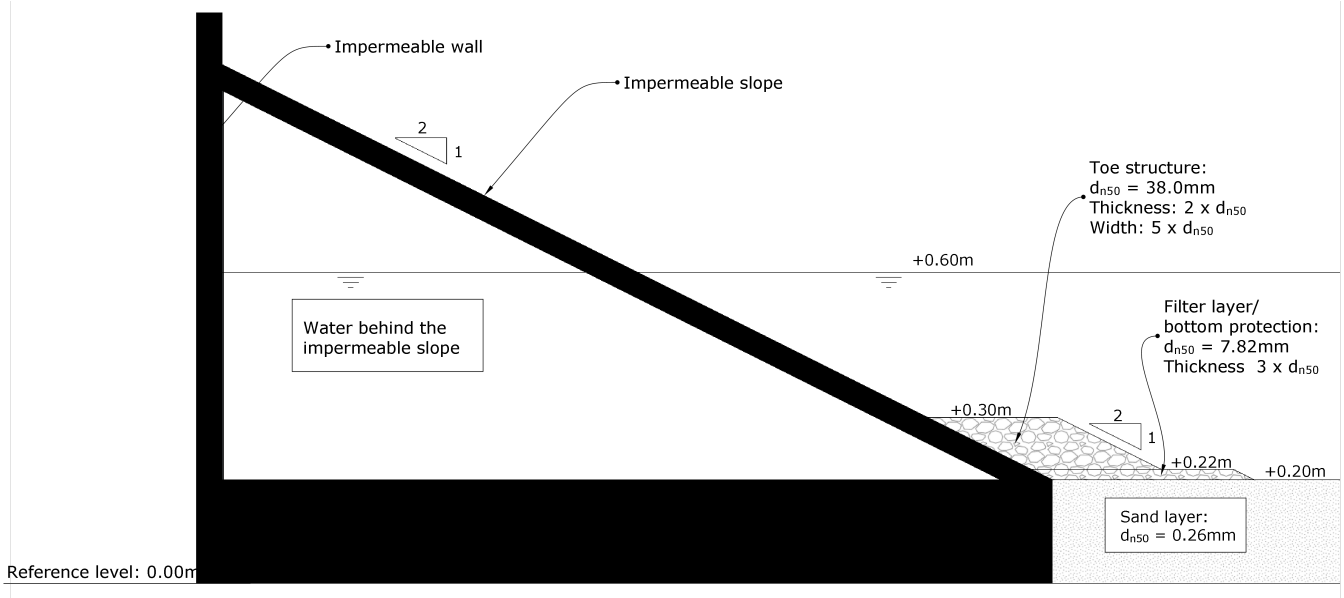

Figure A.2: Impermeable smooth slope cross section, from Jantzen (2020)

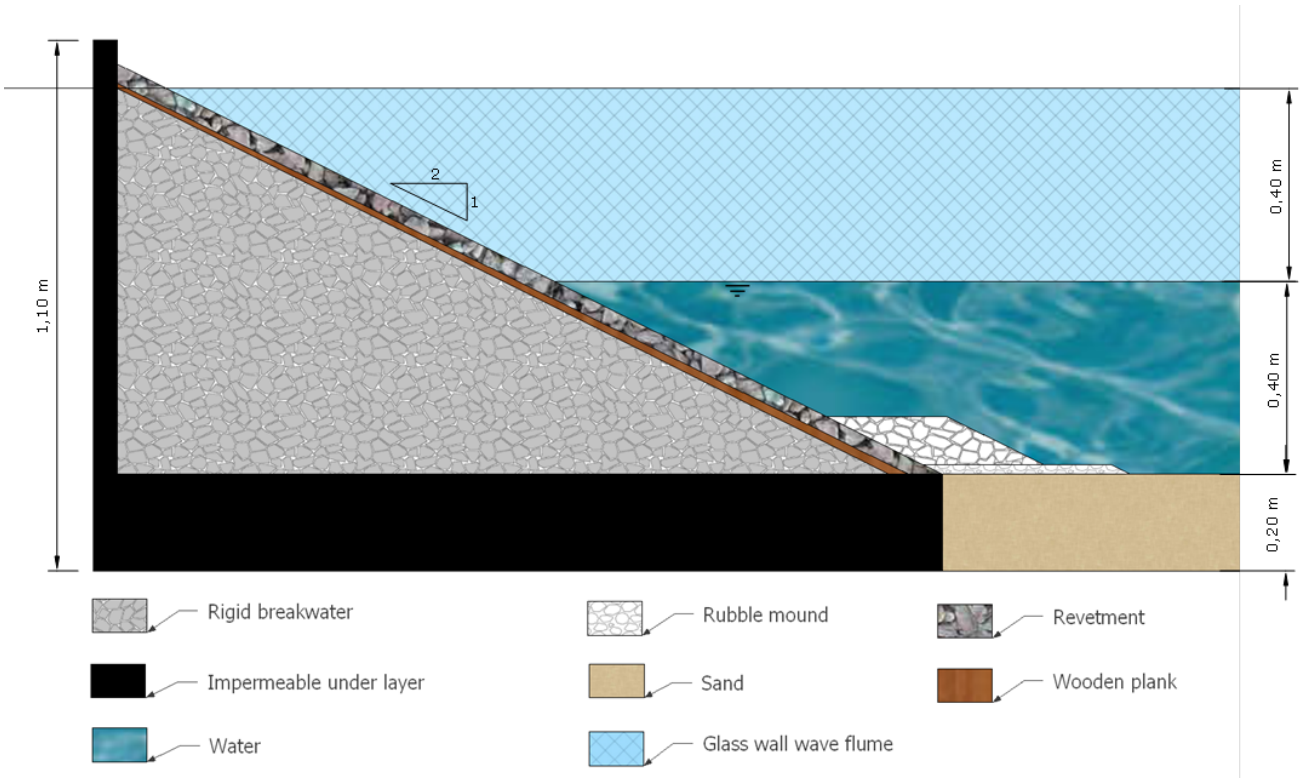

Figure A.3: Impermeable revetment cross section

A.2 Materials

A.2.1 Stones used for permeable breakwater, revetment & toe structure

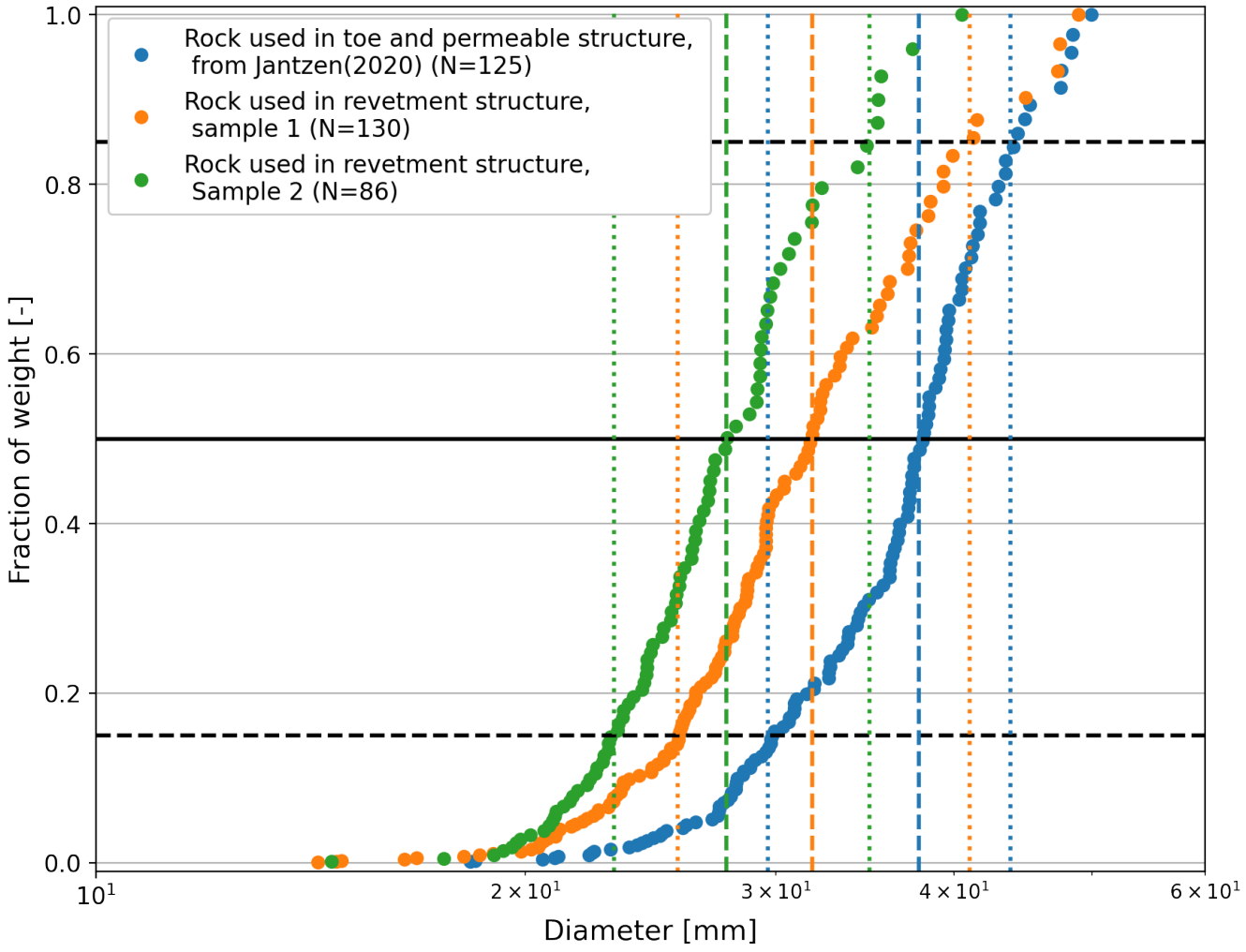

Figure A.4: Grading material used in armour layer and toe

Table A-1: Grading of armour layer and toe material

Sample	N [-]	d_{n15} [mm]	d_{n50} [mm]	d_{n85} [mm]
Material used by Jantzen (2020)	125	29.6	37.8	43.8
Present study - sample 1	130	25.6	31.8	41
Present study - sample 2	86	23.1	27.7	34.9

A.2.2 Stones used for filter layer

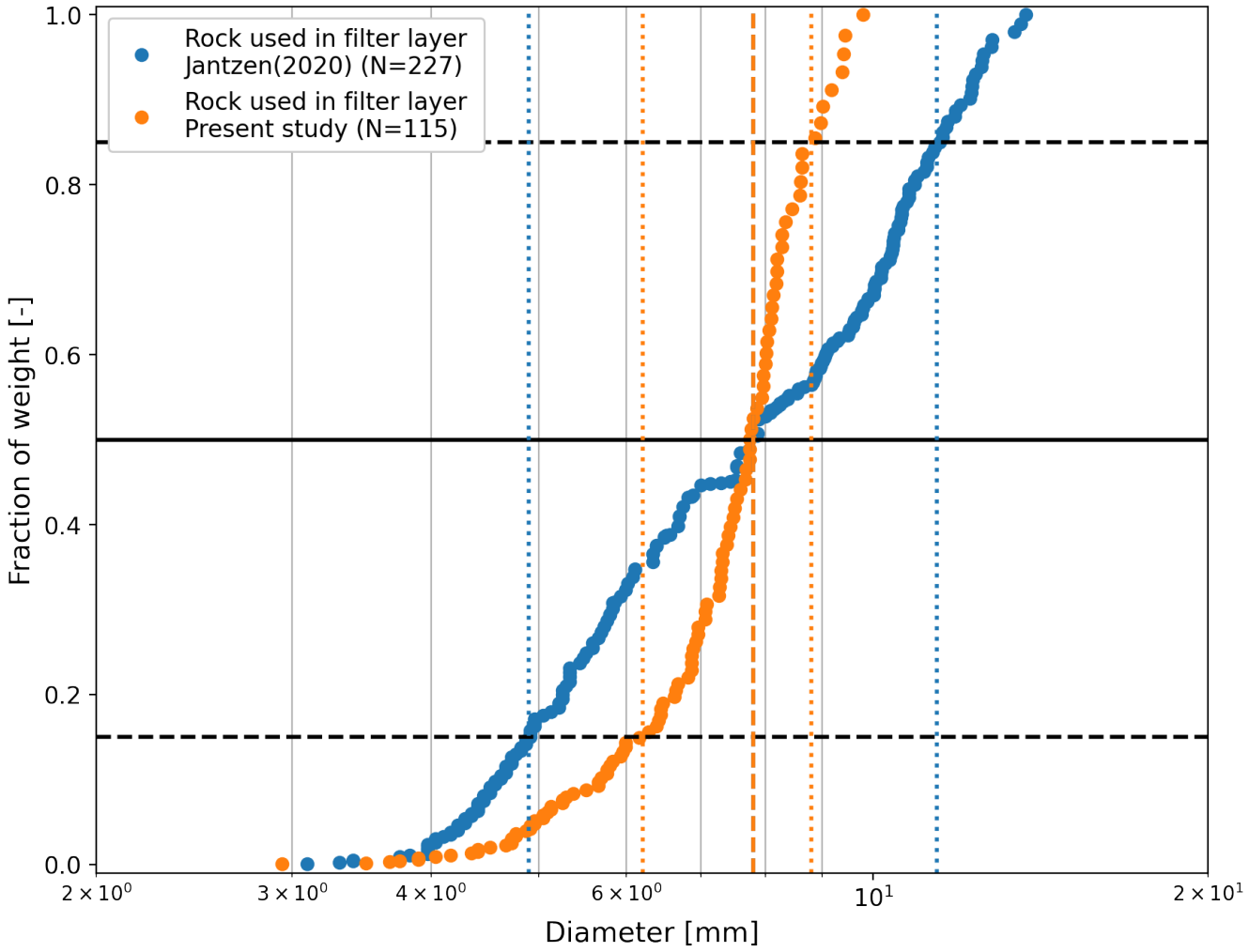

Figure A.5: Grading material used in filter layer

Table A-2: Grading of filter layer material

Sample	N [-]	d_{n15} [mm]	d_{n50} [mm]	d_{n85} [mm]
Material used by Jantzen (2020)	227	4.9	7.8	11.4
Present study	115	6.2	7.8	8.8

A.2.3 Sieving curves sand

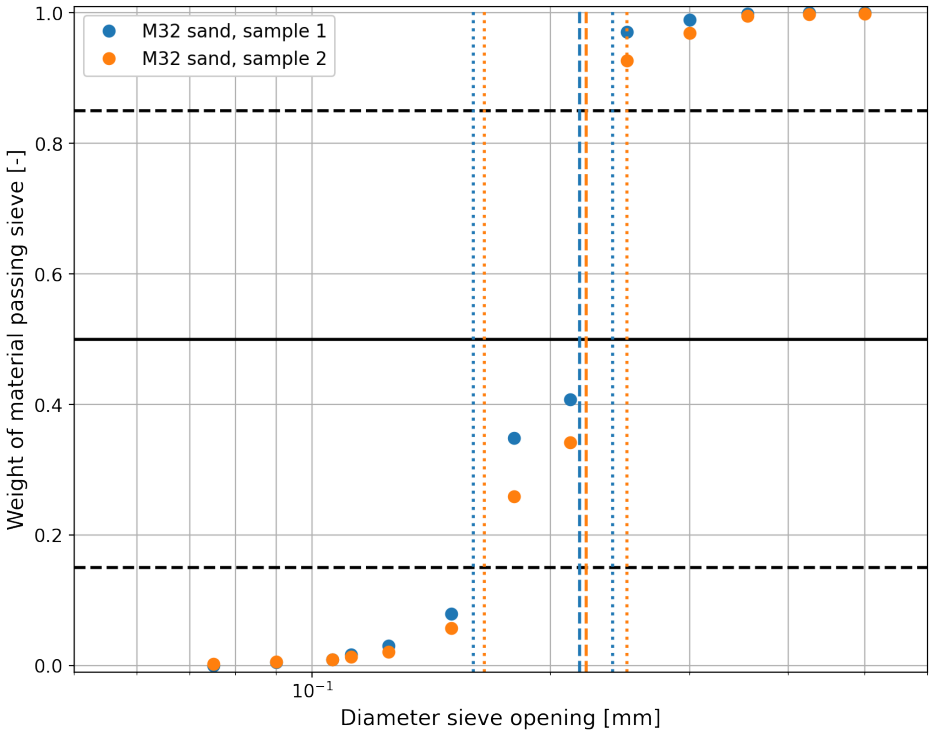

Figure A.6: Sieving curve M32 sand

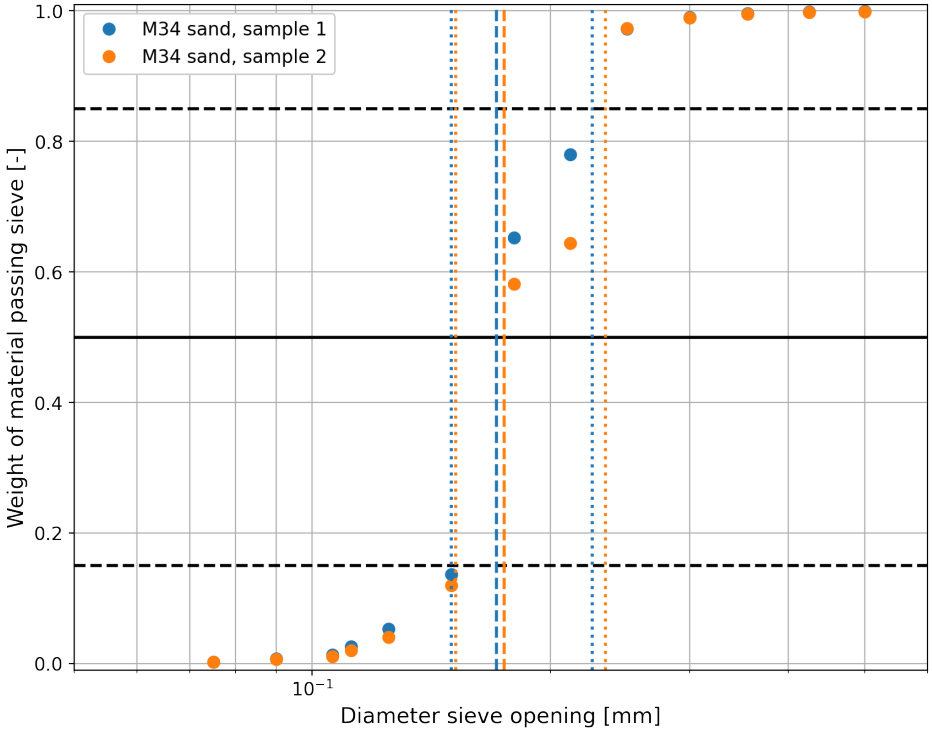

Figure A.7: Sieving curve M34 sand

Table A-3: Results sieving of sand

Material	$\mathbf{d_{15}}$ **[mm]**	$\mathbf{d_{50}}$ **[mm]**	$\mathbf{d_{85}}$ **[mm]**
Jantzen (2020) - M32	0.21	0.26	0.32
Present study - M32 - sample 1	0.16	0.22	0.24
Present study - M32 - sample 2	0.17	0.22	0.25
Present study - M34 - sample 1	0.15	0.17	0.23
Present study - M34 - sample 2	0.15	0.18	0.24

,

B Appendix - Wave conditions

Table B-1: Wave conditions during tests

Test	Structure	Target H_s [m]	T_p[s]	h_o [m]	h_n [m]	$H_{s,o}$[m]	$\lambda_{o,p}$[m]	$s_{o,p}$[%]	$H_{s,n}$[m]	$\lambda_{n,p}$[m]	$s_{n,p}$[%]	Kr [%]
Per_D22_H14_T25_NoToe	Permeable	0.14	2.5	0.6	0.4	0.141	9.76	1.4	0.127	4.74	2.7	36
Per_D22_H14_T25_Toe	Permeable	0.14	2.5	0.6	0.4	0.141	9.76	1.4	0.125	4.74	2.6	33
Per_D22_H14_T16_NoToe	Permeable	0.14	1.6	0.6	0.4	0.136	4.00	2.9	0.116	2.84	4.1	23
Per_D22_H14_T16_Toe	Permeable	0.14	1.6	0.6	0.4	0.136	4.00	2.9	0.116	2.84	4.1	24
Per_D22_H14_T16_ToeProt	Permeable	0.14	1.6	0.6	0.4	0.136	4.00	2.9	0.116	2.84	4.1	24
Per_D17_H14_T25_NoToe	Permeable	0.14	2.5	0.6	0.4	0.141	9.76	1.4	0.127	4.74	2.7	37
Per_D17_H14_T25_Toe	Permeable	0.14	2.5	0.6	0.4	0.141	9.76	1.4	0.127	4.74	2.7	34
Per_D17_H14_T25_Toe_b	Permeable	0.14	2.5	0.6	0.4	0.143	9.76	1.4	0.130	4.74	2.7	34
Per_D17_H14_T25_ToeProt	Permeable	0.14	2.5	0.6	0.4	0.141	9.76	1.4	0.127	4.74	2.7	37
Per_D17_H14_T16_NoToe	Permeable	0.14	1.6	0.6	0.4	0.137	4.00	3.4	0.117	2.84	4.1	26
Per_D17_H14_T16_Toe	Permeable	0.14	1.6	0.6	0.4	0.137	4.00	3.4	0.110	2.84	3.9	26
Per_D17_H14_T16_ToeProt	Permeable	0.14	1.6	0.6	0.4	0.137	4.00	3.4	0.117	2.84	4.1	27
Per_D17_H14_T21_NoToe	Permeable	0.14	2.1	0.6	0.4	0.140	6.89	1.8	0.126	3.91	3.2	32
Per_D17_H14_T19_NoToe	Permeable	0.14	1.9	0.6	0.4	0.138	5.64	2.2	0.124	3.48	3.6	28
Per_D17_H14_T21_Toe	Permeable	0.14	2.1	0.6	0.4	0.138	6.89	1.9	0.133	3.91	3.4	41
Per_D17_H18_T25_Toe	Permeable	0.18	2.5	0.6	0.4	0.182	9.76	1.7	0.163	4.74	3.4	41
Per_D17_H14_T25_ToeProt*	Permeable	0.14	2.5	0.6	0.4	0.143	4.74	1.4	0.132	9.76	2.8	36
Rev_D17_H14_T25_NoToe	Revetment	0.14	2.5	0.6	0.4	0.141	4.74	1.4	0.127	9.76	2.7	51
Rev_D17_H14_T25_Toe	Revetment	0.14	2.5	0.6	0.4	0.141	4.74	1.4	0.127	9.76	2.7	51
Rev_D17_H14_T25_ToeProt	Revetment	0.14	2.5	0.6	0.4	0.140	4.74	1.4	0.126	9.76	2.7	51
Rev_D17_H14_T16_NoToe	Revetment	0.14	1.6	0.6	0.4	0.138	4.00	3.5	0.119	2.84	4.2	33
Rev_D17_H14_T16_Toe	Revetment	0.14	1.6	0.6	0.4	0.138	4.00	3.5	0.119	2.84	4.2	34
Rev_D17_H14_T16_ToeProt	Revetment	0.14	1.6	0.6	0.4	0.137	4.00	3.5	0.119	2.84	4.2	33

Table B-2: Wave conditions during tests Jantzen (2020)

Test	Structure	Target H_s [m]	T_p[s]	h_o [m]	h_n [m]	$H_{s,o}$[m]	$\lambda_{o,p}$[m]	$s_{o,p}$[%]	$H_{s,n}$[m]	$\lambda_{n,p}$[m]	$s_{n,p}$[%]	Kr [%]
Im_D26_H14_T16_NoToe	Impermeable	0.14	1.6	0.6	0.4	0.161	4.00	3.6	0.144	2.84	5.1	63
Im_D26_H14_T25_NoToe	Impermeable	0.14	2.5	0.6	0.4	0.174	9.76	1.8	0.175	4.74	3.7	81
Im_D26_H14_T25_Toe	Impermeable	0.14	2.5	0.6	0.4	0.174	9.76	1.8	0.174	4.74	3.7	78
Im_D26_H14_T25_ToeProt	Impermeable	0.14	2.5	0.6	0.4	0.177	9.76	1.8	0.172	4.74	3.6	77
Im_D26_H14_T16_Toe	Impermeable	0.14	1.6	0.6	0.4	0.155	4.00	3.6	0.144	2.84	5.1	61
Per_D26_H14_T25_NoToe	Permeable	0.14	2.5	0.6	0.4	0.152	9.76	1.5	0.143	4.74	3.0	35
Per_D26_H14_T25_Toe	Permeable	0.14	2.5	0.6	0.4	0.152	9.76	1.5	0.143	4.74	3.0	36
Per_D26_H18_T25_Toe	Permeable	0.18	2.5	0.6	0.4	0.194	9.76	1.8	0.176	4.74	3.7	36
Per_D26_H14_T25_ToeProt	Permeable	0.14	2.5	0.6	0.4	0.153	9.76	1.5	0.144	4.74	3.0	37
Per_D26_H14_T25_Toe	Permeable	0.14	2.5	0.6	0.4	0.154	9.76	1.5	0.145	4.74	3.0	37

The following equations are used for calculating the relevant wave periods for each test:

$$T_{m-1,0} = \frac{m_{-1}}{m_0}$$

$$T_{m0,1} = \frac{m_0}{m_1}$$

$$T_{m0,2} = \sqrt{\frac{m_0}{m_2}}$$

$$T_{m2,4} = \sqrt{\frac{m_2}{m_4}}$$

Table B-3: Nearshore wave conditions during tests

Test	T_p[s]	h_n [m]	$H_{s,total}$[m]	$H_{s,in}$[m]	$H_{s,out}$[m]	$T_{m-1,0}$ [s]	$T_{m0,1}$ [s]	$T_{m0,2}$ [s]	$T_{m2,4}$ [s]
Per_D22_H14_T25_NoToe	2.5	0.4	0.141	0.127	0.046	2.19	1.85	1.70	1.22
Per_D22_H14_T25_Toe	2.5	0.4	0.141	0.125	0.041	2.19	1.87	1.71	1.23
Per_D22_H14_T16_NoToe	1.6	0.4	0.136	0.116	0.026	1.47	1.38	1.32	1.07
Per_D22_H14_T16_Toe	1.6	0.4	0.136	0.116	0.028	1.47	1.38	1.32	1.07
Per_D22_H14_T16_ToeProt	1.6	0.4	0.136	0.116	0.028	1.47	1.37	1.31	1.04
Per_D17_H14_T25_NoToe	2.5	0.4	0.141	0.127	0.045	2.19	1.86	1.71	1.23
Per_D17_H14_T25_Toe	2.5	0.4	0.141	0.127	0.045	2.20	1.87	1.71	1.23
Per_D17_H14_T25_Toe_b	2.5	0.4	0.143	0.130	0.044	2.20	1.88	1.73	1.25
Per_D17_H14_T25_ToeProt	2.5	0.4	0.141	0.127	0.042	2.18	1.87	1.70	1.25
Per_D17_H14_T16_NoToe	1.6	0.4	0.137	0.117	0.027	1.47	1.38	1.32	1.06
Per_D17_H14_T16_Toe	1.6	0.4	0.137	0.110	0.029	1.47	1.38	1.32	1.06
Per_D17_H14_T16_ToeProt	1.6	0.4	0.137	0.117	0.028	1.47	1.38	1.31	1.06
Per_D17_H14_T21_NoToe	2.1	0.4	0.140	0.126	0.039	1.87	1.66	1.55	1.14
Per_D17_H14_T19_NoToe	1.9	0.4	0.138	0.124	0.035	1.72	1.55	1.46	1.11
Per_D17_H14_T21_Toe	2.1	0.4	0.138	0.133	0.055	2.74	1.80	1.63	1.17
Per_D17_H18_T25_Toe	2.5	0.4	0.182	0.163	0.067	2.76	1.86	1.65	1.10
Per_D17_H14_T25_ToeProt*	2.5	0.4	0.143	0.132	0.046	2.24	1.87	1.71	1.23
Rev_D17_H14_T25_NoToe	2.5	0.4	0.141	0.127	0.065	2.20	1.90	1.75	1.29
Rev_D17_H14_T25_Toe	2.5	0.4	0.141	0.127	0.064	2.22	1.92	1.78	1.33
Rev_D17_H14_T25_ToeProt	2.5	0.4	0.140	0.126	0.064	2.20	1.90	1.75	1.30
Rev_D17_H14_T16_NoToe	1.6	0.4	0.138	0.119	0.039	1.49	1.39	1.33	1.08
Rev_D17_H14_T16_Toe	1.6	0.4	0.138	0.119	0.040	1.49	1.39	1.33	1.08
Rev_D17_H14_T16_ToeProt	1.6	0.4	0.137	0.119	0.039	1.49	1.39	1.33	1.08
Im_D26_H14_T16_NoToe	1.6	0.4	0.144	0.120	0.046	1.50	1.41	1.36	1.12
Im_D26_H14_T25_NoToe	2.5	0.4	0.173	0.135	0.109	2.11	1.76	1.61	1.16
Im_D26_H14_T25_Toe	2.5	0.4	0.172	0.134	0.104	2.49	1.83	1.68	1.27
Im_D26_H14_T25_ToeProt	2.5	0.4	0.171	0.135	0.104	2.14	1.80	1.65	1.19
Im_D26_H14_T16_Toe	1.6	0.4	0.144	0.122	0.075	1.51	1.42	1.37	1.14
Per_D26_H14_T25_NoToe	2.5	0.4	0.143	0.134	0.050	2.20	1.85	1.69	1.18
Per_D26_H14_T25_Toe	2.5	0.4	0.143	0.135	0.050	2.20	1.86	1.69	1.17
Per_D26_H18_T25_Toe	2.5	0.4	0.175	0.163	0.058	2.10	1.92	1.74	1.27
Per_D26_H14_T25_ToeProt	2.5	0.4	0.144	0.137	0.051	2.56	1.89	1.69	1.16
Per_D26_H14_T25_Toe	2.5	0.4	0.145	0.137	0.050	2.62	1.90	1.70	1.18

Table B-4: Offshore wave conditions during tests

Test	T_p[s]	h_n [m]	$H_{s,total}$[m]	$H_{s,in}$[m]	$H_{s,out}$[m]	$T_{m-1,0}$ [s]	$T_{m0,1}$ [s]	$T_{m0,2}$ [s]	$T_{m2,4}$ [s]
Per_D22_H14_T25_NoToe	2.5	0.6	0.147	0.141	0.037	2.23	2.05	1.93	1.48
Per_D22_H14_T25_Toe	2.5	0.6	0.144	0.141	0.032	2.24	2.05	1.94	1.49
Per_D22_H14_T16_NoToe	1.6	0.6	0.139	0.136	0.026	1.45	1.35	1.29	1.03
Per_D22_H14_T16_Toe	1.6	0.6	0.140	0.136	0.027	1.45	1.35	1.29	1.04
Per_D22_H14_T16_ToeProt	1.6	0.6	0.139	0.136	0.027	1.45	1.35	1.29	1.03
Per_D17_H14_T25_NoToe	2.5	0.6	0.145	0.141	0.037	2.23	2.05	1.93	1.48
Per_D17_H14_T25_Toe	2.5	0.6	0.146	0.141	0.034	2.23	2.05	1.94	1.49
Per_D17_H14_T25_Toe_b	2.5	0.6	0.149	0.143	0.036	2.24	2.06	1.95	1.50
Per_D17_H14_T25_ToeProt	2.5	0.6	0.146	0.141	0.034	2.23	2.05	1.94	1.49
Per_D17_H14_T16_NoToe	1.6	0.6	0.140	0.137	0.027	1.45	1.35	1.29	1.04
Per_D17_H14_T16_Toe	1.6	0.6	0.140	0.137	0.028	1.45	1.35	1.29	1.02
Per_D17_H14_T16_ToeProt	1.6	0.6	0.140	0.137	0.027	1.45	1.36	1.29	1.03
Per_D17_H14_T21_NoToe	2.1	0.6	-	-	-	-	-	-	-
Per_D17_H14_T19_NoToe	1.9	0.6	0.142	0.138	0.029	1.71	1.58	1.51	1.18
Per_D17_H14_T21_Toe	2.1	0.6	0.144	0.138	0.031	1.91	1.76	1.68	1.32
Per_D17_H18_T25_Toe	2.5	0.6	0.191	0.182	0.046	2.24	2.03	1.90	1.45
Per_D17_H14_T25_ToeProt*	2.5	0.6	0.151	0.143	0.037	2.24	2.06	1.95	1.51
Rev_D17_H14_T25_NoToe	2.5	0.6	0.153	0.141	0.055	2.42	2.09	1.97	1.51
Rev_D17_H14_T25_Toe	2.5	0.6	0.152	0.141	0.054	2.26	2.07	1.96	1.53
Rev_D17_H14_T25_ToeProt	2.5	0.6	0.151	0.140	0.054	2.26	2.07	1.95	1.51
Rev_D17_H14_T16_NoToe	1.6	0.6	0.144	0.138	0.036	1.46	1.37	1.31	1.06
Rev_D17_H14_T16_Toe	1.6	0.6	0.144	0.138	0.037	1.46	1.37	1.31	1.06
Rev_D17_H14_T16_ToeProt	1.6	0.6	0.143	0.137	0.036	1.46	1.37	1.31	1.07
Im_D26_H14_T16_NoToe	1.6	0.6	0.161	0.143	0.071	1.48	1.41	1.36	1.14
Im_D26_H14_T25_NoToe	2.5	0.6	0.174	0.143	0.095	2.20	1.95	1.82	1.38
Im_D26_H14_T25_Toe	2.5	0.6	0.174	0.145	0.094	2.22	1.98	1.85	1.41
Im_D26_H14_T25_ToeProt	2.5	0.6	0.177	0.145	0.090	2.26	1.99	1.87	1.43
Im_D26_H14_T16_Toe	1.6	0.6	0.155	0.138	0.068	1.48	1.39	1.34	1.11
Per_D26_H14_T25_NoToe	2.5	0.6	0.152	0.144	0.039	2.26	2.06	1.94	1.49
Per_D26_H14_T25_Toe	2.5	0.6	0.152	0.143	0.038	2.24	2.08	1.97	1.56
Per_D26_H18_T25_Toe	2.5	0.6	0.194	0.194	0.076	2.65	2.06	1.92	1.43
Per_D26_H14_T25_ToeProt	2.5	0.6	0.153	0.145	0.039	2.24	2.06	1.95	1.50
Per_D26_H14_T25_Toe	2.5	0.6	0.154	0.145	0.039	2.25	2.06	1.95	1.51

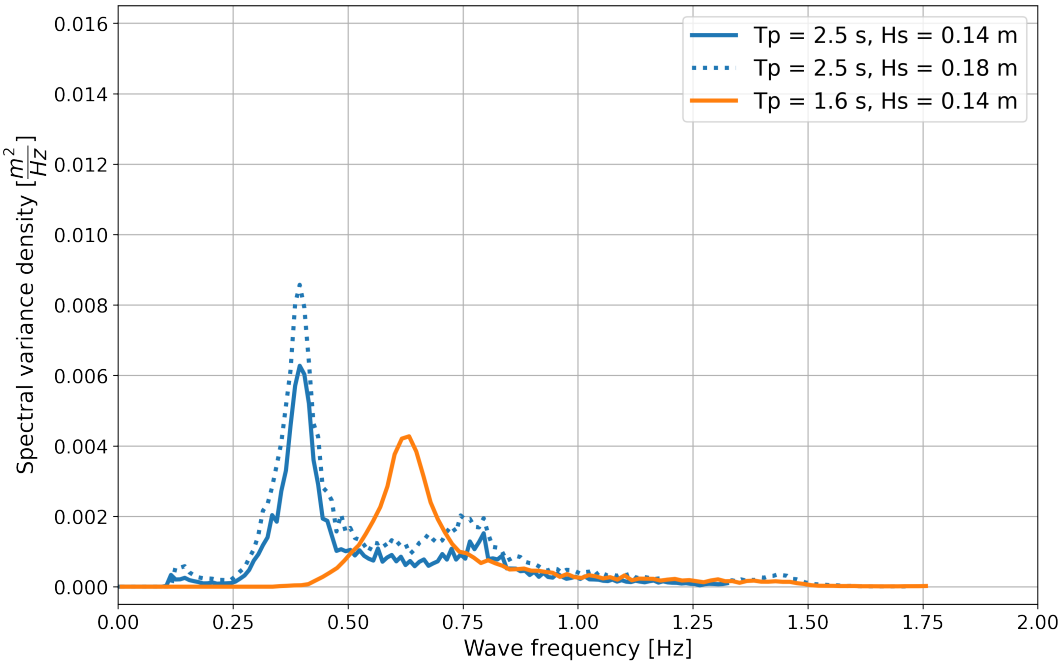

Figure B.1: Variance density spectrum incoming waves - Permeable breakwater - Onshore location

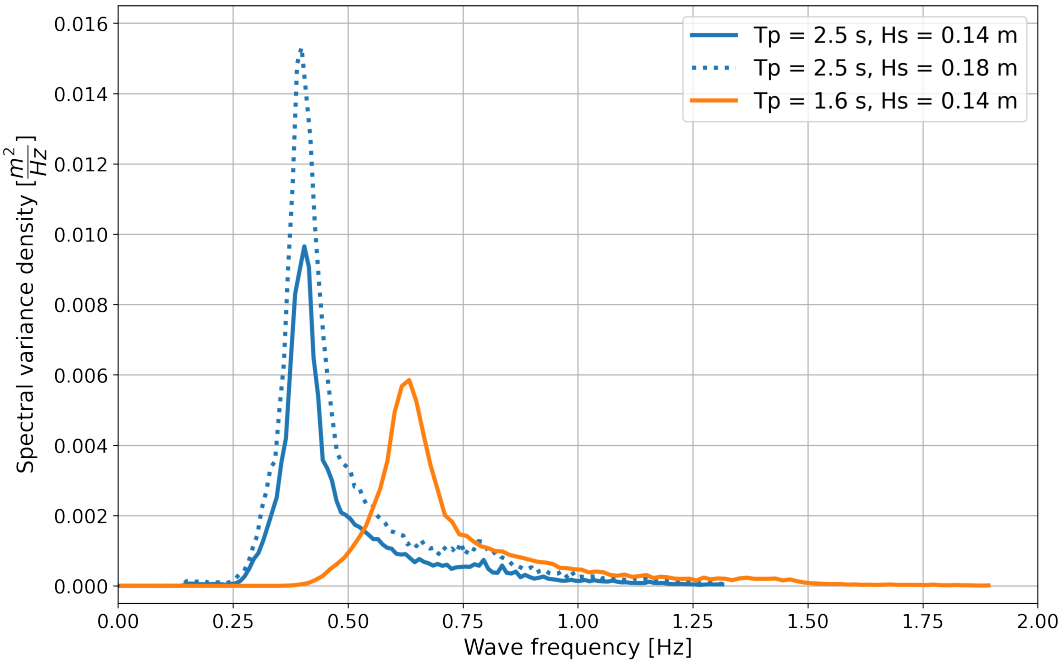

Figure B.2: Variance density spectrum incoming waves - Permeable breakwater - Offshore location

C Appendix - Results

C.1 Bed profiles permeable breakwater

C.1.1 Permeable rubble mound - Coarse sediment tests

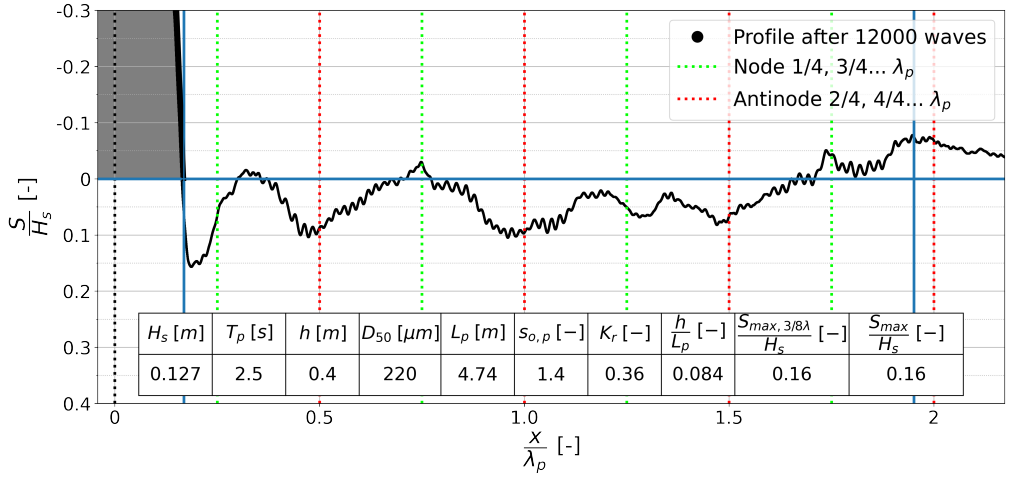

H_s [m]	T_p [s]	h [m]	D_{50} [μm]	L_p [m]	$s_{o,p}$ [−]	K_r [−]	$\frac{h}{L_p}$ [−]	$\frac{S_{max,\,3/8\lambda}}{H_s}$ [−]	$\frac{S_{max}}{H_s}$ [−]
0.127	2.5	0.4	220	4.74	1.4	0.36	0.084	0.16	0.16

Figure C.1: Test Per_D22_H14_T25_NoToe

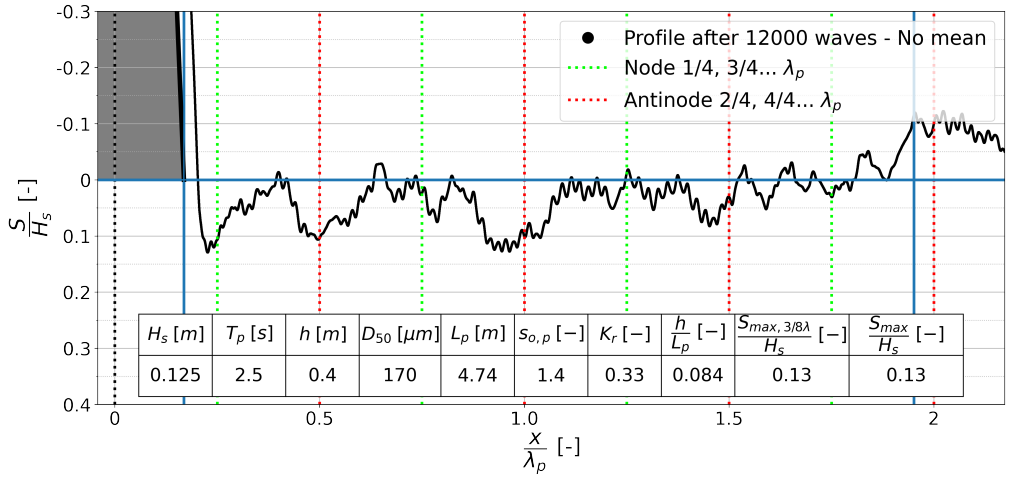

H_s [m]	T_p [s]	h [m]	D_{50} [μm]	L_p [m]	$s_{o,p}$ [−]	K_r [−]	$\frac{h}{L_p}$ [−]	$\frac{S_{max,\,3/8\lambda}}{H_s}$ [−]	$\frac{S_{max}}{H_s}$ [−]
0.125	2.5	0.4	170	4.74	1.4	0.33	0.084	0.13	0.13

Figure C.2: Test Per_D22_H14_T25_Toe

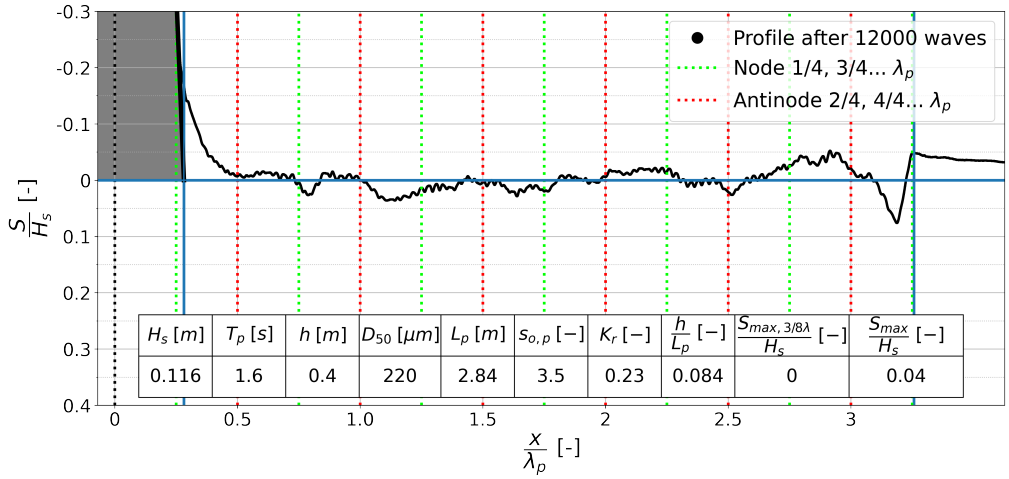

H_s [m]	T_p [s]	h [m]	D_{50} [μm]	L_p [m]	$s_{o,p}$ [−]	K_r [−]	$\frac{h}{L_p}$ [−]	$\frac{S_{max,\,3/8\lambda}}{H_s}$ [−]	$\frac{S_{max}}{H_s}$ [−]
0.116	1.6	0.4	220	2.84	3.5	0.23	0.084	0	0.04

Figure C.3: Test Per_D22_H14_T16_NoToe

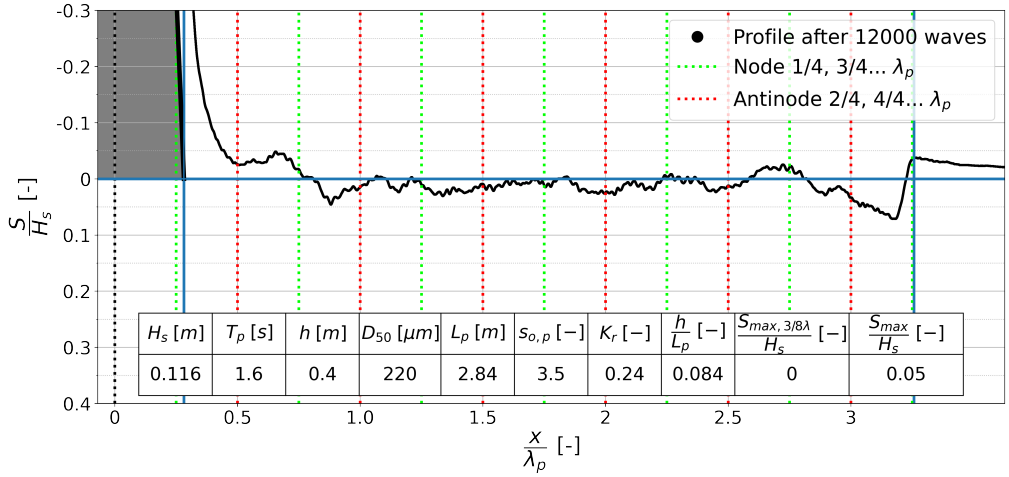

H_s [m]	T_p [s]	h [m]	D_{50} [μm]	L_p [m]	$s_{o,p}$ [−]	K_r [−]	$\frac{h}{L_p}$ [−]	$\frac{S_{max,\,3/8\lambda}}{H_s}$ [−]	$\frac{S_{max}}{H_s}$ [−]
0.116	1.6	0.4	220	2.84	3.5	0.24	0.084	0	0.05

Figure C.4: Test Per_D22_H14_T16_Toe

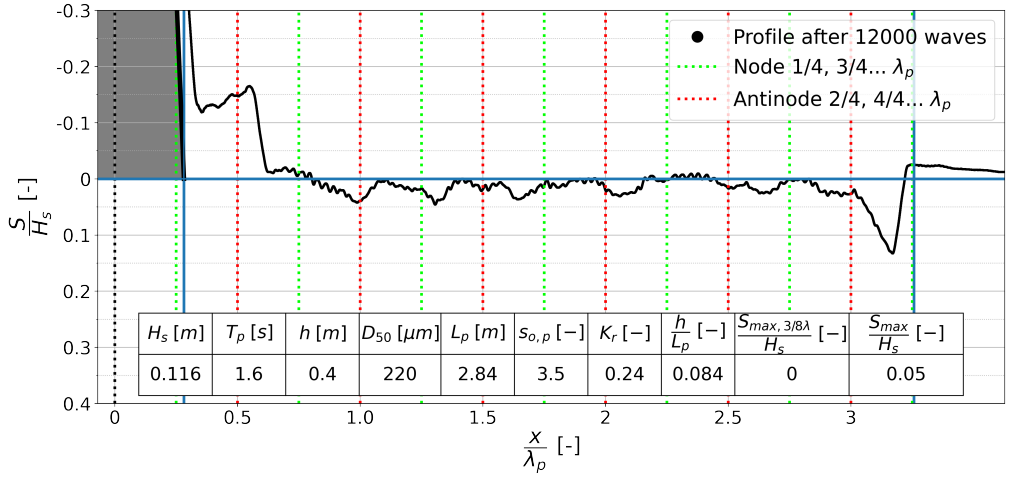

H_s [m]	T_p [s]	h [m]	D_{50} [μm]	L_p [m]	$s_{o,p}$ [−]	K_r [−]	$\frac{h}{L_p}$ [−]	$\frac{S_{max,\,3/8\lambda}}{H_s}$ [−]	$\frac{S_{max}}{H_s}$ [−]
0.116	1.6	0.4	220	2.84	3.5	0.24	0.084	0	0.05

Figure C.5: Test Per_D22_H14_T16_ToeProt

C.1.2 Permeable rubble mound - Fine sediment tests

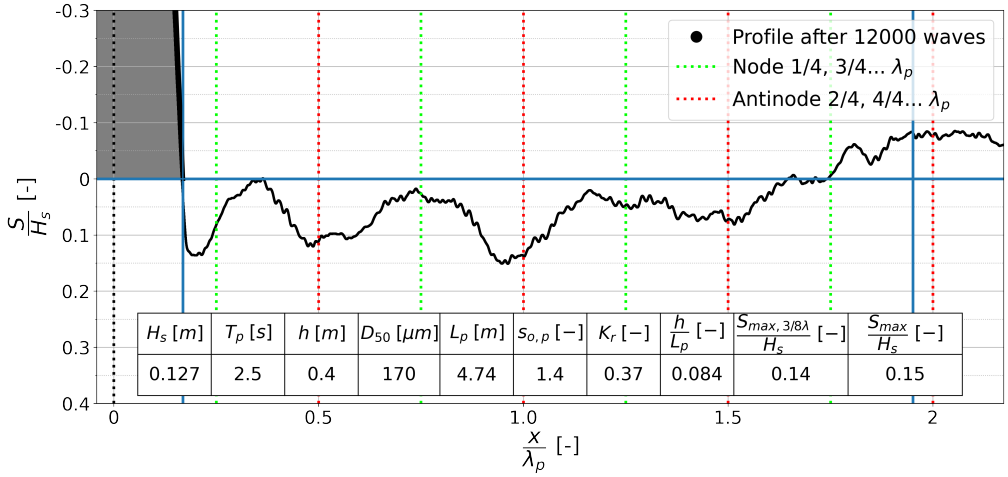

H_s [m]	T_p [s]	h [m]	D_{50} [μm]	L_p [m]	$s_{o,p}$ [−]	K_r [−]	$\frac{h}{L_p}$ [−]	$\frac{S_{max,\,3/8\lambda}}{H_s}$ [−]	$\frac{S_{max}}{H_s}$ [−]
0.127	2.5	0.4	170	4.74	1.4	0.37	0.084	0.14	0.15

Figure C.6: Test Per_D17_H14_T25_NoToe

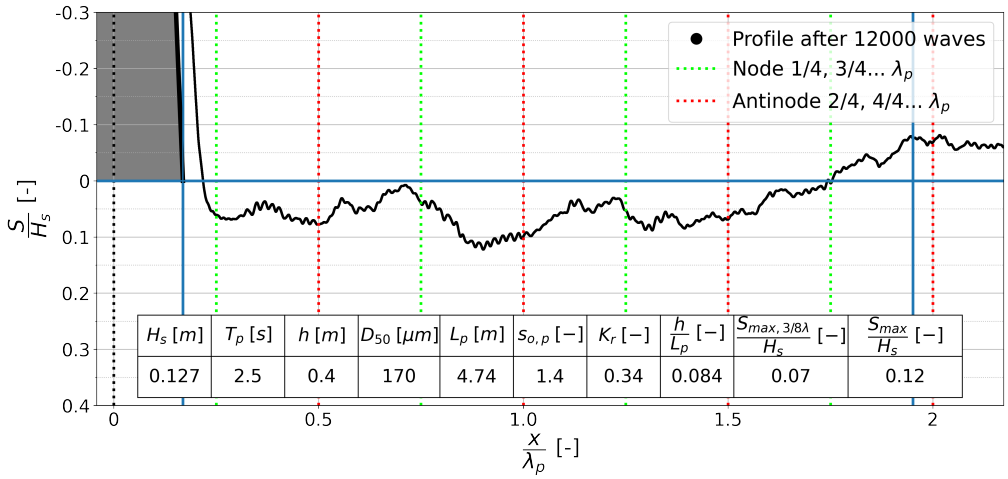

H_s [m]	T_p [s]	h [m]	D_{50} [μm]	L_p [m]	$s_{o,p}$ [−]	K_r [−]	$\frac{h}{L_p}$ [−]	$\frac{S_{max,\,3/8\lambda}}{H_s}$ [−]	$\frac{S_{max}}{H_s}$ [−]
0.127	2.5	0.4	170	4.74	1.4	0.34	0.084	0.07	0.12

Figure C.7: Test Per_D17_H14_T25_Toe

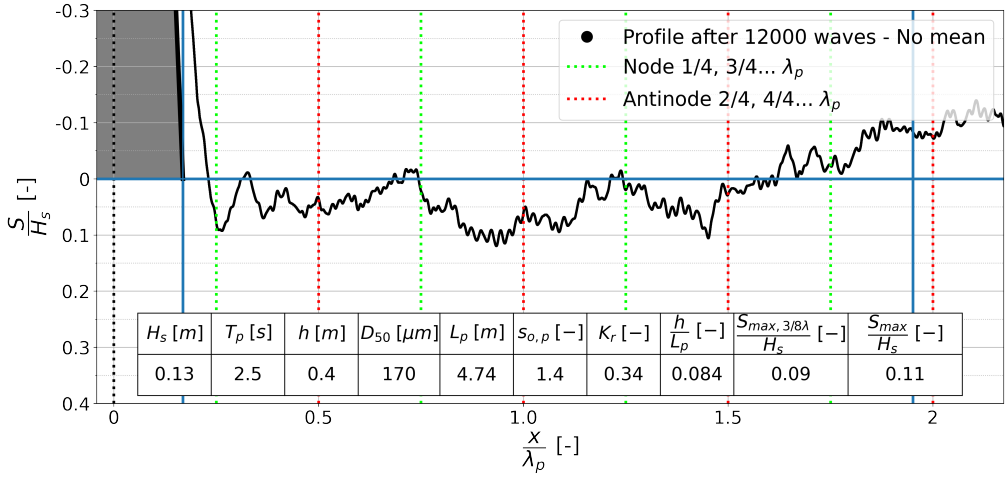

H_s [m]	T_p [s]	h [m]	D_{50} [μm]	L_p [m]	$s_{o,p}$ [−]	K_r [−]	$\frac{h}{L_p}$ [−]	$\frac{S_{max,\,3/8\lambda}}{H_s}$ [−]	$\frac{S_{max}}{H_s}$ [−]
0.13	2.5	0.4	170	4.74	1.4	0.34	0.084	0.09	0.11

Figure C.8: Test Per_D17_H14_T25_Toe_b

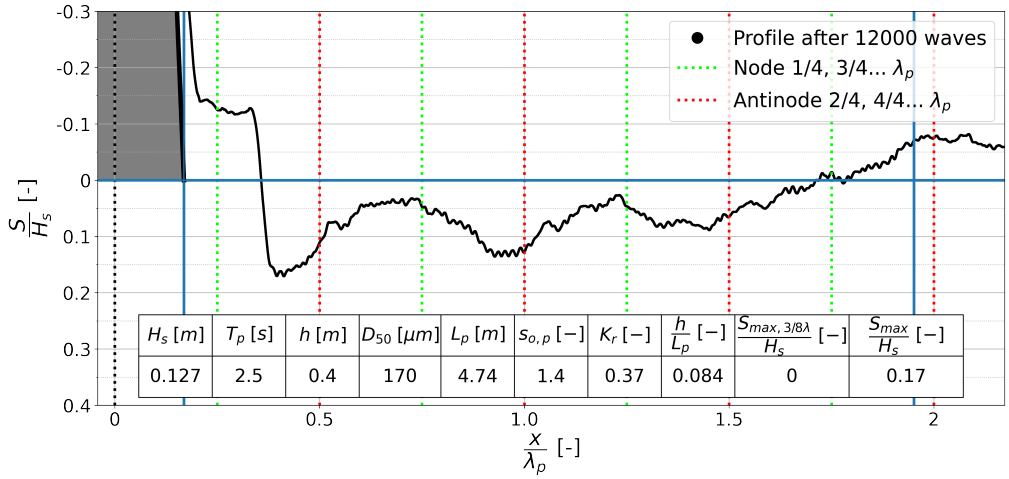

H_s [m]	T_p [s]	h [m]	D_{50} [μm]	L_p [m]	$s_{o,p}$ [−]	K_r [−]	$\frac{h}{L_p}$ [−]	$\frac{S_{max,\,3/8\lambda}}{H_s}$ [−]	$\frac{S_{max}}{H_s}$ [−]
0.127	2.5	0.4	170	4.74	1.4	0.37	0.084	0	0.17

Figure C.9: Test Per_D17_H14_T25_ToeProt

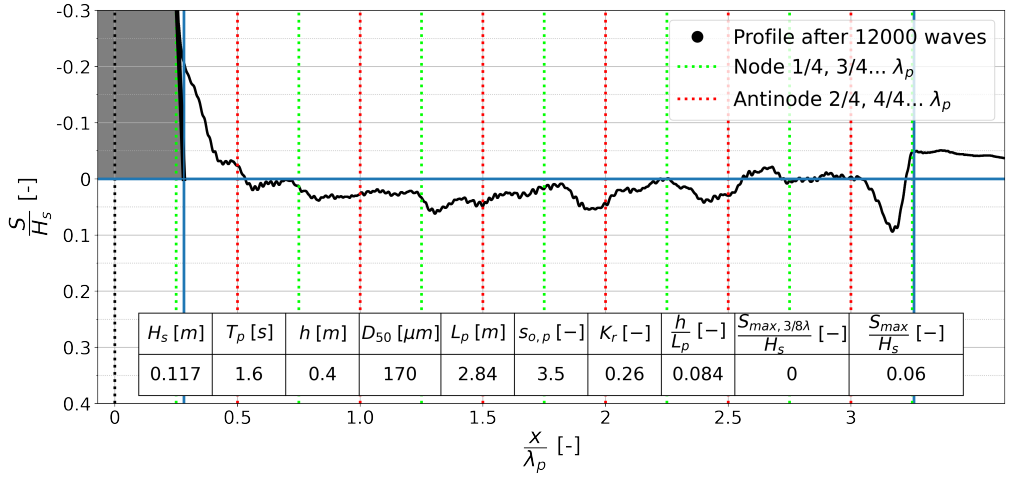

H_s [m]	T_p [s]	h [m]	D_{50} [μm]	L_p [m]	$s_{o,p}$ [−]	K_r [−]	$\frac{h}{L_p}$ [−]	$\frac{S_{max,\,3/8\lambda}}{H_s}$ [−]	$\frac{S_{max}}{H_s}$ [−]
0.117	1.6	0.4	170	2.84	3.5	0.26	0.084	0	0.06

Figure C.10: Test Per_D17_H14_T16_NoToe

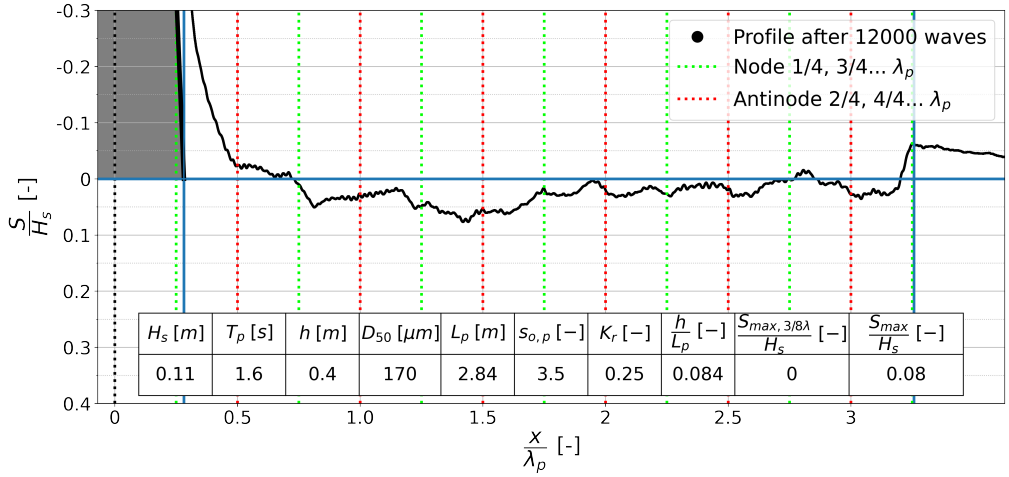

H_s [m]	T_p [s]	h [m]	D_{50} [μm]	L_p [m]	$s_{o,p}$ [−]	K_r [−]	$\frac{h}{L_p}$ [−]	$\frac{S_{max,\,3/8\lambda}}{H_s}$ [−]	$\frac{S_{max}}{H_s}$ [−]
0.11	1.6	0.4	170	2.84	3.5	0.25	0.084	0	0.08

Figure C.11: Test Per_D17_H14_T16_Toe

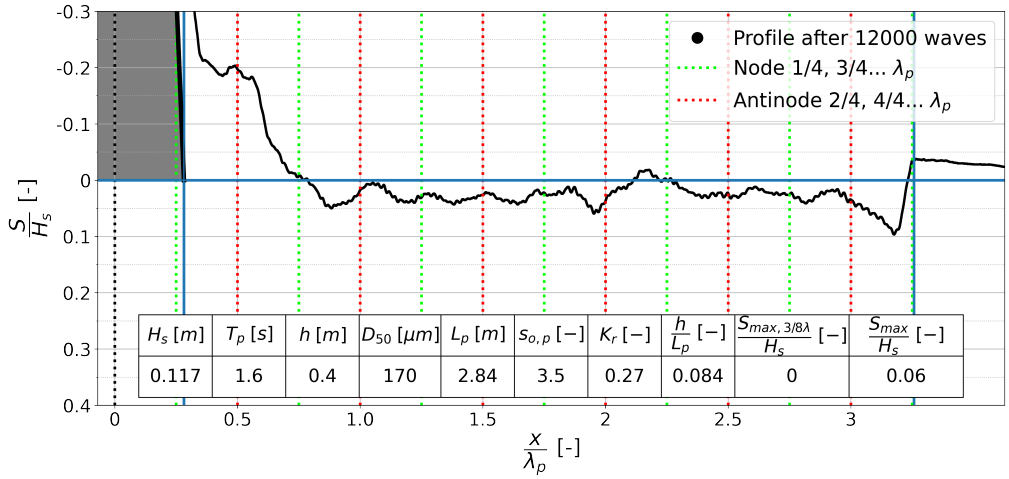

H_s [m]	T_p [s]	h [m]	D_{50} [μm]	L_p [m]	$s_{o,p}$ [−]	K_r [−]	$\frac{h}{L_p}$ [−]	$\frac{S_{max,\,3/8\lambda}}{H_s}$ [−]	$\frac{S_{max}}{H_s}$ [−]
0.117	1.6	0.4	170	2.84	3.5	0.27	0.084	0	0.06

Figure C.12: Test Per_D17_H14_T16_ToeProt

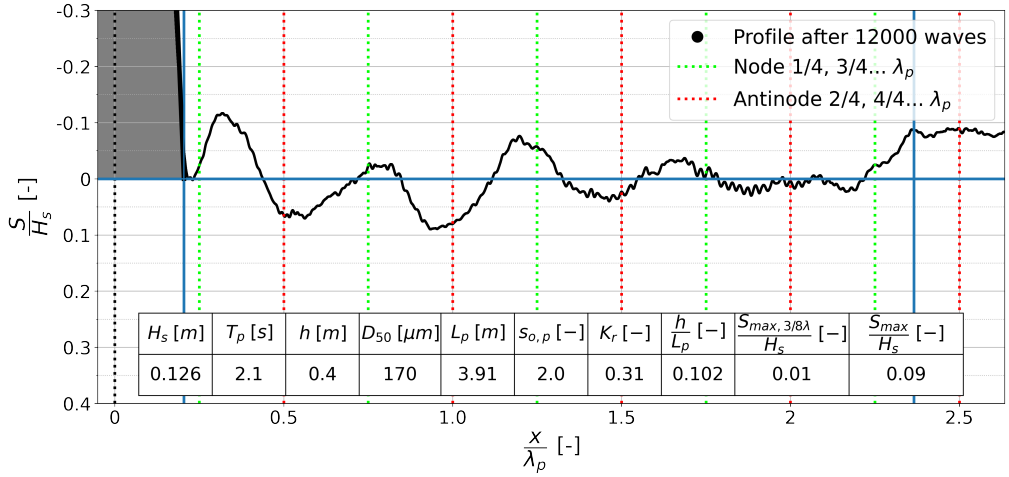

H_s [m]	T_p [s]	h [m]	D_{50} [μm]	L_p [m]	$s_{o,p}$ [−]	K_r [−]	$\frac{h}{L_p}$ [−]	$\frac{S_{max,\,3/8\lambda}}{H_s}$ [−]	$\frac{S_{max}}{H_s}$ [−]
0.126	2.1	0.4	170	3.91	2.0	0.31	0.102	0.01	0.09

Figure C.13: Test Per_D17_H14_T21_NoToe

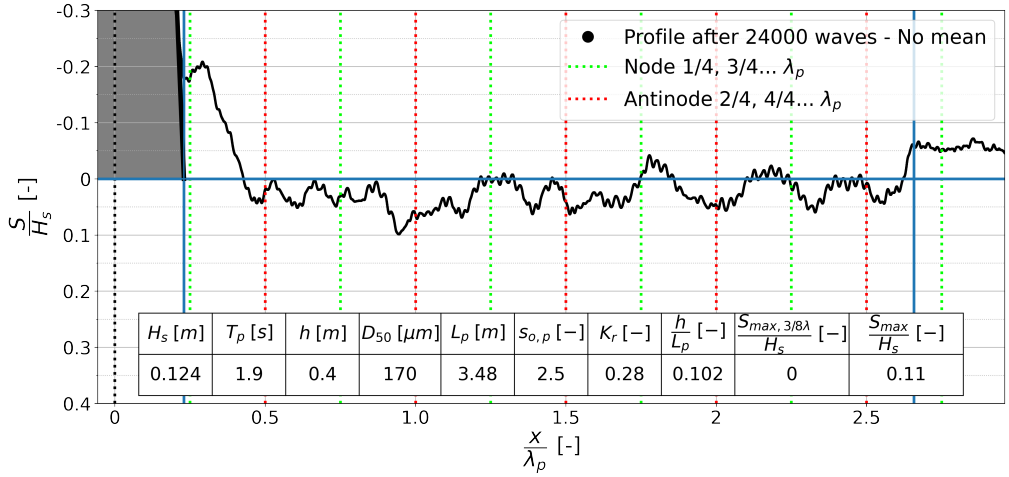

H_s [m]	T_p [s]	h [m]	D_{50} [μm]	L_p [m]	$s_{o,p}$ [−]	K_r [−]	$\frac{h}{L_p}$ [−]	$\frac{S_{max,\,3/8\lambda}}{H_s}$ [−]	$\frac{S_{max}}{H_s}$ [−]
0.124	1.9	0.4	170	3.48	2.5	0.28	0.102	0	0.11

Figure C.14: Test Per_D17_H14_T19_NoToe

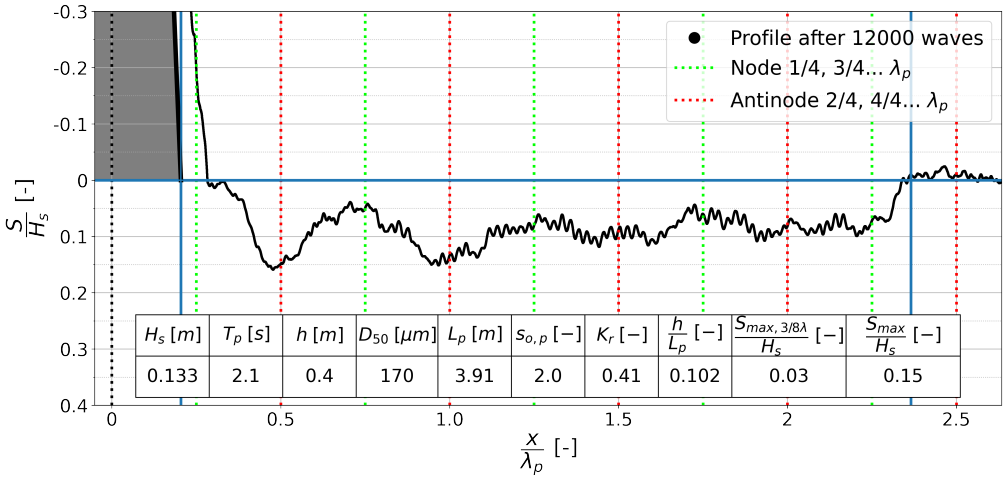

H_s [m]	T_p [s]	h [m]	D_{50} [μm]	L_p [m]	$s_{o,p}$ [−]	K_r [−]	$\frac{h}{L_p}$ [−]	$\frac{S_{max,\,3/8\lambda}}{H_s}$ [−]	$\frac{S_{max}}{H_s}$ [−]
0.133	2.1	0.4	170	3.91	2.0	0.41	0.102	0.03	0.15

Figure C.15: Test Per_D17_H14_T21_Toe

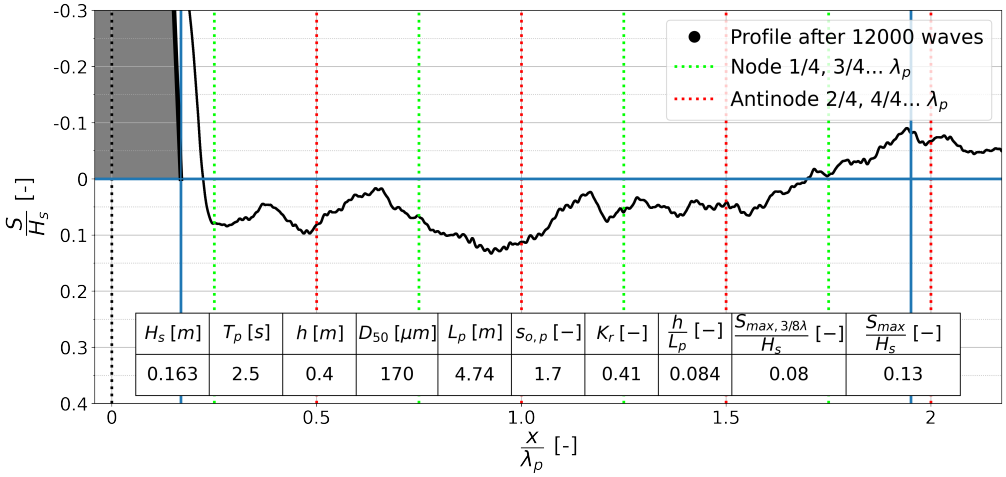

H_s [m]	T_p [s]	h [m]	D_{50} [μm]	L_p [m]	$s_{o,p}$ [−]	K_r [−]	$\frac{h}{L_p}$ [−]	$\frac{S_{max,\,3/8\lambda}}{H_s}$ [−]	$\frac{S_{max}}{H_s}$ [−]
0.163	2.5	0.4	170	4.74	1.7	0.41	0.084	0.08	0.13

Figure C.16: Test Per_D17_H18_T25_Toe

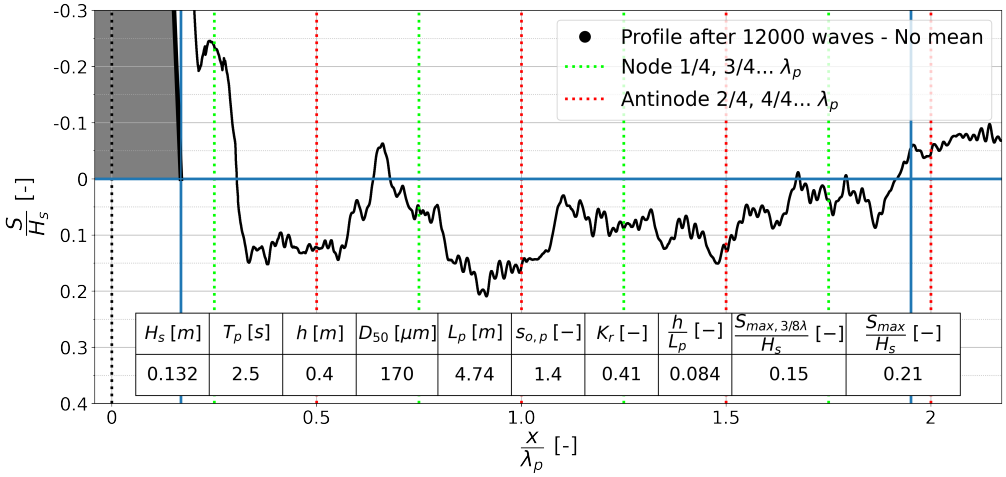

H_s [m]	T_p [s]	h [m]	D_{50} [μm]	L_p [m]	$s_{o,p}$ [−]	K_r [−]	$\frac{h}{L_p}$ [−]	$\frac{S_{max,\,3/8\lambda}}{H_s}$ [−]	$\frac{S_{max}}{H_s}$ [−]
0.132	2.5	0.4	170	4.74	1.4	0.41	0.084	0.15	0.21

Figure C.17: Test Per_D17_H14_T25_ToeProt* After 16 hours

C.2 Bed profiles Revetment

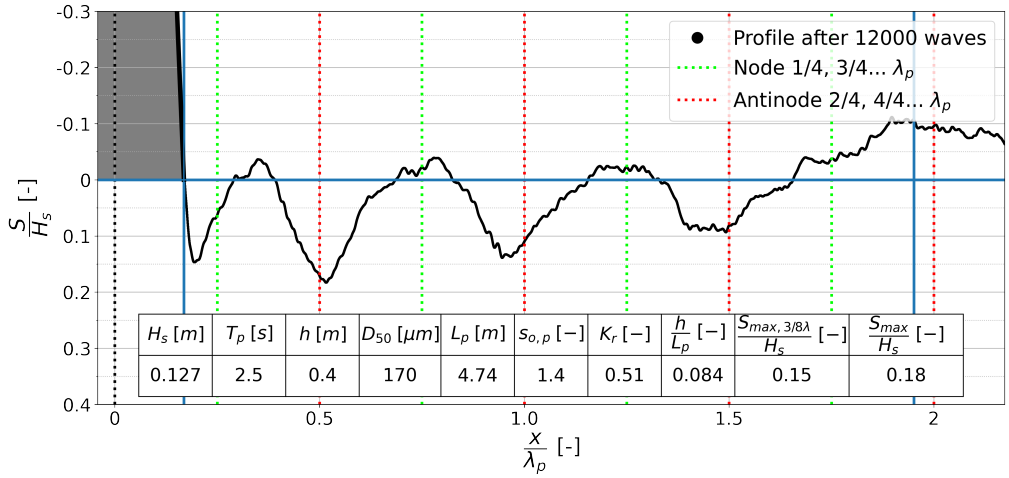

H_s [m]	T_p [s]	h [m]	D_{50} [μm]	L_p [m]	$s_{o,p}$ [−]	K_r [−]	$\frac{h}{L_p}$ [−]	$\frac{S_{max,\,3/8\lambda}}{H_s}$ [−]	$\frac{S_{max}}{H_s}$ [−]
0.127	2.5	0.4	170	4.74	1.4	0.51	0.084	0.15	0.18

Figure C.18: Test Rev_D17_H14_T25_NoToe

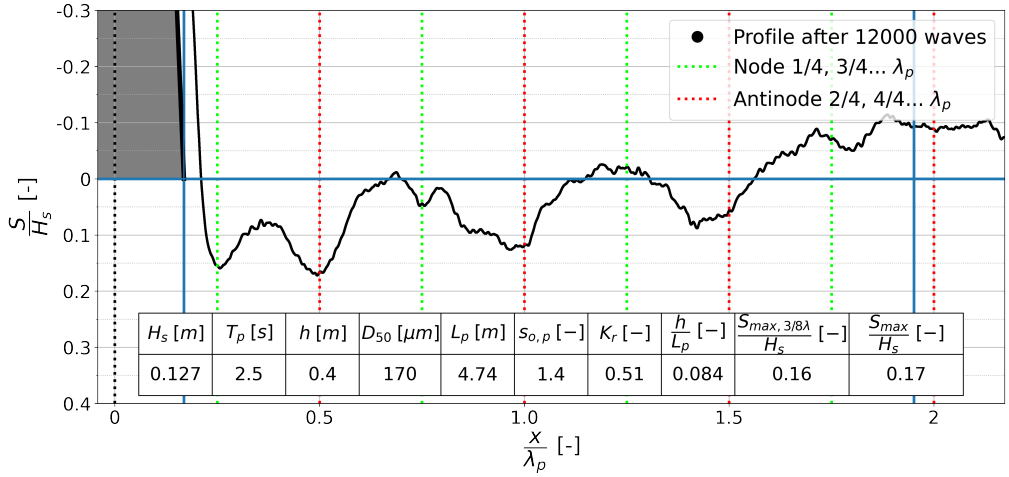

H_s [m]	T_p [s]	h [m]	D_{50} [μm]	L_p [m]	$s_{o,p}$ [−]	K_r [−]	$\frac{h}{L_p}$ [−]	$\frac{S_{max,\,3/8\lambda}}{H_s}$ [−]	$\frac{S_{max}}{H_s}$ [−]
0.127	2.5	0.4	170	4.74	1.4	0.51	0.084	0.16	0.17

Figure C.19: Test Rev_D17_H14_T25_Toe

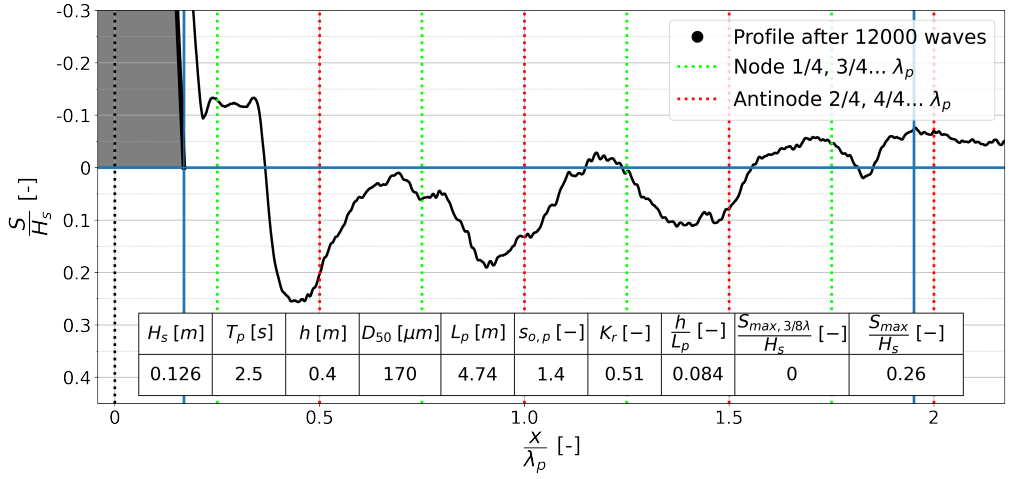

H_s [m]	T_p [s]	h [m]	D_{50} [μm]	L_p [m]	$s_{o,p}$ [−]	K_r [−]	$\frac{h}{L_p}$ [−]	$\frac{S_{max,\,3/8\lambda}}{H_s}$ [−]	$\frac{S_{max}}{H_s}$ [−]
0.126	2.5	0.4	170	4.74	1.4	0.51	0.084	0	0.26

Figure C.20: Test Rev_D17_H14_T25_ToeProt

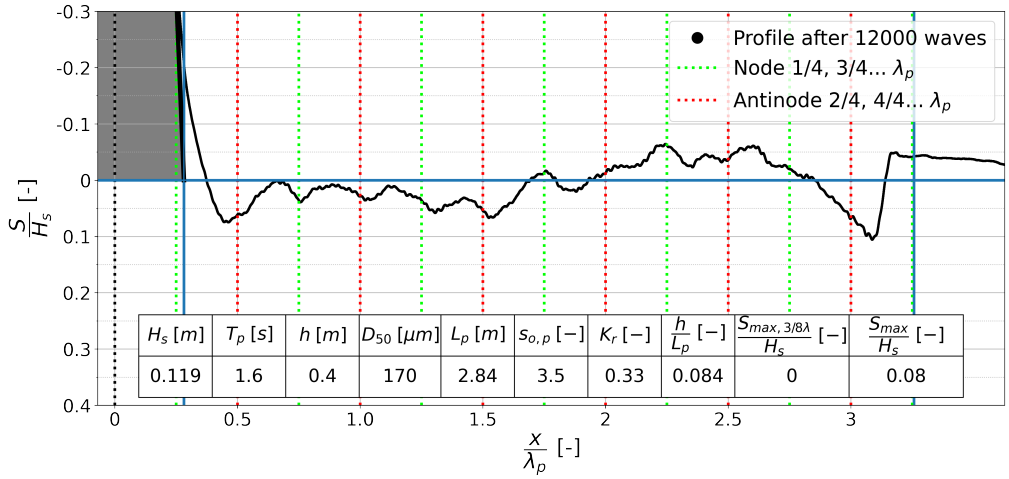

H_s [m]	T_p [s]	h [m]	D_{50} [μm]	L_p [m]	$s_{o,p}$ [−]	K_r [−]	$\frac{h}{L_p}$ [−]	$\frac{S_{max,\,3/8\lambda}}{H_s}$ [−]	$\frac{S_{max}}{H_s}$ [−]
0.119	1.6	0.4	170	2.84	3.5	0.33	0.084	0	0.08

Figure C.21: Test Rev_D17_H14_T16_NoToe

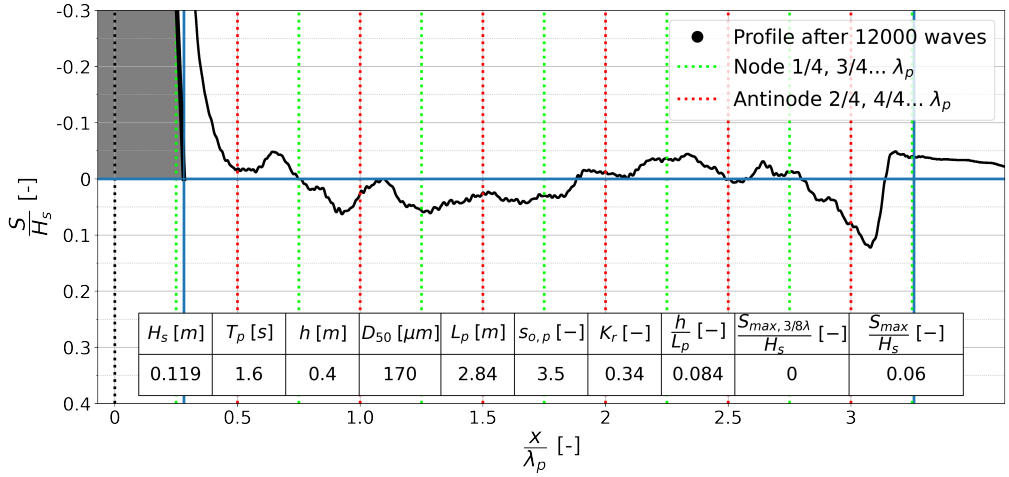

H_s [m]	T_p [s]	h [m]	D_{50} [μm]	L_p [m]	$s_{o,p}$ [−]	K_r [−]	$\frac{h}{L_p}$ [−]	$\frac{S_{max,\,3/8\lambda}}{H_s}$ [−]	$\frac{S_{max}}{H_s}$ [−]
0.119	1.6	0.4	170	2.84	3.5	0.34	0.084	0	0.06

Figure C.22: Test Rev_D17_H14_T16_Toe

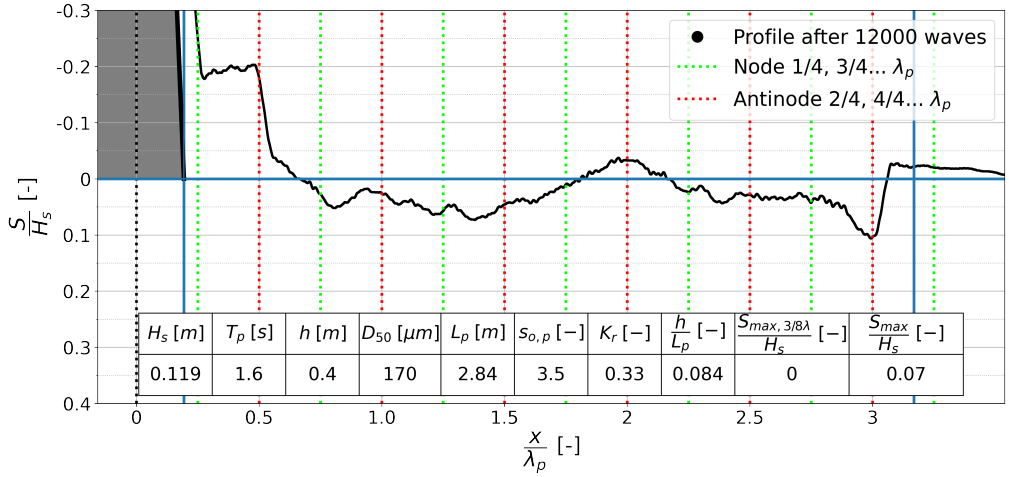

H_s [m]	T_p [s]	h [m]	D_{50} [μm]	L_p [m]	$s_{o,p}$ [−]	K_r [−]	$\frac{h}{L_p}$ [−]	$\frac{S_{max,\,3/8\lambda}}{H_s}$ [−]	$\frac{S_{max}}{H_s}$ [−]
0.119	1.6	0.4	170	2.84	3.5	0.33	0.084	0	0.07

Figure C.23: Test Rev_D17_H14_T16_ToeProt

C.3 Permeable rubble mound - tests Jantzen (2020)

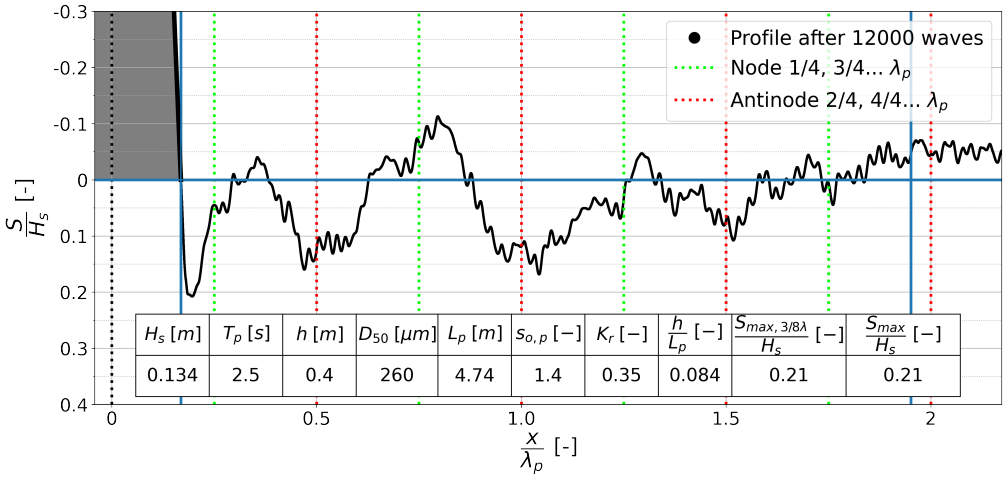

H_s [m]	T_p [s]	h [m]	D_{50} [μm]	L_p [m]	$s_{o,p}$ [−]	K_r [−]	$\frac{h}{L_p}$ [−]	$\frac{S_{max,\,3/8\lambda}}{H_s}$ [−]	$\frac{S_{max}}{H_s}$ [−]
0.134	2.5	0.4	260	4.74	1.4	0.35	0.084	0.21	0.21

Figure C.24: Test Per_D26_H14_T25_NoToe

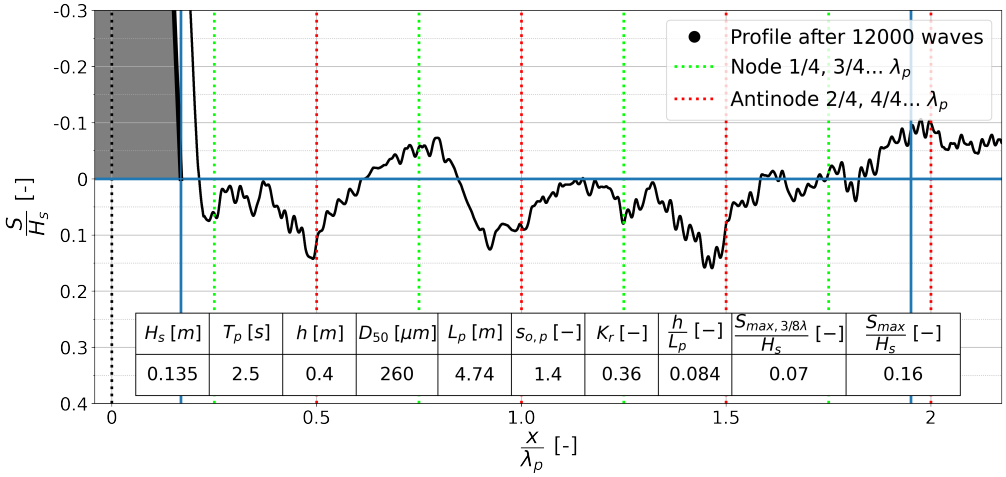

H_s [m]	T_p [s]	h [m]	D_{50} [μm]	L_p [m]	$s_{o,p}$ [−]	K_r [−]	$\frac{h}{L_p}$ [−]	$\frac{S_{max,\,3/8\lambda}}{H_s}$ [−]	$\frac{S_{max}}{H_s}$ [−]
0.135	2.5	0.4	260	4.74	1.4	0.36	0.084	0.07	0.16

Figure C.25: Test Per_D26_H14_T25_Toe

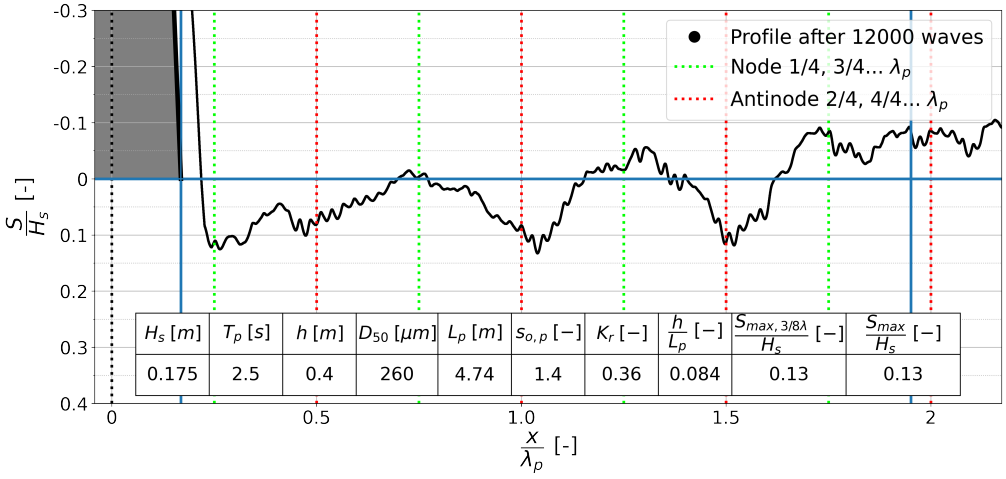

H_s [m]	T_p [s]	h [m]	D_{50} [μm]	L_p [m]	$s_{o,p}$ [−]	K_r [−]	$\frac{h}{L_p}$ [−]	$\frac{S_{max,\,3/8\lambda}}{H_s}$ [−]	$\frac{S_{max}}{H_s}$ [−]
0.175	2.5	0.4	260	4.74	1.4	0.36	0.084	0.13	0.13

Figure C.26: Test Per_D26_H18_T25_Toe

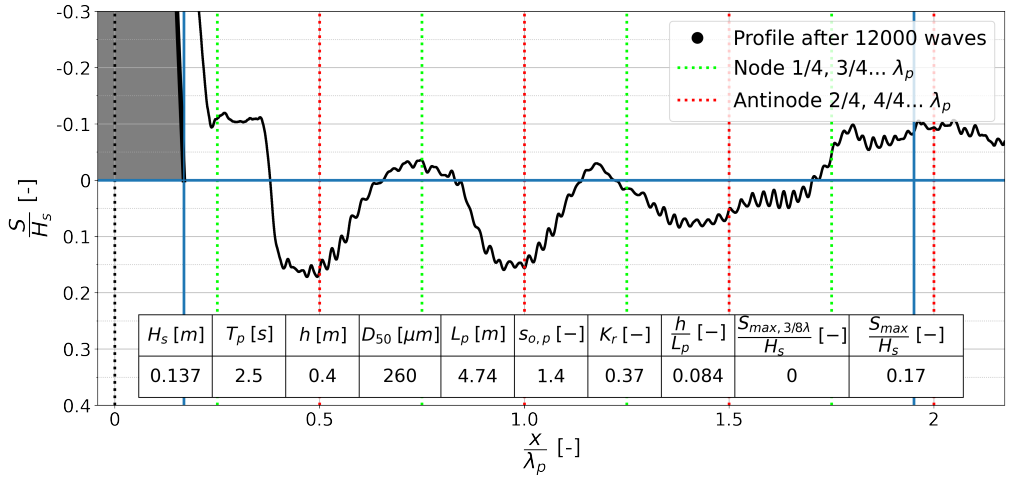

H_s [m]	T_p [s]	h [m]	D_{50} [μm]	L_p [m]	$s_{o,p}$ [−]	K_r [−]	$\frac{h}{L_p}$ [−]	$\frac{S_{max,\,3/8\lambda}}{H_s}$ [−]	$\frac{S_{max}}{H_s}$ [−]
0.137	2.5	0.4	260	4.74	1.4	0.37	0.084	0	0.17

Figure C.27: Test Per_D26_H14_T25_ToeProt

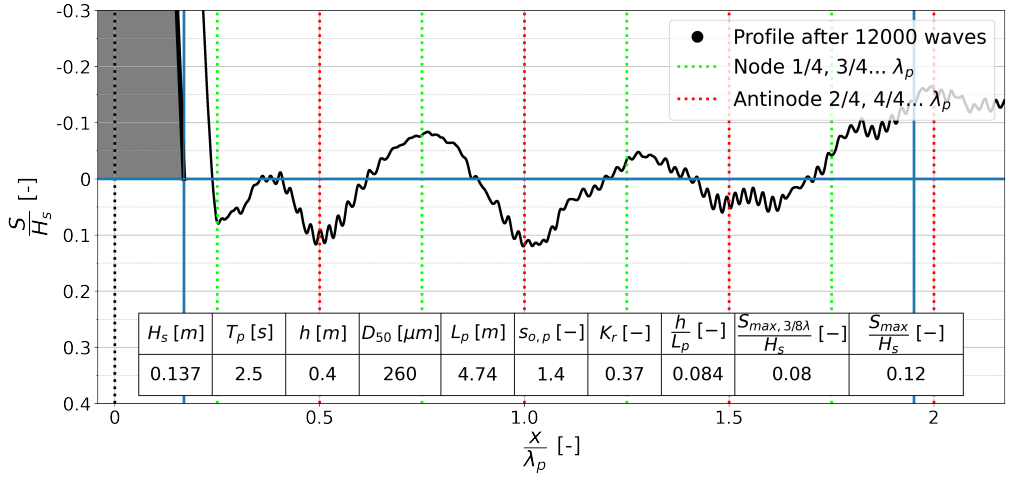

H_s [m]	T_p [s]	h [m]	D_{50} [μm]	L_p [m]	$s_{o,p}$ [−]	K_r [−]	$\frac{h}{L_p}$ [−]	$\frac{S_{max,\,3/8\lambda}}{H_s}$ [−]	$\frac{S_{max}}{H_s}$ [−]
0.137	2.5	0.4	260	4.74	1.4	0.37	0.084	0.08	0.12

Figure C.28: Test Per_D26_H14_T25_Toe

C.4 Bed profiles impermeable slope - tests Jantzen (2020)

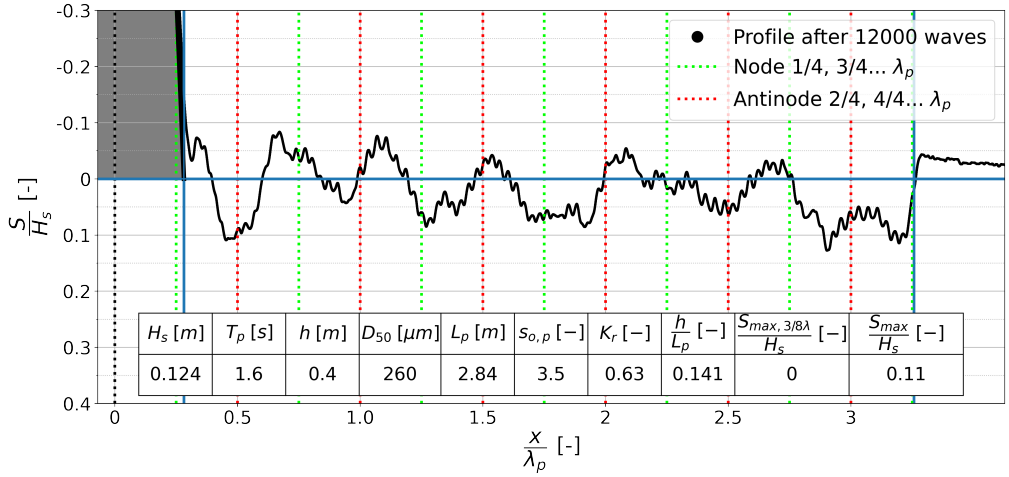

H_s [m]	T_p [s]	h [m]	D_{50} [μm]	L_p [m]	$s_{o,p}$ [−]	K_r [−]	$\frac{h}{L_p}$ [−]	$\frac{S_{max,\,3/8\lambda}}{H_s}$ [−]	$\frac{S_{max}}{H_s}$ [−]
0.124	1.6	0.4	260	2.84	3.5	0.63	0.141	0	0.11

Figure C.29: Test Im_D26_H14_T16_NoToe

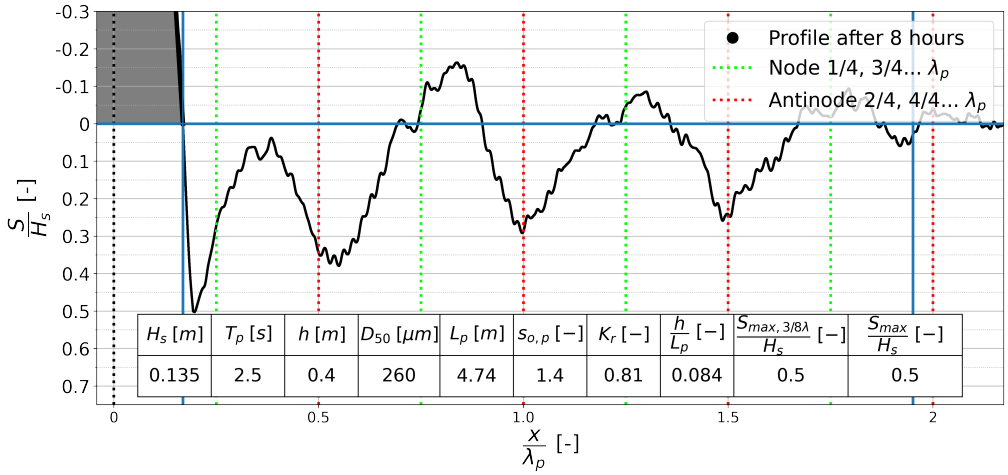

H_s [m]	T_p [s]	h [m]	D_{50} [μm]	L_p [m]	$s_{o,p}$ [−]	K_r [−]	$\frac{h}{L_p}$ [−]	$\frac{S_{max,\,3/8\lambda}}{H_s}$ [−]	$\frac{S_{max}}{H_s}$ [−]
0.135	2.5	0.4	260	4.74	1.4	0.81	0.084	0.5	0.5

Figure C.30: Test Im_D26_H14_T25_NoToe

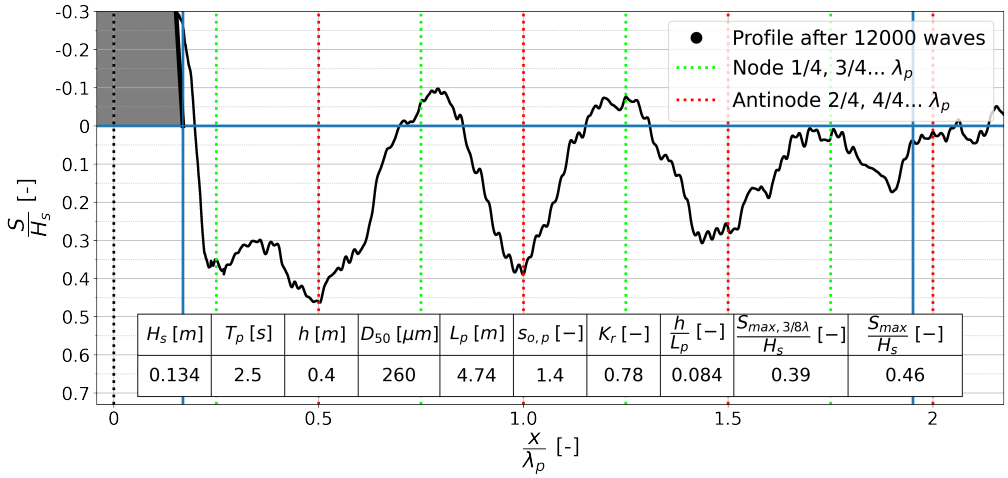

H_s [m]	T_p [s]	h [m]	D_{50} [μm]	L_p [m]	$s_{o,p}$ [−]	K_r [−]	$\frac{h}{L_p}$ [−]	$\frac{S_{max,\,3/8\lambda}}{H_s}$ [−]	$\frac{S_{max}}{H_s}$ [−]
0.134	2.5	0.4	260	4.74	1.4	0.78	0.084	0.39	0.46

Figure C.31: Test Im_D26_H14_T25_Toe

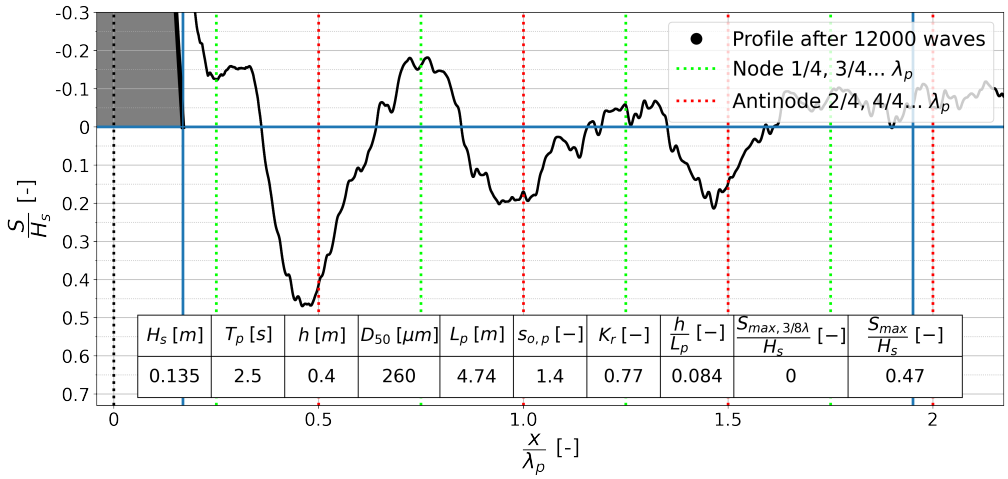

H_s [m]	T_p [s]	h [m]	D_{50} [μm]	L_p [m]	$s_{o,p}$ [−]	K_r [−]	$\frac{h}{L_p}$ [−]	$\frac{S_{max,\,3/8\lambda}}{H_s}$ [−]	$\frac{S_{max}}{H_s}$ [−]
0.135	2.5	0.4	260	4.74	1.4	0.77	0.084	0	0.47

Figure C.32: Test Im_D26_H14_T25_ToeProt

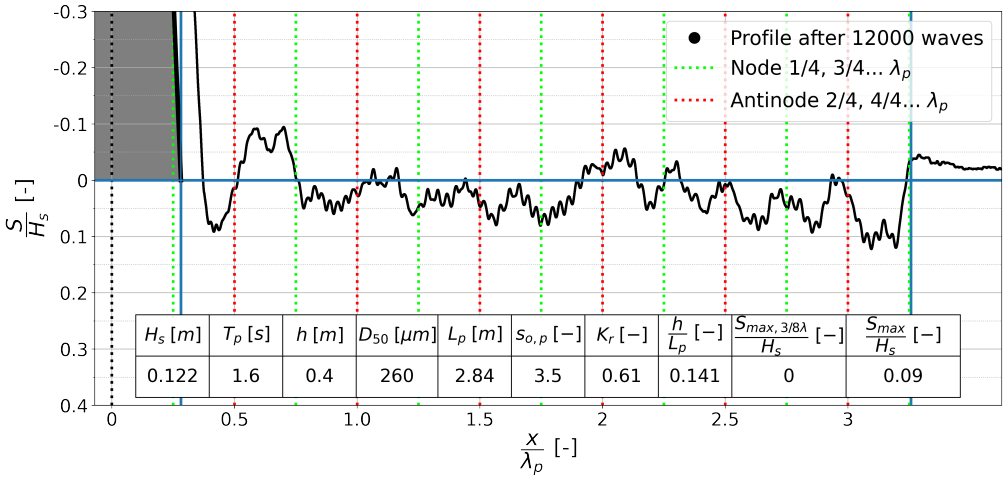

H_s [m]	T_p [s]	h [m]	D_{50} [μm]	L_p [m]	$s_{o,p}$ [−]	K_r [−]	$\frac{h}{L_p}$ [−]	$\frac{S_{max,\,3/8\lambda}}{H_s}$ [−]	$\frac{S_{max}}{H_s}$ [−]
0.122	1.6	0.4	260	2.84	3.5	0.61	0.141	0	0.09

Figure C.33: Test Im_D26_H14_T16_Toe

D Appendix - Flow measurements

In the following tables the results of the flow measurements are given for 7 tests done in the present study and that of Jantzen (2020). Results are given of measurements above the toe of the structure and at 1/2 and 3/4 peak wavelength λ_p from the waterline. For some test measurements have not been done at all these locations.

Measurements have been done at each location for 5 minutes. From these measurements the maximum and minimum measured velocity is presented. Additionally, the velocity that is exceeded 2% is given in both the offshore and onshore direction. This value is also given for the absolute velocity.

Measurements for tests Per_D26_H14_T25_NoToe, Im_D26_H14_T16_Toe and Im_D26_H14_T25_ToeProt are from earlier research by Jantzen (2020). The exact location of the measurements done for these test compared to the standing wave pattern is not know. Therefore, comparison of these measurements with results from the present study only gives an indication of differences in flow velocity.

Table D-1: Measured flow velocities at toe, 0.20 m above initial bed level.

Test	$\mathbf{u_{max}}$ **[m/s]**	$\mathbf{u_{min}}$ **[m/s]**	**Offshore** $\mathbf{u_{2\%}}$ **[m/s]**	**Onshore** $\mathbf{u_{2\%}}$ **[m/s]**	**Absolute** $\mathbf{u_{2\%}}$ **[m/s]**
Per_D17_H14_T16_ToeProt	0.46	-0.58	0.25	-0.29	0.34
Per_D26_H14_T25_NoToe	-	-	-	-	-
Per_D17_H14_T25_Toe_b	0.74	-0.51	0.47	-0.38	0.45
Rev_D17_H14_T16_NoToe	0.43	-0.48	0.28	-0.27	0.31
Rev_D17_H14_T25_Toe	0.86	-0.65	0.55	-0.48	0.58
Im_D26_H14_T16_Toe	-	-	-	-	-
Im_D26_H14_T25_ToeProt	-	-	-	-	-

Table D-2: Measured flow velocities at approximately $1/2\lambda$ from waterline, 0.10 m above initial bed level.

Test	$\mathbf{u_{max}}$ **[m/s]**	$\mathbf{u_{min}}$ **[m/s]**	**Offshore** $\mathbf{u_{2\%}}$ **[m/s]**	**Onshore** $\mathbf{u_{2\%}}$ **[m/s]**	**Absolute** $\mathbf{u_{2\%}}$ **[m/s]**
Per_D17_H14_T16_ToeProt	-	-	-	-	-
Per_D26_H14_T25_NoToe	0.39	-0.31	0.22	-0.21	0.26
Per_D17_H14_T25_Toe_b	0.41	-0.31	0.24	-0.19	0.25
Rev_D17_H14_T16_NoToe	-	-	-	-	-
Rev_D17_H14_T25_Toe	0.37	-0.36	0.24	-0.20	0.26
Im_D26_H14_T16_Toe	0.40	-0.38	0.24	-0.21	0.26
Im_D26_H14_T25_ToeProt	0.42	-0.35	0.18	-0.16	0.21

Table D-3: Measured flow velocities at approximately $3/4\lambda$ from waterline, 0.10 m above initial bed level.

Test	$\mathbf{u_{max}}$ **[m/s]**	$\mathbf{u_{min}}$ **[m/s]**	**Offshore** $\mathbf{u_{2\%}}$ **[m/s]**	**Onshore** $\mathbf{u_{2\%}}$ **[m/s]**	**Absolute** $\mathbf{u_{2\%}}$ **[m/s]**
Per_D17_H14_T16_ToeProt	0.32	-0.40	0.18	-0.22	0.26
Per_D26_H14_T25_NoToe	0.46	-0.45	0.26	-0.23	0.31
Per_D17_H14_T25_Toe_b	0.45	-0.41	0.32	-0.27	0.33
Rev_D17_H14_T16_NoToe	0.32	-0.33	0.20	-0.22	0.24
Rev_D17_H14_T25_Toe	0.51	-0.52	0.34	-0.32	0.36
Im_D26_H14_T16_Toe	0.46	-0.47	0.28	-0.26	0.31
Im_D26_H14_T25_ToeProt	0.51	-0.59	0.30	-0.28	0.34

E Appendix - Velocities from reflected irregular waves

Hughes and Fowler (1995) studied velocity for irregular waves reflected from coastal structures and present a technique for estimating the horizontal and vertical root-mean-squared velocity parameters. This techniques uses empirical relationships for wave reflection and reflection phase. Both a smooth impermeable and a permeable rubble mound structure with a slope of 1:2.0 were investigated.

$$u_{rms}^2 = \sum_{i=1}^{\infty} \left(\frac{g k_i}{\sigma_i} \right)^2 \frac{\cosh^2 k_i (h+z)}{\cosh^2 k_i h} (1 - 2K_{r_i} \cos 2k_i x + \theta_i + K_{r_i}^2) \frac{a_i^2}{2} \tag{E.1}$$

$$w_{rms}^2 = \sum_{i=1}^{\infty} \left(\frac{g k_i}{\sigma_i} \right)^2 \frac{\sinh^2 k_i (h+z)}{\cosh^2 k_i h} (1 + 2K_{r_i} \cos 2k_i x + \theta_i + K_{r_i}^2) \frac{a_i^2}{2} \tag{E.2}$$

Based on first-order wave theory expressions for the horizontal and vertical root-mean-squared (RMS) velocities were developed. These expressions are valid for normally incident, non-breaking irregular waves that are reflected of a coastal structure situated on a flat bottom.

As the tests in the present study are also done with normally incident, irregular non-breaking waves and all tests are done with a flat bed in front of the structure the expressions from Hughes and Fowler (1995) can be applied. In fig. E.1a the horizontal RMS velocity calculated with the expression is given for all three structures. It can be seen that a change in wave reflection influences the velocities caused by the standing wave. For a low amount of wave reflection the maximum velocity over the length is lowest, while for the highest reflection the maximum velocity is largest. Another interesting result is that the lowest reflection gives the largest velocity at the nodes while it results in the lowest velocity at the anti-node. For the largest reflection this is switched.
An opposite pattern is observed for the vertical velocities. These are largest at the nodes and smallest at the anti-nodes. Again the impermeable structure with the largest amount of wave reflection results in the largest maximum and minimum velocities. The vertical velocity pattern is given in fig. E.1b.

The same patterns are observed for the short waves that are tested and can be seen in fig. E.1c and fig. E.1d. As expected for these shorter waves the maximum velocities and the mean velocities are smaller.

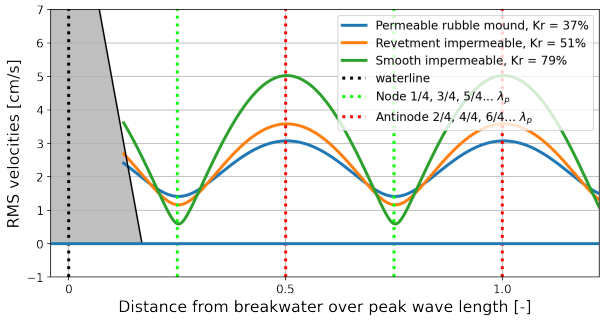

(a) Horizontal RMS velocity long waves, Tp = 2.5 s.

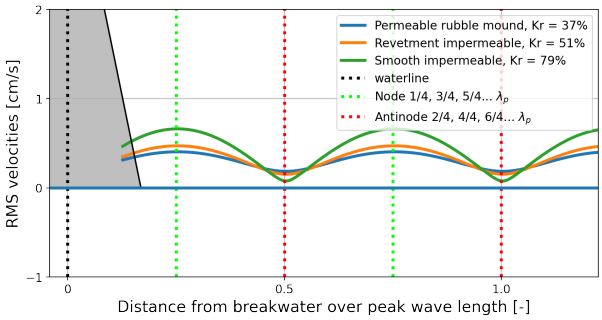

(b) Vertical RMS velocity long waves, Tp = 2.5 s.

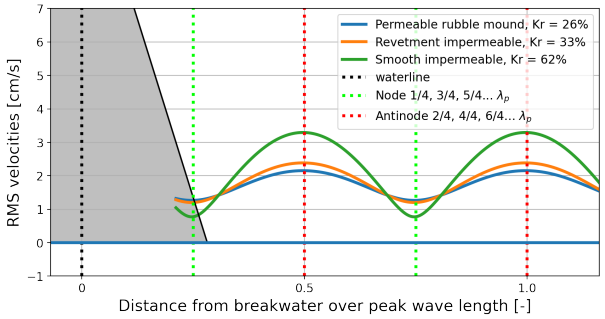

(c) Horizontal RMS velocity short waves, Tp = 1.6 s.

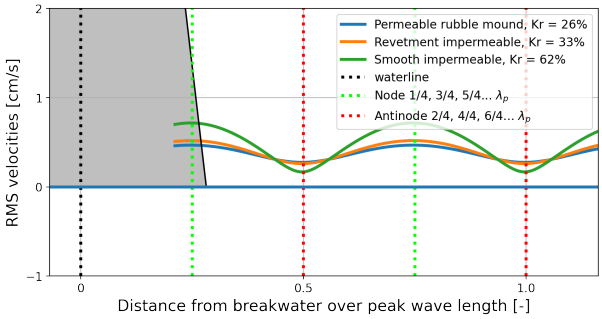

(d) Vertical RMS velocity short waves, Tp = 1.6 s.

Figure E.1: RMS velocities 0.10 m above bed, for tested structures with a 1:2.0 slope.
Calculated with eq. (E.1) and eq. (E.2).

F Appendix - Sediment transport calculations

F.1 Shields and modified Shields

With the modified Shields approach the grain size for which the bed material will start to move can be determined using the maximum orbital velocity $\hat{u}_b$, which is given in eq. (F.1) by Rance and Warren (1969). When rewriting this equation for each type of sediment the orbital velocity for which movement starts can be found. In table F-1 these orbital velocities are given for all types of sand and for the peak wave periods that are tested. These velocities show that for the smaller sand particles initiation of motion begins at lower velocities than for the larger particles. Therefore it is expected that the profiles for the finer sediment will show more suspended material and possibly different patterns. In this table the bottom orbital velocity u_b calculated using linear wave theory is also added. This velocity is higher for every condition than the value of $\hat{u}_b$ for which motion initiates. For every test significant transport of bed material is therefore expected according to the modified Shields approach.

$$d_{n50} = 2.15 \frac{\hat{u}_b^{2.5}}{\sqrt{T}(\Delta g)^{1.5}} \tag{F.1}$$

Table F-1: Initiation of motion for the modified Shields approach

Type of sand	$\mathbf{D_{50,Sand}}[\mu m]$	$\mathbf{T_p}$ **[s]**	$\hat{u}_b$ **[m/s]**	$\mathbf{u_b}$ **[m/s]**
Sand used by Jantzen (2020)	260	1.6	0.155	0.24
Sand used by Jantzen (2020)	260	2.5	0.170	0.31
M32	220	1.6	0.145	0.24
M32	220	2.5	0.159	0.31
M34	170	1.6	0.131	0.24
M34	170	1.9	0.136	0.27
M34	170	2.1	0.138	0.29
M34	170	2.5	0.143	0.31

F.2 Rouse number

Rouse (1937) developed an approach for predicting the mode of sediment transport. In this approach the Rouse number P is calculated. This is a non-dimensional number that describes the mode of transport of sediment. The Rouse number can be calculated using the expression in equation **??** (Rouse, 1937). With the Rouse number transport is divided into three regimes, these are the bed load, the suspended load and the wash load regime. Table F-2 shows which type of transport is present depending on the Rouse number. The Rouse number is based on a flowing fluid and not on wave-induced flow. Therefore the results of the analysis with the Rouse approach are only used to give an indication of the possible sediment transport for the maximum flow velocities.

$$P = \frac{W}{\kappa u_*} \tag{F.2}$$

Where:

W = The sediment settling velocity

κ = The von Karman constant

u_* = The shear velocity

To be able to calculate the Rouse number the settling velocity of the sediment particles has to be known. This settling velocity is calculated using the approach by van Rijn (1989). The formula used here is given in eq. (F.3). The settling velocities of all three types of tested sand are calculated using this formula and are given in table F-3.

Table F-2: Rouse numbers for transport (Rouse, 1937)

Type of transport	Rouse number
Bed load	P > 2.5
Suspended load (50%)	1.2 > P >2.5
Suspended load (100%)	0.8 > P >1.2
Wash load	P < 0.8

$$W_s = \frac{10\nu}{D}\left(\sqrt{1+\frac{0.01\Delta g D^3}{\nu^2}}-1\right) \tag{F.3}$$

Where:

W_s = The settling velocity of the sand particle

ν = The kinematic viscosity

D = The particle diameter

Table F-3: Settling velocities sand particles

Type of sand	$D_{50,Sand}[\mu m]$	Settling velocity W [m/s]
Sand used by Jantzen (2020)	260	0.037
M32	220	0.030
M34	170	0.020

The shear velocity that is used to calculate the Rouse number depends on the hydraulic conditions. As these are varied between tests the velocity is calculated for every individual test. The shear velocity is calculated using eq. (F.4). To use this equation first the bed shear stress, τ_*, is calculated using eq. (F.5) and eq. (F.6).
With the settling velocities of all tested types of sediment and the shear velocity for each individual test condition the Rouse numbers are calculated. These are given in table F-4.

$$u_* = \sqrt{\frac{\tau_*}{\rho_s}} \tag{F.4}$$

$$u_{max} = \frac{\omega \frac{1}{2} H_s}{\sinh kd} \tag{F.5}$$

$$\tau_* = \frac{1}{2}\rho C_f u_{max}^2 \tag{F.6}$$

$$u_* = \sqrt{\frac{\tau_*}{\rho}} \tag{F.7}$$

Table F-4: Rouse transport mode for all tests

Test name		$H_{s,t}$ [cm]	T_p [s]	K_r [%]	$D_{50,s}[\mu m]$	W [cm/s]	u_{max} [cm/s]	τ_* [N/m^2?]	P [-]	Rouse transport mode
Per_D22_H14_T25_NoToe	B.1.1b	13.9	2.5	36	220	2.9	31.4	2.58	1.5	Suspended load (50%)
Per_D22_H14_T25_Toe	B.1.2.b	13.6	2.5	33	220	2.9	30.8	2.50	1.5	Suspended load (50%)
Per_D22_H14_T16_NoToe	B.1.6	12.0	1.6	23	220	2.9	23.4	2.15	1.6	Suspended load (50%)
Per_D22_H14_T16_Toe	B.1.7	12.1	1.6	24	220	2.9	23.6	2.29	1.5	Suspended load (50%)
Per_D22_H14_T16_ToeProt	B.1.8	12.1	1.6	24	220	2.9	23.6	2.29	1.5	Suspended load (50%)
Per_D17_H14_T25_NoToe	B.2.1	13.9	2.5	37	170	2.0	31.5	2.46	1.0	Suspended load (100%)
Per_D17_H14_T25_Toe	B.2.2	13.9	2.5	34	170	2.0	31.5	2.46	1.0	Suspended load (100%)
Per_D17_H14_T25_Toe_b	B.2.2b	13.9	2.5	34	170	2.0	31.5	2.46	1.0	Suspended load (100%)
Per_D17_H14_T25_ToeProt	B.2.3	13.9	2.5	37	170	2.0	31.5	2.46	1.0	Suspended load (100%)
Per_D17_H14_T16_NoToe	B.2.4	12.2	1.6	26	170	2.0	23.8	2.20	1.1	Suspended load (100%)
Per_D17_H14_T16_Toe	B.2.5	12.2	1.6	26	170	2.0	23.8	2.20	1.1	Suspended load (100%)
Per_D17_H14_T16_ToeProt	B.2.6	12.2	1.6	27	170	2.0	23.8	2.20	1.1	Suspended load (100%)
Per_D17_H14_T21_NoToe	B.2.7a	13.6	2.1	32	170	2.0	29.6	2.49	1.0	Suspended load (100%)
Per_D17_H14_T19_NoToe	B.2.7b	13.0	1.9	28	170	2.0	27.3	2.37	1.0	Suspended load (100%)
Per_D17_H14_T21_Toe	B.2.8	13.8	2.1	41	170	2.0	30.0	2.55	1.0	Suspended load (100%)
Per_D17_H18_T25_Toe	B.2.9	17.6	2.5	41	170	2.0	39.8	3.46	0.8	Suspended load (100%)
Per_D17_H14_T25_ToeProt*	B.2.10	14.4	2.5	36	170	2.0	32.6	2.52	1.0	Suspended load (100%)
Rev_D17_H14_T25_NoToe	C.2.1	14.7	2.5	51	170	2.0	33.3	2.66	1.0	Suspended load (100%)
Rev_D17_H14_T25_Toe	C.2.2	14.7	2.5	51	170	2.0	33.3	2.66	1.0	Suspended load (100%)
Rev_D17_H14_T25_ToeProt	C.2.3	14.7	2.5	51	170	2.0	33.3	2.66	1.0	Suspended load (100%)
Rev_D17_H14_T16_NoToe	C.2.4	12.7	1.6	33	170	2.0	24.8	2.32	1.0	Suspended load (100%)
Rev_D17_H14_T16_Toe	C.2.5	12.8	1.6	34	170	2.0	25.0	2.32	1.0	Suspended load (100%)
Rev_D17_H14_T16_ToeProt	C.2.6	12.7	1.6	33	170	2.0	24.8	2.32	1.0	Suspended load (100%)

F.3 Xie transport criterion

The following criterion for the scouring pattern fine has been formulated by Xie:

$$\frac{u_{max} - u_{crit}}{W} \geq 16.5 \tag{F.8}$$

The critical velocity is calculated using the approach by Bagnold (1946):

$$u_{crit} = 2.40\,\Delta^{2/3}\,D_{50}^{0.433}\,T^{1/3} \tag{F.9}$$

Table F-5: Xie criterion for all tests

Test name		$H_{s,t}$ [cm]	T_p [s]	K_r [%]	$D_{50,s}[\mu m]$	W [cm/s]	U_{crit} [cm/s]	u_{max} [cm/s]	$\frac{u_{max}-u_{crit}}{W}$ [-]	Mode
Per_D22_H14_T25_NoToe	B.1.1b	13.9	2.5	36	220	2.9	11.6	31.4	6.7	**Coarse**
Per_D22_H14_T25_Toe	B.1.2.b	13.6	2.5	33	220	2.9	11.6	30.8	6.5	**Coarse**
Per_D22_H14_T16_NoToe	B.1.6	12.0	1.6	23	220	2.9	10.0	23.6	4.6	**Coarse**
Per_D22_H14_T16_Toe	B.1.7	12.1	1.6	24	220	2.9	10.0	23.6	4.6	**Coarse**
Per_D22_H14_T16_ToeProt	B.1.8	12.1	1.6	24	220	2.9	10.0	23.6	4.6	**Coarse**
Per_D17_H14_T25_NoToe	B.2.1	13.9	2.5	37	170	2.0	10.4	31.5	10.5	**Coarse?**
Per_D17_H14_T25_Toe	B.2.2	13.9	2.5	34	170	2.0	10.4	31.5	10.5	**Coarse?**
Per_D17_H14_T25_Toe_b	B.2.2b	13.9	2.5	34	170	2.0	10.4	31.5	10.5	**Coarse**
Per_D17_H14_T25_ToeProt	B.2.3	13.9	2.5	37	170	2.0	10.4	31.5	10.5	**Coarse?**
Per_D17_H14_T16_NoToe	B.2.4	12.2	1.6	26	170	2.0	9.0	23.8	7.4	**Coarse**
Per_D17_H14_T16_Toe	B.2.5	12.2	1.6	26	170	2.0	9.0	23.8	7.4	**Coarse**
Per_D17_H14_T16_ToeProt	B.2.6	12.2	1.6	27	170	2.0	9.0	23.8	7.4	**Coarse**
Per_D17_H14_T21_NoToe	B.2.7a	13.6	2.1	32	170	2.0	9.8	29.6	9.9	**Coarse?**
Per_D17_H14_T19_NoToe	B.2.7b	13.0	1.9	28	170	2.0	9.5	27.3	8.9	**Coarse?**
Per_D17_H14_T21_Toe	B.2.8	13.8	2.1	41	170	2.0	9.8	30.0	10.1	**Coarse?**
Per_D17_H18_T25_Toe	B.2.9	17.6	2.5	41	170	2.0	10.4	39.8	14.7	**Coarse?**
Per_D17_H14_T25_ToeProt*	B.2.10	14.4	2.5	36	170	2.0	10.4	32.6	11.1	**Coarse?**
Rev_D17_H14_T25_NoToe	C.2.1	14.7	2.5	51	170	2.0	10.4	33.3	11.4	**Coarse?**
Rev_D17_H14_T25_Toe	C.2.2	14.7	2.5	51	170	2.0	10.4	33.3	11.4	**Coarse?**
Rev_D17_H14_T25_ToeProt	C.2.3	14.7	2.5	51	170	2.0	10.4	33.3	11.4	**Coarse?**
Rev_D17_H14_T16_NoToe	C.2.4	12.7	1.6	33	170	2.0	9.0	24.8	7.9	**Coarse**
Rev_D17_H14_T16_Toe	C.2.5	12.8	1.6	34	170	2.0	9.0	25.0	8.0	**Coarse**
Rev_D17_H14_T16_ToeProt	C.2.6	12.7	1.6	33	170	2.0	9.0	24.8	7.9	**Coarse**

G Appendix - Performance design formula

Performance of the new design formula is also compared with measurements after 4 and 16 hours of testing. For both the first $3/8\lambda_p$ and the first $2\lambda_p$ comparison is done with measurements. Results are given in fig. G.1 and fig. G.2. The design formula is:

$$\text{For } N \leq 24000 \text{ and } \frac{W_{p,t}}{L_p} < \frac{3}{8} L_p :$$

$$\frac{S_{max}(N)}{H_s} = \frac{0.3}{\left(\sinh \frac{2\pi h}{L_p}\right)^{1.35}} K_r^{1.5} \sqrt{\frac{N}{12000}} \tag{G.1}$$

The resulting RMSE and coefficient of determination R^2 for the formula with these measurements is given in the following table:

Table G-1: Comparison design formula with measurements after 4 and 16 hours of testing.

Area considered	Test duration	Number of tests	R^2 [-]	RMSE - all tests [-]	RMSE - small wave steepness [-]	n	RMSE - large wave steepness [-]	n
First $3/8\lambda$	4 hours	17	0.70	0.041	0.041	17	**Sedimentation**	-
First $3/8\lambda$	16 hours	5	0.96	0.037	0.037	5	**Sedimentation**	-
First 2λ	4 hours	24	0.68	0.046	0.044	14	0.048	8
First 2λ	16 hours	6	0.92	0.050	0.032	5	0.107	1

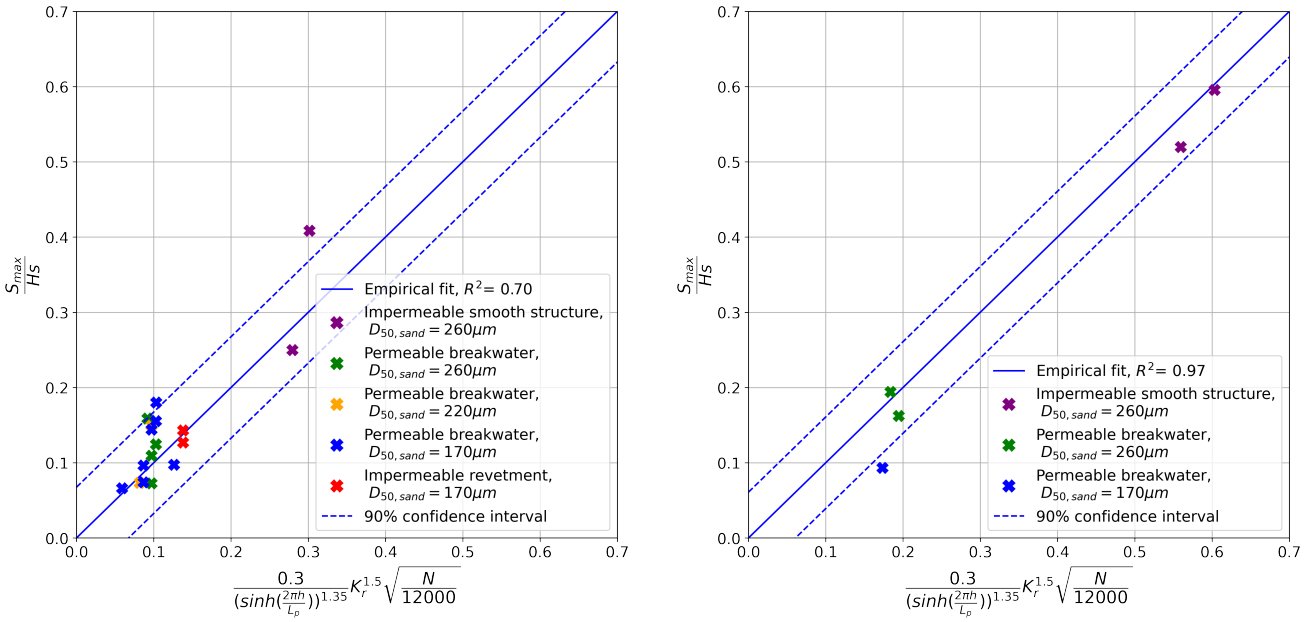

(a) Maximum depth after 4 hours of testing

(b) Maximum depth after 16 hours of testing

Figure G.1: Comparison new design formula with measurement data, first $3/8\lambda_p$

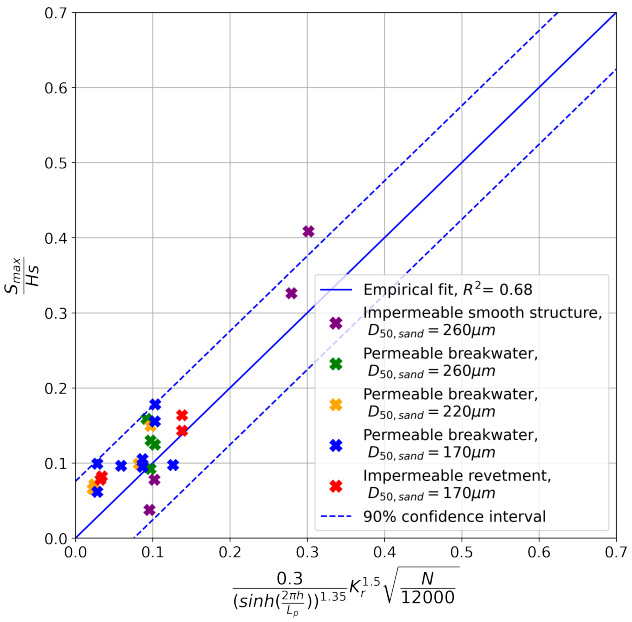

(a) Maximum depth after 4 hours of testing

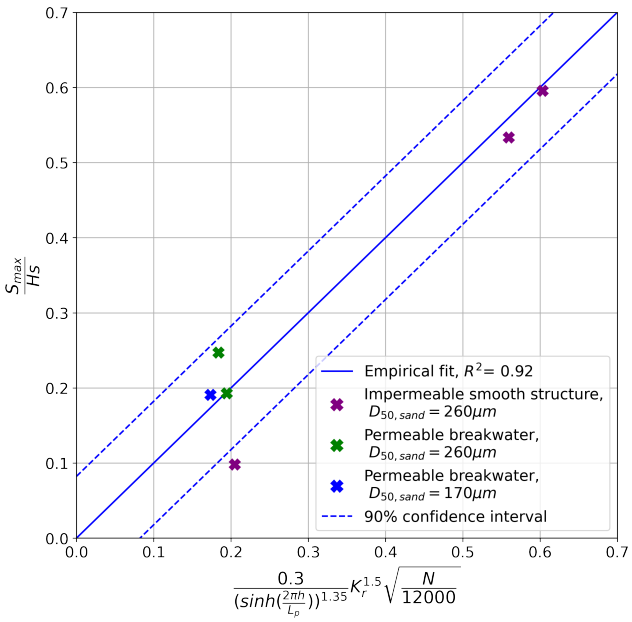

(b) Maximum depth after 16 hours of testing

Figure G.2: Comparison new design formula with measurement data, first $2\lambda_p$